ELECTRIC CURRENT AND MAGNETIC FIELD EFFECTS ON BACTERIAL BIOFILMS

by

Elizabeth Louise Sandvik

A dissertation submitted in partial fulfillment
of the requirements for the degree

of

Doctor of Philosophy

in

Chemical Engineering

MONTANA STATE UNIVERSITY
Bozeman, Montana

July 2014

ACKNOWLEDGEMENTS

First, I would like to thank my advisors Dr. Phil Stewart and Dr. Bruce McLeod. I owe much of my current knowledge of electromagnetic theory and application to Bruce's teaching and guidance. I would like to thank Phil for your introspective approach to research and science. It has been a joy working with both of you. I would also like to thank the members of my committee, Dr. Robin Gerlach, Dr. Joseph Seymour, and Dr. Gregory Johnson. I've immensely enjoyed our discussions and your input on this multidisciplinary project.

I would like to thank all researchers, graduate and undergraduate students, postdocs, and staff I have worked alongside during my time at the CBE. The collaborative spirit encompassed here has enriched my research and my daily experience. I would like to thank Dr. Al Parker for statistics guidance and for your time during many multi-hour meetings. I would like to thank Betsey Pitts for your incredible enthusiasm, assistance with all things microscopy, and lab camaraderie. I would like to thank Kerry Williamson for your expertise and guidance learning molecular techniques as well as Kate McInnerney, Joanna Gress, Pat Secor, and Jake Valenzuela. I would like to thank Dr. Mike Franklin for your input and discussions during lab meetings and members of the Biofilm Control lab, past and present, for discussions and suggestions. I would like to thank John Neuman and Ann Willis for support with equipment and supplies. John was a wonderful friend. I would like to thank Shelley Thomas, Carol Leist, Margie Hansen, Tricia Cook, Nancy Carrasco, and Muriel Holmquest for keeping everything in order.

Finally, I would like to thank my family and friends for all of their support.

TABLE OF CONTENTS

TABLE OF CONTENTS - CONTINUED

TABLE OF CONTENTS - CONTINUED

TABLE OF CONTENTS - CONTINUED

LIST OF TABLES

LIST OF TABLES - CONTINUED

LIST OF FIGURES

LIST OF FIGURES - CONTINUED

LIST OF FIGURES - CONTINUED

LIST OF FIGURES - CONTINUED

GLOSSARY AND NOMENCLATURE

CFU	bacterial colony forming units
DC	direct electric current
ELF	extremely low-frequency (in reference to an electromagnetic field)
ELF-MF	extremely low-frequency magnetic field
EMF	electromagnetic field
EPS	extracellular polymeric substance
FC	fold change of gene expression of a treated sample compared to a control sample
ICR	ion cyclotron resonance
LD	log cell density [$\log_{10}(CFU/cm^2)$ or $\log_{10}(CFU/mL)$]
LR	log reduction in log cell density compared to at control
MF	magnetic field
PBS	phosphate buffered saline
TSA	tryptic soy agar
TSB	tryptic soy broth
SD	standard deviation
SEM	standard error of the means

ABSTRACT

The ability of bacteria to form and grow as biofilm presents a major challenge in clinical medicine. Through this work, two alternative electromagnetic treatment strategies were investigated to combat bacterial biofilms like those that cause chronic infections on indwelling medical devices. Direct electric current (DC) was applied at current densities of 0.7 to 1.8 mA/cm^2 alone and in conjunction with antibiotic. Unlike most previous studies, chloride ions were included in the treatment solution at a physiologically-relevant concentration. Using this approach, low levels of DC alone were demonstrated to have a dose-responsive, biocidal effect against *Staphylococcus epidermidis* and *Pseudomonas aeruginosa* biofilms with no synergistic enhancement of antibiotic activity. Through a series of experiments using chemical measures, cell viability, and global gene expression, electrolytic generation of chlorine, a potent disinfectant, was identified as the predominant mechanism by which DC kills bacteria in biofilm. The second treatment strategy investigated weak, extremely low-frequency magnetic fields (ELF-MFs) as a noninvasive approach, involving an extension of concepts from well-studied ELF-MF effects observed in eukaryotic systems to bacterial biofilm. *S. epidermidis* biofilms grown in weak, extremely low-frequency magnetic fields (ELF-MFs) at Ca^{2+} and K^+ ion resonance frequencies were assessed using global gene expression to determine if *S. epidermidis* in biofilm detect and respond to ELF-MFs. Frequency-dependent changes in gene expression were observed with upregulation of genes involved in transposase activity, signal transduction systems, and membrane transport processes indicating possible effects consistent with theories of ELF-MF induced changes in ion transport reported in eukaryotic cells. This is the first transcriptome study to indentify ELF-MF effects in bacteria. While no direct biocidal effect was observed with ELF-MF treatment, alteration of membrane transport processes could potentially modify biofilm susceptibility to certain antibiotics. The ELF-MF responses identified in this work provide a platform for future study.

CHAPTER 1: INTRODUCTION

Bacterial Biofilms

Biofilms are communities of bacteria that form when cells attach to a surface and secrete a matrix of extracellular polymeric substance (EPS). A hallmark characteristic of biofilms is their tolerance to antimicrobials. Killing microorganisms in biofilms can require 100 to 1,000 times the concentrations of antimicrobials effective on their planktonic counterparts. Biofilms are also tolerant of host immune defenses making them a challenging adversary in clinical medicine. As the study of biofilms has progressed, our knowledge of the complexity of these organisms has grown to include their ability to communicate, build complex multi-cellular communities, and persist in many environments.

Biofilm formation is characterized by initial surface attachment of planktonic cells that grow into microcolonies and mature into highly heterogeneous structures consisting of towers, streamers, and bridges. The development of these complex structures is mediated by cell-to-cell communication via quorum sensing. Davies et al. demonstrated that the complex, heterogeneous biofilm structure produced by *P. aeruginosa* was reduced to a thin, tightly packed slab biofilm in a mutant strain lacking the gene to produce the signaling molecule *lasI* (Davies et al., 1998). In contrast, the wildtype biofilm formed large microcolonies and towers separated by water channels. While the *lasI* mutant was capable of the early attachment stages of biofilm growth, the differentiation into the mature biofilm state was halted and when challenged with a

detergent biocide, most or all of the cells detached and dispersed. The wildtype was unchanged by this treatment (Davies et al., 1998). This ability to organize as a community of cells and build multicellular structures may be critical in the development of the characteristic resistant properties of biofilms. In *S. epidermidis*, the initial attachment has been linked to the release of extracellular DNA. The eDNA has been attributed to autolysis of a small subpopulation of cells that releases genomic DNA upon death, promoting surface attachment of the remaining population which in turn incorporates the DNA in the matrix structure (Qin et al., 2007). In *P. aeruginosa*, eDNA has been found as an intercellular connector, providing structural stability to the matrix (Yang et al., 2007). These examples of coordinated, community based processes demonstrate the complexity of these "simple" single-celled organisms.

In the process of building a multicellular structure, the physical properties of the extracellular structure begin to impede mass transport processes through the biofilm. The makeup of extracellular polymeric substance (EPS) matrix varies greatly between organisms and within the same organism grown under different conditions (Buckingham-Meyer et al., 2007) but includes exopolysaccharides (a major fraction of the matrix), extracellular enzymes and structural proteins, eDNA, surfactants and lipids. Water is nevertheless the largest component (Flemming and Wingender, 2010). Consequently, compounds can still migrate through the matrix via diffusion but at an effective diffusion rate less than for the same compound in water. When the compound is a reactive compound as would be the case for nutrients, including oxygen, or antimicrobials, reaction-diffusion limitations are manifested as concentration gradients through the

biofilm. In many cases this results in a penetration depth of compounds less than that of the biofilm thickness. This produces an active zone at boundaries, for example, at the top of the biofilm near the air or liquid interface or at the base of the biofilm if grown on a medium substratum such as agar. Direct measurements of decreasing oxygen concentrations in *Pseudomonas aeruginosa* biofilms have been determined with microelectrodes moved from the bulk fluid into the biofilm matrix with complete depletion of oxygen at the bottom portion of microcolonies (Borriello et al., 2004; DeBeer et al., 1994b; Kuhl et al., 2007; Rani et al., 2007). Measurements of oxygen profiles in the pore space between the microcolonies has shown elevated oxygen levels providing evidence for enhanced convective transport via channeling (DeBeer et al., 1994b) and a possible purpose for development of complex topography. The effect of these nutrient gradients has been seen in corresponding gradients of bacterial activity. Rani et al. measured DNA and protein synthetic activity in colony biofilms under aerobic and anaerobic conditions. Under aerobic conditions, DNA and protein synthetic activity were observed in thin bands at the air/biofilm interface and at the base of the biofilm at the nutrient agar interface. In contrast, under anaerobic conditions, those same activity bands were only observed at the nutrient interface (Rani et al., 2007). Using microdissection microscopy, Lenz et al. found constant levels of 16S rRNA throughout the biofilm but a large decrease in the activity of the housekeeping gene *acpP* in the middle and base of biofilms when grown on glass slides or in the middle of colony biofilms with a slight increase in levels at the agar interface indicating that gene expression can be affected by localized conditions in the biofilm (Lenz et al., 2008).

A number of factors contribute to biofilms notorious tolerance to antimicrobials and immune defenses. The same reaction diffusion limitations discussed above can also apply to reactive antimicrobial compounds diffusing into the biofilm. For highly reactive, non-specific agents like chlorine, this can result in incomplete penetration. Direct measurement of chlorine with biofilm depth have shown steep concentration gradients in *Pseudomonas aeruginosa* and *Klebsiella pneumoniae* biofilms with chlorine never reaching the interior of biofilm microcolonies (patchy colonies: 200-300 μm wide, 150-200 μm in depth) even after 2 hours (DeBeer et al., 1994a). Reduced transport and limited penetration has also been proposed to explain the ineffectiveness of antibiotics. Several reports have used a modified colony biofilm method reported by Anderl et al. that measures migration of antibiotics from antibiotic agar plates through the colony biofilm to a small absorbent disk set atop the colony (Anderl et al., 2000). Anderl et al. reported complete penetration of ciprofloxacin in less than 20 minutes but no penetration by ampicillin in a wildtype *K. pneumoniae* biofilm. Transport of ampicillin through a β-lactamase deficient biofilm occurred in under 10 minutes (Anderl et al., 2000). Zheng and Stewart reported complete penetration of rifampin without killing of a *S. epidermidis* biofilms (Zheng and Stewart, 2002). Singh et al. reported no decrease in diffusion of ciprofloxacin and amikan through *S. epidermidis* and *S. aureus* biofilms. They observed retarded but complete diffusion of oxacillin, cefotaxime, and vanomycin over 24 hours (Singh et al., 2010). Most recently, fluorescently-labeled vancomycin was shown to penetrate a biofilm in 2-8 minutes depending on the *S. aureus* strain (Oubekka et al., 2012). Taken together, diffusion limitation of antibiotic compounds cannot fully explain

antimicrobial tolerance as many antibiotics fully penetrate biofilms unless organisms have means to inactivate the compound.

The reduced and slowed growth rate of bacteria in the biofilm state is known to be a major component of antibiotic tolerance. The activity studies have demonstrated the majority of the bottom or middle of biofilms are inactive, and as demonstrated by complete antibiotic penetration, the antibiotics are simply not effective despite reaching the cells (Zheng and Stewart, 2002). Borriello et al. demonstrated that anaerobic conditions in *P. aeruginosa* biofilm correlated to antimicrobial resistance to several antibiotics. The oxygen limitation was linked to biofilm age as actively growing four-hour-old biofilms were much more susceptible to antibiotics than 48-hour-old biofilms where the majority of cells were in a oxygen-limited, extremely slow growing state (Borriello et al., 2004). Slow growth can go to an extreme called the persister state, a small subpopulation of cells that remain in a non-growing state that can reactivate to normal cells and repopulate the biofilm following eradication of the rest of the population (Lewis, 2012).

Given these attributes, bacterial biofilms are incredibly difficult to treat. Standard antimicrobial treatments are often not effective and novel treatment strategies need to be considered.

Electric Current Treatment of Bacteria

DC Treatment of Planktonic Cultures

One of the early reports of electric current as a microbial control strategy investigated 10 second exposures of planktonic cultures of *E. coli* to alternating current

at 25-110 mA and 50 Hz (Pareilleux and Sicard, 1970). The study found a bactericidal effect that was dose-responsive with respect to both current level and the duration of time cells remained in the treated media after exposure before being sampled for viability. Following observation of biocidal effects of corrosion products released from platinum, gold, stainless steel and platinum electrodes against *S. aureus* on agar plates (Barranco et al., 1974), the intentional release of electrolytically generated metallic ions was studied as a possible antifungal (Berger et al., 1976a). Electrolytic generation of silver ions was further studied for antibacterial effects against *S. aureus* and mammalian cells (Berger et al., 1976b) and was used in a clinical trial to successfully treat chronic osteomyelitis in twelve of fifteen participants (Becker and Spadaro, 1978). Davis et al. reported bacteria specific gold iontophoretic killing of planktonic cultures in a model catheter system with complete killing of *E. coli* and *S. aureus* but ineffective killing of several other bacteria (Davis et al., 1982). They went on to study effects of electrode material on iontophoresis. With a gold cathode, anodes made of carbon or platinum were reported to be the most effective while silver, nickel, or copper corroded to the point of breakage during experiments (Davis et al., 1989). In a study of electrode lifetime of gold versus platinum electrodes in synthetic urine, breakage of gold electrodes with 400 μA of current occurred between 9 and 31 days depending on the electrode diameter while platinum electrodes were still intact after 180 days of continuous current (the termination of the experiment). While more stable than many of the previous electrode materials, the time to breakage for gold electrodes scaled with current level as well indicating release of electrode material (Davis et al., 1991). With the use of these more inert gold and

platinum electrodes, chloride was identified as a critical medium component for successful killing of planktonic *E. coli, S. saprophyticus,* and *C. albicans* (Davis et al., 1993; Davis et al., 1992). In a thorough electrochemical analysis of chloride-dependent DC effect, levels of free chlorine, chlorine dioxide, monochloramine, and dichloramine were measured in electrolyzed sodium chloride and synthetic urine solutions. Species differentiation of these compounds were dependent on the other components in solution (Davis et al., 1994).

Theory: Electrolysis of a Sodium Chloride Solution

The reactive chlorine species observed by Davis et al. can be explained by the electrolytic generation of chlorine. To further understand this concept, the treatment well can be considered as an electrolytic cell along with its associated half reactions. For this example we will ignore the organics in the nutrient solution and examine DC application to a sodium chloride solution as seen in Figure 1.1.

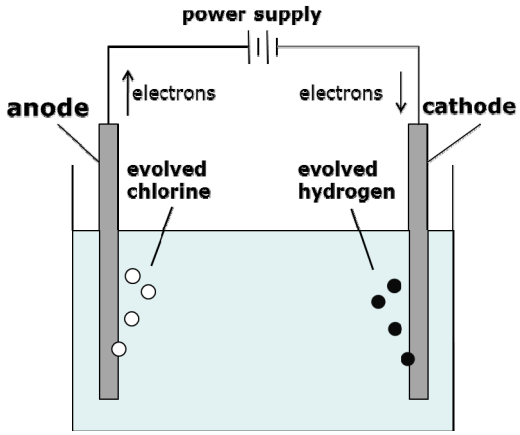

Figure 1.1 Electrolysis of a sodium chloride solution with inert electrodes. Electron flow is indicated from the anode to the cathode. Oxidation of chloride ions in solution will evolve chlorine gas at the anode whereas reduction of water at the cathode will generate hydrogen gas.

At the cathode, reduction will occur and the following reactions are possible are:

$$Na^+ + e^- \rightarrow Na(s) \qquad E^o_{red} = -2.71\ V \qquad (1.1)$$

$$2H_2O\ (l) + 2e^- \rightarrow H_2\ (g) + 2OH^-\ (aq) \qquad E^o_{red} = -0.83V \qquad (1.2)$$

Equation 1.2 will predominate because of the higher reduction potential and H_2(g) will be evolved along with an increase in pH at the cathode.

At the anode, oxidation will occur and the following reactions are possible:

$$2Cl^-\ (aq) \rightarrow Cl_2(g) + 2e^- \qquad E^o_{ox} = -1.36\ V \qquad (1.3)$$

$$2H_2O\ (l) \rightarrow O_2(g) + 4H^+\ (aq) + 4e^- \qquad E^o_{ox} = -1.23\ V \qquad (1.4)$$

The oxidation potentials for these two reactions are very close and they might both occur. However, it is generally observed that Equation 1.3 predominates due to the overvoltage required for the oxidation of water and generally Cl_2(g) generation is considered the primary reaction (Chang, 1987).

Chlorine Chemistry. The generated chlorine gas will go into solution to form hypochlorite (OCl^-) and hypochlorous acid (HOCl) as in Equations 1.5 and 1.6.

$$Cl_2(g) + 2OH^-\ (aq) \rightarrow Cl^-\ (aq) + OCl^-\ (aq) + H_2O\ (l) \qquad (1.5)$$

$$HOCl \rightarrow H^+\ (aq) + OCl^-\ (aq) \qquad (1.6)$$

HOCl and OCl^- are active oxidizing agents responsible for disinfection and the distribution between the two is pH dependent with equilibrium between the two species at pK_a=7.5. The combined concentration of the two species is called the "free chlorine" in a solution, i.e. the chlorine available to react with compounds. If the pH is increasing due to the reaction at the cathode, OCl^- would predominate and Equation 1.5 can be used.

If we combine equations Equations 1.2, 1.3, and 1.5 we arrive at the overall reaction seen below.

$$Cl^- (aq) + H_2O (l) \rightarrow OCl^- (aq) + H_2(g) \quad (1.7)$$

The rates of generation for the half reactions can be used to determine changes for a system with a known current level. The molar rate of electrons introduced to the well by the current, I [A], can be represented as r_{e^-}. This electron rate can be related to the rates of generation or chlorine gas, Cl_2, where q_v is a loss term for the rate of volatilization of Cl_2(g).

$$r_{e^-} = I\left(\frac{C/s}{A}\right)\left(\frac{e-}{1.602*10^{-19}C}\right)\left(\frac{mole^-}{6.022*10^{23}e^-}\right) \quad [\text{mol } e^-/\text{s}] \quad (1.8)$$

$$r_{Cl_2} = V\frac{\partial[Cl_2]}{\partial t} = r_{e^-}\left(\frac{molCl_2}{2mole^-}\right) - q_v \quad [\text{mol } Cl_2/\text{s}] \quad (1.9)$$

The molar concentration of free chlorine, $[Cl_2]$, after current is applied for a given time, t, can also be determined with the volume of liquid, V:

$$[Cl_2] = r_{Cl_2}\frac{t}{V} \quad [\text{mol } Cl_2/\text{L}] \quad (1.10)$$

$$C_{freechlorine} = r_{Cl_2}\frac{t}{V}\left(\frac{70.9*10^3 mgCl_2}{molCl_2}\right) \quad [\text{mg/L or ppm free chlorine}] \quad (1.11)$$

Electric Current Treatment of Biofilms and the Bioelectric Effect

Treatment of bacterial biofilms with low levels of direct current (DC) was first reported by Blenkinsopp et al. (1992). Biofilms were grown on stainless steel studs in a modified Robbins device and treated in chloride-free medium. They reported that while a

biocide or direct current alone had little to no effect on bacterial survival, the combination of direct current and industrial biocides (kathon, quaternary ammonium compound, or gluteraldehyde) was shown to significantly increase killing efficacy. This synergistic phenomenon was termed the bioelectric effect (Blenkinsopp et al., 1992a). Subsequent investigations studied the use of electric current with antibiotics (Costerton et al., 1994; del Pozo et al., 2009b; Jass et al., 1995; Jass and Lappin-Scott, 1996; Khoury et al., 1992; McLeod et al., 1999; Stewart et al., 1999; Wattanakaroon and Stewart, 2000; Wellman et al., 1996). Nearly all of these studies used stainless steel electrodes (Costerton et al., 1994; del Pozo et al., 2009b; Jass et al., 1995; Jass and Lappin-Scott, 1996; Khoury et al., 1992; McLeod et al., 1999; Stewart et al., 1999; Wattanakaroon and Stewart, 2000) and chloride free medium (Blenkinsopp et al., 1992a; Costerton et al., 1994; Jass et al., 1995; Jass and Lappin-Scott, 1996; Khoury et al., 1992; McLeod and Sandvik, 2010; Stewart et al., 1999; Wellman et al., 1996). Costerton et al. studied biofilms grown on stainless steel electrodes and saw a nearly 3-log reduction in viable cells including biofilm cells on passive stainless steel electrodes between the active electrodes (Costerton et al., 1994). Jass et al. reported less pronounced results of DC and tobramycin when *P. aeruginosa* biofilms were grown on a membrane in the center of the well, away from reactions occurring directly at the electrode surfaces (Jass et al., 1995). Stewart et al. linked DC-enhanced tobramycin efficacy in *P. aeruginosa* biofilms to electrolytic generation of oxygen (Stewart et al., 1999).

Studies of electric current effects without antibiotics were also reported. Stoodley et al. reported expansive and retractive deformation of mixed species biofilms

of *K. pneumoniae*, *P. fluorescens*, and *P. aeruginosa* grown on platinum electrodes in chloride-free medium coupled with pH shifts as the electrode polarities were reversed (Stoodley et al., 1997). Shirtliff et al. reported no effect of electric current to remove mixed-species water distribution biofilms on stainless steel slides in the presence of chloride even when coupled with a free chlorine dose (Shirtliff et al., 2005). Electrolytic removal of *S. epidermidis* biofilms from stainless steel electrodes was demonstrated with gas evolution and a rapid removal event after 30 seconds of connection to a 6 V battery (Rabinovitch and Stewart, 2006).

A number of mechanisms have been proposed for the bioelectric effect. Electric current has been proposed to apply electrophoretic forces that enhance transport of antimicrobials through the biofilm matrix, overcoming diffusion limitations (Blenkinsopp et al., 1992a; Costerton et al., 1994; Jass and Lappin-Scott, 1996; Khoury et al., 1992). It has also been suggested that DC enhances uptake of antimicrobials at the cell membrane via electroporation (Blenkinsopp et al., 1992a; Costerton et al., 1994). A number of explanations involve products of electrolysis including the production of gases such as oxygen that increase metabolic and thus antimicrobial activity (Jass et al., 1995; Stewart et al., 1999), the generation of electrolysis products including chlorine species (Davis et al., 1994; Liu et al., 1997; Rabinovitch and Stewart, 2006), hydrogen peroxide (Liu et al., 1997), and those affecting pH (Rabinovitch and Stewart, 2006; Stoodley et al., 1997). In other studies, DC is reported to affect bacterial adherence or stimulate detachment of biofilm to conducting surfaces (Hong et al., 2008; Poortinga et al., 2001b; Rabinovitch and Stewart, 2006; van der Borden et al., 2005; van der Borden et al., 2004b). When

external electric fields were applied with insulated electrodes (i.e. no current flow), enhanced bacterial killing by antibiotics was not observed (McLeod et al., 1999) nor were modification of bacterial adhesion (Poortinga et al., 2001a).

Magnetic Fields

Electromagnetic fields (EMFs) are known to affect biological processes (Binhi and Savin, 2003; Funk et al., 2009; Funk and Monsees, 2006; Milyaev and Binhi, 2006). The reports of magnetic field EMF effects range from negative consequences and implications in human diseases, such as cancer (Lacy-Hulbert et al., 1998), to current therapeutic applications in EMF modulation of bone repair and the healing of chronic wounds (Pilla, 2006). Interest in EMF effects on biological systems arose from concerns of human impacts of the rising levels of weak EMFs experienced daily in the modern human environment. In a paper by Delgado et al., weak, extremely low-frequency electromagnetic fields at 100 Hz and 1.2 μT had a pronounced effect on chick embryo development, delaying or arresting early division processes and specialization of tissues. Interestingly, maximum occurrences of abnormalities in embryos occurred at specific frequency and power "windows" (more occurrences at 100 Hz versus 10 or 1,000 Hz; more occurrences at 1.2 μT versus 0.12 or 12 μT) (Delgado et al., 1982). The response to the report of these "windows" lead to a wide range of research of weak MF effects in the extremely low-frequency range (0-300 Hz) studying frequency and field-dependent effects in many organisms, the majority at magnetic field magnitudes on the order of Earth's magnetic field: 25-70 μT (250-700 mG) (Liboff, 1985). The relatively new field

of magnetobiology studies the biological reactions and mechanisms of these weak (below 1 mT) magnetic fields (Binhi and Savin, 2003).

Biological Responses to ELF-MFs

Over the last 30 years, a large body of evidence has presented biological responses to MFs in the extremely low-frequency (ELF) range. Despite the multitude of reports, the mechanisms for these observed effects is unknown.

A few of the wide range of responses to the application of ELF-MFs include enhanced bone growth in birds and mammals now used in human medicine (Aaron et al., 2004), modified exploratory and anxiety behavior of rats (He et al., 2011; Jadidi et al., 2007), increased diatom motility (McLeod et al., 1987; Smith et al., 1987), modified protein activity (Blank, 1992, 2008), DNA stress (Blank, 2008; Blank and Goodman, 1997, 2008), increase Ca^{2+} saturation in plant roots (Belyavskaya, 2004), and increased measures of heat shock and stress proteins in *E. coli* (Cairo et al., 1998; Chow and Tung, 2000a, b; Del Re et al., 2006; Del Re et al., 2009; Li and Chow, 2001). The physical mechanism for these effects are highly debated. Proposed mechanisms include several theories for EMF effects on ion transport through membrane channels based on ion cyclotron resonance (Liboff, 1985), ion binding with protiens based on parametric ion resonance (Blanchard and Blackman, 1994; Lednev, 1991), effects on charge transfer in proteins, including membrane proteins, and DNA (Blank, 2005; Blank and Goodman, 1997, 2008; Blank and Soo, 2001a), and forced vibration of free ions on the surface of the cell membrane (Panagopoulos et al., 2002). As all of these theories have some basis on charged molecules we will first examine the basic physics of charges in an MF.

Theory: Magnetic Force on a
Charged Molecule in Vacuum

The force exerted on a free charged particle of charge q with a velocity $\vec{u}$ in the presence of an electromagnetic field is a sum of the forces from an electric flux density, $\vec{E}$, and a magnetic flux density, $\vec{B}$, and is described by the Lorentz equation:

$$\vec{F} = \vec{F}_e + \vec{F}_m = q\vec{E} + q\vec{u} \times \vec{B} \tag{1.12}$$

Several important features can be seen in this equation. First, the force exerted on a charged particle by an electric field does not depend on the velocity and thus can act on a moving particle or a particle at rest. In contrast, a magnetic field can only act on a moving particle. The force applied to a charged particle by an electric field, $\vec{E}$, will be applied in the direction of the $\vec{E}$ field while the force applied by a magnetic field, $\vec{B}$, as a cross product of the velocity and $\vec{B}$, will be perpendicular to both the velocity vector, $\vec{u}$, and the $\vec{B}$ field. The effect of the magnetic force is to change the direction of the charged particle, however, because the applied force is always perpendicular to the velocity, the magnetic field cannot change the velocity of a charged particle or change the kinetic energy, it can only change the particle's path of motion.

For magnetic field applications, consider the path of a charged particle in a magnetic field with no electric field ($\vec{E}$=0). When we expand the cross product the force on a charge in a magnetic field will be:

$$\vec{F} = \vec{F}_m = q\vec{u} \times \vec{B} = q\hat{n}uB\sin(\theta) \tag{1.13}$$

where θ is the angle between the velocity, $\vec{u}$, and magnetic field, $\vec{B}$, vectors, u and B are the magnitudes of the vectors , and $\hat{n}$ is the unit normal vector. If $\vec{u}$ is parallel to $\vec{B}$ the cross product will be zero and the magnetic field will not exert a force on the ion (Figure 1.2A). If $\vec{u}$ is perpendicular to $\vec{B}$ the cross product (and the magnetic force) will be at a maximum and the particle will move in a circular path around the magnetic field lines as seen in Figure 1.2B. When $\vec{u}$ and $\vec{B}$ are neither parallel nor perpendicular, the force will again cause circular motion however the component of the vector parallel to the magnetic field will remain unchanged thus maintaining the "forward" motion resulting in a spiral path of the particle as seen in Figure 1.2C.

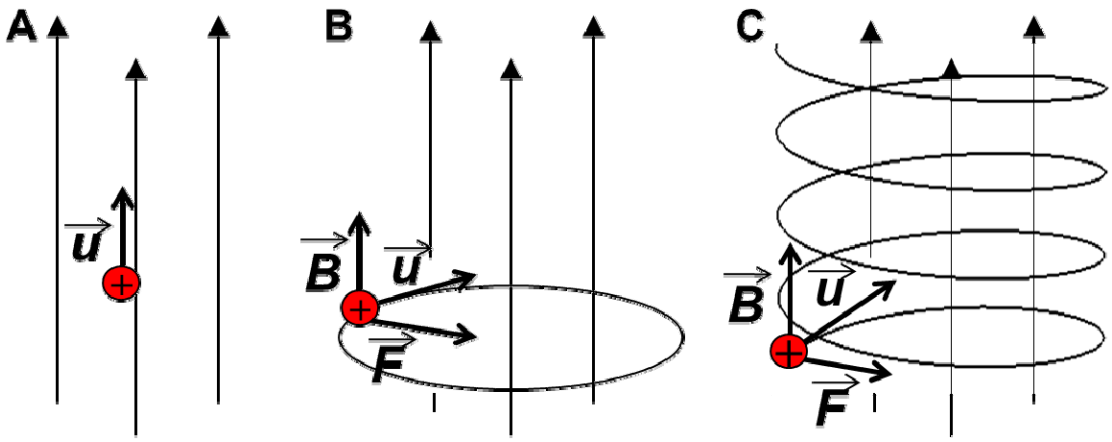

Figure 1.2 The motion of a charged molecule in a magnetic field. Motion is depicted for a positively charged molecule with a velocity (A) parallel to the magnetic field lines, (B) perpendicular to the magnetic field lines, or (C) neither parallel nor perpendicular to the magnetic flux density thus resulting in a forward moving, helical path.

For a given particle of mass, m, and charge, q, the frequency, f, of these revolutions is:

$$f=\frac{qB_o}{2\pi m} \tag{1.14}$$

This is the frequency of a time-varying magnetic field but it is only a function of the static magnetic field component (independent of the magnitude of the time-varying element). The frequency is also independent of the velocity of the particle. As mass and charge are intrinsic properties of the ion, each ion has a fixed charge to mass ratio, *q/m*. Thus for a given $B_{o,}$ there will be a frequency that satisfies the above equation for each ion, called the ion resonant frequency.

While the Lorentz equation helps to gain a fundamental concept of electromagnetic effects on charged particles, it fails to account for interactions seen in a real material such as collisions with other particles and drag forces of the moving particle through a fluid. A common correction is addition of a damping term that we will refer to here as F_{damp} to account for collisions of particles. Liboff sets this term proportional to the velocity as $F_{damp}= \vec{u}\, m/\tau$ where τ is the mean time interval between collisions (Liboff, 2005). Another term might be a drag term for particle moving through the fluid. If creeping flow is assumed for this term and we roughly estimate the charged particle as a solid sphere, we can define a drag force using Stoke's Law where $F_{drag}=6\pi\mu\,\vec{u}\,R,$ where μ is the viscosity of the fluid and *R* the radius of the particle. With the correction terms added to Equation 1.5 we arrive at the following for additional forces in a complex medium:

$$\vec{F}=\vec{F}_e+\vec{F}_m-\vec{F}_{damp}-\vec{F}_{drag}=q\vec{E}+q\vec{u}\times\vec{B}-\frac{\vec{u}m}{\tau}-6\pi\mu\vec{u}R \tag{1.15}$$

Ion Resonance-based Theories for ELF-MF Effects

An ion cyclotron resonance mechanism of electromagnetic field interactions with biological systems was first proposed by Liboff (Liboff, 1985). His observation was that the optimal frequency "windows" seen by Delgado et al. (Delgado et al., 1982) and in other EMF studies, correlated with resonance frequencies for a number of biologically relevant ions based on static magnetic fields within the range of the geomagnetic field. He posited that biological effects were the result of MF forces on ion transport through helical interstitial protein channels (Liboff, 1985). Experimental tests designed to test the model used a marine diatom previously reported to require calcium for motility (Cooksey and Cooksey, 1980). The experiment found enhanced diatom motility in the presence of a magnetic field tuned to a Ca^{2+} ion resonance frequency (McLeod et al., 1987b). Subsequent studies found effective frequencies not only at the resonance frequency, but additionally at odd harmonic frequencies for those ions in the diatom system (McLeod et al., 1987b; Smith et al., 1995) and in a study of radish seed germination reporting stimulatory effects of Ca^{2+} tunings, inhibitory effects of K^{+} tunings and no effect of Mg^{2+} tunings, also only at odd harmonics (Smith et al., 1995). During that same time Ca^{2+} tunings were demonstrated to increase bone healing in chick (Smith et al., 1991) and rabbit (Deibert et al., 1994) models. The current ICR theory predicts effective frequencies by:

$$f_n = \frac{qB_o n}{2\pi m} \qquad \textit{where } n=1,3,5,7,\ldots \tag{1.16}$$

A substantial amount of experimental data fits the resonance frequencies for biologically relevant ions. A summary of systems, tunings, and responses from a review of over 65 studies of living systems and 11 cell free systems fitting ICR frequencies are listed in Table 1.1 (summarized from Tables 1-8 (Liboff, 2005)). The ion resonance frequency specificity has been supported by studies that reported pronounced effects with a specific tuned fields that ceased when the tuning was nonspecific. In some studies, effects were reversed by tuning to a different ion.

The ion magnetic parametric resonance model was proposed by Lednev (Lednev, 1991) and clarified by Blanchard and Blackman (Blanchard and Blackman, 1994). Ion magnetic parametric resonance theory also predicts effects at the ion cyclotron resonance frequency and subharmonics:

$$f_n = \frac{qB_o}{2\pi mn} \qquad \textit{where } n=1,2,3,4,... \qquad (1.17)$$

Note that the fundamental frequency (n=1) is the same as the ion cyclotron resonance model (Equation 1.16). The proposed mechanism of ion parametric resonance was modified binding of ions in protein complexes and subsequent biological responses (Lednev, 1991).

Table 1.1 Summary of systems, tunings, and responses fitting the ion resonance frequencies compiled from Tables 1-8 of Liboff (2005). The tables reported results of over 65 studies of living systems and 11 cell free systems including specific tuning parameters and responses.

System	ICR Tuned to:	Types of Responses
Bone (*in-vitro* and *in-vivo*)	Ca^{2+}, Mg^{2+}	Enhanced fibroblast, osteosarcoma, and human bone cell proliferation; increased chick femur length/diameter; inhibition of chondrocytes; enhanced protoglycan synthesis in bovine cartilage; Increased fibular stiffness in rabbits after ostectomy; reduced bone loss in rats
	K^+	Decreased chick femoral diameter, inhibited bone growth (opposite effects of Ca^{2+}, Mg^{2+} in same system)
Rat Behavior	Mg^{2+}	Enhanced learning; enhanced locomotor exploratory behavior
	Ca^{2+}	Loss of short-term memory; inhibited learning; reduced locomotor exploratory behavior (opposite effects of Mg^{2+} in same system)
Diatom Motility	Ca^{2+}	Enhanced motility (no effect at even harmonics)
	K^+	Inhibited motility
Cell Cultures	Ca^{2+}	Increased incorporation of ^{45}Ca in lymphocytes (effect disappears with calcium blocker); increased micronuclei formation in human lymphocytes; enhanced fibroblast proliferation
	K^+	Reduced fibroblast proliferation (opposite when Ca^{2+} tuned in same system); enhanced proliferation of human lymphoma cells
Neural Cell Culture	Co^{2+}, Fe^{2+}, H^+, Ca^{2+}, Mg^{2+}	Enhanced proliferation in neuroblastoma cells; changes in neurite outgrowth
Complex Biological Systems	Ca^{2+}	Reduced synthesis/release of rat pineal melatonin; maximal hear rate fluctuation in Daphnia; delayed cephalic regeneration, enhanced rate of blastema growth during flatworm regeneration; maximum effects on bioluminescence in marine plankton; enhanced snail analgesia
	K^+	No change in flatworm regeneration rate; modulated snail opioid analgesia reversed with K^+ channel blocker
Plants	Ca^{2+}, Mg^{2+}	Stimulated radish growth, delayed germination; no effects on mustard plants, possible effect on barley plant; enhanced gravitropic response in millet, flax and clover seeds at Ca^{2+} (no effect at Mg^{2+})
	K^+	Reduced radish growth, enhanced germination; inhibited gravitropic response in millet, flax and clover seeds
Cell-free Systems	K^+, H^+	No changes in gram A channel conductance in lipid bilayer
	Ca^{2+}	No enhancement of Ca2+ binding to calcium-modulated protein (calmodulin)
	Asn^+, Arg^{2+}, Glu^+, Tyr^+	Enhanced aqueous conductivity in amino acid solutions (ICR effect disappears at AC/DC ratio=0.2 vs 0.002, when DC fields are very small, and when AC and DC fields are at 90°)
	$H_3O^+(H_2O)$, H_3O^+, H^+	Long-term increases in ultra-pure water conductivity

The controversy surrounding either of these concepts is that ion resonance is based on free ions in vacuum, a far extreme from what would be seen in the aqueous

cellular milieu of biological systems. Ions are typically hydrated and would not achieve the motion predicted by resonance theory and would have substantial dampening effects due to the surrounding fluids and structures. While these theories indeed predict frequencies for maximum effects, the mechanism of the interactions of ELF-MF in biological systems remains highly debated.

ELF-MF Effects on Electron Transfer

The large body of work by Blank and Goodman has also studied mammalian systems using both electric and magnetic fields. In a recent review, the lack of a mechanism or principle that could be applied to all EMF studies was again discussed (Blank and Goodman, 2008). They propose that a number of the observed biological response to EMF could be explained by changes in transcription due to MF effects of electron transfer in DNA during transcription initiation (Blank and Goodman, 2004) or as a charge transfer-induced acceleration of the Na^+,K^+-ATPase and ion pumping (Blank, 2005).

A series of reports by Blank and colleagues have observed EMF frequency specific changes in the ATP-driven transmembrane protein Na^+,K^+-ATPase from mouse kidney extracts, a transmembrane protein used to selectively pump ions against their gradient across cell membrane in eukaryotic cells (Blank, 1992, 1995, 2005; Blank and Soo, 1993, 1996a, b, 1997, 2001b; Blank et al., 1995). They conclude from these studies that under normal activity, electric fields inhibit the protein transporter activity, while magnetic fields enhance transport, however both field types can be stimulatory when the enzyme activity is low (Blank, 2005). They propose that an electric or magnetic field can

modify electron distribution along the interior of these protein channels and shift the conformational state of the protein to an open or closed state (Blank, 2008). Na^+,K^+ATPase is a primary transporter involved with Ca^{2+}/H^+ and Na^+/H^+ antiporters to maintain ion homeostasis in eukaryotic cells (Nelson, 1994). As such, the disruption of the normal ion gradient could act as a "trigger" for a cascade of biological effects (Blank, 2008).

The second explanation is based on an induced stress response due to charge disruption in DNA (Blank, 2008; Blank and Goodman, 1997, 2002, 2008; Blank and Goodman, 2009). They propose that EMFs induce electron charge displacement of hydrogen ions in DNA chains, disaggregating DNA, and initiating transcription (Blank and Goodman, 2008). This can in turn stress the cell and induce a number of changes in cell processes (Blank and Goodman, 2009).

Dissertation Summary

The work presented in the following chapters sought to explore two alternative electromagnetic strategies to combat the unique properties of bacterial biofilms that contribute to their tolerance.

Direct current has been proposed to increase transport of antibiotics through the EPS matrix, increase bacterial uptake of antibiotics across the cell membrane, and generate stimulatory as well as potentially biocidal chemical changes within the system. While numerous theories have been proposed, the mechanism of the bioelectric effect remains unknown. The intent of this work was to explore DC treatment of biofilms at conditions more relevant to treatment *in vivo* by including a physiologically relevant

saline concentration. It was furthermore desired to determine mechanistic effects for DC efficacy under these conditions.

To our knowledge, extremely low-frequency magnetic field (ELF-MF) effects have not been studied on biofilms. Based on the large body of evidence for frequency-specific ELF-MFs affecting cell membrane and ion-related responses in eukaryotes, it was hypothesized that similar effects modifying membrane transport could be observed in bacteria. Additionally, MFs move through living tissue with little obstruction presenting ELF-MF application as an attractive noninvasive treatment strategy capable of penetrating both biofilm and biofilm on indwelling medical devices. The studies to date in planktonic bacteria have focused on possible mutagenic effects of anthropogenic EMFs. The majority of bacterial experiments in the weak ELF-MF range measured several heat-shock and stress response proteins, transfer of transposable elements between subpopulations, and cell growth and morphology in 50 or 60 Hz, 0.2-1.5 mT (2,000-15,000 mG) magnetic fields (bacterial EMF responses will be reviewed in Chapter 4). Reports of frequency-specific effects on *E. coli* DNA relaxation in much weaker fields (30 μT) may support a frequency-dependent mechanism (Alipov and Belyaev, 1996; Alipov et al., 1994; Belyaev and Alipov, 2001; Binhi et al., 2001). The focus of this study involved a transition of the concepts involving applied weak ELF-MF in mammalian systems to that of single-celled bacteria in biofilm. It was desired to study ELF-MF effects at magnetic field strengths lower than previously used with bacteria (<0.15 mT), on the same order as the geomagnetic magnitude, and additionally to investigate frequency-dependent effects using several ion cyclotron frequencies for

biologically relevant ions. If the resonance frequency tuning did impact ion transport or membrane processes, the implications of increasing or decreasing the influx of ions into a cell could modify gene expression, negatively impact growth due to the introduction of a undesirable ion or through disruption of chemical and charge gradients, or inversely, increase metabolism of these relatively slow growing bacteria thus increasing the susceptibility of biofilms to antibiotics (Zheng and Stewart, 2002) interfering with metabolic processes.

In both approaches, our experimental designs were based around a potential target application for the treatment of orthopedic device-related infections. As a model organism, coagulase-negative *Staphylococcus epidermidis* was selected, recently reported as the most prominent organism present in joint-prosthesis infections (Montanaro et al., 2011). Additionally results were complemented with study of *Pseudomonas aeruginosa* biofilms.

In Chapter 2, DC killing effects against *S. epidermidis* biofilms under physiologic saline conditions in conjunction with the antibiotic ciprofloxacin will be presented. *S. epidermidis* biofilm results include: (1) a dose-responsive DC killing effect, (2) a lack of synergy or any killing effect of ciprofloxacin with or without DC, (3) measurement of electrolytically generated chlorine species, (4) effective mimicking of DC dose response curves with chlorine dosing in the absence of current, and (5) little or no DC killing effect in chloride-free medium.

In Chapter 3, a global transcriptomic assessment of DC effect in *S. epidermidis* biofilms will be reported. A comparison of gene expression profiles for DC and chlorine

treated biofilms will be presented and results of a DC gene response that is (1) similar to the gene response to chlorine, (2) related to oxidative stress, and (3) indicative of a stressed cell state.

In Chapter 4, a global transcriptomic assessment of ELF-MF effects on *S. epidermidis* biofilms at Ca^{2+} and K^{+} ion resonance frequencies will be presented. Changes in gene expression in response to ELF-MF will be discussed that (1) are frequency-dependent, (2) field magnitude-dependent (and/or dependent on the ratio of time-varying and static magnetic field components), (3) include upregulation of genes involved in environmental sensing and signal transduction, substrate and ion transport, transposition activity , translation, and (5) also include downregulation of genes related to cell division and cell wall repair.

In Chapter 5, conclusions from these investigations and the potential for future study in these areas will be further discussed.

CHAPTER 2: DIRECT ELECTRIC CURRENT TREATMENT UNDER PHYSIOLOGIC SALINE CONDITIONS KILLS STAPHYLOCOCCUS EPIDERMIDIS BIOFILMS VIA ELECTROLYTIC GENERATION OF HYPOCHLOROUS ACID

Contribution of Authors and Co-Authors

Manuscript in Chapter 2

Author: Elizabeth L. Sandvik

Contributions: Collaborated to design the experimental setup, ran experiments, collected and analyzed data, wrote manuscript.

Co-Author: Bruce R. McLeod

Contributions: Collaborated on experimental design, provided discussion and feedback on results and manuscripts.

Co-Author: Albert E. Parker

Contributions: Provided statistical expertise during data analysis.

Co-Author: Philip S. Stewart

Contributions: Provided discussion and feedback on the experimental design, results and manuscript.

Manuscript Information Page

Elizabeth L. Sandvik, Bruce R. McLeod, Albert E. Parker, Philip S. Stewart
PLoS ONE
Status of Manuscript:
____ Prepared for submission to a peer-reviewed journal
____ Officially submitted to a peer-review journal
____ Accepted by a peer-reviewed journal
_X_ Published in a peer-reviewed journal

Published by PLOS
Submitted August 27, 2012
Accepted December 19, 2012
Published February 4, 2013
Volume 8, Issue 2: e55118

The manuscript that follows was published in PlosOne and describes a mechanistic analysis of DC killing efficacy in bacterial biofilms. Supplemental material of corrosion issues observed during electrode selection, data not shown in the text, and electrolyte assessment of medium components and alternate electrolytes can be found in Appendix A. Discussion of these parameters, and a detailed assessment of electrochemistry in the presence and absence of chloride, sulfate, nitrate, and phosphate, beyond what is found in the manuscript, can be found in Chapter 5.

Abstract

The purpose of this study was to investigate the mechanism by which a direct electrical current reduced the viability of *Staphylococcus epidermidis* biofilms in conjunction with ciprofloxacin at physiologic saline conditions meant to approximate those in an infected artificial joint. Biofilms grown in CDC biofilm reactors were exposed to current for 24 hours in $1/10^{th}$ strength tryptic soy broth containing 9 g/L total NaCl. Dose-dependent log reductions up to 6.7 $\log_{10}$CFU/cm^2 were observed with the application of direct current at all four levels (0.7 to 1.8 mA/cm^2) both in the presence and absence of ciprofloxacin. There were no significant differences in log reductions for wells with ciprofloxacin compared to those without at the same current levels. When current exposures were repeated without biofilm or organics in the medium, significant generation of free chlorine was measured. Free chlorine doses equivalent to the 24 hour endpoint concentration for each current level were shown to mimic killing achieved by current application. Current exposure (1.8 mA/cm^2) in medium lacking chloride and amended with sulfate, nitrate, or phosphate as alternative electrolytes produced diminished kills of 3, 2, and 0 log reduction, respectively. Direct current also killed *Pseudomonas aeruginosa* biofilms when NaCl was present. Together these results indicate that electrolysis reactions generating hypochlorous acid from chloride are likely a main contributor to the efficacy of direct current application. A physiologically relevant NaCl concentration is thus a critical parameter in experimental design if direct current is to be investigated for *in vivo* medical applications.

Introduction

The treatment of medical implant-associated infections is challenging. A 2004 article in *The New England Journal of Medicine* reported that of 600,000 joint prostheses implanted in the U.S. annually, approximately 12,000 will develop infections (Darouiche, 2004). The most common culprits of these infections are staphylococcal species (Ehrlich et al., 2004; König et al., 2001; Montanaro et al., 2011; Pavoni et al., 2004; Saginur et al., 2006; Zimmerli et al., 1998) constituting over 80% of infections associated with medical devices (Ehrlich et al., 2004; Montanaro et al., 2011). In a 2011 assessment of the most frequent pathogens in orthopedic infections, *Staphylococcus epidermidis* was identified as the most prevalent bacterial species in both knee and hip arthroprostheses infections, occurring in half of infections documented, followed by *Staphylococcus aureus* (around 20% of cases), and *Pseudomonas aeruginosa* (around 10% and 4% of cases, respectively) (Montanaro et al., 2011), supporting reports of coagulase-negative *Staphylococcus* as an increasingly recognized or emerging pathogen in medical device-related infections (Montanaro et al., 2011; von Eiff et al., 2002). These infections are particularly persistent when the bacteria produce a protective matrix and establish as biofilms (Vergidis and Patel, 2012), a bacterial mode of growth known to be significantly more tolerant to antimicrobial agents when compared to planktonic cultures of the same organism. While long-term antimicrobial therapy with multiple antibiotics can be effective in some cases (König et al., 2001; Pavoni et al., 2004; Zimmerli et al., 1998), treatment failure may require the removal and replacement of the device in a one or two stage surgical process accompanied with an extensive course of antibiotics (Pavoni et al.,

2004) and an estimated average cost of medical and surgical treatment of $30,000 (Darouiche, 2004). With these consequences, the development of novel strategies for treatment is desirable.

One proposed strategy is the use of direct current to enhance or replace existing antibiotic regimens. The reports of direct current effects vary. Direct current has been demonstrated to have killing efficacy against planktonic bacteria in static and flowing systems (Davis et al., 1982; Davis et al., 1992; Davis et al., 1989) with effects dependent on the electrode material and the medium composition. A 1992 paper used direct current in conjunction with industrial biocides to combat bacterial biofilms and reported current to enhance the activity of several agents (Blenkinsopp et al., 1992a). The study reported direct current alone to have little or no effect on the survival of *Pseudomonas aeruginosa* biofilms; however the combination of direct current and biocide was shown to significantly increase killing efficacy of Kathon, glutaraldeyhde, and quaternary ammonium compound. Subsequent investigations studied the use of electric current with antibiotics (Costerton et al., 1994; del Pozo et al., 2009b; Jass et al., 1995; Jass and Lappin-Scott, 1996; Khoury et al., 1992; McLeod et al., 1999; Stewart et al., 1999; Wattanakaroon and Stewart, 2000; Wellman et al., 1996). It was proposed that this synergistic phenomenon, termed the bioelectric effect, could be optimized to enhance antibiotic treatment of recalcitrant biofilm infections when antibiotic treatments were minimally effective. The synergy between antimicrobial and current, central to the bioelectric effect, was reproduced in some studies (Costerton et al., 1994; del Pozo et al., 2009b; Jass et al., 1995; Jass and Lappin-Scott, 1996; Khoury et al., 1992; Stewart et al.,

1999; Wellman et al., 1996), with some reporting conditions with a killing effect of current alone (Costerton et al., 1994; del Pozo et al., 2009b; Stewart et al., 1999; Wattanakaroon and Stewart, 2000), and others concluding current alone to have little or no effect (Blenkinsopp et al., 1992a; Costerton et al., 1994; Jass et al., 1995; Jass and Lappin-Scott, 1996; Khoury et al., 1992). Proposed mechanisms for the effect included electrophoretic enhanced transport of antimicrobials through the biofilm matrix (Blenkinsopp et al., 1992a; Costerton et al., 1994; Jass and Lappin-Scott, 1996; Khoury et al., 1992), electroporation enhanced uptake of antimicrobials (Blenkinsopp et al., 1992a; Costerton et al., 1994), production of gases such as oxygen that increase metabolic and antimicrobial activity (Jass et al., 1995; Stewart et al., 1999), and generation of electrolysis products including chlorine (Liu et al., 1997; Rabinovitch and Stewart, 2006), hydrogen peroxide (Liu et al., 1997), and those affecting pH (Rabinovitch and Stewart, 2006; Stoodley et al., 1997). In other studies, direct current is reported to affect bacterial adherence or stimulate detachment of biofilm to conducting surfaces (Hong et al., 2008; Poortinga et al., 2001b; Rabinovitch and Stewart, 2006; van der Borden et al., 2005; van der Borden et al., 2004b). When external electric fields have been applied with insulated electrodes (i.e. no current flow), enhanced bacterial killing by antibiotics (McLeod et al., 1999) or modification of bacterial adhesion (Poortinga et al., 2001a) has not been observed.

One notable feature of nearly all of the *in vitro* work on the bioelectric effect with antibiotics has been the omission of chloride from the media during electric current exposure (Blenkinsopp et al., 1992a; Costerton et al., 1994; Jass et al., 1995; Jass and

Lappin-Scott, 1996; Stewart et al., 1999; Stoodley et al., 1997; van der Borden et al., 2005; van der Borden et al., 2004b; Wellman et al., 1996). This has been done deliberately to preclude the electrolytic generation of chlorine. *In vivo*, however, chloride is abundant and this omission is not relevant. The purpose of the work reported in this article was to investigate the effect of direct electric current against a mature bacterial biofilm under conditions of physiologic saline and a dilute nutrient solution meant to approximate *in vivo* conditions such as those found in an artificial joint. As a model organism we chose *S. epidermidis* but we also present data for gram-negative *P. aeruginosa*. We first sought to determine whether electric current exposure by itself had an effect on bacterial biofilm in the presence of chloride and whether synergy between current and antibiotic could be observed in this milieu. Second, if electric current had an effect on biofilm in the presence of chloride, we sought to establish whether this effect could be attributed to electrolytic generation of hypochlorous acid.

Methods

Biofilm Growth

The CDC Biofilm Reactor (Biosurface Technologies Corp., Bozeman, MT, Model CBR90-1DS) is designed to grow repeatable biofilm on polycarbonate disks (called coupons) in a high shear environment. The reactor is a one-liter glass beaker with a side-arm discharge port at approximately 400 mL for effluent drainage by gravity. Eight polystyrene rods, each holding three 1.27 cm diameter polycarbonate coupons, are inserted through the lid, suspending the coupons in the bulk fluid of the reactor. A baffled magnetic stir bar in the center of the reactor provides mixing as well as uniform

fluid shear on each coupon. During continuous flow operation, a peristaltic pump is used to pump fresh medium into the reactor through an influent port in the lid. An in-line, glass flow break in the influent feed line prevents back-contamination of the feed carboy. A second port in the lid is attached to a bacterial air vent for gas exchange. A total of 24 coupons are available in the reactor for sampling.

Biofilms were grown on polycarbonate coupons in the CDC Biofilm Reactor using a standard growth protocol for each organism. The *S. epidermidis* growth protocol is analogous to the ASTM E2562-07 "Standard Test Method for Quantification of *Pseudomonas aeruginosa* Biofilm Grown with High Shear and Continuous Flow using CDC Biofilm Reactor" (ASTM E2562 - 07, 2007) but has been adapted for the main study organism, *S. epidermidis* RP62A (ATCC#35984): The sterilized reactor containing 450 mL of full strength (30 g/L) TSB (tryptic soy broth, Soybean-Casein Digest Medium, Difco) with the effluent tube clamped was inoculated from a frozen stock of *S. epidermidis*. The reactor was placed on a magnetic stir plate in a 37°C incubator and operated in batch with stirring at 125 rpm for 24 hours. After 24 hours, a continuous flow of sterile $1/10^{th}$ strength TSB was started with a reactor residence time of 30 minutes and overflow drainage to a waste carboy by gravity. Continuous flow ran for 16 hours at the end of which biofilm-coated coupons were ready for use in experimental protocols. It should be noted that the two faces of the coupon (facing inward towards the baffled stir bar versus outwards towards the glass) experience different amounts of shear stress which is a critical factor in biofilm growth. For all experiments the inward face of the coupon was defined as the sample surface. At the end of the growth protocol (just prior to

treatment) coupons had a mean LD of 8.46 $\log_{10}$(CFU/cm^2) with a repeatability SD of 0.34 $\log_{10}$(CFU/cm^2) over 25 experiments with 30% of error due to between experiment sources (sampling method follows).

P. aeruginosa ERC-1 (ATCC#70088) biofilms were also grown in the CDC reactor with a similar protocol. The medium concentrations, temperature, and timing were the same as those found in the standard method ASTM E2562-07 and differed from the *S. epidermidis* growth protocol as follows: Batch phase was operated for 24 hours with 1/100th strength (0.3 g/L) TSB at room temperature. Continuous flow was run for 24 hours with 1/300th strength (0.1 g/L) TSB at room temperature. At the end of the growth protocol (just prior to treatment) coupons had a mean LD of 8.08 $\log_{10}$(CFU/cm^2) with a repeatability SD of 0.25 $\log_{10}$(CFU/cm^2) over 28 experiments with 96% of error due to between experiment sources (sampling method follows).

Exposure to Direct Current and/or Antibiotic

The treatments were performed in small enclosed wells designed at the Center for Biofilm Engineering, described previously (McLeod et al., 1999). Inner dimensions were 7.1 cm long by 1.6 cm wide by 3.4 cm tall (Figure 2.1). Rubber sheeting lined the lid to prevent contamination. Twenty-four gauge platinum electrodes, 3.8 cm long, were pushed through the lid at opposite ends of the wells and extended 2.5 cm from the lid into the treatment well. The anode was connected to the positive terminal of the power supply and the cathode to the negative. A small strip of 3 mm thick rubber sheeting on the bottom of the well, 4.0 cm from the cathode, loosely held the coupons in place so that the positions of the three coupons were the same in all experiments. Each well had a

separate circuit with an inline ammeter and current controller (Wavelength Electronics, No. LDD200-1M) on a power supply that generated the direct current. The current controllers maintained a constant current level while voltage fluctuated slightly with changes in the resistive loads across each well.

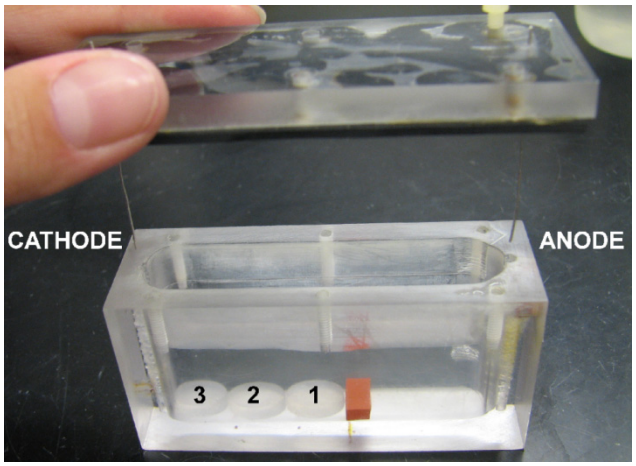

Figure 2.1 Polycarbonate treatment well. A piece of rubber sheeting on the bottom of the well held the biofilm-coated coupons at the same position (labeled 1-3) for each experiment. Platinum electrodes were inserted through the lid at opposite ends of the well and current was applied lengthwise. The anode was connected to the positive terminal of the power supply and the cathode to the negative.

After growth, biofilm-coated coupons were aseptically removed from the rods of the CDC reactor, dipped in 10 mL of sterile buffered dilution water (42.2 mg KH_2PO_4/L, 406.5 mg/L $MgCl_2 \cdot 6H_2O$/L in reagent-grade water) to remove planktonic cells and placed in sterile treatment wells with the inner face of the coupon (from the CDC reactor) facing up in the well. Twenty mL of a sterile treatment solution (with antibiotic when indicated) was gently added to each well. Direct current was applied across the length of the well.

Staphylococcus epidermidis treatments were performed for 24 hours at 37ºC. The treatment solution was 1/10th strength TSB with 9 g/L total NaCl (accounting for the salt

in TSB) with 2.5 μg/mL ciprofloxacin (Sigma-Aldrich) when indicated. This concentration of ciprofloxacin was approximately 40X the minimum inhibitory concentration (MIC) determined for an aerobic, planktonic culture of the bacteria (data not shown). Direct current levels of 2.0, 3.0, 4.0, and 5.0 mA were applied across the wells with an effective current density of 0.7, 1.1, 1.4, and 1.8 mA/cm^2, respectively (based on the minimum cross-sectional area of the liquid in the treatment well when coupons were present). Experiments were performed in parallel wells, with and without ciprofloxacin, at each current level. Control wells without current, with and without ciprofloxacin, were run with every experiment. When one current level was investigated, this resulted in four parallel wells corresponding to four treatment levels: (1) a control with no ciprofloxacin and with no current, (2) a well with ciprofloxacin but no current, (3) a well with current but no ciprofloxacin, and (4) a well with both ciprofloxacin and current. In some experiments two current levels were applied for a total of six parallel treatment wells. Three coupons were sampled from exposed wells when only one current level (four wells total) was studied. For experiments with two current levels (six wells total), only the two extreme coupons (positions 1 and 3) were sampled in each well. At least three independent experiments were performed at each current level (N=11 experiments total).

While *S. epidermidis* was the primary study organism, treatment of gram-negative bacteria with electric current was also investigated with varying NaCl concentrations. Treatment of *Pseudomonas aeruginosa* biofilms were performed for 20 hours at room temperature. The treatment solution was $1/300^{th}$ strength TSB (to match continuous flow

conditions from the growth reactor) with varying concentrations of NaCl from no added salt (0.017 g/L NaCl from the TSB) to 9 g/L total NaCl. Tobramycin was added when indicated at 10.0 μg/mL tobramycin sulfate (Sigma-Aldrich) to parallel previous bioelectric effect studies using the same concentration (Jass et al., 1995; Khoury et al., 1992) or half the concentration (5.0 μg/mL) (Costerton et al., 1994; Khoury et al., 1992; McLeod et al., 1999; Stewart et al., 1999; Wellman et al., 1996) of tobramycin against *P. aeruginosa.* The MIC data reported in those studies indicate 10.0 μg/mL tobramycin sulfate to be 10X the MIC for the *P. aeruginosa* strains studied (Costerton et al., 1994; Jass et al., 1995; Khoury et al., 1992; McLeod et al., 1999; Wellman et al., 1996). Three coupon spacing regimes were used: no spacers, grouped at the cathode (as in the *S. epidermidis* experiments), and an extreme spacing with coupons at the anode, middle, and cathode. For this reason, *P. aeruginosa* results are presented as mean LD for coupons (n=2 or 3 coupons per well) from a given treatment well. A total of N=14 experiments applied current with and without antibiotic and N=5 experiments applied current only, resulting in 34 wells with only current and 16 treatment wells with current and tobramycin. Applied current levels between 0.13 and 2.0 mA (0.05 to 0.71 mA/cm^2) were restricted by the salt concentration and the range of the current controllers.

Determination of Biofilm Viable Cell Numbers

At the end of the treatment, coupons were sampled and analyzed as described in ASTM E2562-07 (ASTM E2562 - 07, 2007) with slight modifications: Treated coupons were gently removed from the treatment well with a sterile hemostat and placed on a sterile surface for sampling. While holding the coupon with the hemostat, the top surface

of the coupon was scraped with a sterile wooden stick held perpendicular to the surface for 30 seconds. The stick was swirled in 9 mL of sterile buffered dilution water and then used to scrape the coupon a second and a third time. The coupon was scraped a total of three times for 30 seconds each in this same manner. After swirling the third time, the stick was discarded. The coupon was held over the dilution tube and the scraped surface was rinsed with 1mL of dilution water to remove any remaining biofilm resulting in a final volume of 10 mL in the dilution tube. The sample was homogenized at 10,000 rpm for one minute to disaggregate biofilm clumps, serially diluted and drop plated using the drop plate method (ten 0.01 mL drops per dilution) on agar. *S. epidermidis* samples were plated on tryptic soy agar (Difco) and *P. aeruginosa* samples were plated on R2A agar (Difco). The colony forming units (CFU) on the plates were counted following overnight incubation at 37°C. A biofilm log density (LD) of viable cells for each coupon was calculated using the mean CFUs counted over 10 drops, the volume of each drop, the surface area of the coupon, the volume of liquid the biofilm was scraped into (the zero dilution), and the dilution at which the colonies were counted:

$$LD = \log_{10}\left(\frac{CFU}{cm^2}\right) = \log_{10}\left(\left(\frac{\overline{CFU_{drop}}}{vol_{drop}}\right)\left(\frac{vol_{zerodilution}}{SA_{coupon}}\right)\left(10^{dilution}\right)\right) \qquad (2.1)$$

Log reductions (LR) of biofilm cell densities were calculated for each sample based on comparison of the treated sample to the mean of the no-current, no-antimicrobial control (1-3 controls per experiment) within the same experiment:

$$LR = \overline{LD_{control}} - LD \qquad (2.2)$$

We used a LR per sample, as opposed to a LR per experiment, in order to explicitly model the effect of the location in the well on the mean LR. Either definition of the LR generated the same mean LR, but the SEMs and degrees of freedom for the t-tests based on LRs per sample were larger.

Growth control coupons were sampled directly following the growth protocol each time the reactor was run and sampled in the same fashion. Growth coupons were aseptically removed from the reactor and the coupon holder, dipped in 10 mL of sterile dilution water to remove planktonic cells, and placed on a sterile sampling board. The scraping procedure at this point was the same as above.

Measurement of Chlorine Generated by Electric Current Exposure

Both biofilm and medium organics can be sources of chlorine demand, which react quickly with available chlorine in the system thereby lowering measurable free chlorine. Consequently, to determine if free chlorine species were generated during the course of electric current exposure, the experiments were repeated without biofilm and without the organics in the medium. The same current levels used in the *S. epidermidis* experiments were applied to 20 mL of a 9 g/L NaCl, 0.25 g/L K_2HPO_4 solution equivalent to the salt and buffer concentrations present in the treatment solution. After 24 hours of application, the current was turned off, the lid was gently removed, and liquid samples (0.1 mL each) were pipetted simultaneously at each electrode. Samples were measured by the DPD chlorine method using HACH DPD Free Chlorine Reagent (5mL Powder Pillows) read on a spectrophotometer at 530 nm. Samples were diluted in

reagent-grade water to be within the manufacturer's range of the reagents. These chlorine concentrations, referred to as "endpoint free chlorine measurements", were assumed to represent the cumulative amount of reactive chlorine species generated over the 24 hour treatment time.

Measurement of pH Following Electric Current Exposure

For an estimate of pH changes, the *S. epidermidis* biofilm experiments were repeated without biofilm. The same current levels were applied to 20 mL of the standard treatment solution (3 g/L TSB, 9 g/L total NaCl) at 37°C for 24 hours. For each well, the current was turned off and the pH was immediately measured with a pH meter at each electrode. In a cruder method, pH strips (EMD colorpHast, 0-14 pH range) were spaced at 1 cm spacing and simultaneously dipped into the treatment well while the current was running.

Chlorine Dosing Experiments to Mimic Electric Current Exposure

In another variation, free chlorine concentrations equivalent to the 24 hour "endpoint free chlorine measurements" for each current level were used to treat *S. epidermidis* biofilms in place of the electric current. For each current level, the previously measured free chlorine concentrations were grouped for both electrodes and averaged. Four free chlorine solutions (corresponding to the four current levels) were made with bleach and sterile laboratory-grade water. Sterile water (no added bleach) was used for the control. Due to the rapid nature of chlorine reactions, the nutrients were added to the chlorine solutions just prior to application to the biofilm as follows. Each

free chlorine solution was adjusted to 105% of the target free chlorine concentration. A 20X sterile medium solution was made such that the resulting 1X concentration would be the standard 3 g/L TSB with 9 g/L total NaCl. *S. epidermidis* biofilms were grown in the CDC reactor and transferred to the treatment wells as before. At time zero, 1 mL of the 20X medium solution was added to 19 mL of the given free chlorine solution in a sterile glass vial, swirled, and gently added to the treatment well containing the biofilm-coated coupons. This was done for all five wells. Wells were then treated like the biofilms exposed to current with a 24 hour incubation at 37°C after which biofilms were sampled as usual. No antibiotic was used in this experiment.

Exposure of Biofilm to
Electric Current with Alternate
Electrolytes (Omitting Chloride)

In this variation, the electric current was applied to *S. epidermidis* biofilms in treatment solutions without chloride. An electrolyte was still needed for current flow so in place of the 0.154 M Cl^- (9 g/L NaCl) in the standard treatment solution, 0.154 M SO_4^{2-} (as 21.9 g/L Na_2SO_4), 0.154 M NO_3^- (as 13.1 g/L $NaNO_3$), or 0.154 M PO_4^{3-}(as 10.7 g/L Na_2HPO_4 and 9.2 g/L NaH_2PO_4 accounting for K_2HPO_4 contributions already in the medium) was used with the other components of TSB added individually (at $1/10^{th}$ strength: 1.7 g/L pancreatic digest of casein (BD Bacto Tryptone), 0.3 g/L enzymatic digest of soybean meal (BD Difco Soytone Peptone), 0.25 g/L dextrose, and 0.25 g/L K_2HPO_4). For each alternate electrolyte, applications of 0, 2.0, and 5.0 mA (0, 0.7, and 1.8 mA/cm^2 respectively) were performed in parallel and all three coupons in the wells were sampled. Other than substitution of the treatment solutions, the growth, treatment,

and sampling protocols were the same as the previous *S. epidermidis* experiments with current application. No antibiotic was present in these experiments.

Staining and Microscopy of
Detached Cells and Biofilm

Three wells containing *S. epidermidis* biofilms were treated with 3.0 mA (1.1 mA/cm^2) of direct current for 24 hours with parallel triplicate control wells without current (as described above). Bulk fluid and biofilm samples were stained using the LIVE/DEAD BacLight Bacterial Viability Kit (Molecular Probes) as well as sampled for viability on TSA. The staining kit contains green-fluorescent SYTO 9 and red-fluorescent propidium iodide to distinguish between cells with intact membranes ("live") and cells with damaged membranes ("dead"), respectively. One mL samples of the undiluted bulk fluid and a 1:10 dilution of the bulk fluid (in sterile PBS) were removed from each well and incubated at room temperature with 3 μL of a 1:1 solution of Component A (SYTO 9) and Component B (propidium iodide) in the dark for 15 minutes. Each stained sample was filtered onto a black polycarbonate membrane (GE Water & Process Technologies, 0.22 μm pore size, 25 mm diameter). The membrane was transferred to a glass microscope slide, a drop of Type FF immersion oil (Cargille) was applied to the filter and a cover slip applied. The samples were visualized with a Nikon Eclipse E800 epifluorescence microscope (100X oil objective, 1.40 NA) with a standard FITC filter (ex: 480/30, DM: 505 LP, em: 535/40) for visualizing green SYTO 9 fluorescence and a standard TRITC filter (ex: 540/25, DM: 565 LP, em: 605/55) for viewing red propidium iodide fluorescence. Paired green and red images were taken at

twenty random views (16,389 μm^2) for each sample using MetaVue software (Universal Imaging Corporation). The area of cell coverage was measured on each digital image using MetaMorph software (Universal Imaging Corporation). A calibration of the measured cell area versus manual cell counts of the digital image was done for 50 clusters ranging in size from 1-32 cells. The calibrated mean area per cell was used to convert the measured area to cell counts for each image resulting in cell counts of "live" and "dead" cells for n=20 views for each bulk fluid sample. To complement these measurements, the bulk fluid was also sampled, serially diluted, and plated on TSA for viable cell counts.

Biofilm samples from the same treatment wells were removed, stained on the coupon with LIVE/DEAD solution at a ratio of 3 μL of the 1:1 SYTO 9 and propidium iodide solution to 1 mL of filter sterilized PBS, and incubated at room temperature in the dark for 30 minutes. Following incubation, the stain was pipetted from the side of the coupon and the sample was gently rinsed with filter sterilized PBS to remove excess stain. The stained samples were then imaged with confocal microscopy or embedded for cryosectioning. Confocal images of the biofilm were taken fully hydrated in a petri plate using a Leica TCS SP5 Confocal (25XW LWD, 0.95 NA). SYTO 9 and propidium iodide fluorescence was excited using 488 nm and 561 nm lasers with detector slits set to 499-551 nm and 579-647 nm, respectively. Images were processed using Imaris software (Bitplane). For cryosectioning, stained coupon samples were cryoembedded in O.C.T. Compound tissue embedding medium (Tissue-Tek) on dry ice as previously described [26]. Five μm thick slices of the embedded samples were cut in a Leica CM1850 cryostat

at -20°C and placed on poly-L-lysine coated microscope slides (SuperFrost Plus, FisherBrand). A coverslip was placed over the dry cryosection samples, a drop of water placed on top of the cover slip and the cryosections were imaged using a 60XWI objective (1.20 NA) with the Nikon E800 epifluoresence microscope and filters described above. Green and red images of the cryosections were color combined using MetaMorph software (Universal Imaging Corporation).

Statistical Methods

Statistical analyses were performed using linear mixed effects (lme) models in the nonlinear mixed effects (nlme) package (Pinheiro et al., 2011) in the free statistical and graphing program R (R Development Core Team, 2010). The lme models accounted for electric current density, position in the well, and salt concentration (*P. aeruginosa* experiments only) as covariates. Antimicrobial treatment, treatment source (electric current versus mimicked electric current for chlorine dosing experiments), and electrolyte were categorical variables. Experiment was a random factor in all models. As unequal variances existed between the no-current controls and current-exposed data (as expected), statistical analyses were performed on LR data sets (compared to the no-current, no-antibiotic control) that were truncated to exclude the controls with antibiotic but no current. The following model selection process was used to determine the most appropriate model for the data. Initially, all two-way interactions amongst the factors were included in the lme model. Interactions were investigated by significance tests and interaction plots. Insignificant and unimportant interactions were dropped.

The following models resulted from the selection process. To assess *S. epidermidis* killing effects of direct current in the presence and absence of ciprofloxacin, LRs for each sample were evaluated as a function of antibiotic presence/absence, current density, and position in the well with an interaction between antibiotic and current density. Differential killing across the well was analyzed using a subset of the data as the LR difference between the extreme coupons (coupons 1 and 3) from the same well as a function of current density and antibiotic presence/absence with an interaction term between the two variables. To assess killing of *S. epidermidis* with chlorine doses, LRs for each sample in the chlorine dosing experiment were analyzed as a function of mimicked current density. The chlorine dosing experiment (N=1) was compared to the no antimicrobial, current exposed experiments (N=11) as mean LRs across each well as a function of applied (or mimicked) current density and treatment type (direct current or chlorine dose) with an interaction term between current density and treatment type. Current exposure with alternate electrolytes was analyzed in one model using the nitrate, sulfate, and phosphate data as well as the 2.0 and 5.0 mA data when chloride served as the electrolyte. LR (in comparison to the no-current control of the same electrolyte) was analyzed as a function of current density, electrolyte, and position with an interaction term between current density and electrolyte.

Free chlorine generation was analyzed at each electrode as the free chlorine concentration as a function of current density. Gradients of chlorine across the well were analyzed as the difference in free chlorine concentration between electrodes in the same well (simultaneous samples) as a function of current density.

For *P. aeruginosa* experiments, the following *lme* models were used. To assess the effect of salt on growth, LDs of the no-current controls with and without tobramycin were analyzed separately as a function of salt concentration, and jointly as LDs as a function of antibiotic presence/absence and salt concentration with an interaction term between the two variables. As several spacing regimes were used in the *P. aeruginosa* experiments during electric current treatment, mean LRs across each current-treated well were used as the response. Data from biofilms exposed to current without antibiotic was used to examine current effects at different salt levels. Mean LRs over individual treatment wells were assessed as a function of salt concentration and current density as covariates with an interaction term between the two variables. Tobramycin effects with current at varying salt concentrations were assessed only for experiments with parallel wells with and without antibiotic. Mean LR's were analyzed as a function of current density, salt concentration, and antibiotic presence/absence. Initially all two way interactions were in the model but nonsignificant interactions between antibiotic and current (p-value=0.32) and antibiotic and salt (p-value=0.52) were removed from the model resulting in one interaction term between current and salt for the tobramycin experiments.

The repeatability standard deviation (SD) for lme models was calculated from the R output of within-experiment variance, σ_{within}^2, and between-experiment variance, $\sigma_{between}^2$:

$$repeatabilitySD = \sqrt{\sigma_{within}^{\ 2} + \sigma_{between}^{\ 2}} \tag{2.3}$$

The percent contributions of each source of variance were calculated as the variance for that source divided by the square of the repeatability SD. To maintain a familywise false discovery rate of 5%, the Benjamini-Hochberg procedure was implemented (Benjamini and Hochberg, 1995). Thus, hypothesis tests with individual p-values<0.0186 were considered statistically significant.

Results

Electric Current Alone

Killed *S. epidermidis* Biofilms

Significant reductions of *S. epidermidis* biofilms were observed when direct current was applied for 24 hours at 37ºC at all four current levels (0.7, 1.1, 1.4, and 1.8 mA/cm^2), both in the presence and absence of ciprofloxacin (Figure 2.2A andB). Data are plotted as individual data points for each coupon sampled. Larger reductions in biofilm viable cell density were observed at higher current levels with mean LRs up to 6.68 $\log_{10}(CFU/cm^2)$ at the highest current level (1.8 mA/cm^2) with ciprofloxacin (p-value<0.0001). The repeatability SD of LR on coupons exposed to current was 1.71 $\log_{10}(CFU/cm^2)$ with 24% of variance due to between experiment sources. Statistical analyses were performed based on LR as a function of current level, position, and the presence/absence of antibiotic. A significant linear relationship of increasing LR with increasing current level was observed for wells without antibiotic (p-value=0.0001) as well as those with ciprofloxacin (p-value=0.004) demonstrating a dose-responsive effect due to current alone.

Combining Antibiotic with
Electric Current did not Increase
Killing of *S. epidermidis* Biofilms

As killing was observed both in the presence and absence of ciprofloxacin, the linear relationships of LR and current level were compared to investigate the role of the antibiotic. No statistically significant difference in killing were observed when 2.5 μg/mL ciprofloxacin was present during direct current exposure (p-value=0.75). The

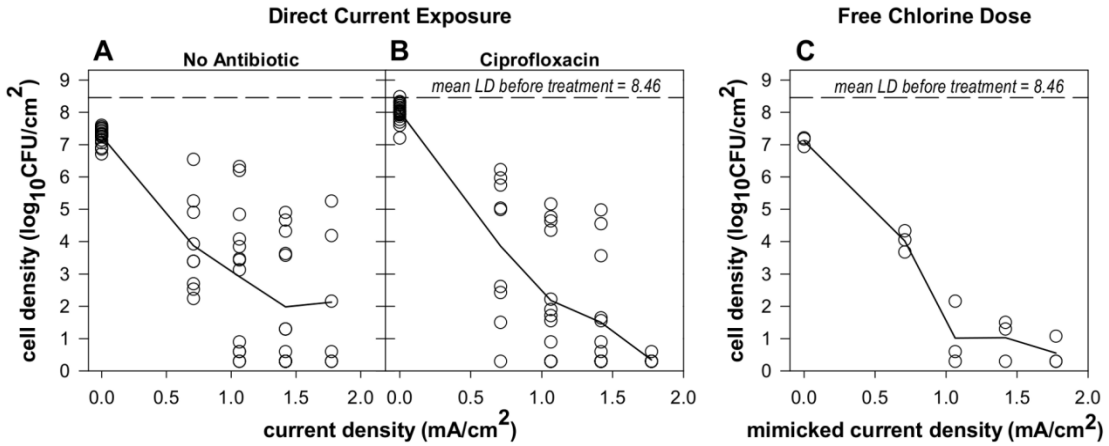

Figure 2.2 Treatment of *S. epidermidis* biofilm with electric current or a mimicked current exposure using chlorine. Direct current was applied in parallel to wells (A) with no antibiotic and (B) with 2.5 μg/mL ciprofloxacin at one or two current levels for N=11 experiments. (C) An initial dose of free chlorine corresponding to each current level was used to mimic the direct current exposure in the absence of current for N=1 experiment (no antibiotic). All wells contained 3 g/L TSB and 9 g/L total NaCl and treatments lasted 24 hours. Each data point denotes the LD for an individual coupon and lines show connected mean LDs for each current level.

interaction between current and antibiotic was not significant (p-value=0.33) indicating that the presence of 2.5 μg/mL ciprofloxacin additionally did not affect the rate of the dose-responsive killing with current level. As the bioelectric effect is discussed as a synergistic increase in killing efficacy when antibiotics are used in conjunction with

electric current, an interaction between antibiotic and current would be observed if this type of synergy was present. In these experiments, no statistically significant synergistic or additive responses were observed when 2.5 μg/mL ciprofloxacin was present during direct current exposure.

S. epidermidis Biofilms Closer to the Cathode Experienced Greater Killing than those More Distant

An unexpected but significant observation was the relationship between log reductions and the position of the sample in the treatment well during current exposure (p-value=0.0005). To determine if a definitive killing trend existed across the treatment wells, the difference in LR for the coupon at the cathode (coupon 3) with respect to the coupon near the center of the well (coupon 1) from the same current exposed well was examined for the *S. epidermidis* experiments (Figure 2.3). Non-zero differences would indicate differential killing due to position. Five of the thirty-nine wells exposed to current had total kill (below detection limit) on both coupons and thus had a position difference of zero. In 28 of the 34 remaining experiments, larger reductions in bacterial density were observed at coupon 3 compared to coupon 1 as indicated by a positive LR difference. These LR differences between the extreme coupons did not change significantly with current level (p-value=0.71) or the presence or absence of ciprofloxacin (p-value=0.13) but the pooled difference across all wells was significantly positive on the average (p-value=0.0003). These data thus indicate a trend of increased killing at the cathode (coupon 3) compared to samples in the center of the well when direct current is

applied. When no current was applied (control samples), position did not have a statistically significant effect.

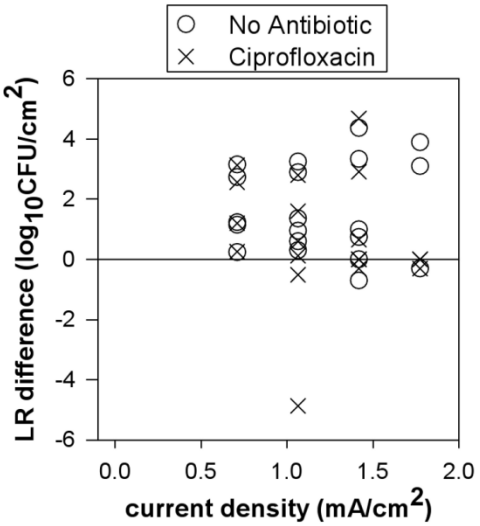

Figure 2.3 Increased killing of *S. epidermidis* biofilm adjacent to the cathode. Within each well, a trend of larger reductions at coupon 3 (adjacent to the cathode) compared to coupon 1 (near the center of the well) was observed following electric current treatment, as indicated by positive values. Each symbol denotes the measurement of the difference in LR between the extreme coupon positions (coupon 3 minus coupon 1) in a current-exposed well.

Electric Current Resulted in
the Generation of Free Chlorine

Due to the chloride in the medium, chlorine generated from electrolysis was suspected as a possible etiologic agent for observed reductions in biofilm density. During electric current exposure, free chlorine would be generated continuously but the available chlorine would react quickly with biofilm and the organics in the medium and was not measurable when those sources of chlorine demand were present. Therefore, the direct current exposures were repeated without the sources of chlorine demand (biofilm and organics) and sampled for chlorine at 24 hours. These measurements are referred to as

"endpoint free chlorine concentrations" and approximate the cumulative chlorine generated over the course of treatment without reaction. Significant concentrations of free chlorine were generated at all four current levels over 24 hours (Figure 2.4A). Concentrations ranged from 400-680 ppm free chlorine at the lowest current level (0.7 mA/cm^2) to 930-1400 ppm free chlorine at the highest current level (1.8 mA/cm^2). A strong linear relationship was observed with increasing free chlorine with increasing current levels (p-value<0.0001 for anode samples as well as cathode samples). A significant gradient of free chlorine was also observed across the well (Figure 2.4B). On average, free chlorine concentrations were higher at the cathode compared to the anode within the same well (p-value=0.012). Any changes in the magnitude of the chlorine difference with increasing current levels were not significant at the comparison value (p-value=0.038). When these same experiments were performed with the organics in the solution, free chlorine was undetectable at 24 hours. It is important to note that these chlorine concentrations are cumulative and would be nowhere near as high at any given time during electric current treatment when biofilm and organic sources of chlorine demand are present.

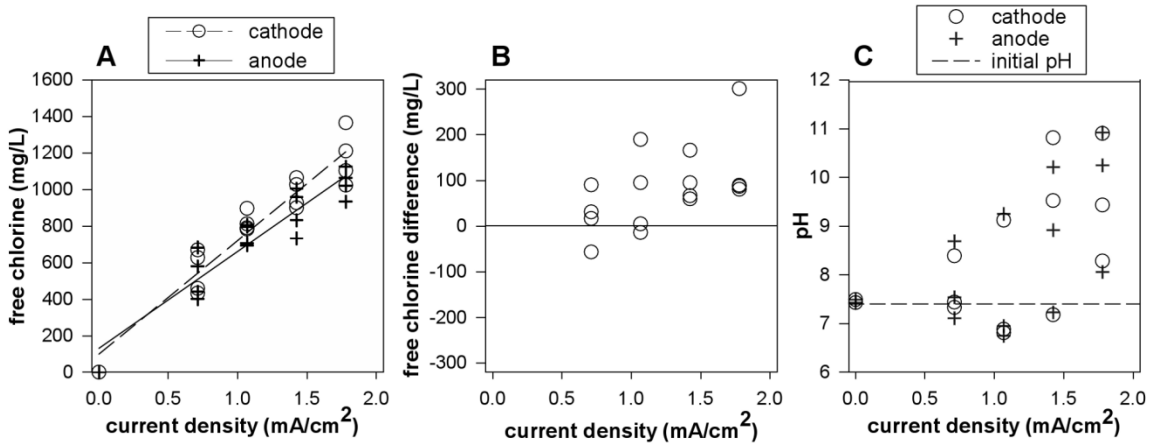

Figure 2.4 Chlorine generation and pH changes with electric current in the absence of biofilm. (A) Free chlorine was measured at each electrode after 24 hours of current when the direct current exposures were repeated without sources of chlorine demand (biofilm and organics in the medium). These "endpoint free chlorine concentrations" approximate the cumulative chlorine generated over the course of treatment without reaction. (B) The free chlorine differences between electrodes (cathode minus anode) in each well indicated a trend of higher free chlorine concentrations at the cathode as indicated by positive values. (C) pH measurements were taken at each electrode after direct current was applied for 24 hours to the standard treatment solution (with organics). Symbols indicate individual measurements and lines (A) show linear mixed effects models.

Electric Current Resulted in pH Changes

pH measurements were taken after 24 hours of direct current application to the treatment solution (3 g/L TSB, 9 g/L total NaCl, no biofilm) to investigate an overall change in pH as well as pH gradients across the well. After 24 hours, the current was turned off and measurements were immediately taken at each electrode with a pH meter (Figure 2.4C). Slight increases in pH were generally observed after current was applied, however the increases were not statistically significant when compared to the initial pH (p-values=0.059 and 0.062 for measurements at the anode and cathode, respectively). Comparisons of these measurements within each well were inconsistent with respect to pH being higher at one electrode over the other and no statistically significant difference

was observed that would indicate a pH gradient across the wells (p-value=0.97). However, to validate these observations, pH measurements were taken with pH strips while the current was running. At five minutes, pH gradients around 3 at the anode and 9 at the cathode were observed at the four current levels studied with values between 6 and 7 at the center of the wells (Figure A.3). Any pH gradient across the well would be expected to rapidly dissipate when current was stopped due to diffusive and convective mixing. These observations indicate a large pH gradient across the wells when the current is running, but no net change in the pH of the solution.

Free Chlorine Addition in the Absence of Electric Current Mimicked Biofilm Killing by Current

To investigate the contribution of chlorine generation to direct current effects, the following experiment was performed to determine if a free chlorine dose, representative of the concentrations measured when sources of chlorine demand were absent, could be used to mimic direct current exposure. For each current level, the mean endpoint free chlorine concentrations for both electrodes (Figure 2.4A) were used to determine the treatment concentration of free chlorine to mimic the direct current effect. The averaged concentrations were 0, 560, 730, 920, and 1,120 ppm free chlorine for 0, 0.7, 1.1, 1.4, and 1.8 mA/cm^2, respectively. Because the nutrients present a very large source of chlorine demand, chlorine solutions were made in water and the nutrients were added immediately preceding application of the chlorine-nutrient solution to the biofilm samples for a 24 hour exposure. This approach accounted for simultaneous chlorine reactions with the biofilm and the organic medium components. Significant reductions in cell density were

observed with chlorine doses at all levels (Figure 2.2C). The reductions followed a dose-responsive pattern with a linear trend of increasing LR with increasing mimicked current level (i.e. chlorine dose, p-value=0.003). When the mimicked current with chlorine dosing (*N*=1 experiment) was compared to direct current exposure (*N*=11 experiments, Figure 2.2A) as a function of current density (or mimicked current density), no statistically significant difference was observed between treatment with current versus mimicked current with the chlorine dosing (p-value=0.98), nor was there a significant difference in the LR trend over current (p-value=0.76). While dose-responsive biofilm reductions with increasing chlorine doses would be expected, the specificity of the applied dose to each current level to generate similar reductions demonstrates more than a partial contribution to efficacy. These results indicate that chlorine generation plays a predominate role in direct current effects in this system but additionally do so in a dose-responsive manner that is based on the current level applied and subsequent amount of free chlorine produced.

Electrolytes Other than Chloride Produced Less Biofilm Killing by Electric Current

Indications of the importance of chlorine generation in direct current efficacy led us to question if electric current effects would be observed without chloride in the system. In the next variation, current was applied to *S. epidermidis* biofilms in the absence of chloride using alternate electrolytes in the treatment solution (Figure 2.5). Sodium chloride is not only an electrolyte but also a parameter affecting growth of *S. epidermidis* and thus an ideal electrolyte was difficult to determine. As other halide salts

would generate similar biocidal products, nitrate, sulfate, and phosphate were used as electrolytes in these experiments. Growth curves of planktonic cultures in the three alternative electrolytes solutions versus the chloride containing solution were similar during exponential phase but final log densities were half to one log order lower than those with chloride (data not shown). Thus, for these experiments, biofilms were grown in the CDC reactor using the standard growth protocol (with chloride) and the application of the alternative electrolyte solutions (and subsequent removal of chloride) only occurred during current application. Controls without current were run in parallel to account for any effects of the alternative electrolyte on biofilm growth or survival over the treatment time. The lowest and highest current levels from the chloride experiments were applied to each solution for 24 hours (Figure 2.5). Reductions in biofilm were observed with direct current application when sulfate or nitrate served as the electrolyte with a statistically significant dose response of LR with current level for sulfate (p-value=0.013) but not for nitrate (p-value=0.066). Reductions were larger for electric current exposure with sulfate as the electrolyte (a 3-log mean reduction at the highest current density) compared to nitrate (a 2-log mean reduction at the highest current density), however, neither showed as strong of an effect as the 5-log reduction seen at the highest current level when direct current was applied with chloride present. In contrast, when phosphate was used as the electrolyte, the application of electric current at the same current levels had no effect on biofilm viability (p-value=0.58).

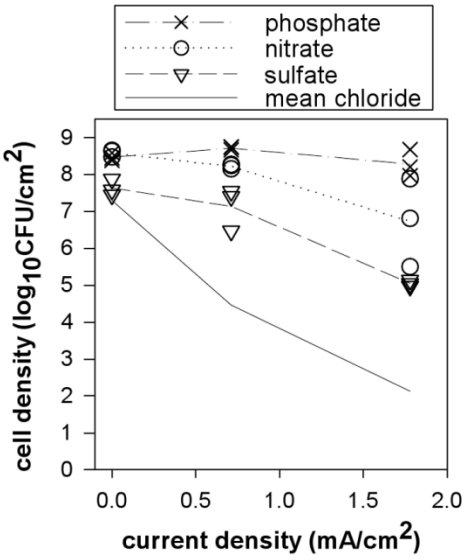

Figure 2.5 Treatment of *S. epidermidis* biofilm with electric current using various electrolytes. Direct current was applied to biofilms for 24 hours. The treatment solutions had all of the components of TSB except NaCl. Chloride was replaced with nitrate, phosphate, or sulfate at the same molarity (0.154 M) used for chloride experiments. The mean chloride results for 2 and 5mA are shown for comparison (full data set in Figure 2.2A). Each symbol indicates the LD for an individual coupon and lines show the connected means for each current level.

Observation of a Paradoxical
Increase in *S. epidermidis* Biofilm
Cell Numbers with Antibiotic Treatment

Control treatment wells (one without antibiotic, one with ciprofloxacin) were run in parallel with every experiment and received no current for the duration of the 24 hour treatment. The mean LD for no-current controls without antibiotic was 7.24 $\log_{10}$(CFU/cm^2) with a repeatability SD of 0.27 $\log_{10}$(CFU/cm^2) with variance mainly due to between experiment sources (85%). The mean LD for no-current controls with ciprofloxacin was 8.00 $\log_{10}$(CFU/cm^2) with a repeatability SD of 0.28 $\log_{10}$(CFU/cm^2) with variance mainly due to between experiment sources (83%). The LR due to ciprofloxacin in the no-current controls was statistically significant ($p<0.001$). We are

95% confident that the *increase* in log density when ciprofloxacin is present is between 0.66 and 0.89 $\log_{10}(CFU/cm^2)$. While this seems contradictory to the action of an antibiotic, in this system it can be explained by differential detachment of cells from the coupon surface over the course of the 24 hour treatment. The mean LD on coupons at the start of the 24 hour treatment was 8.46 $\log_{10}(CFU/cm^2)$ so LDs decrease over the course of treatment in both control types. We hypothesize that in the presence of ciprofloxacin, more cells remained attached to the coupon surface versus detaching into the harsher environment of the bulk fluid containing the antibiotic. In contrast, detachment may have been less inhibited in the absence of antibiotic. This observation is supported by the fact that control wells with no current and no antibiotic were typically turbid after treatment while the corresponding no-current wells with ciprofloxacin were not. The absence of any killing efficacy of the antibiotic against biofilm bacteria shows that this model system captures the remarkable tolerance of biofilm towards antibiotics.

Cell Detachment was Observed in
Control and Electric Current Treated Samples

Biofilm detachment was assessed with viable cell counts on TSA and LIVE/DEAD staining of the bulk fluid and biofilm following exposure to 3.0 mA (1.1 mA/cm^2) of direct current for 24 hours. The LIVE/DEAD BacLight kit uses two stains to distinguish between cells with intact membranes (green “live” cells) and cells with damaged membranes (red “dead” cells). While membrane integrity is an important parameter in cell viability, green staining of cells is not a strict parameter for live cells nor does red staining strictly indicate non-viability, thus plate counts and staining are

complementary methods. Viable cells in the bulk fluid where considerably higher in the no-current control wells with a mean LD +/- SD of 8.01 +/- 0.09 $\log_{10}$(CFU/mL) compared to 1.15 +/- 0.78 $\log_{10}$(CFU/mL) viable cells in the bulk fluid of the current exposed wells. Total cell counts of filtered bulk fluid samples were calculated from the combined number of stained cells ("live" and "dead") via microscopy. Detached total cells in the bulk fluid after 24 hours of treatment were 1-log higher in control wells with mean log total cell counts +/- SD of 8.72 +/- 0.01 $\log_{10}$(cells/mL) in control wells and 7.67 +/- 0.45 $\log_{10}$(cells/mL) in the current exposed wells; however the ratios of green "live" or red "dead" cells to total cells in the images showed 92% "live" cells in the bulk fluid of control wells (8.68 +/- 0.03 $\log_{10}$("live" cells/mL)) compared to only 2% "live" cells of the total detached cells in the wells exposed to 3.0 mA direct current (5.40 +/- 1.12 $\log_{10}$("live" cells/mL)).

LIVE/DEAD stained biofilm samples from the same treatment wells were imaged with confocal microscopy and cryosectioning. The topography of the unexposed control biofilms was very heterogeneous with many columns, towers, and streamers characteristic of a mature biofilm (Figure 2.6A and D). The majority of distinguishable cells stained green although intermittent distinct red cells were found with searching in both the confocal and cryosectioned images. Broader red staining was also observed on the surface of tower structures.

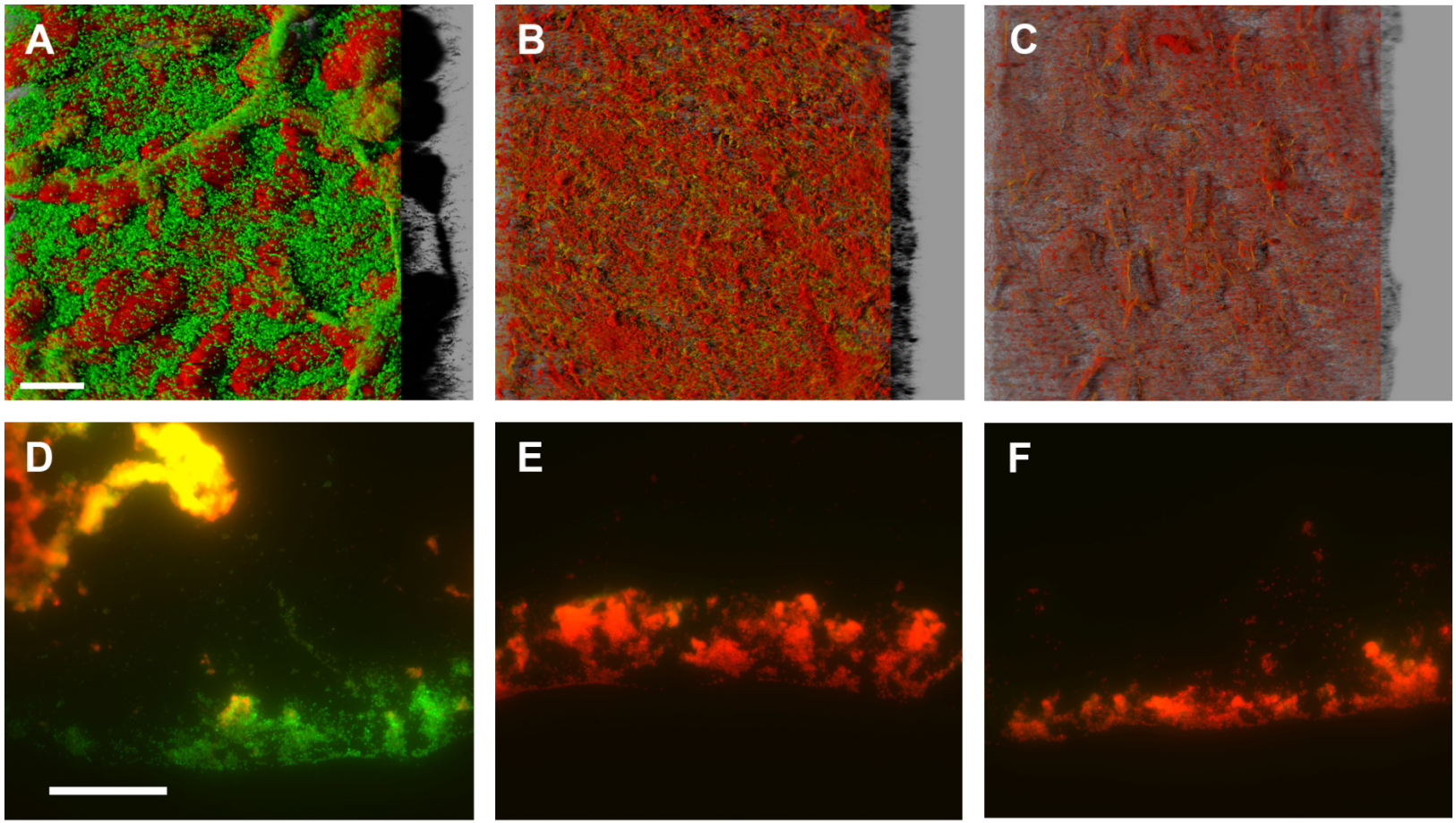

Figure 2.6 Images of *S. epidermidis* biofilm after 24 hours of no current and 3 mA direct current exposure. Biofilms are stained with LIVE/DEAD BacLight stains. Green color indicates cells with intact membranes ("live" cells) while red color indicates cells with damaged membranes ("dead" cells). (A) Confocal and (D) cryosection images of the control biofilm. Confocal and cryosection images of biofilm exposed to 3 mA of current are shown for position 1 (B and E) and position 3 (C and F) from the same treatment well. The scale bar for confocal images is 100 μm. The scale bar for cryosection images is 50 μm.

In contrast, electric current treated biofilms were thinner and flatter with the majority of distinguishable cells staining red, indicating damaged cells, for biofilm samples at the center of the well at position 1 (Figure 2.6B and E) as well as adjacent to the cathode at position 3 (Figure 2.6C and F). Some broad red staining and sparse green staining was observed in areas of clustered red cells and seemed to be associated with loose matrix material as distinct green cells were not observed. Biofilm samples from position 1 in the center of the well were visually observed to be slightly denser than those at the cathode with more observations of dim green with red cell clusters. Biofilm samples from position 3 near the cathode showed mainly red cells that ranged from dense clusters of red cells to areas of sparse biofilm only several cells thick. This reduced topography is pronounced considering all biofilm samples (control and treated) came from the same growth reactor and at time zero were mature biofilms resembling the control biofilm.

These biofilm and bulk fluid measurements can be used to assess the components of observed biofilm reductions due to detachment versus killing. Detached cells were found in the bulk fluid of the treatment wells, however more viable cells, total cells ("live" and "dead"), and "live" cells were observed in control wells compared to the wells with electric current indicating that, while biofilm detachment occurs, it is not a treatment specific event. "Dead" stained biofilm was observed still attached to the surface of coupons following electric current exposure although it was reduced in thickness and visually seemed to have decreased total cell density per volume biofilm. During the dose-response experiments described previously, electric current treated biofilms were observed to be looser than controls when sampling for viability. These

observations may indicate detachment mechanism and thus an assessment of the LR components (killing versus detachment) should be considered. Due to the heterogeneity of thickness and density of the biofilm samples, quantitative estimates of LR based on biofilm structure in the microscope images would be very difficult but the following hypothetical scenarios may aid in interpretation. If a homogeneous slab biofilm is assumed and the effect of electric current exposure is proposed to only cause biofilm detachment (i.e. no effects on viability), a 2/3 reduction in biofilm thickness would only represent a 0.5 LR of biofilm. If, in addition, the treatment was hypothesized to affect matrix structure such that the number of cells per volume in the remaining slab biofilm was reduced, for example, to 25% of the cells per biofilm volume in the untreated control, the combined decrease in thickness and density would only represent a 1.1 LR. While these values are hypothetical, the detachment and thinning scenarios cannot completely explain the 4.34 $\log_{10}(CFU/cm^2)$ mean LR observed at 3.0 mA (1.1 mA/cm^2) with no antibiotic (Figure 2.2A), indicating a large effect due to killing. Together, these results suggest that electric current exposure prevented the growth of and killed biofilm and planktonic phase bacteria. While some detachment occurred during electric current treatment and was observed to impact biofilm structure, the predominant effect on the biofilm was loss of viability.

Electric Current has a Killing Effect
on *Pseudomonas aeruginosa* Biofilms.

A dose-responsive killing effect of current was observed against gram-negative *P. aeruginosa* biofilms over a twenty hour treatment (Figure 2.7). Each data point in Figure

2.7 is the mean LD across coupons (n=2 or 3) sampled from the same treatment well in the same experiment. The standard errors (SE) associated with each data point (i.e. the SE of the mean LD of the coupons in each well exposed to current over 50 wells in N=19 experiments) were between 0.05 and 1.75 $\log_{10}$(CFU/cm^2) with the exception of eight wells in which all samples were below the detection limit and thus had no variability. Most of this within-experiment variability was observed for direct current levels of 0.18-0.43 mA/cm^2 for no-antibiotic wells and 0.07-0.43 mA/cm^2 with tobramycin while standard errors less than 0.32 $\log_{10}$(CFU/cm^2) were observed outside these ranges. In these experiments, TSB was again used as the nutrient in the treatment solution but at 3% of the concentration that was used in the wells during treatment of *S. epidermidis* biofilms and thus represents a system with lower chlorine demand from organic medium components.

Experiments were first analyzed for the effect of the salt concentration during electric current exposure. While the sodium chloride levels are grouped in ranges of concentrations in Figure 2.7 for clarity of presentation, salt concentration was used as a covariate for analysis. In the absence of current, the salt concentration in the control wells over the 20 hour treatment had no significant effect on the LD in control wells (p-value=0.12) and was determined not to affect biofilm growth or survival during the treatment time. The mean LD of the no-current, no-antibiotic controls across salt levels was 7.50 $\log_{10}$(CFU/cm^2) with a repeatability SD of 0.34 $\log_{10}$(CFU/cm^2) with 66% of variance due to between experiment sources. For any well with current, two boundaries for chlorine were calculated: the maximum free chlorine concentration if all the chloride

in the treatment solution was converted to free chlorine, and the theoretical chlorine concentration if all the current that runs through the treatment solution goes to reactions that generate free chlorine. Experimental parameters where the theoretical maximum chlorine concentration based on current level exceeded the available chloride in the system were defined as theoretically "salt limited". The mean LRs were analyzed as a function of current density and salt concentration for the no-antibiotic data. Figure 2.7A indicates that the mean LD of organisms on the coupons decreased as direct current increased with the same rate regardless of salt concentration. The increasing LR with current level was statistically significant (p-value=0.008) but was not found to be affected by the salt concentration (p-value=0.72) and no significant interaction was observed between the two factors (p-value=0.83). The repeatability SD of mean LR for wells exposed to current was 1.35 $\log_{10}(CFU/cm^2)$ with 100% of variance due to within experiment sources. As the rates of biofilm reductions with current level were the same across the salt concentrations, it was concluded that the treatment wells had sufficient chloride available and were thus not "salt limited" in the range studied. Looking back at the chlorine generation measured for the *S. epidermidis* current levels (all of which had excess salt available), the mean endpoint free chlorine measurements across each well (Figure 2.4A) were only 12-21% of the theoretical maximum free chlorine level that would be achieved if all current flow went to the generation of free chlorine. If the type of electrolytic "efficiency" seen with excess salt also applied to the salt and current parameters in the *P. aeruginosa* experiments, the actual chloride required in the medium may be much lower than the theoretical extremes used to define salt limitation, providing

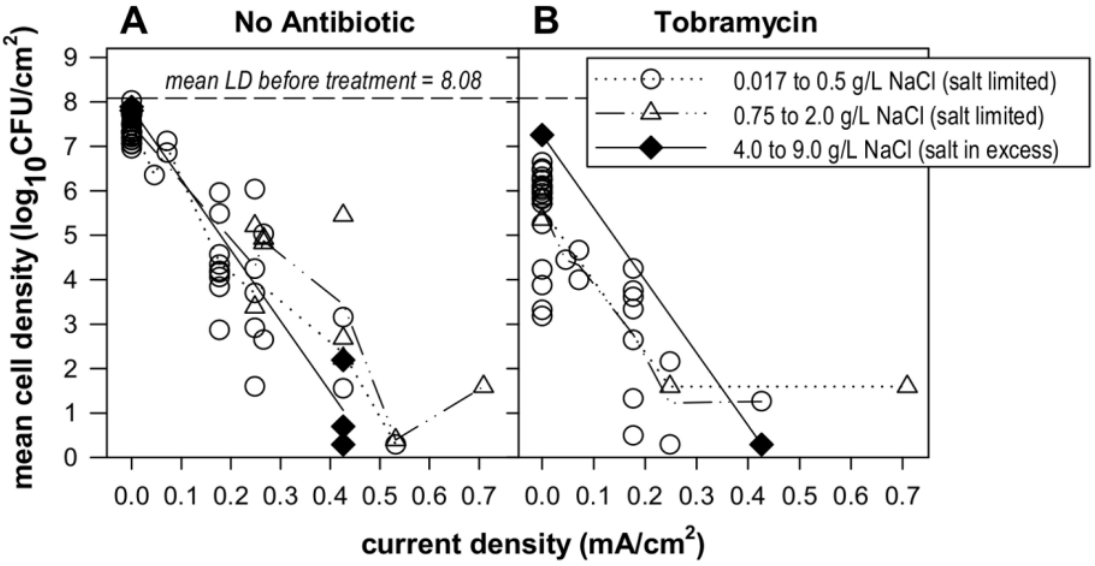

Figure 2.7 Treatment of *P. aeruginosa* biofilm with direct current. Direct current was applied to biofilm in wells containing (A) no antibiotic and (B) 10 µg/mL tobramycin sulfate for 20 hours. All wells contained 0.1 g/L TSB with varying amounts of total NaCl. References to theoretical salt limitation or excess salt apply only to wells with current. Each symbol indicates a mean LD on coupons across one well and lines show connected means for each current level.

a possible explanation for the lack of NaCl effects at the experimental conditions studied.

The effect of tobramycin with varying salt concentrations and current densities was then analyzed (Figure 2.7B). In the absence of current, biofilms treated with tobramycin had a significant mean LR of 1.92 $\log_{10}(CFU/cm^2)$ compared to no-current, no-antibiotic controls (p-value<0.0005) with a repeatability SD of 0.78 $\log_{10}(CFU/cm^2)$ with no change in LR due to the salt concentration (p-value=0.45). When current was applied, a significant linear trend of increasing biofilm reductions with increasing current was again observed (p-value=0.001). A statistically significant increase in LR of 1.70 $\log_{10}(CFU/cm^2)$ was observed when tobramycin was present in wells with current compared to wells without antibiotic (p-value=0.001), however the interaction between tobramycin and current level (which would indicate synergy between the antibiotic and

electric current) was not significant (p-value=0.33). The repeatability SD of mean LR for wells exposed to current was 1.17 $\log_{10}(CFU/cm^2)$ with 100% of variance due to within experiment sources. The tobramycin effect during current application is very close to that seen in the no-current controls and the lack of interaction with current level fails to demonstrate synergy between current and tobramycin. Thus, in this system the killing by tobramycin seems to be a separate, additive effect that is not enhanced by the application of current.

Discussion

The purpose of this study was to investigate the application of direct current under conditions physiologically relevant to the milieu of an infected artificial joint. While past biofilm experiments in this area of research have typically used a chloride-free solution to minimize electrolysis effects, in this system a salt concentration of normal saline (0.9% NaCl) was used in order to mimic the physiologically relevant environment.

Our results are consistent with electrolytic generation of hypochlorous acid, a potent disinfectant, at the anode leading to biofilm killing. The half-reactions for electrolysis of a sodium chloride solution are:

$$2H_2O\,(l) + 2e^- \rightarrow H_2\,(g) + 2OH^-\,(aq) \qquad \text{(cathode)} \qquad (2.4)$$

$$2Cl^-\,(aq) \rightarrow Cl_2(g) + 2e^- \qquad \text{(anode)} \qquad (2.5)$$

Chlorine gas has limited disinfection power however when generated in water, produces reactive free chlorine compounds including hypochlorous acid (HOCl) and hypochlorite (OCl^-):

$$Cl_2(g) + H_2O\,(l) \rightarrow Cl^-\,(aq) + HOCl\,(aq) + H^+\,(aq) \qquad (2.6)$$

$$HOCl\ (aq) \rightarrow H^{+}\ (aq) + OCl^{-}\ (aq) \quad (2.7)$$

When combined, the overall electrolysis reaction is:

$$H_2O\ (l) + Cl^{-}\ (aq) \rightarrow H_2\ (g) + OCl^{-}\ (aq) \quad (2.8)$$

Although the overall reaction would result in no net pH change, the cathodic and anodic reactions indicate localized pH decreases at the anode and increases at the cathode consistent with our observations.

This mechanism of electrolytic generation of chlorine in the presence of aqueous chloride is consistent with the following experimental observations: 1) Killing effects associated with direct current exposure were observed against *S. epidermidis* and *P. aeruginosa* biofilms in the absence of antibiotic (Figure 2.2A and Figure 2.7A). 2) Biofilm reductions were dose responsive with increased killing observed with increasing current density (Figure 2.2A and B, Figure 2.7). Increasing the current density is expected to increase the rate of chlorine generation. 3) High concentrations of free chlorine were measured in the system when exposed to electric current (Figure 2.4). The amount of chlorine generated also follows a linear dose response with current density. 4) The effect of electric current was accurately mimicked by dosing of an equivalent concentration of chlorine (Figure 2.2C). 5) Less killing was observed during electric current treatment at the same current levels when nitrate and sulfate were used in place of chloride during current exposure (Figure 2.5). 6) No killing effect was observed when current was applied at the same levels when phosphate was used in place of chloride. 7) Biofilm killing was greater on the coupon immediately adjacent to the cathode where higher chlorine concentrations were also observed (Figure 2.3). We conclude that

electrolytic generation of chlorine is likely to be important *in vivo* where chloride ions are naturally and invariably present.

The bioelectric effect is typically discussed as a synergistic effect between biocide and direct current when either alone would have minimal to no impact. There was no effect of ciprofloxacin in the *S. epidermidis* experiments (Figure 2.2A and B). The reduction due to tobramycin in *P. aeruginosa* experiments (Figure 2.7) was comparable when current was present or absent and determined to be an additive effect, independent of the presence of direct current. Thus, the results reported here do not conform to the bioelectric effect model as we find substantial killing by current alone and no synergistic enhancement of killing provided by combining current and antibiotic.

Electrolytic generation of chlorine explains the direct current efficacy observed in this study when the experiment accounted for physiologic saline conditions (9 g/L NaCl). Doses of chlorine alone at concentrations of 25 to 100 mg/L have been reported to partially kill or remove *S. epidermidis* (Buckingham-Meyer et al., 2007; Davison et al., 2010) or *S. aureus* biofilms (Ueda and Kuwabara, 2007) and those results are furthermore confirmed in this study. Considered a rapid speed kill agent, chlorine works as a disinfectant by oxidizing organic material (Chapman, 2003). Active against many organisms, chlorine and hypochlorite salts are the most common disinfectant in municipal water treatment facilities (Brezonik, 1994). HOCl is also produced in the phagolysosomes of human neutrophils from Cl^- and H_2O_2 by myeloperoxidase to kill and digest foreign microbes for immune defense (Foote et al., 1983; King et al., 1997; Sam and Lu, 2009). Although seemingly supportive of chlorine in the body, HOCl is isolated

to the phagolysosomes within these cells and release of chlorine species from ruptured neutrophils has been implicated in host tissue damage (King et al., 1997) although host systems to prevent HOCl tissue damage are also reported (Xulu and Ashby, 2010). HOCl reacts with a number of cellular targets (Winterbourn, 2002) demonstrating broad reactivity with bacterial and host cells (Chapman et al., 2002). Electrolytic generation of chlorine gas in an aqueous solution is a means of generating this potent disinfectant. Although chlorine would be generated at the anode, free chlorine was found throughout the system due to convective mixing (Figure 2.3A). However, due to the highly reactive nature of chlorine, the free chlorine would remain very low during the course of treatment and may be difficult to detect when chlorine demand is high in the system. Chlorine was not detected over the course of 7 days of electric current in a recent study with 0.5 g/L NaCl from TSB (del Pozo et al., 2009c). In our system, chlorine was only detected when the organics were removed from the system.

The speciation of free chlorine is pH dependent as predominantly hypochlorous acid (HOCl) below pH 7.5 and hypochlorite ion (OCl^-) above. Hypochlorous acid is known to be 100 times more reactive than the hypochlorite ion and a stronger disinfectant. In the study reported here, a pH gradient around 3 at the anode to 9 at the cathode was observed across the treatment wells when the current was running. While the pH gradient alone could have substantial effects on bacterial viability, it may also affect chlorine speciation and efficacy. Insight into the effects of pH versus chlorine can be drawn from emerging use of electrolyzed water (EW) as a disinfectant in the food industry. EW is typically generated from the electrolysis of dilute sodium chloride

solutions that is then collected at each electrode for subsequent application with hypothesized action due to pH, chlorine, and the oxidation-reduction potential (ORP) of the solutions. A recent comparison of acidic EW and basic EW treatment of *S. aureus* biofilms by Sun et al. demonstrated high killing efficacy but no removal of biofilm with acidic EW solutions but high removal and no killing of biofilm with basic EW (Sun et al., 2012). The removal effect was partially reproduced by increasing the pH without EW but representative decreases in pH did not reproduce the killing effect indicating other EW properties, such as chlorine or oxidative properties, to be responsible for killing efficacy. In other studies, reductions by previously electrolyzed acidic EW against planktonic *E. coli* and *L. monocytogenes* were reproduced with a free chlorine concentration close to those found in the respective EW solution (Venkitanarayanan et al., 1999). In our study, we used non-electrolyzed free chlorine solutions to effectively mimic direct current. Reductions were very similar when chlorine doses were used indicating chlorine as a major factor although pH may affect localized changes across the treatment well and ORP might be an additional contributing factor.

The significance of chloride in the system was further demonstrated when the same current levels were applied without chloride in the system. No electric current effect was seen when *S. epidermidis* biofilms were treated with phosphate serving as the electrolyte. Intermediate 2-log and 3-log mean reductions were observed at the highest current level when nitrate or sulfate served as the electrolyte but neither had as strong of an effect as the 5-log mean reduction when chloride was present in the system (Figure 2.5). The effects with sulfate and nitrate are hypothesized to be due to electrolysis

reactions and products other than those generating chlorine. Davis et al. found similar results with electrolyte variations in the medium during direct current treatment of planktonic *E. coli* cultures (Davis et al., 1992). They reported an initial 8-log planktonic cell culture to be very minimally reduced when phosphate was used in the medium, a 1-log reduction with sulfate, a 2-log reduction with nitrate, but no survival when chloride was present over a 4 hour treatment with 400 μA across a 10 mL culture. In studies of electrochemical disinfection of wastewater in a plug flow reactor, Li et al. observed reduction efficiencies of *E. coli* when wastewater contained NaCl but no disinfection efficacy was observed when water contained $NaNO_3$ or Na_2SO_4 (Li et al., 2004). Wattanakaroon and Stewart reported a 4-log increase in *Streptococcus gordonii* biofilm killing when 2 g/L NaCl was added to the solution during electric current treatment although also reported extensive corrosion of the stainless steel electrodes with chloride present (Wattanakaroon and Stewart, 2000). Sun et al. reported that while acidic electrolyzed water generated from the electrolysis of a 0.1% NaCl solution had strong killing efficacy against *S. aureus* biofilm, the same pH electrolyzed water generated from a 0.1% $NaNO_3$ solution had minimal efficacy (Sun et al., 2012). These observations show chloride as an important parameter demonstrated to increase killing efficacy of electric current.

Another point of consideration is electrode material. Davis et al. reported the electrode material to be a critical parameter in studies of electric current application to planktonic cultures (Davis et al., 1989). With a gold cathode, anodes made of carbon or platinum were reported to be the most effective while silver, nickel, or copper corroded to

the point of breakage during experiments. In other studies, the release of metals from the electrodes has been intentionally used to deliver silver for treatment (Berger et al., 1976a; Berger et al., 1976b). Stainless steel has predominantly been used for both electrodes (Costerton et al., 1994; del Pozo et al., 2009b; del Pozo et al., 2009c; Jass et al., 1995; Jass and Lappin-Scott, 1996; Shirtliff et al., 2005; Stewart et al., 1999; Wattanakaroon and Stewart, 2000), as one electrode alternating polarity throughout exposure as anode or cathode (Blenkinsopp et al., 1992a; Khoury et al., 1992), or as the cathode (van der Borden et al., 2005; van der Borden et al., 2004a; van der Borden et al., 2004b) in studies investigating electrical effects on biofilm although use of platinum (Stoodley et al., 1997; Wellman et al., 1996) and graphite (del Pozo et al., 2009b; del Pozo et al., 2009c) are also reported. In some of these studies, corrosion or discoloration has been reported as an observation with stainless steel electrodes. We also began our study with ferrous electrodes (no data shown). These electrodes experienced significant corrosion and precipitation of colored corrosion products (Figures A.1 and A.2). These products were observed to have lethal effects in our system which led to the use of platinum electrodes. Recent studies have also linked the use of stainless steel electrodes to both corrosion products and higher bacterial reductions when compared to graphite electrodes (del Pozo et al., 2009b; del Pozo et al., 2009c). It has been suggested that use of stainless steel electrodes may have contributed to the larger reductions reported in previous studies of the bioelectric effect (del Pozo et al., 2009b). These types of observations might be difficult to detect in a flowing system.

So how do our findings relate back to treatment of an infection *in vivo*? In the past, the bioelectric effect has been suggested as a way to enhance antibiotic treatment of infections. Our *in vitro* results suggest a mechanistic basis for the efficacy of electric current alone when chloride is present. This may be part of the explanation for antimicrobial efficacy of electrical treatments reported in prior studies in animals. Successful electrical current treatment of *S. epidermidis* has been demonstrated in a goat model along surgical pin tracts connecting an external fixation frame to bone for use in reconstructive bone surgery with the pin acting as an electrode (van der Borden et al., 2007). The anode, which would be the site of generation of hypochlorous acid, was a platinum ring contacting the skin with the stainless steel fixation pin serving as the cathode. Secinti et al. used titanium and silver coated titanium screws as anodes to study the intentional release of silver particles to treat *S. aureus* on vertebral implants in rabbits (Secinti et al., 2008). While both electrically treated screws decreased cell counts, release of titanium was associated with significant bone tissue inflammation where none was reported with silver. del Pozo et al. showed killing efficacy of electric current application against *S. epidermidis* on stainless steel implants in the tibia of rabbits without antibiotic over a 21 day exposure although discoloration of the bone was also noted (del Pozo et al., 2009a).

Here we have reported killing efficacy of direct current against *S. epidermidis* and *P. aeruginosa* biofilms and conclude these effects to be due to electrolytic generation of free chlorine. Localized generation of an antimicrobial at the site of infection is an attractive strategy for indwelling, device-related infections. However, while

electrolytically generated chlorine may have antimicrobial properties, as we have demonstrated here, it is also likely to have cytotoxic effects in the surrounding host tissue. We do not necessarily advocate the application of direct electric current as a therapeutic strategy. The message from this investigation is that if a direct current is established *in vivo*, where chloride is abundant, the generation of chlorine is an inevitable consequence. The potential for host tissue damage needs to be addressed if electric current therapies are to be considered. In future work, it will be important to be aware of electrochemistry that can lead to free chlorine when considering the application of direct current technologies *in vivo*.

Acknowledgments

We would like to thank Betsey Pitts at the Center for Biofilm Engineering for providing expert assistance with confocal microscopy. Microscopy equipment at the facility was purchased with funds provided by the M. J. Murdock Charitable Trust and the NSF Major Research Instrumentation program.

CHAPTER 3: GLOBAL GENE EXPRESSION OF DIRECT CURRENT TREATED STAPHYLOCOCCUS EPIDERMIDIS BIOFILMS IN COMPARISON TO CHLORINE

Abstract

The purpose of this study was to investigate direct electric current (DC) induced changes in global gene responses of *S. epidermidis* biofilms to better understand the mechanisms of biocidal DC effects. Previous work demonstrated dose-responsive killing of these biofilms with DC exposure that was linked to electrolytic generation of reactive chlorine species. In this work, biofilms grown in a CDC biofilm reactor were treated with 2 mA (0.7 mA/cm^2) of direct electric current via platinum electrodes in 1/10th strength tryptic soy broth containing 9 g/L total NaCl for 4 hours. In parallel experiments, the biofilms were treated with a single dose of 70 mg/L HOCl solution, the mean free chlorine concentration measured after 4 hour DC exposures to the treatment medium in the absence of organic and biofilm sources of chlorine demand. Microarray results of DC and chlorine treatments revealed 103 significantly upregulated genes and 94 significantly downregulated genes in response to DC exposure. Statistically significant overlaps of 59 genes upregulated in both DC and chlorine treatments and 41 genes downregulated in both treatments were identified, supporting a mechanism of action related to chlorine generation. The DC gene response was linked to upregulation of central catabolic metabolism, translation and upregulation of genes related to oxidoreductase activity. These data suggest an oxidative stress response due to chlorine generation, adding to the evidence for an electrolytically generated chlorine mechanism of antimicrobial activity by DC treatments in the presence of chloride.

Introduction

Bacterial biofilms are notoriously resistant to antimicrobials and immune defenses. One proposed strategy to combat these infections has been the use of direct electric current (DC) to treat biofilm-related infections *in vivo*. The biocidal effects of DC against bacteria have been reported in both planktonic and biofilm cultures. Other studies have reported minimal effects of electric current alone but a synergistic effect of antimicrobials and antibiotics when the treatments occurred simultaneously.

In our previous work, we reported dose-responsive killing of *S. epidermidis* and *P. aeruginosa* biofilms over 24 hour direct current treatments at levels between 0.7-1.8 mA/cm^2 (Sandvik et al., 2013). DC was not observed to increase or decrease the efficacy of the antibiotics ciprofloxacin with *S. epidermidis* and tobramycin with *P. aeruginosa* and thus a mechanism for DC efficacy alone was systematically investigated. One of the key features of the system was DC exposure at a physiologically-relevant chloride concentration, removed from the medium in other studies to preclude electrolytic byproducts, but clearly present if this treatment strategy were to be used *in vivo*. High levels of electrolytically-generated free chlorine were measured over the duration of treatment and were used in the absence of current to effectively mimic the dose-responsive kill curve observed with DC treatment. Little or no killing effect was observed at the same current levels when the chloride was removed from the medium and substituted with electrolytes of sulfate, nitrate, or phosphate (Sandvik et al., 2013).

By addressing individual parameters in the experimental system using chemical and biofilm viability measures, we concluded the effects of DC to be due to electrolytic

generation of free chlorine species, potent disinfectants. In this study we sought to understand bacterial responses beyond viability by examining gene level responses of *S. epidermidis* biofilms to direct current exposure in the same system. As chlorine generation was strongly indicated in our previous work, we also wished to compare similarities and differences in global gene responses to DC and chlorine using chlorine concentrations representative of chlorine generated during the course of DC treatment within this study.

Methods

Biofilm Growth

The CDC Biofilm Reactor (Biosurface Technologies Corp., Bozeman, MT, Model CBR90-1DS) is designed to grow repeatable biofilm on polycarbonate disks (called coupons) in a high shear environment under continuous flow conditions. The reactor is a one-liter glass beaker with a side-arm discharge port at approximately 400 mL for effluent drainage by gravity. Eight polystyrene rods, each holding three 1.27 cm diameter polycarbonate coupons, are inserted through the lid, suspending the coupons in the bulk fluid of the reactor. A baffled magnetic stir bar in the center of the reactor provides mixing as well as uniform fluid shear on each coupon. During continuous flow operation, a peristaltic pump is used to pump fresh medium into the reactor through an influent port in the lid. An in-line, glass flow break in the influent feed line prevents back-contamination of the feed carboy. A second port in the lid is attached to a bacterial air vent for gas exchange. A total of 24 coupons are available in the reactor for sampling.

Biofilms were grown on polycarbonate coupons in the CDC Biofilm Reactor using a standard growth protocol for each organism. The *S. epidermidis* growth protocol is analogous to the ASTM E2562-07 "Standard Test Method for Quantification of *Pseudomonas aeruginosa* Biofilm Grown with High Shear and Continuous Flow using CDC Biofilm Reactor" (ASTM E2562 - 07, 2007) but has been adapted for the study organism, *S. epidermidis* RP62A (ATCC#35984): The sterilized reactor containing 450 mL of full strength (30 g/L) TSB (tryptic soy broth, Soybean-Casein Digest Medium, Difco) with additional NaCl to a total concentration of 9 g/L NaCl (accounting for NaCl in TSB) was inoculated from a frozen stock of *S. epidermidis*. The reactor was placed on a magnetic stir plate in a 37ºC incubator and operated in batch with stirring at 125 rpm for 24 hours. After 24 hours, a continuous flow of 1/10th strength TSB (9 g/L total NaCl) was started with a reactor residence time of 30 minutes and overflow drainage to a waste carboy by gravity. Continuous flow ran for 16 hours at the end of which biofilm-coated coupons were ready for use in experimental protocols. For all experiments the face of the coupon facing inward (towards the stir bar) was defined as the sample surface.

Direct Current Treatment of Biofilm

The treatments were performed in small enclosed wells designed at the Center for Biofilm Engineering, described previously (McLeod et al., 1999; Sandvik et al., 2013). Inner dimensions were 7.1 cm long by 1.6 cm wide by 3.4 cm tall (Figure 2.1). Rubber sheeting lined the lid to prevent contamination. Twenty-four gauge platinum electrodes, 3.8 cm long, were pushed through the lid at opposite ends of the wells and extended 2.5 cm from the lid into the treatment well. The anode was connected to the positive

terminal of the power supply and the cathode to the negative. Each well had a separate circuit with an inline ammeter and current controller (Wavelength Electronics, No. LDD200-1M) connected to a DC power supply. The current controllers maintained a constant current level while voltage fluctuated slightly with changes in the resistive loads across each well.

After growth, biofilm-coated coupons were aseptically removed from the rods of the CDC reactor, dipped in 10 mL of sterile phosphate buffered saline (PBS: 8 g/L NaCl, 0.2 g/L KCl, 1.15g/L Na_2HPO_4, 0.2 g/L KH_2PO_4 in reagent-grade water, pH=7.2) to remove planktonic cells and placed in sterile treatment wells with the inner face of the coupon (from the CDC reactor) facing up in the well. Five coupons were placed in each well, four of which would be pooled for RNA extraction with the fifth sampled for viability. Twenty mL of sterile 3 g/L tryptic soy broth (TSB) with 9 g/L total NaCl was gently added to each well. Direct current at a level of 2.0 mA (an effective current density of 0.7 mA/cm^2 based on the minimum cross-sectional area of the liquid in the treatment well) was applied across the length of the well for four hours at 37ºC. Parallel control treatment wells contained 20 mL of the same treatment solution without current. At the end of treatment, biofilm were scraped for viability and RNA extractions.

Chlorine Treatment of Biofilm

Determination of the chlorine dose concentration to mimic DC was done as described previously (Sandvik et al., 2013) at the current levels and durations of interest in this study. The treatment medium was first exposed to DC in the absence of biofilm to measure free chlorine generation. The same current level used in DC exposures (0.7

mA/cm^2) was applied to 20 mL of a 9 g/L NaCl, 0.25 g/L K_2HPO_4 solution equivalent to the salt and buffer concentrations present in the treatment solution with organic sources of chlorine demand removed. After 4 hours of application, the current was turned off, the lid was gently removed, and liquid samples (0.1 mL each) were pipetted simultaneously at each electrode. Samples were measured by the DPD chlorine method using HACH DPD Free Chlorine Reagent (5 mL Powder Pillows) read on a spectrophotometer at 530 nm. These "endpoint free chlorine measurements" were assumed to represent the cumulative amount of reactive chlorine species generated over the 4 hour treatment time in the absence of chlorine demand. The mean concentration of these measurements was used as an initial chlorine dose for chlorine treatments.

Biofilms were grown and transferred to the treatment wells as described above for DC treated samples. Due to the rapid nature of chlorine reactions, the nutrients were added to the chlorine solution just prior to application to the biofilm. The chlorine solution was made with bleach and laboratory-grade water and adjusted to 105% of the target free chlorine concentration. A 20X sterile medium solution was made such that the resulting 1X concentration would be 3 g/L TSB with 9 g/L total NaCl. At time zero, 1 mL of the 20X medium solution was added to 19 mL of the given free chlorine solution in a sterile glass vial, swirled, and gently added to the treatment well containing the biofilm-coated coupons. The treatment wells were then treated like the DC-treated wells with a 4 hour incubation at 37°C. Parallel control wells were run with each treatment as described above for DC experiments. At the end of treatment, biofilm were scraped for viability measurements and RNA extractions.

Sampling Biofilm for Viability

The center coupon from each well was sampled for viability following treatment as described in the ASTM standard method (ASTM E2562 - 07, 2007) with slight modifications: Treated coupons were gently removed from the treatment well and transferred to a sterile surface for sampling. The top surface of the coupon was scraped with a sterile wooden stick held perpendicular to the surface for 30 seconds and then swirled in a dilution tube containing 9 mL of sterile PBS. This was repeated three times after which the stick was discarded. The coupon was then held over the dilution tube and the scraped surface was rinsed with 1mL of PBS to remove any remaining biofilm resulting in a final volume of 10 mL in the dilution tube. Samples were homogenized at 10,000 rpm for one minute to disaggregate biofilm clumps, serially diluted, and drop plated using the drop plate method (ten 0.01 mL drops per dilution) on tryptic soy agar (TSA). The colony forming units (CFU) on the plates were counted following overnight incubation at 37ºC. A biofilm log density (LD) of viable cells for each coupon was calculated using the mean CFUs counted over 10 drops, the volume of each drop, the surface area of the coupon, the volume of liquid the biofilm was scraped into (the zero dilution), and the dilution at which the colonies were counted (Equation 3.1):

$$LD = \log_{10}\left(\frac{CFU}{cm^2}\right) = \log_{10}\left(\left(\frac{\overline{CFU_{drop}}}{vol_{drop}}\right)\left(\frac{vol_{zerodilution}}{SA_{coupon}}\right)\left(10^{dilution}\right)\right) \quad (3.1)$$

Statistical analyses of viability were performed using linear mixed effects (*lme*) models in the nonlinear mixed effects (*nlme*) package (Pinheiro et al., 2011) in the free statistical and graphing program *R* (R Development Core Team, 2010). Sources of

variance for growth in the CDC Reactor used a mixed effects model with experiment as the random factor (to account for n=1 or 2 coupons sampled for viability per well). The repeatability standard deviation (SD) was calculated from the R output of within-experiment variance, σ_{within}^2, and between-experiment variance, $\sigma_{between}^2$ (Equation 3.2):

$$repeatabilitySD = \sqrt{\sigma_{within}^{\ 2} + \sigma_{between}^{\ 2}} \tag{3.2}$$

The percent contributions of each source of variance were calculated as the variance for that source divided by the square of the repeatability SD. The LD of treated and control data following a 4 hour treatment were compared with a linear mixed effects model as a factor of treatment (control, DC, or chlorine) with experiment as a random variable.

RNA Extraction from CDC Coupons

Biofilm from four coupons in each treatment well were pooled for each RNA extraction sample with the fifth, center coupon sampled for viability as described above. Each coupon was gently removed from the treatment well to a sterile sampling surface. A sterile, chloroform-treated (for RNase inactivation) Teflon policeman was used to scrape the surface of each coupon and transfer biofilm to a 15 mL conical centrifuge tube initially containing 4 mL of 2:1 by volume RNA stabilizing agent (Qiagen RNA Protect):PBS. After scraping, the coupon was held over the tube and rinsed with 1 mL of fresh 2:1 RNA Protect:PBS to remove any remaining biofilm on the coupon surface. The remaining coupons from the same well were scraped and rinsed into the same tube to pool biofilm from each treatment for the extraction sample. Each pooled sample was then vortexed briefly and incubated at room temperature with the stabilizing agent for 5 minutes. Samples were centrifuged at 6,000 rpm for 8 minutes at 25˚C and the

supernatant was discarded. RNA extractions were then performed using a modified protocol for enzymatic lysis with mechanical disruption using the RNeasy Protect Bacteria Mini Kit (Qiagen). The biofilm pellet was resuspended in 20 µL of a 0.3 mg/mL (≥150 U/mL) lysostaphin (Sigma-Aldrich) solution in 200 µL TE buffer (pH 8.0, Amresco) and incubated in a 37˚C shaker for 10 minutes, followed by 2 minutes on ice. A volume of 700 µL Buffer RLT (provided with kit) with β-mercaptoethanol (1% by volume) was added to the sample which was then transferred to a 2 mL conical screw-cap microcentrifuge tube containing 0.05 g of acid-washed glass beads (150-212 µm diameter, Sigma). Samples were processed in a cell disrupter (Savant /Bio101 FastPrep FP120) at the maximum speed (setting 6.5) for four 30 second intervals with 20 second intervals on ice between each run. Samples were then centrifuged for 2 min (the centrifugation settings from this point on were 12,000 × *g* at room temperature (RT) unless otherwise indicated). The supernatant was transferred to a fresh microcentrifuge tube with 470 µL of 100% ethanol and incubated at RT for 3 minutes. The lysate was transferred to an RNeasy Mini spin column (provided with kit) and centrifuged for 30 seconds in 700 µL volumes until all of the sample had run through the column. Each volume was spun through twice (i.e. the flow-through from the first spin was reapplied to the column and spun through a second time before being discarded). The column was washed with 350 µL of Buffer RW1 (provided with kit), centrifuged for 30 seconds and the flow-through was discarded. An on-column DNase digestion was performed per the RNeasy Mini Kit optional protocol using an RNase-Free DNase Set (Qiagen). In brief, 80 µL of a DNase 1 solution (70 µL of Buffer RDD, 10 µL of a 1,500 Kunitz units/uL

DNase I stock solution) was added directly to the spin column membrane and incubated at RT for 15 minutes. A 350 µL volume of Buffer RW1 was added to the column and incubation continued for an additional 5 minutes. The column was centrifuged for 30 seconds and transferred to a new 2 mL collection tube with the flow-through discarded. A wash step was performed twice by incubating 500 µL of Buffer RPE (provided with kit) on the column for 3 minutes at RT and centrifuging for 30 seconds with the flow-through discarded. The column was then centrifuged for 1 minute to dry the membrane. If at this point additional liquid was identified, the column was transferred to a fresh 2 mL collection tube and dried for an additional minute by centrifugation. The RNA sample was then eluted from the column in 50 µL of RNase-free water with a 5 minute incubation at RT prior to 1 minute centrifugation. Samples were immediately frozen and stored at -70˚C. Aliquots of RNA samples were confirmed for quantity and chemical purity with a NanoDrop ND-100 spectrophotometer and for nucleic acid integrity on an RNA NanoChip with an Agilent Bioanalyzer 2100.

cDNA Synthesis

cDNA syntheses were performed with minor modification to the NimbleGen Arrays User's Guide adapted protocol for the Invitrogen SuperScript Double-Stranded cDNA Synthesis Kit (unless otherwise indicated, reagents were provided with this kit): RNA samples were transferred to nuclease-free 0.2 mL PCR tubes and concentrated to ≤10 µL in a SpeedVac vacuum concentrator. The volumes of samples were brought to 10 µL with DEPC water. For the first strand synthesis, one µL of random primers (Invitrogen) was added to the samples and incubated in a thermocycler for 10 minutes at

70˚C, followed by 5 minutes at 4˚C. A solution containing 4 µL 5X First Strand Buffer, 2 µL 0.1M DTT, and 1 µL 10mM dNTP Mix was added to each tube and incubated for 2 minutes at 42˚C. Two µL of SuperScript II RT was added to each tube which were then incubated for 4 hours at 42˚C. Upon removal, samples were placed on ice or stored at -20˚C. For the second strand cDNA synthesis, a solution consisting of 91 µL DEPC Water, 30 µL 5X Second Strand Buffer, 3 µL 10 mM dNTP mix, 1 µL 10 U/µL DNA Ligase, 4 µL 10 U/µL DNA Polymerase I, and 1 µL 2 U/µL RNase H was added to each tube and incubated for 2 hours at 16˚C. Following incubation, 2 µL of 5 U/µL T4 DNA polymerase was added to each tube and incubated at 16˚C for an additional 5 minutes. Samples were moved to a PCR chiller rack and 10 µL of 0.5 M EDTA (pH 8.0, Invitrogen) was added to each sample prior to storage at -20˚C. cDNA cleanup and precipitation were performed as follows: The samples were incubated for 10 minutes at 37˚C with 1 µL of 4 mg/mL RNase A (≥70 Kunitz units/mg protein, Sigma-Aldrich) in 10 mM Tris-Cl, pH 7.8. Each sample was transferred to a tube with 163 µL phenol:chloroform:isoamyl alcohol and vortexed well. The samples were transferred to Phase Lock Tubes and centrifuged at 12,000 × *g* for 5 minutes. The upper, aqueous layer was transferred to a clean microcentrifuge tube and combined with 16 µL 7.5 M ammonium acetate, 5 µL of 15 µg/mL GlycoBlue (Invitrogen), and 326 µL of ice-cold 100% ethanol with mixing by inversion between each addition. Samples were centrifuged at 12,000 × *g* for 20 minutes at RT and the supernatant was discarded. The pellet was washed twice by mixing 500 µL volumes of iced 80% ethanol (by volume in

DEPC water) to the pellet, centrifuging for 5 minutes and discarding the supernatant. The pellet was dried in a SuperVac vacuum concentrator. The pellet was then rehydrated in 20 µL of DEPC water. Samples were immediately frozen and stored at -70˚C. Aliquots of the cDNA samples were confirmed for quantity and chemical purity with a NanoDrop ND-100 spectrophotometer and for nucleic acid integrity on an RNA NanoChip with an Agilent Bioanalyzer 2100. One µg of cDNA was run on each array.

Microarrays

Microarrays were run on four-plex (4 arrays/chip) 4x72K NimbleGen microarrays (Roche) with a custom design for *S. epidermidis* RP62A. The design had targets for the transcripts of all the 2,526 protein-coding genes in the genome (2,494 genomic loci, 32 plasmid loci) with 14 probes per target transcript and an identical design on the same array for data confirmation. The arrays were processed by the Functional Genomics Core Facility (Montana State University) following the NimbleGen Protocol. The cDNA was labeled using a NimbleGen One-Color DNA Labeling Kit, hybridized to the array with a HS4 Hybridization System, scanned on an MS 200 Microarray Scanner with MS 200 Data Collection Software and images processed using NimbleGen's NimbleScan software. Following NimbleGen protocols for array processing, the software implemented a robust multi-array average (RMA) algorithm to normalize expression across arrays for comparison as described by Irizarry (Irizarry et al., 2003) and subsequent data were background corrected, log2 transformed, normalized with quantile normalization, and protected from outliers using a median polish robust procedure using

NimbleScan to generate expression levels . The mean expression level of the two replicate designs on each array was used for further data analysis.

Differential Gene Expression

The normalized expression data were compared with Welch's t-tests (for unequal variance) for each gene in the gene expression program FlexArray 1.6.1.1 treating all samples with the same treatment (control, DC, or chlorine) as replicates across experiments. The same control treatments were used for DC and chlorine experiments and thus all DC and chlorine gene expression profiles were compared to the same set of controls generating fold-changes in gene expression with respect to the untreated control. Fold changes (FC) are presented as linear, symmetric FCs centered on no change (equivalent to any FC=+/-1) with positive FCs representing upregulated genes and negative FCs representing downregulated genes. A p-value≤0.05 was used as a cutoff for significant genes.

Biological patterns and themes in the enriched gene lists were explored using the freely accessible Functional Annotation Tools in the NIH bioinformatics Database for Annotation, Visualization and Integrated Discovery (DAVID) v6.7 (Huang et al., 2009a, b). DAVID is designed to explore biological relationships between genes based on annotated categories for each gene collected in the DAVID knowledgebase from dozens of public databases (see Supplemental File 2 of (Huang et al., 2009a) for information on sources). The following categories and specific annotations were selected for analyses (DAVID default settings): Functional Categories (Clusters of Orthologous Groups (COG) ontology, COG_ONTOLOGY; Swiss-Prot (SP) Protein Information Resource

(PIR) keywords, SP_PIR_KEYWORDS; Universal Protein Resource (UniProt) sequence feature, UP_SEQ_FEATURE), Gene Ontology (for biological process, GOTERM_BP_FAT; for cellular component, GOTERM_CC_FAT; for molecular function, GOTERM_MF_FAT), Pathways (KEGG Pathway, KEGG_PATHWAY), and Protein Domains (InterPro classification, INTERPRO; Protein Information Resource (PIR) SuperFamily classification, PIR_SUPERFAMILY; Simple Modular Architecture Research Tool (SMART) classification, SMART). Given a list of gene identifiers for a list of interest (i.e. significantly upregulated genes, significantly downregulated genes, or all significantly changing genes), DAVID identified enriched categories under which multiple genes fell. As the only input for these lists were gene identifiers without expression levels, any FC or statistical cutoffs were implemented before input of gene lists into DAVID. The Functional Annotation Chart identifies genes falling under a single annotation and provided statistical outputs for the probability of that same overlap by random chance using the number of background genes, the number of genes in the input list, the number of genes in the list that had the annotation of interest, and the number of possible genes in the background list that have the annotation of interest. The Functional Annotation Clustering tool further draws correlations between similar gene ontology (GO), pathways, or other annotations using fuzzy heuristics and generates an enrichment score for that group of genes.

Genome Comparison Tool

Homologous genes for comparison of similar treatments from other organisms in the literature were obtained from the Multi-Genome Homology Comparison tool from the

JCVI Comprehensive Microbial Resource (cmr.jcvi.org, (Peterson et al., 2001)) using a 40% minimum percent similarity between proteins in the two genomes. The generated homologue file was used to match locus identifiers in the comparison study organism to *S. epidermidis* RP62A SERP identifiers. Additional gene annotation files with gene names and descriptions for each study organism were obtained from the microbesonline.org database.

Results

Selection of a Treatment Level with Minimal Loss of Viability

In our previous work using this experimental system, up to 7-log reductions (LR) in biofilm viability with DC treatment were observed with high concentrations of free chlorine measured over the course of a 24 hour treatment (as high as 1,100 ppm free chlorine at 5 mA or 1.8 mA/cm^2) when chloride was present (Sandvik et al., 2013). In this study, we were interested in achieving a treatment level at which the organisms would respond to treatment with limited killing to maximize the chance of recovering intact genetic material for gene expression analysis. Following preliminary experiments decreasing both current level and duration (see Appendix C, Figure A.1), a 4 hour exposure at 2 mA (0.7 mA/cm^2) was chosen for DC treatment. The endpoint free chlorine concentration +/- SD measured for that current level and duration (in the absence of organics and biofilm) was 67.8 +/- 26.4 mg/L free chlorine (see Appendix C, Figure A.2 for additional current levels). A 70 mg/L free chorine dose was used as an equivalent chlorine dose for these experiments. The viable cell density following 4 hour treatments

are reported in Figure 3.1. Control samples had a mean LD +/- repeatability SD of 7.86 +/- 0.50 $log_{10}CFU/cm^2$ with a majority of error due to between experiment sources (96%). Direct current treated samples had a mean LD +/- repeatability SD of 7.42 +/- 0.87 $log_{10}CFU/cm^2$ with 49% of error due to between experiment sources. Chlorine treated samples had a mean LD +/- repeatability SD of 7.87 +/- 0.34 $log_{10}CFU/cm^2$ with 53% of error due to between experiment sources. No statistically significant differences were found for treatments with current (p-value=0.14) or chlorine (p-value=0.34) when compared to the control.

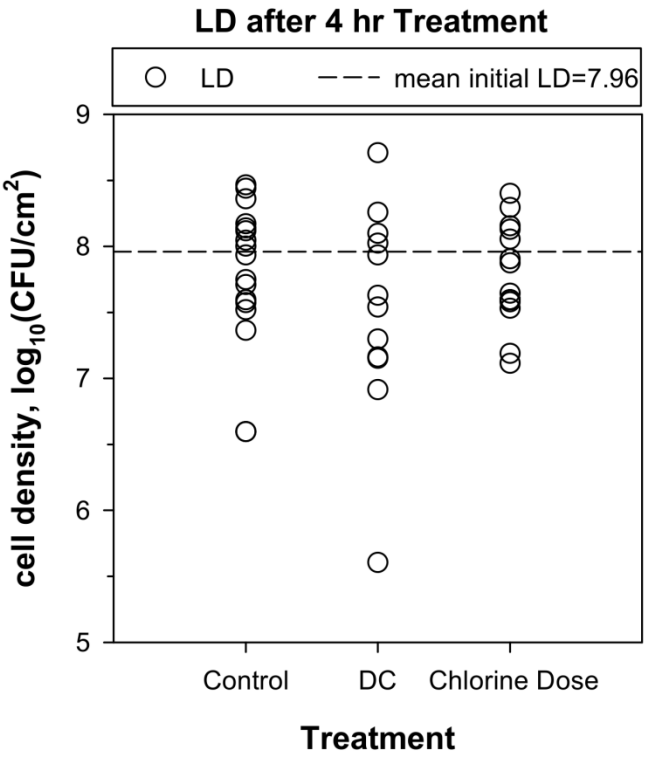

Figure 3.1 Biofilm viability following 4hr treatments with DC or chlorine. Direct current (DC) was applied at 2 mA (0.7 mA/cm^2) throughout the duration of treatment. The chlorine dose corresponding to the current level was a 70 ppm free chlorine dose applied at t=0. Symbols indicate the LD for individual coupons.

DC and Chlorine Treatments
Modified Gene Expression

For both of the selected DC and chlorine treatment levels, significant changes in gene expression were observed in comparison to the control. Fold-changes (FCs) in gene expression for the DC exposure were relatively small with all significant FCs falling between -2.2 and 2.2, identifying 103 upregulated and 94 downregulated significant genes (p-value≤0.05, any FC). The response to chlorine treatment was greater with respect to the number of significantly different genes (546 upregulated genes, 482 downregulated genes) and the magnitude of the change in expression levels with FCs between -7.2 to 10.1 in addition to one significant gene with higher expression at FC=20.9.

A tally of the number of differentially expressed genes for DC and chlorine treatments is seen in Table 3.1 using several cutoffs for gene lists. In the literature, a number of cutoffs for FC and p-value have been used in gene expression analysis including frequently used criteria of |FC|≥2 or |FC|≥1.5 with a p-value≤0.05. However, a growing opinion has suggested that statistically detectable changes in microarray expression may still be important even if the fold changes are small. In a comparison study of the same data with different cutoffs, Dalman et al. demonstrated that the selection of cutoffs for FC and p-value could drastically change study conclusions (Dalman et al., 2012). Thus, the numbers of differentially expressed genes for each condition are presented for multiple cutoffs.

Table 3.1 Tally of differentially expressed genes for DC and chlorine microarrays experiments using various cutoffs. Perturbed gene are the combined upregulated and downregulated gene lists. Each treatment was compared to the same set of controls with Welch's t-tests and resulting p-values and foldchange (FC) are with respect to those control samples. The 10% false-discovery rate (FDR) are the result of Benjamini-Hochberg corrections.

Treatment	n arrays	PERTURBED GENES		UPREGULATED GENES				DOWNREGULATED GENES			
		p-value≤0.05	10%FDR	p-value≤0.05			10%FDR	p-value≤0.05			10%FDR
		any FC	any FC	any FC	FC≥1.5	FC≥2	any FC	any FC	FC≤-1.5	FC≤-2	any FC
Control	4	---	---	---	---	---	---	---	---	---	---
DC	4	196	0	103	32	5	0	93	36	3	0
Chlorine	4	1028	872	546	452	179	474	482	366	160	398

Overlap of Differentially Expressed Genes between DC and Chlorine Treatments

Based on our previous work, it was suggested that DC treatment in the presence of chloride generated reactive free chlorine species, potent disinfectants, which were responsible for DC efficacy against bacterial biofilms. To investigate this theory, the response to DC treatment was compared to the chlorine treatment for overlap of significant differentially expressed genes. Over half of the upregulated DC response genes (any FC) were also upregulated in the chlorine treatment regardless of FC cutoffs (Figure 3.2).

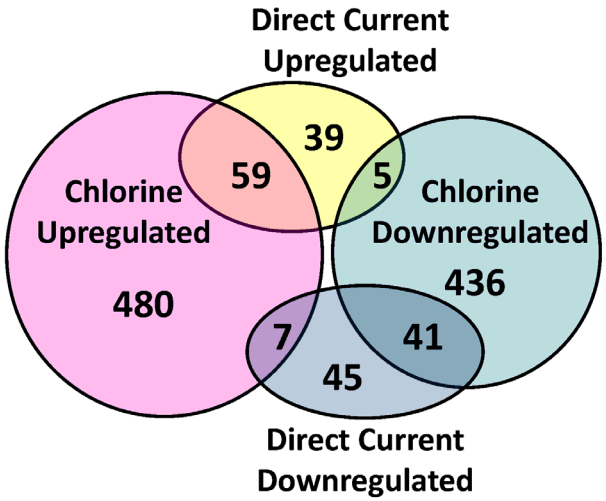

Figure 3.2 Overlap of differentially expressed genes between DC and chlorine treatments. Treatment were applied for 4hrs, the above gene tallies are for all genes significant with p-value≤0.05 (all FCs).

Table 3.2 Significance of overlap between DC and chlorine treatments. The table reports the probability of two gene lists of the given lengths having the observed overlap due to factors greater than random chance. The expected overlap is the product of the two list lengths over the total genes tested (2,526 genes on the array).

Probabilities of Overlap Between Two Gene Lists

	Cutoff	DC Genes	Chlorine Genes	Observed Overlap	Expected Overlap	p-value for observed overlap
Perturbed	any FC	197	1028	112	80	**1.4E-06**
Upregulated DC/ Upregulated Chlorine	any FC>0	103	546	59	22	**$<10^{-15}$**
	FC≥1.5	32	542	21	7	**7.6E-08**
	FC≥2	5	179	3	0	**0.003**
Downregulated DC/ Downregulated Chlorine	any FC<0	94	482	41	18	**2.3E-08**
	FC≤ -1.5	36	366	17	5	**2.4E-06**
	FC≤-2.0	3	160	3	0	**2.5E-04**
Upregulated DC/ Downregulated Chlorine	any FC	103	482	5	20	1.000
	|FC|≥1.5	32	366	1	5	0.994
	|FC|≥2	5	160	0	0	1.000
Upregulated Chlorine/ Downregulated DC	any FC	94	546	7	20	1.000
	|FC|≥1.5	36	542	1	8	1.000
	|FC|≥2	3	179	0	0	1.000

The significance of the overlap between the treatments was calculated as p-values based on a hypergeometric mean distribution to determine if the observed overlap between two

lists was greater than the expected overlap due to random chance (Table 3.2). The overlap of genes upregulated in response to DC and chlorine treatment was highly significant regardless of FC cutoff (all p-values≤0.003). Significant overlap was also observed for downregulation of genes with slightly less than half of the genes downregulated with DC treatment also downregulated during chlorine treatment. downregulated in the chlorine treatment, with a significant overlap (p-value=2.3 x 10^{-8}). Twelve genes were indicated to be upregulated in one treatment and downregulated in the other, however, ten of these inverse genes had |FC|≤1.5 and were no longer observed when FC cutoffs were implemented.

Genes of the DC Response

All significant genes ($p \leq 0.05$) differentially expressed following DC exposure are listed in Table 3.3. FCs of overlapping significant chlorine response genes are also reported for comparison. A full list of all differentially expressed chlorine response genes can be found in Appendix A, Table A.2). Only five genes were found with FC≥2 in response to DC treatment. Interestingly two of the five highest upregulated genes represent single gene operons coding for secretory antigen precursors SsaA (SERP1880, FC=2.1; SERP2136, FC=2.2). Both of these genes were also significantly upregulated in the chlorine treatment. This secreted protein was reported as a novel antigen identified in a patient suffering with a severe septic *S. epidermidis* infection (Lang et al., 2000). The remaining three genes with FC≥2 were hypothetical proteins, one of which overlapped also had FC≥2 in the chlorine treatment.

Examining multiple genes upregulated on the same operon, both genes of a two gene operon involved in fatty acid biosynthesis, *fabH* and *fabF*, were upregulated for both DC and chlorine treatments. A repressor for an arsenical resistance operon, *arsD,* and one gene, *arsB*, on an adjacent three-gene operon coding for an arsenical pump were upregulated in the DC whereas all 5 genes of these two operons (SERP2427-2428 and SERP2429-2431) were upregulated during chlorine treatment. This might indicate a moderate response in DC that might be amplified at higher current levels. Interestingly genes for another arsenical pump were also found to be significantly upregulated in the chlorine data (arsC-1, SERP0210, and arsR-1) but the only significant DC gene on this operon, the arsenate reductase, *arsC-1,* was significantly downregulated at a FC=-1.3 for DC treatment. Fewer operons containing multiple significant genes were identified as downregulated. The largest downregulated FC in response to DC treatment was for a hypothetical protein (SERP0028, FC=-2.2) on a two gene predicted operon for a transcriptional regulator that was also significantly downregulated (SERP0029, FC= -1.6). This operon was significantly downregulated for both DC and chlorine treatments. All genes on the operon coding for the sigma factor B, *rpoF*, and *rsbWVU* were downregulated with the same FC= -1.3.

The significant overlap of genes responding to both chlorine and DC treatments support our previous measurements of electrolytically generated free chlorine species during DC treatment. However, while chlorine generation may be a predominate mechanism of DC efficacy in the presence of chloride, current flow may result in effects unique to DC treatment. A response unique to the DC treatment was upregulation of

three of five genes on the *dltABCD* operon (SERP0517, *dltC*, and *dltD*) with FC between 1.4 and 2.2. The two additional genes on the operon were upregulated but were not significant at α=0.05 (*dltA*, FC=1.6, p-value=0.063 and *dltB*, FC=1.5, p-value=0.070). In *S. aureus*, the gene products of the *dltABCD* operon modify the cell envelope by replacing negatively charged components in teichoic acids with positively charged D-alanine effectively increasing the net positive surface charge of the organism (Peschel et al., 1999; Weidenmaier et al., 2005). This modification of the electrostatic properties of the cell envelope is proposed as a bacterial mechanism to decrease binding of host cationic antimicrobial peptides (Peschel et al., 1999; Weidenmaier et al., 2005), but in the context of electric current flow may indicate some effect of DC on the electrostatic nature of the cell surface. Another response unique to the DC treatment was upregulation of five ribosomal genes (*fplR, fplX, fplV, rpsS,* and *rplW*) that were not significant in the chlorine treatment. Only one gene on the rest of this very large operon was significant in the chlorine treatment (SERP1821, FC= -1.4).

Direct Current Induced Genes Related to Translation, Central Catabolic Metabolism, and Oxidoreductase Activity and Repressed DNA Recombination Processes

Within the DC gene list, three clusters of upregulated genes and one cluster of downregulated genes were identified in the DAVID Functional Annotation tool with enrichment scores greater than 1 using genes with p-value≤0.05 and any FC (Figure 3.3). In addition to clusters found in upregulated or downregulated genes, the lists were combined to generate perturbed gene clusters. The cluster with the largest FCs comprised fifteen genes clustered in U^{III} with annotation related to oxidation reduction

reactions including four genes with FC≥1.5, three of which were oxidoreductase family proteins. All of the genes of this cluster and 8 downregulated genes made up the second perturbed cluster (P^{II}). Eleven of the fifteen genes in this third upregulated cluster and thirteen of the twenty-three genes in the perturbed cluster were also significantly upregulated in the chlorine treatment. All but one of these genes were either upregulated in both treatments or downregulated indicating oxidation reduction transformations as an important factor in DC and chlorine treatments. The upregulated cluster with the highest enrichment score, U^{I}, included a number of ribosomal proteins of translation activity. The majority of these changes were very small with 1.1 to 1.3 FCs and three with FCs between 1.4 to 1.6. The second upregulated cluster related to catabolic processes in central metabolism used for energy generation and production of metabolic precursors via the pentose phosphate pathway. All of the FCs in this cluster were ≤1.3 indicating significant but small effects on these catabolic pathways.

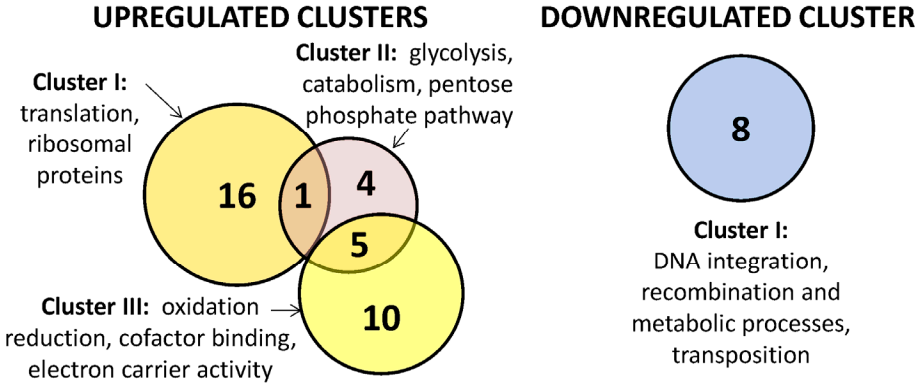

Figure 3.3 Clusters of significantly changing genes in response to DC exposure with enrichment score (ES)≥1. Enrichment scores: U1 (17 genes, ES=1.93), U^{II} (10 genes, ES=1.67), U^{III} (15 genes, ES=1.04), and D^{I} (8 genes, ES=1.03). Perturbed clusters (not shown) include P^{I} (11 genes with 5 genes of U^{III}, ES=1.44), P^{II} (23 genes including all the oxidation reduction genes of U^{III}, ES=1.32), and P^{III} (15 genes including all of U^{II}, ES=1.11). Sixty-seven upregulated genes and 85 downregulated genes did not cluster.

Table 3.3 Differentially expressed genes following 4 hours of DC treatment (all p-values≤0.05). Genes that were also significant in the chlorine treatment are included for comparison. The fold change (FC) and p-values are for each treatment compared to the parallel no-treatment controls. The DC clusters identified in DAVID are identified for upregulated (U), downregulated (D), and the combined "perturbed" (P) gene lists with superscripts identifying specific clusters. Color coding is denoted below.

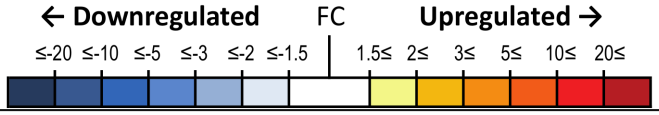

Upregulated Genes

Locus	Gene Name	Gene Description	Predicted SERP	DC Cluster	DC FC	Chlor FC
SEA0009		transcriptional regulator, putative	0009		1.4	1.5
SERP2427	*arsD*	arsenical resistance operon trans-acting repressor	2427-2428		1.8	3.7
SERP0059	*ahpF*	alkyl hydroperoxide reductase, F subunit	0060-0059	U^{III},$P^{I,II}$	1.3	1.5
SERP0096		hypothetical protein	0096-0099		1.3	2.0
SERP0113		acetyltransferase, GNAT family	0113-0114		1.5	
SERP0156	*lysS*	lysyl-tRNA synthetase	0156	U^{I}	1.2	
SERP0159		hypothetical protein	0158-0159		1.5	-1.7
SERP0178	*rplK*	ribosomal protein L11	0178-0182	U^{I}	1.3	
SERP0179	*rplA*	50S ribosomal protein L1	0178-0182	U^{I}	1.5	
SERP0183	*rpoB*	DNA-directed RNA polymerase beta subunit	0183-0184		1.2	1.3
SERP0188	*fusA*	translation elongation factor G	0185-0189	U^{I}	1.2	
SERP0189	*tuf*	elongation factor Tu	0185-0189	U^{I}	1.1	
SERP0202		deoxynucleoside kinase family protein	0203-0202		1.4	
SERP0205		hydrolase, haloacid dehalogenase-like family	0205-0206		1.3	1.8
SERP0214		hypothetical protein	0214-0213		1.4	3.1
SERP0224		hypothetical protein	0224		1.2	
SERP0228	*ung*	uracil-DNA glycosylase	0228-0230		1.3	
SERP0242		pyridine nucleotide-disulfide oxidoreductase family protein	0243-0242	U^{III},$P^{I,II}$	1.9	6.9
SERP0243		hypothetical protein	0243-0242		2.2	10.1
SERP0341		ABC transporter, ATP-binding protein, MsbA family	0340-0341		1.4	4.4
SERP0353	*norA*	quinolone resistance protein NorA	0353		1.4	2.4
SERP0432	*trxB*	thioredoxin-disulfide reductase	0428-0432	U^{III},$P^{I,II}$	1.4	3.2
SERP0442	*gapA-1*	glyceraldehyde 3-phosphate dehydrogenase	0441-0446	$U^{II,III}$,$P^{II,III}$	1.2	
SERP0444	*tpiA*	triosephosphate isomerase	0441-0446	U^{II},P^{III}	1.1	
SERP0445	*pgm*	phosphoglyceromutase	0441-0446	U^{II},P^{III}	1.1	
SERP0483		thioredoxin, putative	0483		1.9	2.2
SERP0485	*gcvH*	glycine cleavage system protein H	0484-0485	U^{III},P^{II}	1.3	
SERP0496	*sufC*	FeS assembly ATPase SufC	0496-0499		1.3	1.8
SERP0499		NifU domain protein	0496-0499		1.2	2.0
SERP0517		hypothetical protein	0517-0521		2.2	
SERP0520	*dltC*	D-alanine--poly(phosphoribitol) ligase subunit 2	0517-0521		1.9	
SERP0521	*dltD*	dltD protein	0517-0521		1.4	
SERP0542		NADH-dependent flavin oxidoreductase, Oye family	0542	U^{III},P^{II}	1.7	2.7
SERP0550	*pgi*	glucose-6-phosphate isomerase	0550	U^{II},P^{III}	1.1	
SERP0567	*fabH*	3-oxoacyl-(acyl carrier protein) synthase	0567-0568		1.7	2.7
SERP0568	*fabF*	3-oxoacyl-(acyl-carrier-protein) synthase II	0567-0568		1.4	1.6
SERP0583		hypothetical protein	0583-0581		1.6	1.5
SERP0616		lipoate-protein ligase A family protein	0616		1.6	2.5
SERP0634		hypothetical protein	0634-0633		1.2	1.4
SERP0651	*purC*	phosphoribosylaminoimidazole-succinocarboxamidesynthase	0649-0659		1.7	

Table 3.3 (continued)

Locus	Gene Name	Gene Description	Predicted SERP	DC Cluster	DC FC	Chlor FC
SERP0682	*pdhC*	pyruvate dehydrogenase complex E2 component, dihydrolipoamide acetyltransferase	0680-0683	$U^{II,III}$,$P^{II,III}$	1.1	
SERP0712		hypothetical protein	0712		1.4	
SERP0713		hypothetical protein	0713		1.4	
SERP0729	*uvrC*	excinuclease ABC subunit C	0729		1.4	3.0
SERP0775	*fbe*	fibronectin/fibrinogen binding protein	0775		1.2	2.0
SERP0781	*def-2*	polypeptide deformylase	0781-0786	U^{I}	1.2	1.6
SERP0782	*fmt*	methionyl-tRNA formyltransferase	0781-0786	U^{I}	1.2	
SERP0796	*fabD*	malonyl CoA-acyl carrier protein transacylase	0794-0803		1.4	1.4
SERP0823	*rpsB*	30S ribosomal protein S2	0823-0826	U^{I}	1.1	
SERP0839	*ribF*	riboflavin biosynthesis protein RibF	0837-0841		1.2	1.8
SERP0865	*glpP*	glycerol uptake operon antiterminator regulatory protein	0863-0865		1.5	
SERP0873		GTP-binding protein, putative	0873-0874		1.3	2.7
SERP0912	*tkt*	transketolase	0912	U^{II},P^{III}	1.2	1.3
SERP0920		choline/carnitine/betaine transporter	0920		1.2	-1.4
SERP0922		thioesterase family protein	0922		1.7	
SERP0925	*parE*	DNA topoisomerase IV subunit B	0925-0926	$U^{I,II}$,P^{III}	1.1	
SERP0927		amino acid carrier protein	0927		1.2	1.6
SERP0955		oligoendopeptidase F, putative	0955		1.3	1.6
SERP1000	*msrA-2*	methionine sulfoxide reductase A	1000-1997	U^{III},P^{II}	1.2	1.6
SERP1020	*pbp2*	penicillin-binding protein 2	1019-1020		1.2	-1.2
SERP1047		pyridine nucleotide-disulfide oxidoreductase family protein	1047	U^{III},$P^{I,II}$	1.5	1.5
SERP1052		hypothetical protein	1052		2.1	1.8
SERP1053		hypothetical protein	1053		1.7	1.6
SERP1061		transcriptional regulator, Fur family	1062-1060		1.3	1.8
SERP1067	*zwf-2*	glucose-6-phosphate 1-dehydrogenase	1067	$U^{II,III}$,$P^{II,III}$	1.3	
SERP1071	*gnd*	6-phosphogluconate dehydrogenase	1072-1070	$U^{II,III}$,$P^{II,III}$	1.1	1.1
SERP1085	*nusB*	transcription antitermination protein NusB	1088-1082	U^{I}	1.2	1.7
SERP1187		bacterial luciferase family protein	1187	U^{III},P^{II}	1.7	2.6
SERP1199	*recJ*	single-stranded-DNA-specific exonuclease RecJ	1199-1198		1.1	
SERP1207		hypothetical protein	1211-1202		1.3	1.5
SERP1295	*fhs*	formate--tetrahydrofolate ligase	1295		1.8	1.8
SERP1301		FtsK/SpoIIIE family protein	1305-1300		1.3	1.7
SERP1303		hypothetical protein	1305-1300		1.4	1.2
SERP1315		hypothetical protein	1315	U^{III},$P^{I,II}$	1.3	1.7
SERP1327	*ribE*	riboflavin synthase subunit alpha	1328-1325		1.7	2.6
SERP1328	*ribD*	riboflavin biosynthesis protein RibD	1328-1325		1.6	2.1
SERP1338		CrcB family protein	1337-1339		1.4	1.6
SERP1375		hypothetical protein	1375		1.2	-1.5
SERP1391		RNA methyltransferase, TrmH family, group 2	1392-1391	U^{I}	1.3	
SERP1437	*gatB*	aspartyl/glutamyl-tRNA amidotransferase subunit B	1439-1437	U^{I}	1.3	1.3
SERP1707		hypothetical protein	1707-1705		1.6	1.7
SERP1765		ATP-binding protein, Mrp/Nbp35 family	1766-1765		1.8	2.5
SERP1815	*rplR*	ribosomal protein L18	1832-1810	U^{I}	1.3	
SERP1820	*rplX*	50S ribosomal protein L24	1832-1810	U^{I}	1.6	
SERP1826	*rplV*	ribosomal protein L22	1832-1810	U^{I}	1.4	
SERP1827	*rpsS*	ribosomal protein S19	1832-1810	U^{I}	1.3	
SERP1829	*rplW*	ribosomal protein L23	1832-1810	U^{I}	1.3	
SERP1837		hypothetical protein	1837		1.4	
SERP1880		secretory antigen precursor SsaA	1880		2.1	2.2
SERP1953		DNA-binding response regulator	1953-1954		1.3	2.2

Table 3.3 (continued)

Locus	Gene Name	Gene Description	Predicted SERP	DC Cluster	DC FC	Chlor FC
SERP2016		hypothetical protein	2016		1.2	1.8
SERP2075		DedA family protein	2075		1.6	
SERP2084	*aldA-2*	aldehyde dehydrogenase	2085-2084	$U^{II,III}$,$P^{II,III}$	1.3	2.2
SERP2093		hypothetical protein	2093		1.2	
SERP2109		esterase, putative	2110-2109		1.4	1.7
SERP2136		secretory antigen precursor SsaA	2136		2.2	2.3
SERP2182	*nrdG*	anaerobic ribonucleoside-triphosphate reductase activating protein	2183-2182	U^{III},P^{II}	1.0	-1.2
SERP2196		transcriptional regulator, MarR family	2196-2194		1.5	9.6
SERP2199		hypothetical protein	2199		1.3	2.0
SERP2265		organic hydroperoxide resistance protein, putative	2265		1.6	3.2
SERP2376		hypothetical protein	2376-2378		1.3	
SERP2398	*aap*	accumulation associated protein	2398		1.6	
SERP2430	*arsB*	arsenical pump membrane protein	2429-2431		1.3	3.2

Downregulated Genes

Locus	Gene Name	Gene Description	Predicted SERP	DC Cluster	DC FC	Chlor FC
SEA0006		site-specific recombinase, resolvase family	0006	D^{I}	-1.3	-1.5
SEA0029		rlx protein, putative	0027-0031		-1.5	
SERP0028		hypothetical protein	0029-0028		-2.2	-2.2
SERP0029		transcriptional regulator, Cro/CI family	0029-0028		-1.6	-1.7
SERP0033		cyclase, putative	0037-0033		-1.3	
SERP0064		hypothetical protein	0066-0064		-1.4	-3.6
SERP0127		methyltransferase, tetrapyrrole family	0122-0127		-1.3	-1.3
SERP0197		alcohol dehydrogenase, zinc-containing	0196-0198	$P^{II,III}$	-1.1	
SERP0209	*arsC-1*	arsenate reductase	0211-0209	$P^{I,II}$	-1.3	1.5
SERP0237		lipoate-protein ligase A family protein	0236-0237		-1.2	-1.2
SERP0255		hypothetical protein	0056-0053		-1.4	-1.4
SERP0256		hypothetical protein	0056-0053		-1.5	
SERP0362		oxidoreductase, aldo/keto reductase family	0362	P^{II}	-1.5	
SERP0363		glycosyl transferase, group 2 family protein	0363		-1.5	
SERP0418		comF operon protein 3	0417-0418		-1.3	
SERP0524		NADH dehydrogenase, putative	0524	$P^{I,II}$	-1.5	-1.7
SERP0759		hypothetical protein	0759		-1.1	
SERP0787		hypothetical protein	0787-0789		-1.1	-1.3
SERP0888		sensor histidine kinase, putative	0886-0889		-1.3	-1.9
SERP0894		hypothetical protein	0894		-1.2	-1.5
SERP0937	*trpE*	anthranilate synthase component I	0937-0943		-1.5	
SERP0938	*trpG*	anthranilate synthase component II	0937-0943		-1.4	
SERP0940	*trpC*	indole-3-glycerol phosphate synthase	0937-0943		-1.2	1.5
SERP0970	*lysA*	diaminopimelate decarboxylase	0963-0970		-1.2	
SERP1011	*ebh*	cell wall associated fibronectin-binding protein	1011		-1.7	
SERP1066		AtsA/ElaC family protein	1066		-1.3	-2.3
SERP1135	*cdd*	cytidine deaminase	1138-1133		-1.1	
SERP1224	*tnpA-1*	Tn554, transposase A	1226-1223	D^{I}	-1.4	
SERP1257	*icd*	isocitrate dehydrogenase	1258-1257	$P^{II,III}$	-1.3	
SERP1269		universal stress protein family	1269		-1.2	-2.5
SERP1316		cell wall surface anchor family protein	1316		-1.4	
SERP1345	*tnpC-2*	Tn554, transposase C	1345		-1.2	-1.6
SERP1347	*tnpA-2*	Tn554, transposase A	1347-1346	D^{I}	-1.4	
SERP1494		fructokinase, putative	1495-1494		-1.4	-1.4
SERP1495	*cscA*	sucrose-6-phosphate hydrolase	1495-1494		-1.3	

Table 3.3 (continued)

Locus	Gene Name	Gene Description	Predicted SERP	DC Cluster	DC FC	Chlor FC
SERP1497	*scrR*	sucrose operon repressor	1498-1496		-1.5	-1.5
SERP1506		hypothetical protein	1506-1503		-1.4	
SERP1508		thioredoxin, putative	1508	P^{I}	-1.4	-1.3
SERP1509		hypothetical protein	1509		-1.5	
SERP1510	*nrdF-2*	ribonucleotide-diphosphate reductase beta subunit	1510	P^{II}	-1.4	
SERP1512		HNH endonuclease family protein	1512		-1.4	1.5
SERP1513		truncated ribonucleoside-diphosphate reductase 2, alpha subunit	1513		-1.4	
SERP1517		hypothetical protein	1517		-1.6	
SERP1524		methyltransferase domain protein	1526-1523		-1.5	
SERP1526		hypothetical protein	1526-1523		-1.5	
SERP1574		hypothetical protein	1575-1574		-1.2	
SERP1590		single-stranded-DNA-specific exonuclease RecJ, putative	1592-1590		-1.4	-1.4
SERP1593		hypothetical protein	1593		-1.3	-2.0
SERP1595		hypothetical protein	1595-1594		-1.4	-2.1
SERP1596		hypothetical protein	1596		-1.6	-2.1
SERP1608		hypothetical protein	1608		-1.6	-1.9
SERP1614		hypothetical protein	1614		-2.1	-2.1
SERP1620		hypothetical protein	1620		-1.5	
SERP1621		DNA-binding protein HU, putative	1621		-1.7	-2.4
SERP1677	*rpoF*	sigma factor B	1680-1677		-1.3	-1.5
SERP1678	*rsbW*	serine-protein kinase RsbW	1680-1677		-1.3	1.3
SERP1679	*rsbV*	anti-anti-sigma factor RsbV	1680-1677		-1.3	
SERP1680	*rsbU*	sigma factor B regulator protein	1680-1677		-1.3	-1.7
SERP1792	*lacD*	tagatose 1,6-diphosphate aldolase	1795-1789	P^{III}	-1.2	1.2
SERP1795	*lacA*	galactose-6-phosphate isomerase	1795-1789	P^{III}	-1.2	
SERP1868		transporter, putative	1868		-1.4	
SERP1894		inositol monophosphatase family protein	1894		-1.4	
SERP1931		DNA-3-methyladenine glycosylase	1931	D^{I}	-1.7	
SERP1945		drug transporter, putative	1945-1944		-1.3	-2.0
SERP1948	*tcaA*	tcaA protein	1048-1947		-1.3	-1.7
SERP1999		glutaredoxin, putative	2000-1999	P^{I}	-1.4	-2.5
SERP2031		amino acid ABC transporter, ATP-binding protein	2031-2028		-1.2	1.3
SERP2038		ABC transporter, ATP-binding protein	2038-2037		-1.3	
SERP2060	*glpT*	glycerol-3-phosphate transporter	2060		-1.5	
SERP2061		transcriptional regulator, MerR family	2061		-1.2	
SERP2118		transcriptional regulator, LysR family	2118		-1.4	-1.6
SERP2120		secretory antigen precursor SsaA-related protein	2120		-1.4	
SERP2142		amino acid permease family protein	2142		-1.5	-1.4
SERP2161		lipoprotein, putative	2161		-1.5	-1.8
SERP2162		cell wall surface anchor family protein	2162		-1.3	
SERP2165		pyridine nucleotide-disulfide oxidoreductase	2165	$P^{I,II}$	-1.8	
SERP2184		hypothetical protein	2184		-2.0	-2.7
SERP2206		DNA-binding response regulator	2207-2203		-1.5	-1.8
SERP2244		capA-related protein	2244		-1.6	-2.7
SERP2255		hypothetical protein	2255-2256		-1.5	-1.5
SERP2261	*manA-2*	mannose-6-phosphate isomerase, class I	2259-2261	P^{III}	-1.5	
SERP2285		phosphonate ABC transporter, ATP-binding protein	2286-2283		-1.4	
SERP2351	*arcB-2*	ornithine carbamoyltransferase	2351-2352		-1.1	-1.6
SERP2371		peptide ABC transporter, permease protein, putative	2375-2367		-1.5	
SERP2380		drug transporter, putative	2382-2380		-1.2	
SERP2381		NADH:flavin oxidoreductase/fumarate reductase, flavoprotein subunit	2382-2380	$P^{I,II}$	-1.2	
SERP2385		hypothetical protein	2384-2386		-1.5	1.8

Table 3.3 (continued)

Locus	Gene Name	Gene Description	Predicted SERP	DC Cluster	DC FC	Chlor FC
SERP2454		hypothetical protein	2454	D^{I}	-1.5	-2.5
SERP2456		hypothetical protein	2463-2455		-1.5	-2.6
SERP2472	*hsdM*	type I restriction-modification system, M subunit	2474-2471	D^{I}	-1.8	-2.0
SERP2485	*kdpC*	K+-transporting ATPase, C subunit	2485-2487		-1.7	-2.7
SERP2506	*tnpA-3*	transposase A	2506-2507	D^{I}	-1.5	
SERP2542		hypothetical protein	2543-2542		-1.6	
SERP2550	*recF*	recombination protein F	2551-2548	D^{I}	-1.2	

In addition, all genes of this upregulated cluster (U^{II}) and 5 downregulated clusters made up Perturbed Cluster III (P^{III}) with the largest FC= -1.5. Finally, the only cluster of downregulated genes (independent of the genes grouping in the perturbed clusters) indicated downregulation of DNA integration and metabolic processes. Three of these 8 genes were independent operons for a Tn554 transposase A (*tnpA-1*, *tnpA-2*, *tnpA-3*).

Overlap of DC, Chlorine, and Hydrogen Peroxide Responses in Other Organisms

To investigate response themes to similar treatments, the gene responses to DC and chlorine treatment were compared to several types of treatments reported in the literature. As no *S. epidermidis* comparison studies were found, comparisons were made for homologous genes in several gram-positive organisms. All of the comparison studies were for treatment of planktonic cultures. In a study by Szkotak et al, planktonic cultures of *B. subtilis* 168 were exposed to 0, 25, 83, and 250 $\mu A/cm^2$ direct current for 15 minutes in chloride-containing LB medium using stainless steel electrodes. The study compared treated samples at each current level to 15 minute exposures to pre-treated medium for each current level to "minimize the influence of electrochemical products on gene expression" and reported genes with $|FC| \geq 2$ after implementation of the study's tests

for significance (Szkotak et al., 2011). For our comparison, genes upregulated at 1 or more current levels were used excluding any gene significantly upregulated at one current level and downregulated at another. The focus of a study by Palazzolo-Ballance et al. compared the response of methicillin-resistant *S. aureus* MW2 (USA400) to hypochlorous acid and hydrogen peroxide treatment for 15, 30, 60, and 120 minutes reporting genes with $|FC| \geq 2$ after implementation of the study's tests for significance (Palazzolo-Ballance et al., 2008). For our comparison, genes reported to be upregulated at two or more of the four time points in response to the given treatment were included in the analysis. Two studies by Chang et al. reported *S. aureus* responses to 10 and 20 minute exposures to hydrogen peroxide (Chang et al., 2006) and hypochlorous acid (Chang et al., 2007) reporting genes with $|FC| \geq 2$ in comparison to untreated controls at the same time points following the studies test for significance (Chang et al., 2007). For our comparison, upregulated genes significant at both time points in response to either treatment were used.

The first step in this comparison was converting the selected gene lists from each study to homologous genes in *S. epidermidis* RP62A ("SERP" identifiers). The three *S. aureus* studies reported locus IDs for the respective organism. However, the *B. subtilis* study only reported gene names in tables. Thus, *B. subtilis* gene names were first matched with a respective *B. subtilis* locus ID using a gene annotation file from JCVI. Three of the gene names reported by Szkotak matched two *B. subtilis* 168 (BSU) locus IDs, both of which were included in the comparison locus list. Two gene names could not be matched with a BSU locus. Next, the gene locus IDs for each organism were

individually compared to the *S. epidermidis* RP62A genes used in this study using protein matches with ≥40% similarity identified with the JCVI Multi-Genome Homology Comparison tool. Over half the genes in each study list were found to have a homologous gene in *S. epidermidis* (SERP locus) however some were unique to the study organism and thus could not be compared. Furthermore, a few unique genes in the comparison organisms matched the same homolgous SERP gene reducing each comparison list to unique SERP identifiers. The reduction of these lists is summarized in Table 3.4. All gene lists were compared to the DC and chlorine responses in this study based on the SERP identifier. Additional homology between the comparison strains may exist but was not investigated for this comparison.

Table 3.4 Summary of homologous genes found in *S. epidermidis* RP62A (SERP loci) and the respective organism in each comparison study. Multiple locus identifiers were reported in each *S. aureus* study as MW (*S. aureus* MW2), SACOL (*S. aureus* subsp. aureus COL), Mu50 (*S. aureus* Mu50), SA (*S. aureus* N315), and SH (*S. haemolyticus* JCSC1435) presumably based on available annotations at the time of each study. Gene lists are for upregulated genes selected based on the parameters discussed in the text.

Comparison Gene Lists and Homology with *S. epidermidis* RP62A

				Number of Genes in Comparison List			
Study	**Treat**	**Organism**	**Identifier**	**Reported**	**With Locus ID**	**With SERP homologue**	**Unique SERP IDs**
Szkotak et al 2011	DC	*B. subtilis* 168	gene name	233	232	131	122
Chang 2007	HOCl	*S. aureus* (strain unspecified)	locus ID (SACOL, SA)	109	109	65	64
Palazzolo-Ballance 2008	HOCl	*S. aureus* MW2	locus ID (MW, SH, SERP)	145	145	95	92
	H_2O_2	*S. aureus* MW2	locus ID (MW, SH, SERP)	300	300	263	251
Chang 2006	H_2O_2	*S. aureus* NCTC 8325	locus ID (SACOL, Mu50, N315)	20	20	20	20

When the comparison lists of unique SERP IDs were compared to the DC and chlorine responses in this study, overlap was observed. All comparison studies reported significant genes with FC≥2 only (significance tests varied). Five upregulated genes in response to DC treatment and 179 upregulated genes in response to chlorine treatment in this study were found to fit this criterion. Of the *S. epidermidis* genes or homologous genes identified in other researcher's work, 132 were significant with a FC≥2 for two or more conditions and at least one comparison study and are listed in Table 3.5. Forty-two of those genes overlapped with one or both treatments in this study. FCs for any significant gene from the microarray data are presented alongside the comparison lists to investigate although the cutoff for inclusion in the table remained two or more conditions or studies with FC≥2, thus significant genes from the DC treatment and only one other comparison lists were not included.

Two genes were upregulated with FC≥2 in both of our treatments, both chlorine comparison studies, and one of the hydrogen peroxide comparison studies with a third gene just below the cutoff with a DC FC=1.9. The first was the single-gene operon for the secretory antigen precursor SssA (SERP1880) with a 2.1 FC with DC treatment and a 2.2 FC with chlorine treatment. A second secretory antigen precursor SssA operon (SERP2136) was significant with a FC≥2 in both treatments but not in comparison studies (Table 3.3). The other two genes upregulated in both treatments in this study and three comparison studies were on the same operon, SERP0243-0242.

Table 3.5 Overlap of homologous genes in DC, chlorine, and hydrogent peroxide treatments in various organisms. *S. epidermidis* FC data are for significant genes in this study and are color coded as in Table 3.3. Because of differences in statistical tests, all comparison studies are colored to indicate the minimum criteria for inclusion in this list, FC≥2. DC treatment for *B. subtilis* 168 (Szkotak et al., 2011), chlorine and hydrogen peroxide treatment of *S. aureus* MW2 (Palazzolo-Ballance et al., 2008), *S. aureus* chlorine treatment (Chang et al., 2007), and hydrogen peroxide treatment of *S. aureus* NCTC 8325 (Chang et al., 2006) are reported by the homologous gene name in the comparison organism ("-" represents an unnamed homologue).

Upregulated Genes in Response to Direct Current, Chlorine, and Hydrogen Peroxide

			DC		HOCl			H_2O_2	
			S. epi RP62A	*B. subtilis* 168	*S. epi* RP62A	*S. aureus*	*S. aureus* MW2	*S. aureus* NCTC 8325	*S. aureus* MW2
SERP	SERP	SERP Gene Description	FC	gene	FC	gene	gene	gene	gene
SERP0009		hypothetical protein			-1.6		-	-	
SERP0010		hypothetical protein					-	-	
SERP0019		hypothetical protein			2.0				-
SERP0020		ABC transporter, permease protein					*vraE*		*vraE*
SERP0035		bifunctional homocysteine S-methyltransferase/5,10-			2.1				-
SERP0036		trans-sulfuration enzyme family protein			2.1	-			*metC*
SERP0042		hypothetical protein			-1.4			-	-
SERP0059	*ahpF*	alkyl hydroperoxide reductase, F subunit	1.3	*ahpF*	1.5		*ahpF*		*ahpF*
SERP0060	*ahpC*	alkyl hydroperoxide reductase, C subunit			1.3		*ahpC*		*ahpC*
SERP0068	*pbuX*	xanthine permease			-1.3		*pbuX*		*pbuX*
SERP0097		ABC transporter, ATP-binding protein			2.1				*abcC*
SERP0164		putative ATP:guanido phosphotransferase		*mcsB*	2.2				
SERP0165	*clpC*	ATP-dependent Clp protease, ATP-binding subunit			1.9	*clpC*		-	
SERP0179	*rplA*	50S ribosomal protein L1	1.5				*rplA*		*rplA*
SERP0206		azoreductase				-			-
SERP0207		sdrG protein			2.0	*fnbB*	*fnbB*		
SERP0208		glycosyl transferase, group 1 family protein					-		-
SERP0211	*arsR-1*	arsenical resistance operon repressor			2.5		*arsr*		
SERP0214		hypothetical protein	1.4		3.1				-
SERP0242		pyridine nucleotide-disulfide oxidoreductase family	1.9		6.9	-	*lpd*		*lpd*
SERP0243		hypothetical protein	2.2		10.1	-	-		-
SERP0273		hydrolase, alpha/beta hydrolase fold family			4.1				*mhpC*
SERP0289		Na+/H+ antiporter, putative		*nhaK*	2.1				*nhaP*
SERP0305		hypothetical protein		*ydeO*	-1.3				-
SERP0306		iron compound ABC transporter, ATP-binding protein		*yusV*					*fhuA*
SERP0324	*scdA*	scdA protein					*scdA*	*scdA*	
SERP0340		ABC transporter, ATP-binding protein, MsbA family		*cydC*	4.8				
SERP0353	*norA*	quinolone resistance protein NorA	1.4		2.4				-
SERP0357		transcriptional regulator, DeoR family		*fruR*	1.9	-			
SERP0359	*fruA*	PTS system, fructose-specific IIABC components		*fruA*	2.0				
SERP0365	*saeR*	DNA-binding response regulator SaeR					*saeR*		*saeR*
SERP0367		lipoprotein, putative				-	-		-
SERP0387	*hisC*	histidinol-phosphate aminotransferase				*hisC*	*hisC*		*hisC*
SERP0389		alcohol dehydrogenase, iron-containing			-1.2		*adhE*		*adhE*
SERP0422		LysM domain protein			1.7	-			*ssaA*
SERP0426	*uvrB*	excinuclease ABC subunit B			2.2			*uvrB*	*uvrB*
SERP0427	*uvrA*	excinuclease ABC, A subunit			2.0			*uvrA*	*uvrA*

Table 3.5 (continued)

			DC		HOCl			H_2O_2	
			S. epi RP62A	*B. subtilis* 168	*S. epi* RP62A	*S. aureus*	*S. aureus* MW2	*S. aureus* NCTC 8325	*S. aureus* MW2
SERP	SERP	SERP Gene Description	FC	gene	FC	gene	gene	gene	gene
SERP0432	*trxB*	thioredoxin-disulfide reductase	1.4	*yumC*	3.2				
SERP0542		NADH-dependent flavin oxidoreductase, Oye family	1.7		2.7	-			*yqiG* (2)
SERP0570	*oppB*	oligopeptide ABC transporter, permease protein			1.4		*oppB*		*oppB*
SERP0571	*oppC*	oligopeptide ABC transporter, permease protein					*dppC*		*dppC*
SERP0572	*oppD*	oligopeptide ABC transporter, ATP-binding protein		*appD*			*oppD*		*oppD*
SERP0574	*oppA*	oligopeptide ABC transporter, oligopeptide-binding					*oppA*		*oppA*
SERP0579		competence protein, putative			4.0	-			
SERP0616		lipoate-protein ligase A family protein	1.6		2.5				*lplA*
SERP0618		ComK family protein					*comK*		*comK*
SERP0649	*purE*	phosphoribosylaminoimidazole carboxylase, catalytic		*purE*					*purE*
SERP0673	*cydB*	cytochrome d ubiquinol oxidase, subunit II			4.9	-			
SERP0692		Mn2+/Fe2+ transporter, NRAMP family				-			*mntH*
SERP0704	*pyc*	pyruvate carboxylase			-1.3		*pycA*		*pycA*
SERP0739		phenol soluble modulin beta 1					*psmB*		*psmB* (2)
SERP0790	*rpmB*	ribosomal protein L28					*rpmB*		*rpmB*
SERP0798	*acpP*	acyl carrier protein			-2.3		*hmrB*		*hmrB*
SERP0896		aspartate kinase			1.6		-		-
SERP0897	*hom*	homoserine dehydrogenase		*hom*		*dhoM*	*dhoM*		*dhoM*
SERP0899	*thrB*	homoserine kinase				*thrB*	*thrB*		*thrB*
SERP0905	*rpsN-1*	30S ribosomal protein S14			3.0	*rpsN*			
SERP0909	*lexA*	LexA repressor						*lexA*	*lexA*
SERP0910		hypothetical protein			-1.6			-	-
SERP0911		hypothetical protein			3.0	-	-		
SERP0935		ImpB/MucB/SamB family protein						-	-
SERP0956		phosphate transport system regulatory protein PhoU					*phoU*		*phoU*
SERP0957		phosphate ABC transporter, ATP-binding protein		*pstBB*			*pstB*		*pstB*
SERP0958		phosphate ABC transporter, permease protein		*pstA*			*pstA*		
SERP0959		phosphate ABC transporter, permease protein		*pstC*			*pstC*		*pstC*
SERP0960		phosphate ABC transporter, phosphate-binding		*pstS*					*pstS*
SERP0966	*dapB*	dihydrodipicolinate reductase			2.1	*dapB*			*dapB*
SERP0972		cold shock protein, CSD family					*cspA*		*cspA*
SERP0981		hypothetical protein			-1.4	-			-
SERP0989	*arlR*	DNA-binding response regulator ArlR					*arlR*		*arlR*
SERP1039		ubiquinone/menaquinone biosynthesis			1.3		*smtA*		*smtA*
SERP1046	*ansA*	L-asparaginase			1.6		*ansA*		*ansA*
SERP1187		bacterial luciferase family protein	1.7		2.6	-			-
SERP1249		hypothetical protein					-		-
SERP1288	*serA*	D-3-phosphoglycerate dehydrogenase					*serA*		*serA*
SERP1316		cell wall surface anchor family protein	-1.4				*fmtB*		*fmtB*
SERP1397	*sspA*	glutamyl endopeptidase precursor SspA			-7.2		*splA*		*splC*
SERP1403		ABC transporter, permease/ATP-binding protein		*cydD*	2.8				
SERP1431		ferritin family protein					*fer*		*fer*
SERP1458		hypothetical protein			1.8			-	-
SERP1665	*ilvD*	dihydroxy-acid dehydratase			1.6	*ilvD*	*ilvD*		*ilvD*
SERP1666	*ilvB*	acetolactate synthase, large subunit, biosynthetic type				*ilvB*			*ilvB*
SERP1667		acetolactate synthase, small subunit, truncation				-			*ilvH*
SERP1668	*ilvC*	ketol-acid reductoisomerase				*ilvC*	*ilvC*		*ilvC*
SERP1670	*leuB*	3-isopropylmalate dehydrogenase				*leuB*	*leuB*		
SERP1671	*leuC*	isopropylmalate isomerase large subunit			1.7	*leuC*	*leuC*		

Table 3.5 (continued)

			DC		HOCl			H_2O_2	
			S. epi RP62A	*B. subtilis* 168	*S. epi* RP62A	*S. aureus*	*S. aureus* MW2	*S. aureus* NCTC 8325	*S. aureus* MW2
SERP	SERP	SERP Gene Description	FC	gene	FC	gene	gene	gene	gene
SERP1672	*leuD*	3-isopropylmalate dehydratase, small subunit			1.7	*leuD*	*leuD*		
SERP1702	*sceD*	sceD protein			2.4		*sceD*		*sceD*
SERP1724		modification methylase, HemK family					*hemK*		*hemK*
SERP1748		Dps family protein		*mrgA*		*dps*	*dps*	-	*dps*
SERP1749		hypothetical protein			-3.1	-		-	-
SERP1756		cation efflux family protein		*czcD*	-2.1				*czrB*
SERP1771		hypothetical protein			-1.9			-	-
SERP1774		hypothetical protein			-1.3		-		-
SERP1778		hypothetical protein			2.1				-
SERP1779		hypothetical protein			1.9	-			*sbnC*
SERP1866		acyl-CoA dehydrogenase-related protein		*ydbM*	1.7	-			
SERP1880		secretory antigen precursor SsaA	2.1		2.2	*lytM*	*ssaA*		*lytM*
SERP1884		secretory antigen precursor SsaA, putative					*ssaA*		*ssaA*
SERP1897		hypothetical protein					-		-
SERP1917		oxidoreductase, short chain dehydrogenase/reductase		*yhxD*	2.1				
SERP1918		amidohydrolase family protein		*yxeP*	2.8				*abgB*
SERP1953		DNA-binding response regulator	1.3		2.2				-
SERP1997		formate/nitrite transporter family protein		*ywcJ*	-1.9		*focA*		
SERP2004		amino acid ABC transporter, permease protein		*yxeN*	2.1				
SERP2008		cation efflux family protein		*yeaB*					*czcD*
SERP2024	*lytS*	sensor histidine kinase LytS					*lytS*		*lytS*
SERP2025	*lytR*	response regulator LytR			-1.3		*lytR*		*lytR*
SERP2043		peptidase, M42 family			2.2				*frvX*
SERP2082		acetyltransferase, GNAT family					-	-	-
SERP2083		glyoxalase family protein			3.6	-			
SERP2115		pyruvate oxidase		*ydaP*		-			
SERP2120		secretory antigen precursor SsaA-related protein	-1.4				-		-
SERP2182	*nrdG*	anaerobic ribonucleoside-triphosphate reductase activating	1.0		-1.2		*nrdG*		*nrdG*
SERP2183	*nrdD*	anaerobic ribonucleoside triphosphate reductase			-1.2		*nrdD*		*nrdD*
SERP2211		hypothetical protein					-		-
SERP2304	*hisB*	imidazoleglycerol-phosphate dehydratase		*hisB*	1.6		*hisB*		
SERP2305	*hisD*	histidinol dehydrogenase		*hisD*	2.0				
SERP2323		IS1272-like transposase, degenerate			1.9		-		-
SERP2338		peptide synthetase		*ppsB*			-		-
SERP2358		amino acid ABC transporter, ATP-binding protein			1.6		*opuCA*		*opuCA*
SERP2384		hypothetical protein			2.4	-			
SERP2391	*sspC*	SspC protein					-		-
SERP2418		hypothetical protein					-		-
SERP2434		rhodanese-like domain protein			2.7	-			
SERP2435		metallo-beta-lactamase family protein			3.1	-			-
SERP2465		lipoprotein, putative					*lpl10*		*lpl10*
SERP2489	*kdpD*	sensor histidine kinase KdpD					*kdpD*		*kdpD*
SERP2513		hypothetical protein			2.5	-	-		
SERP2514		hypothetical protein			2.5	-			
SERP2520	*mecR1*	methicillin-resistance regulatory protein MecR1			-2.0		*mecR1*		*mecR1*
SERP2542		hypothetical protein	-1.6				-		-

The operon codes for a hypothetical protein (SERP0243) predicted to be a transcriptional regulator and a pyridine nucleotide-disulfide oxidoreductase family protein (SERP0242) annotated with GO terms for cell redox homeostasis, electron transport, and oxidoreductase activity. This operon was also among the top ten highest FCs for the 197 genes on the DC perturbed gene list as well as the 1,033 genes on the chlorine perturbed gene list with the 11^{th} and highest absolute FCs for DC and the 8^{th} and 2^{nd} highest absolute FCs for chlorine for SERP0242 and SERP0243, respectively. Two single gene operons were significant below the 2 FC cutoff for DC but were also upregulated in the chlorine treatment of this study and the chlorine and hydrogen peroxide comparison studies by Chang et al. (Chang et al., 2007; Chang et al., 2006). SERP1187 is annotated as a bacterial luciferase family oxidoreductase. SERP0542 is described as an Oye family NADH-dependent flavin oxidoreductase. SERP0242, SERP1187, and SERP0542 also grouped in the DC cluster U^{III}.

Two additional genes or homologue genes were identified in all the chlorine treatments but not the DC or H_2O_2 treatments. SERP0207 codes for an SdrG protein, a fibronectin binding adhesin. SERP2513 and SERP2514 are predicted to be on a two gene operon coding two hypothetical proteins, the later which only overlapped with the chlorine treatment reported by Chang et al. (Chang et al., 2007) but might reflect an important but unknown chlorine response operon.

It is important to note that our gene lists and all but the Szkotak study reported FC in the treatment compared to a parallel, untreated control sample (Chang et al., 2007; Chang et al., 2006; Palazzolo-Ballance et al., 2008). In contrast, the Szkotak et al. study

reported FC for DC treatment compared to the same 15 minute duration exposure to pretreated medium to minimize responses to electrolytic products in the results (Szkotak et al., 2011). Thus, many of the effects we have hypothesized to be the cause of DC effects on with a FC≥2 for our FC in compared biofilms, such as chlorine production, may not be reflected in the Szkotak et al. results. No overlap between the two DC treatments (this study and *B. subtilis*) were observed to the control and the FC reported by Szkotak et al. thus our DC treatments were compared to the other oxidative treatment.

Two genes that fit the FC≥2 cutoff for inclusion in the table for two or more studies including the Szkotak et al. DC study and were significant for our DC treatment but at FC<2 were *ahpF* with a FC=1.3 for our DC treatment and *trxB* (*yumC* in *B. subtilis*) at FC=1.4 for our DC treatment and FC=3.2 for our chlorine treatment. The *ahpFC* operon codes for two subunits of an alkyl hydroperoxide reductase, identified to protect the cell from DNA damage by alkyl hydroperoxides (STRING database, (Jensen et al., 2009)). *trxB* codes for a thioredoxin reductase. Both of these genes have been identified as *S. aureus* oxidative stress response enzymes that include catalase (KatA), alkyl hydroperoxide reductase (AhpCF), thiol peroxidase (Bcp) and thioredoxine reductase (TrxB) all of which are regulated by a manganese- and iron-responsive peroxide operon regulator, PerR (Horsburgh et al., 2001a; Horsburgh et al., 2001b). Upregulation of transcripts for these enzymes has been reported in response to hydrogen peroxide stress in *S. aureus* even though levels of the regulator PerR were unchanged (Horsburgh et al., 2001a). A fifteen minute exposure to 3 mg/L HOCl was also reported

to induce *trxB, bcp, katA*, and *mrgA* on the PerR regulon but not *ahpC* (Maalej et al., 2006).

As the only study reporting gene responses to DC exposure, an attempt was made to further compare the work by Szkotak et al. to this study using a measure of FC for direct current treatment compared to the chlorine treatment. There were several problems with this comparison. The number of differentially expressed genes in the chlorine treatment was five times that of the DC treatment at the same cutoff, typically with much larger FCs. Thus a moderately upregulated DC gene and a highly upregulated chlorine gene would be calculated as a downregulated FC for DC with respect to chlorine. This comparison does not work. A better measure of unique effects due to electric current flow through biofilm could be seen by comparing genes that were significantly changed in our DC treatment and not in our chlorine treatment or upregulated in our DC treatment and downregulated in our chlorine treatment. Eleven of the genes from the Szkotak et al. list were significant in the DC treatment (any FC list, DC FCs between -1.3 to 1.7). Seven of these genes were significant for both DC and chlorine treatments with the same trend (upregulated in both treatments or downregulated in both treatments) and were not considered as a response unique to DC treatment but not chlorine. SERP2031 had small and opposite FCs of FC=-1.2 for DC and FC=1.3 for chlorine but as this gene was downregulated (not upregulated) for DC treatment, this is not indicated as a DC specific response over chlorine treatment that would correlate to the comparison of Szkotak et al. Two genes (*rsbV* and SERP2061) were significantly downregulated following our DC treatment but not significant for chlorine treatment but again the direction of the

difference does not correlate to the upregulation reported by Szkotak et al. The only gene that was significantly upregulated in our DC treatment (FC=1.6, p-value=0.033) but not significant in the chlorine treatment for α=0.05 (FC=1.5, p-value=0.054) was SERP2075 indicated to code for a DedA family protein. As the p-value for the chlorine treatment was just outside the significance level of this study, further experiments would be warranted to confirm a DC-unique response. Taken together, this comparison fails to strongly identify DC-unique gene responses found in both this study and the previous DC treatment of *B. subtilis* (Szkotak et al., 2011) that were not also observed with chlorine or hydrogen peroxide treatments.

Discussion

Direct electric current (DC) has been proposed as a treatment strategy for biofilm infections *in vivo*. We have previously reported a significant killing efficacy due to DC application to bacterial biofilms at approximate physiologic conditions, particularly in respect to a physiologically relevant chloride concentration (9 g/L NaCl). At these conditions the mechanism of the effect appears to be electrolytic generation of Cl_2 gas which immediately reacts to HOCl and OCl^- in an aqueous solution, two forms of free chlorine with strong disinfection power. This mechanism is supported by demonstrations of similar efficacy of medium pre-treated with DC (Davis et al., 1992; Pareilleux and Sicard, 1970; Sun et al., 2012) or by a representative dose of free chlorine (Sandvik et al., 2013; Venkitanarayanan et al., 1999) where bacteria were never directly exposed to current.

In the work reported here we went beyond viability measures of DC effects by using global gene expression to investigate gene level changes due to electric current exposure. To our knowledge, this is the first global transcriptome study of electric current effects in biofilm complementing the only previous global transcriptome study of electric current effects on planktonic bacteria (Szkotak et al., 2011). The pattern of gene expression resulting from DC treatment demonstrated significant overlap with the set of genes associated with chlorine treatment. This finding is consistent with the proposed mechanisms of action of DC effects in the presence of chloride. In this study, a 4 hour, 0.7 mA/cm^2 DC exposure was compared to a single dose of HOCl representative of the cumulative chlorine electrolytically generated over the exposure time. The chlorine treatment would approximate a pretreated solution with respect to chlorine but would lack any additional residual biocidal properties unique to a previously electrolyzed solution. Electrolysis of a medium may produce oxidized chemical species in addition to chlorine that would not be found in a HOCl solution. In response to DC treatment, 103 significantly upregulated genes and 93 significantly downregulated genes were identified (p-value≤0.05) although the magnitude of gene responses were generally small with maximum significant FC=2.2 and -2.2 (32 upregulated and 36 downregulated genes had |FC|≥1.5, Table 3.3). In contrast, 546 upregulated genes and 482 downregulated genes were identified in response to chlorine treatment at the same significance level with large changes in transcript levels with maximum FCs of -7.2 to 20.9 (452 upregulated and 366 downregulated genes had |FC|≥1.5, 179 upregulated and 160 downregulated genes had |FC|≥2, see gene list in APPENDIX A, Table A.2). When comparing the study design,

we report gene responses to a continuously replenished disinfectant at a low concentration (DC treatment) compared to a gene response and recovery following initial contact and incubation with a very high concentration of disinfectant (chlorine treatment). While these two treatments generated similar killing efficacy at higher current levels (Sandvik et al., 2013) and no killing at the treatment levels used in this study (Figure 3.1), electrolytically generated Cl_2 would occur over time and not in the sudden manner of the chlorine dose. While the DC treatment resulted in fewer significantly different genes with much smaller FCs in comparison to the chlorine treatment, a highly significant overlap was observed in the two gene responses. These results support HOCl generation as a predominant mechanism of direct current antimicrobial efficacy.

Analysis of the genes changing in response to DC treatment indicate a general stress response with upregulation of translation and catabolic metabolism to generate energy accompanied by downregulation of DNA metabolic processes that might indicate a decreased priority of replication and cell division . An oxidative stress response is possible. While this response could be attributed to chlorine species, some indication of a hydrogen peroxide response can be discerned based on upregulation of the staphylococcal antioxidants *trxB* and *ahpF* on the peroxide response PerR regulon, the identification of a cluster of upregulated genes annotated with oxidation reduction function in addition to several unclustered genes such as SERP0483, FC=1.9 coding for a putative thioredoxin and SERP2265, FC1.6 coding for an organic H_2O_2 resistance protein. Genes of the DC response overlapped with a large list of homologous genes upregulated in response to H_2O_2 in *S. aureus* (Table 3.5) although many of those same

genes also overlapped with chlorine treatments. The PerR regulon for antioxidant proteins was also reported to be upregulated by HOCl (Maalej et al., 2006). Liu et al. proposed H_2O_2 generation as a mechanism of electric current effects in bacteria (Liu et al., 1997). Our results do not support a hydrogen peroxide-only mechanism as our previous work failed to see similar levels of DC killing efficacy in the absence of chloride in the medium (Sandvik et al., 2013); presumably if H_2O_2 were produced electrochemically and was masked by larger chlorine effects, it would become evident when the chloride was absent. These results indicate a general oxidative stress response with DC treatment that could be induced by either agent, consistent with the general concepts of free chlorine as an oxidizing agent.

In this study global gene expression was used to compare treatment of *S. epidermidis* biofilms with DC and chlorine to elucidate mechanisms of DC killing efficacy. The strong overlap of genes of the *S. epidermidis* DC response with chlorine treatments in this study as well as homologues in chlorine treatments in other organisms (Table 3.5) provides additional evidence for a mechanism of direct current efficacy based on electrolytic generation of chlorine. While other mechanisms have been proposed based on studies in chloride-free medium *in vitro*, the inevitable presence of chloride in the body may dominate and mask those effects when chlorine electrochemistry is present. Knowledge of this chemistry is important to consider if DC is pursued as a treatment strategy in *vivo.*

CHAPTER 4: BIOLOGICAL EFFECTS OF EXTREMELY LOW-FREQUENCY MAGNETIC FIELDS ON STAPHYLOCOCCUS EPIDERMIDIS BIOFILMS

Abstract

Colony biofilms were studied using global transcriptomics to determine whether *S. epidermidis* detect or exhibit a response to growth in extremely low-frequency magnetic fields (ELF-MF). Biofilms were inoculated on porous membranes on tryptic soy agar containing 9 g/L total NaCl (physiologic saline concentration) and grown at 37˚C in the presence or absence of a magnetic field for 24 hours. The 60 μT (600 mG) static component of the magnetic field was at the range of the geomagnetic field in all treatments. Changes in gene expression were compared at two ELF-MF frequencies, 23.5 and 45.9 Hz, the ion resonance frequencies for K^+ and Ca^{2+}, respectively. An additional comparison examined the effect of the magnitude of the time-varying magnetic field component, B_{AC}, at 40 μT (400 mG) and 108 μT (1080 mG) when the frequency remained constant. Gene expression in each field tuning was compared to control biofilms grown in the static magnetic field only. At B_{AC}=40 μT (400 mG), microarray results identified more significantly changing genes at 23.5Hz (174 genes) compared to 45.9Hz (10 genes). The effect of varying B_{AC} was examined at 23.5 Hz. More differentially expressed genes (725 genes) were identified at B_{AC}=108 μT (1,080 mG) compared to the 174 genes identified at B_{AC}=40 μT (400 mG). Analysis of the 725 genes differentially expressed at 23.5Hz at the higher B_{AC}, indicated upregulation of two-component signal transduction systems including the *kdp*ATPase potassium uptake system and the *lytRS* system reported to respond to dissipation of the proton motive force

(PMF) in *S. aureus*, as well as ABC-transporters, ion transport systems including six Na^+/H^+ antiporters, and osmoprotectant systems indicating a possible membrane transport related effect. Transposition activity was also highly upregulated in the ELF-MF compared to control samples and could suggest cell damage caused by the ELF-MF. This frequency specific membrane transport response is consistent with eukaryotic studies and may have potential as a means of modifying cell homeostasis and stressing bacterial cells in biofilms.

Introduction

The study of electromagnetic effects on biological systems has been a subject of enduring interest and scientific inquiry for over fifty years. Much of the early motivation stemmed from societal concerns of daily exposure to anthropogenic sources such as power line frequencies of 50 or 60Hz and the magnetic fields (MFs) they emit. These magnetic fields have frequencies in the extremely low-frequency (ELF) range, 3-300Hz, and most are considered weak, on the order of the 25-65μT (250-650mG) geomagnetic field. While initial studies examined potential mutagenic effects of ELF-MF, many biological responses have since been associated with weak ELF-MF exposure across a range of frequencies in a variety of biological systems (Blank and Goodman, 2009; Liboff, 2005; Madkan et al., 2009).

Studies of ELF-MF effects primarily vary three properties: the magnitude of the static component of the MF, B_o; the magnitude of the time-varying MF component, B_{AC}; and the frequency of the MF, f. Additionally, the MF signal type may be varied from a continuous sinusoidal field (used in most studies) to intermittent or pulsed MFs. Based

on these parameters, studies can be grouped into two primary classes. The first class studies potential mutagenic effects at the fixed 50 or 60Hz power line frequencies. Most of these studies have examined time-varying MF components several orders of magnitude higher than the geomagnetic field. Many eukaryotic studies and the majority of *E. coli* studies focus on potential mutagenic effects. The second class of studies report biological responses at distinct frequencies of the ELF-MF. Early studies of combined electromagnetic field (EMF) effects in biological tissues found ranges of frequency in which maximal electromagnetic responses were observed. These responses were measureable as calcium efflux from avian brain tissues and were referred to as "frequency windows" (Bawin and Adey, 1976; Blackman et al., 1985; Blackman et al., 1982). These types of responses do not scale linearly with increasing frequency.

Liboff proposed a theory to explain these frequency-dependent responses, based on observation that these "frequency windows" correlate with ion resonance frequencies of biologically relevant ions (Liboff, 1985). The resonance frequency for a given ion is proportional to the product of the charge to mass ratio, q/m, specific to that ion and the static magnetic field component, B_o, but is independent of B_{AC}. Thus if B_o remains constant, each ion has a fundamental resonance frequency that is generally unique. Therefore, the peak windows of activity could be described by resonance frequencies for certain ions. The original hypothesis proposed a mechanism for enhanced calcium and potassium ion transport through membrane channels based on an ion cyclotron resonance (ICR) model, leading to changes in cellular functioning and signaling (Liboff, 1985). An alternate explanation based on an ion parametric resonance (IPR) model proposed that

ion resonance frequencies alter ion binding at interaction sites in calcium-binding proteins (Blanchard and Blackman, 1994; Lednev, 1991; Liboff, 1985). While these models effectively predict the frequencies for biological responses, the physical mechanisms describing the ELF-MF interactions are based on models at conditions far from the complexity of biological systems. For example, vacuum is assumed for modified ion motion with ICR. Liboff countered these issues proposing that within the ion channels, ions would no longer be hydrated or subject to the many damping factors that would preclude this type of motion in liquid (Liboff, 1985; Liboff, 2005), however this explanation is still debated. Consequently, after three decades of adapted models, there is no widely accepted mechanism to describe ELF-MF responses despite a continually growing body of evidence for biological responses at those frequencies. The body of evidence is primarily reported in eukaryotes, some with "opposite" responses for frequencies of different ions (for a review see Liboff, 2005). As examples, calcium is required for diatom mobility (Cooksey and Cooksey, 1980). Diatom motility is enhanced in an ELF-MF at a Ca^{2+} resonance frequency (McLeod et al., 1987a; McLeod et al., 1987b; Smith et al., 1987). However, ELF-MF exposure to a K^{+} resonance frequency inhibits motility (McLeod et al., 1987b). ELF-MFs have been reported to enhance bone growth at Ca^{2+} or Mg^{2+} resonance frequencies, whereas at a K^{+} frequency bone diameter and healing were reduced in the same studies (Deibert et al., 1989; Deibert et al., 1994; Regling, 2001; Smith et al., 1991). These stimulatory effects have led to current technologies utilizing ELF-MF in human medicine for bone healing and wound healing.

In the study presented in this Chapter, ELF-MF effects were investigated in bacterial biofilms at ion resonance frequencies. A discussion of previous ELF-MF effects reported in bacteria follows. As can be seen in the summary of experimental settings (Figure 4.1), a majority of these studies have used a 50Hz powerline frequency. ELF-MF effects in bacteria have primarily focused on mutagenic responses and several bacterial studies identify frequency windows of peak biological responses. Studies in bacteria started with concern of possible mutagenic properties of ELF-MFs found in homes, work environments, and the modern world. Bacteria were considered simple,

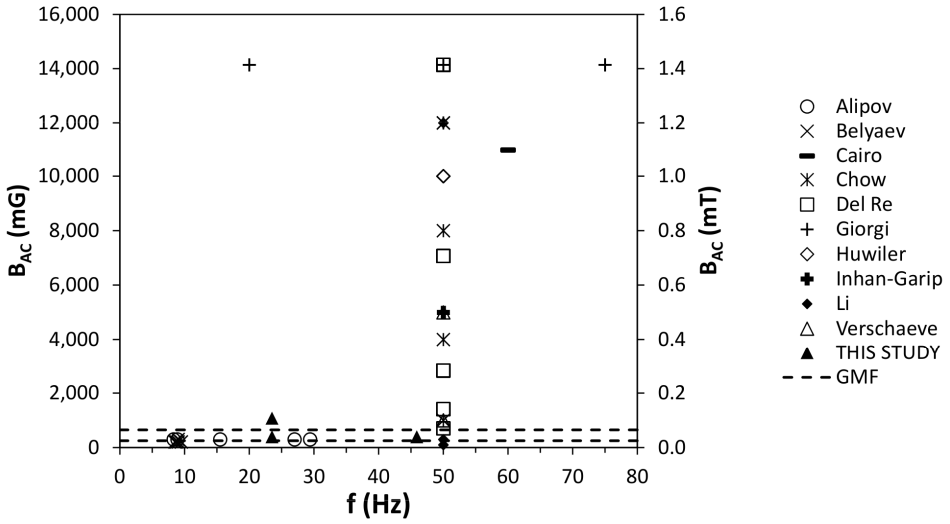

Figure 4.1 Summary of ELF-MF settings studied in bacterial system. Bacterial species were as follows. *Escherichia coli* was studied by Belyaev (Belyaev, 2011; Belyaev et al., 1998; Belyaev et al., 1995), Cairo (Cairo et al., 1998), Chow (Chow and Tung, 2000a, b), Del Re (Del Re et al., 2004; Del Re et al., 2006; Del Re et al., 2003; Del Re et al., 2009), Giorgi (Giorgi et al., 2011), Huwiler (Huwiler et al., 2012), Inhan-Garip (Inhan-Garip et al., 2011), Li (Li and Chow, 2001); *Enterococcus faecalis, Klebsiella pneumoniae, Pseudomonas aeruginosa, Staphylococcus aureus* were studied by Inhan-Garip (Inhan-Garip et al., 2011); *Salmonella typhimurium* was studied by Vershaeve (Verschaeve et al., 2011); and *Staphylococcus epidermidis* was studied by Inhan-Garip (Inhan-Garip et al., 2011) as well as the study presented in this Chapter. Symbols indicate settings by lead author and may represent multiple studies. The 250 and 650 mG boundaries of the geomagnetic field (GMF) are indicated.

well-known systems in which to study ELF-MF effects without compounding factors found *in vivo*. The bulk of this work was done with *E. coli* at frequencies of 50 or 60 Hz and magnetic field strengths ranging from 0.07-1.4 mT (700-14,000 mG), predominantly using two heat shock proteins or transposition activity as measures of a response.

Measures of mutagenic effects have included measures of stress response as mRNA coding for σ^{32}, the heat shock proteins DnaK/J and GroEL, and transposition of transposable DNA elements that could indicate genomic instability. Cairo et al. reported that MFs induced upregulation of *E. coli* mRNA coding for σ^{32}, a protein involved in bacterial recognition of stress promoters by RNA polymerase (Cairo et al., 1998). Chow and Tung reported several studies in which ELF–MFs were found to stimulate production of the DnaK/J and GroEL proteins, two heat shock proteins (Chow and Tung, 2000a, b). While elevation of heat shock proteins could indicate stress, a surprising finding suggested instead of being mutagenic, the ELF-MF enhanced DNA repair (Chow and Tung, 2000a), although the group also reported DNA degradation from ELF-MF exposure (Li and Chow, 2001). Studies by Del Re et al. confirmed the increased production of DnaK and GroEL proteins in *E. coli* with a sinusoidal MF, however saw decreased protein production with a pulsed MF in comparison to a sham control indicating the MF wave shape may affect outcomes (Del Re et al., 2006). To determine if the MFs were simply inducing a heat shock response, an *E. coli* mutant unable to trigger production of DnaK and GroEL in response to a 42˚C heat shock treatment was, instead, exposed to the ELF-MF. The mutant produced elevated levels of DnaK and GroEL in response to the ELF-MF, implying the ELF stress response and the heat stress

response to be two separate pathways with similar responsive elements (Del Re et al., 2009). Measurements of the SOS response as an indicator of DNA damage or genotoxic effects in *Salmonella typhimurium* compared 1 and 2 hr exposures to four chemical mutagens vs. a 50 Hz field at 0.1 and 0.5 mT. Results found no SOS-dependent DNA damage due to the MF alone and no synergy between the agents and the magnetic field (Verschaeve et al., 2011).

Transposition of DNA elements in bacteria has also been studied as a measure of genetic stability in response to 50Hz ELF-MFs in *E. coli*, with contradictory results. Chow and Tung reported MF-enhanced transposition activity of a transposable DNA element (Tn5) within a mix of Tn5 and non-Tn5 cells accompanied with higher levels of DnaK in a sinusoidal field (Chow and Tung, 2000b). As transposition is known to depend on supercoiling of the DNA, it was proposed that the magnetic field induced a stress response and the production of DnaK, which binds with DNA gyrase, leading to supercoiling of the DNA and enhanced transposition activity (Chow and Tung, 2000b). In contrast, othere studies observed a decrease in transposition activity of a Tn10 element with sinusoidal MFs however increased transposition activity was reported with a pulsed magnetic field (Del Re et al., 2004; Del Re et al., 2003; Giorgi et al., 2011). These transposition trends for the sinusoidal and pulsed wave shapes held across varying frequencies and time with no difference at 20, 50, and 75 Hz or treatment times of 15 and 90 minutes (Giorgi et al., 2011).

Finally, the effects of ELF-MF on bacterial viability and colony morphology also show contradictory responses. Del Re et al. reported enhanced viability with a sinusoidal

MF and decreased viability for pulsed MF at 0.07-1.4mT B_{AC} (Del Re et al., 2004; Del Re et al., 2003). Growth stimulatory effects were also reported in the frequency-dependent studies at 0.02-0.03mT $B_{AC,}$ magnitudes below the geomagnetic field (Belyaev, 2011). In contrast, Fojt et al. reported a decrease in *Staphylococcus aureus*, *Escherichia coli*, and *Leclercia adecarboxylata* colony forming units (CFUs) in less than 30 minutes with a 50 Hz, higher magnitude 10 mT B_{AC} (Fojt et al., 2004). Decreased growth rates and modified cell morphology of *E. coli, Enterococcus faecalis, Pseudomonas aeruginosa, Klebsiella pneumonia, S. aureus,* and *S. epidermidis* have also been found following a 6 hr exposure in a 50 Hz, 0.5 mT B_{AC} (Inhan-Garip et al., 2011). In a recent study, optical density (OD), CFU, cell morphology, and global gene expression with microarray were measured in *E. coli* in response to 2.5 and 15 hr exposures to sinusoidal, sinusoidal intermittent, and pulsed MF (50 Hz, 1 mT). No changes in OD, CFU, cell morphology, or significant changes in gene expression were seen for any condition at the study cutoffs ($|foldchange| \geq 2$, p-value≤ 0.01) (Huwiler et al., 2012)

With exception of the Giorgi et al. study which studied 20 and 75 Hz in addition to 50 Hz (Giorgi et al., 2011), all of the above studies used either 50 or 60 Hz and B_{AC} many orders of magnitude higher than the geomagnetic field. Work by Belyaev, Alipov, et al. have used anomalous viscosity time dependency (AVTD) to study conformational changes in DNA and protein/DNA association. They report finding one or more "frequency windows" of peak of maximum effects of a much lower 30 μT (300 mG) ELF MF over a range of 7-37 Hz for various strains of *E. coli* (Alipov and Belyaev, 1996; Alipov et al., 1994; Belyaev, 2011; Belyaev and Alipov, 2001; Belyaev et al., 1998;

Belyaev et al., 1995). These peak measurements represent peaks of DNA relaxation or changes in protein association with DNA. In some of the studies, frequency windows shifted between two strains of *E. coli* (Alipov and Belyaev, 1996; Belyaev and Alipov, 2001). The SOS-response, activated in response to DNA damage, was also assessed in comparison and in conjunction with the genotoxic agent nalidixic acid (NAL). Decreases in AVTD and an SOS response were observed with NAL, a response characteristic of DNA damage. However, ELF-MF exposure increased AVTD and bacterial growth (increased OD and CFU counts) but no induction of the SOS stress response was observed and the ELF-MFs were concluded to have a non-toxic, growth stimulatory effect on *E. coli* (Belyaev, 2011).

Belyaev and Alipov also compared their frequency-dependent responses with the theoretical models proposed in eukaryotic systems. The first was the ion cyclotron resonance (ICR) model (Liboff, 1985; McLeod et al., 1987b; Smith et al., 1987) predicting ELF effects at:

$$f_n = nf = \left(\frac{n}{2\pi}\right)\left(\frac{q}{m}\right)B_o \text{ where } (n = 1,3,5 \ldots) \quad (4.1)$$

The second was the ion magnetic parametric resonance (Blanchard and Blackman, 1994; Lednev, 1991) predicting ELF effects at frequencies:

$$f_n = \frac{f}{n} = \left(\frac{1}{2\pi n}\right)\left(\frac{q}{m}\right)B_o \text{ where } (n = 1,2,3 \ldots) \quad (4.2)$$

where q is the charge of the ion, m is the mass of the ion, B_o is the static magnetic field component, and n represent harmonics or subharmonics of the two models, respectively. They found the *E. coli* resonance frequency windows could be explained by one or both

models for harmonics or subharmonics of Na, K, Ca, Mg, and Zn ions indicating support of resonance frequencies in the study of biological and bacterial systems (Belyaev and Alipov, 2001).

The controversy surrounding the resonance theories is that ion resonance is usually assumed to occur in vacuum, a far extreme from what would be seen in the aqueous milieu of biological systems. In a recent review by Blank and Goodman, the lack of a mechanism or principle that could be applied to all MF study was again discussed (Blank and Goodman, 2008). They propose that the variety of reported effects might be explained by changes in transcription due to EMF alteration of electron transfer in DNA during transcription initiation (Blank and Goodman, 2004) or as an effect of acceleration of the Na,K-ATPase and ion pumping as has been reported in eukaryotes (Blank, 2005). Regardless of the mechanism, evidence exists for ELF-MF effects on membrane associated ion transport in higher organisms.

In this study ELF-MF effects were investigated in bacterial biofilms. Bacteria in biofilms are difficult to kill with antibiotics because of their slow metabolism and poor antibiotic delivery through the biofilm matrix. We previously investigated whether those bacteria would be susceptible to direct current (DC) either alone or in synergy with antibiotics (Chapters 2 and 3). DC has killing efficacy against biofilm, however, current flow *in vivo* requires insertion of electrodes and may be inhibited through a variety of tissue types. In contrast, ELF-MF will penetrate skin tissue without hindrance. ELF-MFs were studied in biofilm at a fundamental level. Effects could be inhibitory or stimulatory. Stimulatory effects could be advantageous as increased metabolic activity

may render antibiotics more effective. To our knowledge, no previous studies have addressed ELF-MF effects on biofilms.

The purpose of this investigation was to study *S. epidermidis* biofilm responses to growth in weak, extremely low-frequency magnetic fields (ELF-MF) on the order of the geomagnetic field. As the potential effects of ELF-MF were unknown, a global transcriptomic approach using microarrays was employed to detect any change in gene expression that could be indicative of a bacterial response. Based on evidence for modification of ion-transport processes in higher organisms, we further hypothesized that ELF-MF may modify ion transport and ion interactions in bacteria. These types of changes could disrupt cell homeostasis and subsequent cell regulation leading to cell damage or conversely could have stimulating effects, boosting metabolism of these relatively slow growing bacteria thus increasing their susceptibility to antibiotics. We chose ELF-MF frequencies based on the ion resonance frequencies for Ca^{2+} and K^{+}, two biologically relevant ions. Under these conditions we addressed a series of questions. The first was to determine if *S. epidermidis* biofilms detect and respond to magnetic fields. If a bacterial response was detected, we would address whether the effects were specific to certain magnitudes or frequencies of the magnetic field. If tuning-specific effects were observed, we sought to determine if those tunings or frequencies were specific to the ion resonance frequencies for biologically relevant ions. And finally, if biological responses were specific to ELF-MF resonance tunings for certain ions, could the changes in gene expression be linked to the target ion?

Methods

ELF Magnetic Field Exposure Setup

The magnetic fields used in these experiments were generated in a 66.0 cm long, 20.3 cm diameter solenoid designed for the magnetic field exposure of bacterial biofilms (Figure 4.2). The design and calibration of this system was previously described in detail (McLeod and Sandvik, 2010), APPENDIX B). Three separate, non-overlapping coils, each 47 turns, were wrapped over a 62 cm length of the solenoid form. One of the coils was connected to a DC power supply for adjustment of the static component of the magnetic field. The other two coils were connected to an AC/DC power supply (Circuitmate Function Generator FG2) with a power amplifier (N4L Laboratory Power Amplifier LPA01) and used in series to generate the time-varying component of the magnetic field. A digital magnetometer (Schonstedt Digital Magnetometer Model 2220-S5), a digital oscilloscope (Tektronix Digital Storage Oscilloscope 2201), and a digital universal frequency counter (Circuitmate Universal Counter UC10) connected to a data recorder (Hewlett Packard 34970A Data Acquisition/Switch Unit with Agilent BenchLink Data Logger 3 Version 4.10.11) were used to monitor the total magnetic field. In all experiments the magnetometer probe was positioned vertically in the center of the solenoid, measuring the combined magnetic field from the two power supplies.

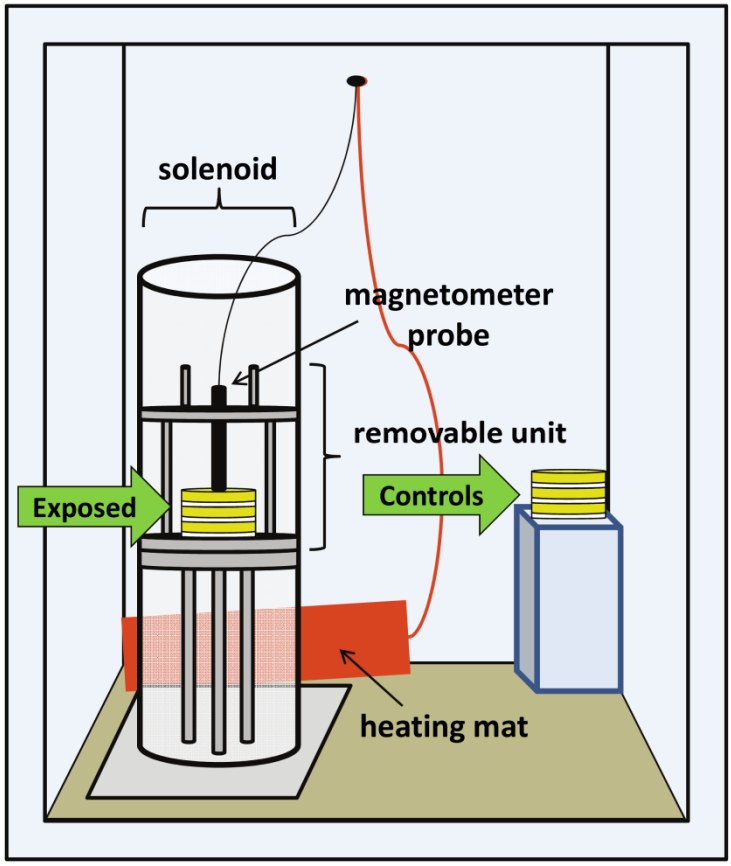

Figure 4.2 Magnetic field exposure setup. A solenoid was used to generate the magnetic field (diameter: 23.3 cm, height: 66 cm). A platform with a removable top unit was used to hold the biofilms in the center of the solenoid during exposure. A magnetometer in the center of the removable top unit was used to monitor the magnetic field parameters during exposure. Control samples were 45 cm away from the edge of the solenoid. The system was housed in an insulated, nonmagnetic chamber with a heating mat for adjusting the chamber temperature.

A platform inside the solenoid was designed to hold biofilm samples in a removable unit centering the samples vertically and radially in the solenoid. For this study, the glass tubes of the removable unit were removed and colony biofilms grown on agar plates were placed in the center of the unit for movement in and out of the field. A slot in the center of the lid of the unit held the magnetometer probe vertical just above the biofilm samples during exposure. The solenoid was housed in a non-magnetic, insulated

chamber to eliminate stray fields often found in conventional laboratory incubators. The temperature was maintained with a silicone heating mat and controller (Barnstead Thermolyne SRL06241).

Colony Biofilm Growth and Exposure

A full transcriptomic approach using microarray was used to detect biological effects in biofilms due to ELF-MF exposure. To optimize the chance of observing such effects, the magnetic field effects were studied for growing (metabolically active) biofilms. Colony biofilms (Figure 4.3) were grown on semipermeable membranes resting on an agar plate with growth and magnetic field exposure occurring simultaneously: An overnight culture of *S. epidermidis* RP62A was grown in tryptic soy broth (TSB) in a 37°C environmental shaker. The following day, the culture was diluted in phosphate buffered saline (PBS) to an OD of 0.05 at 600 nm. Black polycarbonate membranes (GE Water & Process Technologies, 25 mm diameter, 0.2 μm pore size, #K02PB02500) were pretreated under UV light for 10 minutes per side and placed on a tryptic soy agar (TSA) plate with added salt for a total salt concentration of 9 g/L NaCl (physiologic saline concentration).

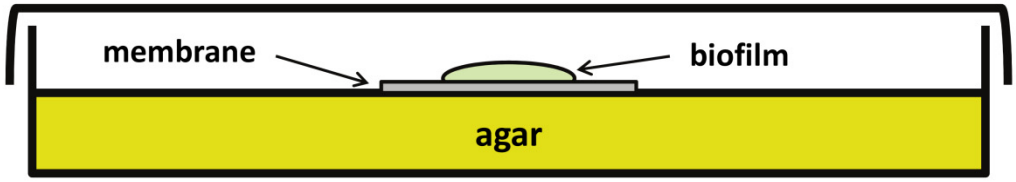

Figure 4.3 Colony biofilm. A porous membrane sits on top of the agar and a dilute planktonic culture is inoculated on the center of the membrane. The 0.22 μm pore size of the membrane allows nutrient to diffuse up into the biofilm but prevents direct contact of the bacteria with the agar.

Each membrane was inoculated with 40 μL of the diluted culture. When the drops had absorbed into the agar, the plates were inverted and moved to the magnetic field exposure chamber. Field-exposed samples were placed in the removable top unit which was placed on the platform inside the solenoid. The biofilm samples were centered vertically and radially in the solenoid. Control samples were exposed to the static field only and were placed outside of the solenoid in the opposite corner of the insulated chamber. The time-varying component of the magnetic field was measured and shown to be zero or negligible at the control location (measurements of the decay of the magnetic field with distance outside of the solenoid were reported previously (McLeod and Sandvik, 2010), Appendix C). Biofilms grew for 24 hours at 37°C in the presence or absence of the magnetic field. Magnetic field parameters used in experiments are given in Table 4.1.

Table 4.1 Magnetic field tuning parameters. The static component of the magnetic field, B_o, was the same in all experiments. The frequency, f, was calculated for the target ion using the ion resonance frequencies as a function of B_o. The time-varying component of the magnetic field is given as B_{AC}. The ratio of the magnetic field components is given by h'. The controls were not in a controlled static field and were subject to B_{earth} approximated by the set point for B_o.

Target Ion	B_o, mG	B_{AC}, mG	f, Hz	$h' = B_{AC}/B_o$
Control	B_{earth}	---	---	---
Ca^{2+} (1st harmonic)	600	400	45.9	0.7
Ca^{2+} (3rd harmonic)	600	400	137.8	0.7
K^+ (1st harmonic)	600	400	23.5	0.7
K^+ (1st harmonic)	600	1080	23.5	1.8
Untuned Field	600	400	39.1	0.7

Bacterial Viability

Control and treated colony biofilms were sampled at the end of the 24 hour exposure. Each membrane with biofilm was lifted off the agar plate and placed in a

dilution tube containing 10 mL of sterile phosphate-buffered saline (PBS). The tubes were vortexed for 1 minute to disaggregate the biofilm from the membrane and each sample was serially diluted and plated on tryptic soy agar with 9 g/L total NaCl using the drop plate method (Herigstad et al., 2001). The colony forming units (CFU) on the plates were counted following overnight incubation at 37ºC. A biofilm log density (LD) of viable cells for each membrane was calculated using the mean CFUs counted over ten drops, the volume of each drop, the volume of liquid the biofilm was disaggregated in (the zero dilution), and the dilution at which the CFUs were counted:

$$LD = \log_{10}\left(\frac{CFU}{membrane}\right) = \log_{10}\left(\left(\frac{\overline{CFU_{drop}}}{vol_{drop}}\right)\left(\frac{vol_{zerodilution}}{membrane}\right)\left(10^{dilution}\right)\right) \quad (4.3)$$

RNA Extraction from Colony Biofilms

RNA extractions were performed using a modified protocol for enzymatic lysis with mechanical disruption using the RNeasy Protect Bacteria Mini Kit (Qiagen). Each membrane and colony biofilm was aseptically transferred to a 15 mL conical centrifuge tube containing 2.5 mL of PBS. Tubes were vortexed for 1 minute to disaggregate the biofilm. The membrane was then removed from the tube. After the membrane was removed, 5.0 mL of an RNA stabilizing agent (Qiagen RNA Protect) was added to the disaggregated sample. The sample was vortexed briefly and incubated at room temperature for 5 minutes. Samples were centrifuged at 6,000 rpm for 8 minutes at 25˚C and the supernatant was discarded.

For cell lysis, the biofilm pellet was resuspended in 20 µL of a 0.3 mg/mL (≥150 U/mL) lysostaphin (Sigma-Aldrich) solution in 200 µL TE buffer (pH 8.0, Amresco) and

incubated in a 37˚C shaker for 10 minutes, followed by 2 minutes on ice. A volume of 700 µL Buffer RLT (provided with kit) with β-mercaptoethanol (1% by volume) was added to the sample which was then transferred to a 2 mL conical screw-cap microcentrifuge tube containing 0.05 g of acid-washed glass beads (150-212 µm diameter, Sigma). Samples were processed in a cell disrupter (Savant /Bio101 FastPrep FP120) at maximum speed (setting 6.5) for four 30 second intervals with 20 second intervals on ice between each run. Samples were then centrifuged for 2 min to remove the beads (the centrifugation settings from this point on were 12,000 × *g* at room temperature (RT) unless otherwise indicated). The supernatant was transferred to a fresh microcentrifuge tube.

For RNA purification, 470 µL of 100% ethanol were added to the lysate and incubated at RT for 3 minutes. The lysate was transferred to an RNeasy Mini spin column (provided with kit) and centrifuged for 30 seconds in 700 µL volumes until all of the sample had run through the same column. Each volume was spun through twice (i.e. the flow-through from the first spin was reapplied to the column and spun through a second time before being discarded). The column was washed with 350 µL of Buffer RWI (provided with kit), centrifuged for 30 seconds and the flow-through was discarded. An on-column DNase digestion was performed per the RNeasy Mini Kit optional protocol using an RNase-Free DNase Set (Qiagen). In brief, 80 µL of a DNase 1 solution (70 µL of Buffer RDD, 10 µL of a 1,500 Kunitz units/uL DNase I stock solution) was added directly to the spin column membrane and incubated at RT for 15 minutes. A 350 µL volume of Buffer RW1 was added to the column and incubation continued for an

additional 5 minutes. The column was then centrifuged for 30 seconds and transferred to a new 2 mL collection tube with the flow-through discarded. A wash step was performed twice by incubating 500 µL of Buffer RPE (provided with kit) on the column for 3 minutes at RT and centrifuging for 30 seconds with the flow-through discarded. The column was then centrifuged for 1 minute to dry the membrane. If at this point additional liquid was identified, the column was transferred to a fresh 2 mL collection tube and dried for an additional minute by centrifugation. The column was transferred to a new 1.5 mL microcentrifuge tube and 50 µL of RNase-free water was added directly to the membrane. The column was incubated for 5 minutes at RT. The RNA sample was then eluted from the column with 1 minute of centrifugation. Samples were immediately frozen and stored at -70˚C. Aliquots of RNA samples were confirmed for quantity and chemical purity with a NanoDrop ND-100 spectrophotometer and for nucleic acid integrity on an RNA NanoChip with an Agilent Bioanalyzer 2100.

cDNA Synthesis

cDNA syntheses were performed with minor modification to the NimbleGen Arrays User's Guide adapted protocol for the Invitrogen SuperScript Double-Stranded cDNA Synthesis Kit (unless otherwise indicated, reagents were provided with this kit). RNA samples were transferred to nuclease-free 0.2 mL PCR tubes and concentrated to ≤10 µL in a SpeedVac vacuum concentrator. The volumes of samples were brought to 10 µL with DEPC water. For the first strand synthesis, one µL of random primers (Invitrogen) was added to the samples and incubated in a thermocycler for 10 minutes at 70˚C, followed by 5 minutes at 4˚C. A solution containing 4 µL 5X First Strand Buffer,

2 µL 0.1M DTT, and 1 µL 10mM dNTP Mix was added to each tube which were then incubated for 2 minutes at 42˚C. Two µL of SuperScript II RT was added to each tube which were then incubated for 4 hours at 42˚C. Upon removal, samples were placed on ice or stored at -20˚C. For the second strand cDNA synthesis, a solution consisting of 91 µL DEPC Water, 30 µL 5X Second Strand Buffer, 3 µL 10 mM dNTP mix, 1 µL 10 U/µL DNA Ligase, 4 µL 10 U/µL DNA Polymerase I, and 1 µL 2 U/µL RNase H was added to each tube and incubated for 2 hours at 16˚C. Following incubation, 2 µL of 5 U/µL T4 DNA polymerase was added to each tube and incubated at 16˚C for an additional 5 minutes. Samples were moved to a PCR chiller rack and 10 µL of 0.5 M EDTA (pH 8.0, Invitrogen) was added to each sample prior to storage at -20˚C. cDNA cleanup and precipitation were performed as follows: The samples were incubated for 10 minutes at 37˚C with 1 µL of 4 mg/mL RNase A (≥70 Kunitz units/mg protein, Sigma-Aldrich) in 10 mM Tris-Cl, pH 7.8. Each sample was transferred to a tube with 163 µL phenol:chloroform:isoamyl alcohol and vortexed well. The samples were transferred to Phase Lock Tubes and centrifuged at 12,000 × *g* for 5 minutes. The upper, aqueous layer was transferred to a clean microcentrifuge tube and combined with 16 µL 7.5 M ammonium acetate, 5 µL of 15 µg/mL GlycoBlue (Invitrogen), and 326 µL of ice-cold 100% ethanol with mixing by inversion between each addition. Samples were centrifuged at 12,000 × *g* for 20 minutes at RT and the supernatant was discarded. The pellet was washed twice by mixing 500 µL volumes of iced 80% ethanol (by volume in DEPC water) to the pellet, centrifuging for 5 minutes and discarding the supernatant. The pellet was dried in a SuperVac vacuum concentrator. The pellet was then rehydrated

in 20 μL of DEPC water. Samples were immediately frozen and stored at -70˚C. Aliquots of the cDNA samples were confirmed for quantity and chemical purity with a NanoDrop ND-100 spectrophotometer and for nucleic acid integrity on an RNA NanoChip with an Agilent Bioanalyzer 2100. One μg of cDNA was run on each array.

Microarrays

Microarrays were run on four-plex (4 arrays/chip) 4x72K NimbleGen microarrays (Roche) with a custom design for *S. epidermidis* RP62A. The design had targets for the transcripts of all the 2,526 protein-coding genes in the genome (2,494 genomic loci, 32 plasmid loci) with 14 probes per target transcript and an identical design on the same array for data confirmation. The arrays were processed by the Functional Genomics Core Facility (Montana State University) following the NimbleGen Protocol. The cDNA was labeled using a NimbleGen One-Color DNA Labeling Kit, hybridized to the array with a HS4 Hybridization System, scanned on an MS 200 Microarray Scanner with MS 200 Data Collection Software and images processed using the NimbleScan software. The robust multi-array average (RMA) algorithm was implemented to normalize expression across arrays for comparison as described by Irizarry (Irizarry et al., 2003). Following the RMA procedure, data were background corrected, log2 transformed, normalized with quantile normalization, and protected from outliers using a median polish robust procedure to generate expression levels in NimbleScan. The mean expression level of the two replicate designs on each array was used for further data analysis.

Differential Gene Expression and Analysis

Gene expression of the normalized data was compared with Welch's t-tests (for unequal variance) in the gene expression program FlexArray 1.6.1.1. All field tunings were compared to the same set of controls generating fold-changes in gene expression for each magnetic field tuning in comparison to the control. Fold changes (FCs) are presented as a symmetric FC centered on no change equivalent to FC=+/-1 (i.e. twice as much expression in the treatment would be a FC of 2, however a 2 fold decrease in expression would be a symmetric FC= -2 instead of FC=0.5). Each Welch's t-test was corrected for multiple comparisons using a standard Benjamini-Hochberg correction (Benjamini and Hochberg, 1995) and are presented for a 5%, 10%, 15%, and 20% false discovery rate (FDR).

Biological patterns and themes in the enriched gene lists were further explored using the freely assessable Functional Annotation Tools in the NIH bioinformatics Database for Annotation, Visualization and Integrated Discovery (DAVID) v6.7 (Huang et al., 2009a, b). DAVID is designed to explore biological relationships between genes based on annotated categories for each gene collected in the DAVID knowledgebase from dozens of public databases (see Supplemental File 2 of (Huang et al., 2009a) for information on sources). The following categories and specific annotations were selected for analyses (DAVID default settings): Functional Categories (Clusters of Orthologous Groups (COG) ontology, COG_ONTOLOGY; Swiss-Prot (SP) Protein Information Resource (PIR) keywords, SP_PIR_KEYWORDS; Universal Protein Resource (UniProt) sequence feature, UP_SEQ_FEATURE), Gene Ontology (for biological process, GOTERM_BP_FAT; for cellular component, GOTERM_CC_FAT; for

molecular function, GOTERM_MF_FAT), Pathways (KEGG Pathway, KEGG_PATHWAY), and Protein Domains (InterPro classification, INTERPRO; Protein Information Resource (PIR) SuperFamily classification, PIR_SUPERFAMILY; Simple Modular Architecture Research Tool (SMART) classification, SMART).

Given a list of gene identifiers for a list of interest (i.e. significantly upregulated genes, significantly downregulated genes, or all significantly changing genes), DAVID identified enriched categories under which multiple genes fell. As the only input for these lists were gene identifiers, any FC or statistical cutoffs were implemented before input into DAVID. The Functional Annotation Chart identifies genes falling under a single annotation and calculated statistics for the probability of that same overlap by random chance using the number of background genes, the number of genes in the input list, the number of genes in the input list that had the annotation of interest, and the number of possible genes in the background list that have the annotation of interest. The Functional Annotation Clustering tool further draws correlations between similar GO, pathways, or other annotations using fuzzy heuristics and generates an enrichment score for that group of genes.

Results

ELF-MFs did not Affect Cell Viability

One of the first questions to address was whether the magnetic field would affect biofilm growth. Colony biofilms were grown in the presence or absence of the magnetic field at seven magnetic field conditions. The results of LD measurements for 24 hour old biofilms grown in the presence or absence of the fields are displayed in Figure 4.4. Each

field tuning was compared to the control samples with t-tests. There were no differences in the LDs of colony biofilms grown in the presence or absence of the magnetic field at any of the conditions studied (control vs Ca^{2+}, 3rd harmonic p-value=0.071, all other p-values>0.26).

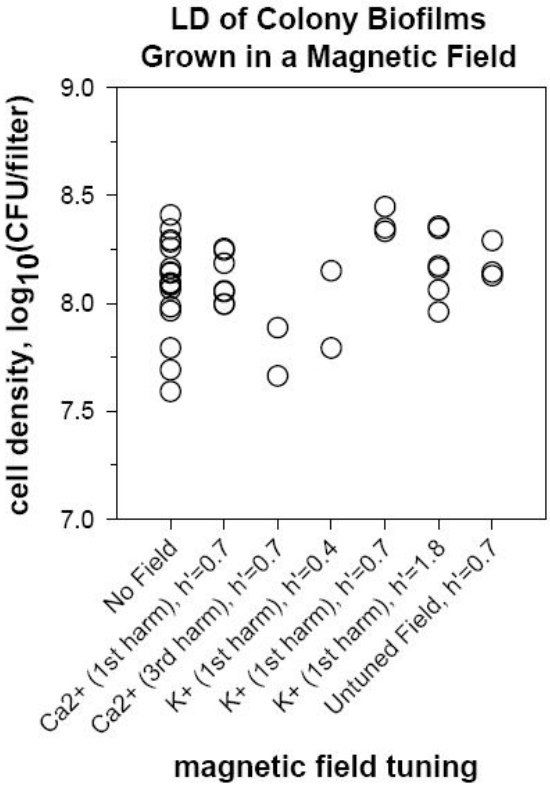

Figure 4.4 Viable of colony biofilms grown in the presence or absence of a magnetic field. All biofilms were grown for 24 hours at 37˚C. Symbols indicate the LD for an individual colony biofilm.

Changes in Gene Expression
were Observed when Biofilms
were Grown in ELF Magnetic Fields

Four magnetic field growth conditions were compared using global gene expression at two frequencies and with two variations in the ratio of field components ($h'=B_{AC}/B_o$): 1) no-field control; 2) Ca^{2+} tuning, h'=0.7; 3) K^+ tuning, h'=0.7; 4) K^+

tuning, h'=1.8. Replicate experiments were performed for each tuning condition with controls performed in parallel with all experiments. Replicate samples for each tuning were pooled across experiments. Welch's t-tests (for unequal variance) were used to compare gene expression levels of the field-grown samples for each field condition to the control samples to generate a fold change (FC) and p-value for each gene. The same control samples were used for all field comparisons. Both FC and p-value are used to distinguish lists of differentially expressed genes and traditional criteria of $|FC| \geq 2$ or $|FC| \geq 1.5$ with a p-value≤ 0.05 are often used. However, selection of the cutoff has been demonstrated to drastically change study conclusions (Dalman et al., 2012). For this study, we used a statistical cutoff but did not implement a FC cutoff for inclusion in tables and analysis. The numbers of differentially expressed genes for each condition were compared for multiple cutoffs and selections of false discovery rate (FDR) to be considered in the list of differentially expressed genes for upregulated, downregulated, and the sum of upregulated and downregulated genes indicated as "perturbed" (Table 4.2). Examining "perturbed" genes can provide insight into regulation where genes may be repressed or upregulated within the same pathway but might be missed if, for instance, only upregulated genes were considered. There were no significant differentially expressed genes for either the calcium or potassium tunings at h'=0.7 (10% FDR), even when the FDR was relaxed to 20%. In contrast, 293 genes differentially expressed genes were significant at the potassium tuning at h'=1.8 (10%FDR).

Table 4.2 Tally of differentially expressed genes for colony biofilms grown under three magnetic field conditions. Commonly used cutoffs for FC (fold-change in gene expression in comparison to the no-field control) and p-value are shown as well as a Benjamini-Hochberg correction for multiple comparisons tests for the indicated FDR (false-discovery rate). A total of 2,526 genes were on array corresponding to the all coding regions in *S. epidermidis*.

Target Ion	h'	n, arrays	PERTURBED GENES		UPREGULATED GENES					DOWNREGULATED GENES				
			p-value≤0.05	10%FDR	p-value≤0.05			15%FDR	10%FDR	p-value≤0.05			15%FDR	10%FDR
			any FC	any FC	any FC	FC≥1.5	FC≥2	anyFC	any FC	any FC	FC≤-1.5	FC≤-2	anyFC	any FC
No Field	0	6	---	---	---	---	---	---	---	---	---	---	---	---
Ca2+	0.7	4	10	none	4	1	0	none	none	6	0	0	none	none
K+	0.7	4	174	none	77	29	8	none	none	102	38	4	none	none
K+	1.8	3	725	293	339	191	41	275	138	386	187	56	326	155

Differential Gene Expression Changed with Frequency and the Magnitude of the Time-Varying Magnetic Field

For this analysis, the number of differentially expressed genes was used as a measure of the overall response to the ELF-MF at different tunings. All of the fields tested had the same static component of the magnetic field (600 mG), but varied in the frequency to target either calcium or potassium using the ion resonance tunings or in the ratio of the time-varying and static field magnitudes.

To assess frequency-dependent effects, the two tunings at h'=0.7 were compared. The only tuning difference between the calcium and potassium tuning when h'=0.7 was the frequency (f=45.9 Hz for calcium versus 23.5 Hz for potassium). When the frequency was 45.9 Hz (Ca^{2+} resonance, h'=0.7), only 8 genes were perturbed (p-value≤0.05), and at very small fold changes (one gene had a |FC|≥1.5). The same field strengths (h'=0.7) at the 23.5 Hz (K^{+} resonance, h'=0.7) frequency had 179 genes perturbed (p-value≤0.05), 66 of which had |FC|≥1.5 suggesting a dependency on the frequency.

In order to investigate the ratio of the time-varying component of the magnetic field to the static component ($h'=B_{AC}/B_o$), we compared the two potassium tunings with the same frequency, differing only in the magnitude of the time-varying component of the MF, B_{AC}. When B_{AC} was increased from 400 mG (h'=0.7) to 1080 mG (h'=1.8), the number of genes differentially expressed genes increased as did the magnitudes of those changes, identifying 725 perturbed genes (p-value≤0.05) of which 378 genes had a |FC|≥1.5 and 97 had a |FC|≥2.0. Additionally, all of the genes with p-values≤0.05 at the higher potassium tuning (h'=1.8) tuning were significant at a 20% FDR or less.

DAVID Analysis of Biological
Responses to K^+-tuned ELF-MF (h'=1.8)

As neither of the h'=0.7 tunings were significant at a 20% FDR, only the gene lists for the higher potassium tuning (h'=1.8) were further explored for biological themes. As pathway identification was desired, a moderate cutoff of all genes differentially expressed with an FDR≤15% was used to capture statistically significant changes in expression that might have small fold-changes but be biologically important in addition to those genes with larger changes in expression. Three gene lists were analyzed: upregulated genes (positive FCs, 275 genes), downregulated genes (negative FCs, 326 genes) and the combined list of all perturbed genes (601 genes).

Several functional annotation tools in DAVID were used to assess biologically important systems. The functional annotation chart tool identified individual gene annotations that were found for two or more genes in the input gene lists and was useful in identifying similar types of systems that might have different functions in the cell. The

chart tool identified 8 annotations in the upregulated gene list, 4 annotations in the downregulated gene list, and 2 annotations in the perturbed list that were significant at a Benjamini corrected p-value≤0.1 (see APPENDIX C, Table C.1). The functional annotation cluster tool grouped the related and redundant annotations in clusters to identify common themes in the input gene list. Five gene clusters were identified in both the upregulated and downregulated gene lists and 4 gene clusters were identified on the perturbed list with a DAVID generated enrichment score>1. Within these results, two KEGG pathways were identified in both the upregulated and the perturbed gene lists in the chart tool. Overlap of genes found in clusters and pathways can be seen in the cluster column in the following tables. Overlap of genes between clusters is shown in Figure 4.5. For specific annotations identified in each cluster see APPENDIX D Table D.1.

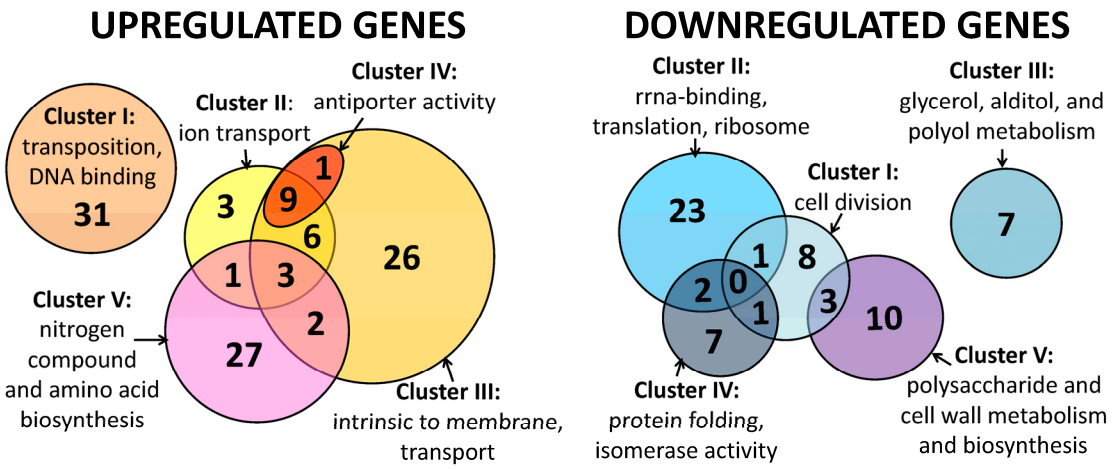

Figure 4.5 Summary of clusters and overlap of related genes identified by DAVID for genes with FDR≤15%. Each cluster was scored with an enrichment score (ES) for multiple clustered annotations (all clusters ES>1). Enrichment scores and the number of related genes in each cluster follow: upregulated gene clusters: I(ES: 3.2, 31 genes), II(ES: 2.04, 22 genes, III(ES: 1.77, 47 genes), IV(ES: 1.42, 10 genes), V(ES: 1.08, 33 genes); downregulated genes: I(ES: 2.05, 13 genes), II(ES: 1.67, 26 genes), III(ES: 1.41, 7 genes), IV(ES: 1.25, 10 genes), V(ES: 1.17, 13 genes). Labels for clusters were summarized from related annotations. Specific annotations within each cluster can be found in APPENDIX D Table D.1.

Growth in a Potassium-tuned Field (h'=1.8) Modifies Two-Component Systems and ABC Transporter Pathways

The genes changing in response to the K^+-tuned ELF-MF (h'=1.8) were analyzed with DAVID to determine what types of bacterial pathways were being affected. Two pathway types were identified based on KEGG_PATHWAY annotations: "two-component systems" (p-value=0.011 and 0.0026, from the upregulated and perturbed gene lists respectively) and "ABC transporter" annotation (p-value=7.3×10^{-5} and 0.013, from the upregulated and perturbed gene lists respectively). Bacterial annotations are often incomplete, thus the identified pathways were used to identify other genes of these systems that lacked the KEGG-specific annotation.

Two-component signal transduction systems (TCSs), considered to be a primary bacterial mode of sensing and responding to environmental changes (Capra and Laub, 2012), generally consist of a sensor histidine kinase that, upon receipt of a signal, phosphorylates a response regulator protein that modifies gene expression in the cell to adapt to change. *S. epidermidis* RP62A has been reported to have fifteen such systems (Gill et al., 2005), however they were not directly indentified, thus the following approach was utilized to identify the specific TCSs in the genome that might also be affected by the ELF-MF. Two types of annotations were used to identify two-component systems (TCSs). Genes with the "KEGG_PATHWAY: two-component system" annotation (47 identified in the genome) code for sensor histidine kinases, response regulators, and additionally as genes regulated by these systems. Using only this annotation, only eight adjacent, paired sensor/response regulator systems were identified.

Thus, TCSs were additionally identified using gene ontology (GO) annotations for "GO:0004871: signal transducer activity" (36 genes) within which were additional annotations for "GO:0000155: two-component sensor activity" (16 genes) and "GO:0000156: two-component response regulator activity" (16 genes). With these additional annotations, fifteen pairs of adjacent sensor histidine kinase and response regulator genes were identified in addition to several unpaired genes annotated with sensor or regulator activity. This approach identified the same number of TCSs reported previously (Gill et al., 2005)and were further assessed for differential expression.

Table 4.3 lists genes of two-component systems (TCSs) that were differentially expressed by growth in the higher magnitude potassium field. The majority of genes associated with two-component systems changed with adjacent genes on the same operon. All of the genes of the *kdpABC* potassium uptake system were significantly upregulated (all FC≥1.5) in response to the higher potassium-tuned field including the potassium limitation sensor histidine kinase, *kdpD*, of the *kdpDE* TCS system for that operon. *kdpC* was also identified with the eighth highest FC of the 275 genes significantly upregulated genes (15% FDR). Other upregulated genes include both genes of the *lytSR* TCS system, indicated to regulate cell death and biofilm formation in response to reduced membrane proton motive force (PMF) (Zhu et al., 2010) as well as three genes of the *trpEGDCFBA* operon indicated to be involved in tryptophan biosynthetic pathways in *S. aureus* (Proctor and Kloos, 1973). Several unknown TCS genes upregulated included an unidentified response regulator (SERP0889) and an ABC transporter permease (SERP0887) on the same operon, and another unidentified sensor

Table 4.3 Differentially expressed genes of two-component systems in response to growth in a potassium tuned magnetic field (h'=1.8). Annotations: KEGG_PATHWAY annotation for "two-component system" (K), "GO: signal transducer activity" (GO), genes without annotation are on the same predicted operon as a gene with one of the previous categories. Paired adjacent genes with "GO: two-component sensor activity" (S) and "GO: two-component response regulator activity" (R) are indicated under TCS function. (SA) indicates "GO: two-component sensor activity" annotation but no identifiable adjacent regulator. FDR corrections are for a 5% FDR (****), 10% FDR (***), 15% FDR (**), and 20% FDR (*). Genes additionally identified in cluster analysis are identified for upregulated (U) and downregulated (D) gene clusters with superscript corresponding to individual clusters.

Two-Component Systems

Locus	*Name*	Gene Description	TCS Functi	Annot.	Predicted SERP Operon	Fold Change	% FDR	Cluster
SEA0003	*blaZ-2*	beta-lactamase		K	0003	-2.0	*	
SERP0218		hydrolase, haloacid dehalogenase-like family			0215-0222	1.7	*	
SERP0220		acetyl-CoA acetyltransferase, putative		K	0215-0222	1.6	***	
SERP0221		hypothetical protein			0215-0222	1.8	**	
SERP0222		hypothetical protein			0215-0222	2.2	***	
SERP0245		transporter, putative		GO	0245-0246	1.4	**	U^{III}
SERP0311		hypothetical protein			0311-0315	-1.2	***	
SERP0428	*hprK*	HPr kinase/phosphorylase	SA	GO	0428-0432	-1.4	**	
SERP0430		acetyltransferase, putative			0428-0432	-1.4	*	
SERP0539	*kapB*	kinase-associated protein B		K	0539	1.6	**	
SERP0705	*ctaA*	cytochrome oxidase assembly protein		K	0705	1.5	*	
SERP0875	*glnR*	glutamine synthetase repressor			0875-0876	-1.2	*	
SERP0889		DNA-binding response regulator, LuxR family	R	GO	0886-0889	1.5	***	U^{I}
SERP0937	*trpE*	anthranilate synthase component I		K	0937-0943	2.2	***	
SERP0938	*trpG*	anthranilate synthase component II			0937-0943	1.3	*	
SERP0942	*trpB*	tryptophan synthase subunit beta		K	0937-0943	1.5	*	
SERP1256	*phoP*	alkaline phosphatase synthesis transcriptional regulatory protein PhoP	R	K,GO	1256-1255	-1.2	***	
SERP1265		NADP-dependent malic enzyme, putative		K	1265	-1.2	***	
SERP1385		sensor histidine kinase	S	GO	1385-1384	1.5	*	
SERP1423	*vraS*	sensor histidine kinase VraS	S	K,GO	1425-1422	-1.5	**	
SERP1425		hypothetical protein			1425-1422	-2.0	**	
SERP1461	*blaZ-1*	beta-lactamase		K	1461	-1.7	**	
SERP1491	*agrD*	accessory gene regulator protein D		K	1490-1493	-1.3	**	
SERP1953		DNA-binding response regulator	R	GO	1953-1954	-1.3	**	
SERP1954		sensor histidine kinase	S	GO	1953-1954	1.2	*	
SERP1982		sensor histidine kinase, putative	S	K,GO	1987-1981	-1.3	***	
SERP1984	*narI*	respiratory nitrate reductase, gamma subunit		K	1987-1981	-1.4	***	
SERP2024	*lytS*	sensor histidine kinase LytS	S	K,GO	2024-2027	1.8	***	U^{III}
SERP2025	*lytR*	response regulator LytR	R	K,GO	2024-2027	1.6	**	U^{I}
SERP2208		alkaline phosphatase family protein		K	2208	1.6	***	
SERP2485	*kdpC*	K+-transporting ATPase, C subunit		K	2485-2487	2.6	***	$U^{II,III}$
SERP2486	*kdpB*	K+-transporting ATPase, B subunit		K	2485-2487	1.5	***	$U^{II,III,V}$
SERP2487	*kdpA*	potassium-transporting ATPase subunit A		K	2485-2487	1.6	***	$U^{II,III}$
SERP2489	*kdpD*	sensor histidine kinase KdpD	S	K,GO	2489-2490	1.2	***	
SERP2531	*yycI*	yycI protein			2534-2531	-1.4	***	
SERP2532	*yycH*	yycH protein			2534-2531	1.3	**	
SERP2534	*yycF*	DNA-binding response regulator YycF	R	K,GO	2534-2531	1.5	***	U^{I}

histidine kinase (SERP1385). The response regulator *yycF* of the *yycFG* TCS system (also called *walKR*), involved in regulation of bacterial membrane and cell wall composition and cell permeability in *S. aureus* (Martin et al., 1999), was also upregulated. Two other genes on the same operon, *yycH* and *yycI,* were significantly upregulated and downregulated, respectively. These genes code for membrane associated proteins located outside the cell (Dubrac and Msadek, 2008) and have been individually identified as negative response regulators of the *yycFG* TCS system although it is not clear if these genes operate separately or together. An unidentified TCS had slight upregulation of the sensor component (SERP1954) and slight down regulation of the response regulator (SERP1953). The sensor protein *vraS* of the *vraSR* TCS, involved with control of the cell wall peptidoglycan biosynthesis in response to cell wall damage (Belcheva and Golemi-Kotra, 2008; Levinger et al., 2012), and a hypothetical protein on the same operon were significantly downregulated. Both beta-lactamases in the genome were also significantly downregulated.

ABC transporters genes were the other set of pathway types modified by growth in the ELF-MF. Table 4.4 lists ABC transport-associated genes that were differentially expressed by growth in the potassium-tuned field (h'=1.8). Two upregulated systems were probable osmoprotectant systems included all five genes of an amino acid ABC transporter predicted operon (SERP2358-2354) and one gene of a separate three gene predicted amino acid ABC transporter operon (SERP2030) both identified by COG designation as transport systems for proline and glycine betaine, osmoprotectants used by *S. aureus* and *S. epidermidis* (Gill et al., 2005).

Table 4.4 Genes of ABC transporters differentially expressed in response to growth in a potassium-tuned ELF-MF (h'=1.8). Annotations: KEGG_PATHWAY: "ABC transporter" (K), GO: "signal transducer activity" (GO), ABC transporter identified by "ABC transporter" in NCBI gene description (n), genes without annotation are on the same predicted operon as a gene with one of the previous categories. FDR corrections are for a 5% FDR (****), 10% FDR (***), 15% FDR (**), and 20% FDR (*). Genes additionally identified in cluster analysis are identified for upregulated (U) and downregulated (D) gene clusters with superscript corresponding to individual clusters.

ABC Transporters

Locus	Name	Gene Description	COG Description	Annot.	Predicted SERP Operon	Fold Change	% FDR	Cluster
SERP0098		ABC transporter, permease protein	ABC-type metal ion transport system, permease component	K	0096-0099	1.6	*	
SERP0267		iron compound ABC transporter, permease protein	ABC-type Fe3+-siderophore transport system, permease component	K	0267-0269	1.3	*	
SERP0296		tagH protein, teichoic acid ABC transporter protein, putative	ABC-type polysaccharide/polyol phosphate transport system, ATPase	K	0296	-1.4	**	
SERP0340		ABC transporter, ATP-binding protein, MsbA family	ABC-type transport system involved in cytochrome bd biosynthesis, ATPase and permease components	K	0340-0341	1.6	***	U^{III}
SERP0341		ABC transporter, ATP-binding protein, MsbA family	ABC-type transport system involved in cytochrome bd biosynthesis, fused ATPase and permease components	K	0340-0341	1.2	*	
SERP0400		iron compound ABC transporter, permease protein	ABC-type enterochelin transport system, permease component	K	0400-0403	1.8	***	U^{III}
SERP0403		transferrin receptor	ABC-type enterochelin transport system, periplasmic component	K	0400-0403	-1.5	***	
SERP0489		ABC transporter, ATP-binding protein	ABC-type metal ion transport system, ATPase component	K	0489-0491	-1.1	**	
SERP0490		ABC transporter, permease protein	ABC-type metal ion transport system, permease component	K	0489-0491	1.3	**	U^{III}
SERP0570	*oppB*	oligopeptide ABC transporter, permease protein	ABC-type dipeptide/oligopeptide/nickel transport systems, permease	K	0570-0574	-1.3	*	
SERP0950		peptide ABC transporter, ATP-binding protein, putative	ABC-type dipeptide/oligopeptide/nickel transport system, ATPase component	K	0953-0950	1.5	*	
SERP0951		peptide ABC transporter, ATP-binding protein, putative	ABC-type dipeptide/oligopeptide/nickel transport system, ATPase component	K	0953-0950	1.4	*	
SERP0959		phosphate ABC transporter, permease protein	ABC-type phosphate transport system, permease component	K	0960-0956	2.1	**	$U^{II,III}$
SERP1475		ABC transporter, ATP-binding protein	ABC-type multidrug transport system, ATPase component	K	1478-1474	-1.5	***	
SERP1775		iron compound ABC transporter, permease protein	ABC-type Fe3+-siderophore transport system, permease component	K	1777-1775	2.1	***	U^{III}
SERP1776		iron compound ABC transporter, permease protein	ABC-type Fe3+-siderophore transport system, permease component	K	1777-1775	1.4	**	U^{III}
SERP1801		cobalt transport family protein	ABC-type cobalt transport system, permease component CbiQ and related	K	1803-1800	1.4	**	$U^{II,V}$
SERP1994		ABC transporter, substrate-binding protein	ABC-type dipeptide transport system, periplasmic component	K	1994	1.5	***	
SERP2030		amino acid ABC transporter, permease protein	ABC-type proline/glycine betaine transport systems, permease component	K	2031-2028	1.7	**	U^{III}
SERP2101		ribose transport protein	ABC-type ribose transport system, auxiliary component	K	2102-2100	1.3	*	
SERP2284		phosphonate ABC transporter, permease protein	ABC-type phosphate/phosphonate transport system, permease component	K	2286-2283	1.4	*	
SERP2355		amino acid ABC transporter, permease protein	ABC-type proline/glycine betaine transport systems, permease component	K	2358-2354	1.5	***	U^{III}
SERP2356		amino acid ABC transporter, amino acid-binding protein	Periplasmic glycine betaine/choline-binding (lipo)protein of an ABC-type transport system (osmoprotectant binding protein)	K	2358-2354	2.7	***	
SERP2357		amino acid ABC transporter, permease protein	ABC-type proline/glycine betaine transport systems, permease component	K	2358-2354	2.1	***	U^{III}
SERP2358		amino acid ABC transporter, ATP-binding protein	ABC-type proline/glycine betaine transport systems, ATPase components	K	2358-2354	1.4	**	
SERP2368		peptide ABC transporter, ATP-binding protein	ABC-type dipeptide/oligopeptide/nickel transport system, ATPase component	K	2375-2367	1.7	***	

Table 4.4 (continued)

Locus	Name	Gene Description	COG Description	Annot.	Predicted SERP Operon	Fold Change	% FDR	Cluster
SERP2369		peptide ABC transporter, ATP-binding protein	ABC-type dipeptide/oligopeptide/nickel transport system, ATPase component	K	2375-2367	1.6	*	
SERP2370		peptide ABC transporter, permease protein	ABC-type dipeptide/oligopeptide/nickel transport systems, permease	K	2375-2367	1.9	**	U^{III}
SERP2371		peptide ABC transporter, permease protein, putative	ABC-type dipeptide/oligopeptide/nickel transport systems, permease	K	2375-2367	2.2	***	U^{III}
SERP2383		ABC transporter, substrate-binding protein	ABC-type metal ion transport system, periplasmic component/surface adhesin	K	2383	1.4	**	$U^{II,III}$
SERP2404		iron compound ABC transporter, iron compound-binding protein, putative	ABC-type Fe3+ transport system, periplasmic component	K	2404-2406	1.5	**	
SERP0021		ABC transporter, ATP-binding protein	ABC-type antimicrobial peptide transport system, ATPase component	n	0021-0019	1.7	***	
SERP0027		ABC transporter, ATP-binding protein, truncation		n	0027	2.0	***	
SERP0292	*sitA*	ABC transporter, ATP-binding protein	ABC-type Mn/Zn transport systems, ATPase component	n	0292-0290	-1.4	*	
SERP0427	*uvrA*	excinuclease ABC, A subunit		n	0426-0427	1.2	***	U^{I}
SERP0887		ABC transporter, permease protein		n	0886-0889	1.9	***	
SERP0956		phosphate transport system regulatory protein PhoU, putative	Phosphate uptake regulator		0960-0956	1.6	*	
SERP1371		ABC transporter, permease protein	Predicted ABC-type exoprotein transport system, permease component	n	1372-1371	1.4	***	
SERP1372		ABC transporter, ATP-binding protein	ABC-type multidrug transport system, ATPase component	n	1372-1371	-1.6	**	
SERP1477		ABC transporter, ATP-binding protein	ABC-type multidrug transport system, ATPase component	n	1478-1474	1.6	***	
SERP1800	*truA*	tRNA pseudouridine synthase A	Pseudouridylate synthase		1803-1800	1.2	*	
SERP2204		ABC transporter, ATP-binding protein	ABC-type antimicrobial peptide transport system, ATPase component	n	2207-2203	1.8	*	
SERP2354		tributyrin esterase EstA, putative			2358-2354	1.6	*	
SERP2367		transporter, putative	Arabinose efflux permease		2375-2367	1.6	***	
SERP2373		hypothetical protein			2375-2367	1.8	***	
SERP2375		diaminopimelate epimerase family protein			2375-2367	1.4	*	
SERP2378		ABC transporter, ATP-binding protein	ABC-type multidrug transport system, ATPase component	n	2376-2378	1.8	**	

Two other unregulated operons included 7 of 9 genes on a large predicted operon (SERP2375-2367) with genes coding for a peptide ABC transporter as well as two of three genes on a separate peptide ABC transporter operon (SERP0950-SERP0951). Both of these operons were identified by COG designation as a dipeptide/oligopeptide/nickel transport system.

Upregulation of other Ion Transport and Membrane Transport Systems in Response to K^+-tuned ELF-MF (h'=1.8)

In addition to the transport systems identified in two-component systems and ABC transporters, other gene systems were identified through clustering in Upregulated Clusters II, III, and IV. Significant overlap was found amongst these three clusters and thus genes are listed together in Table 4.5. Genes of Cluster II were annotated for ion transport with 21 of 22 genes with the annotation GOTERM_BP_FAT: "ion transport" with the remaining gene, SERP2428, and five other genes additionally annotated with GOTERM_MF_FAT: "ATPase activity, coupled transmembrane movement of ions". Genes of Upregulated Cluster III, were identified by location in the membrane and transport-related activity with 42 of 47 genes with the annotation GOTERM_CC_FAT: "intrinsic to membrane" and the remainder falling under SP_PIR_KEYWORDS: "transport", "transmembrane", or "cell membrane". All 10 genes of Upregulated Cluster IV had the annotation GOTERM_MF_FAT: "antiporter activity" and were also found in Upregulated Cluster III. A number of genes previously listed in TCS and ABC transporter systems additionally fell in the membrane associated genes of Cluster III and several under ion transport genes of Cluster II and were not additionally listed in Table 4.5.

Table 4.5 Other genes related to transport and membrane systems identified by Upregulated Clusters II, III, and IV (referenced in other tables as U^{II}, U^{III}, and U^{IV}). Genes without cluster identification were on the same predicted operon as genes identified in this grouping. Additional genes identified in these three clusters were also identified in two-component systems and ABC transporters and are listed in Tables 4.3 and 4.4. FDR corrections are for a 5% FDR (****), 10% FDR (***), 15% FDR (**), and 20% FDR (*). Clusters are identified for upregulated (U) and downregulated (D) gene clusters with superscript corresponding to individual clusters.

Other Ion Transport and Membrane Systems

Locus	Name	Gene Description	Predicted SERP Operon	Fold Change	% FDR	Cluster
SERP0025		major facilitator family transporter	0025	1.2	**	U^{III}
SERP0111		hypothetical protein	0111	2.4	***	U^{III}
SERP0281		Na+/H+ antiporter, MnhA component, putative	0281-0287	1.6	***	$U^{II,III,IV}$
SERP0282		Na+/H+ antiporter, MnhB component, putative	0281-0287	1.9	***	$U^{II,III,IV}$
SERP0283		Na+/H+ antiporter, MnhC component, putative	0281-0287	1.4	**	$U^{II,III,IV}$
SERP0284		Na+/H+ antiporter, MnhD component, putative	0281-0287	1.5	**	$U^{II,III,IV}$
SERP0286		Na+/H+ antiporter, MnhF component, putative	0281-0287	1.3	*	
SERP0289		Na+/H+ antiporter, putative	0289	1.2	***	$U^{II,III,IV}$
SERP0458		sodium transport family protein	0458	1.4	**	U^{II}
SERP0509		hypothetical protein	0508-0510	1.7	***	U^{III}
SERP0533	*mnhF*	Na+/H+ antiporter, MnhF component	0538-0532	1.3	**	$U^{II,III,IV}$
SERP0534	*mnhE*	Na+/H+ antiporter, MnhE component	0538-0532	1.2	*	
SERP0537	*mnhB*	Na+/H+ antiporter, MnhB component	0538-0532	1.4	*	
SERP0590		Na+/H+ exchanger family protein, putative	0585-0590	1.3	*	
SERP0706	*ctaB*	protoheme IX farnesyltransferase	0706-0707	1.4	**	$U^{III,V}$
SERP0707		hypothetical protein	0706-0707	-1.4	***	
SERP1011	*ebh*	cell wall associated fibronectin-binding protein	1011	1.4	**	U^{III}
SERP1245		amino acid permease family protein	1245	1.3	***	U^{III}
SERP1278		hypothetical protein	1280-1278	1.3	**	U^{III}
SERP1280		aminotransferase, class V	1280-1278	1.5	**	
SERP1708	*atpC*	ATP synthase F1, epsilon subunit	1715-1708	-1.5	***	
SERP1709	*atpD*	ATP synthase subunit B	1715-1708	1.1	**	$U^{II,III,V}$
SERP1711	*atpA*	ATP synthase subunit A	1715-1708	1.1	*	
SERP1881	*nhaC*	Na+/H+ antiporter NhaC	1881	1.2	**	$U^{II,III,IV}$
SERP1886	*sugE-1*	sugE protein	1886-1888	1.6	**	U^{III}
SERP1914		Na+/H+ antiporter, putative	1914	1.4	***	$U^{II,III,IV}$
SERP2034		amino acid permease family protein	2034	1.4	**	U^{III}
SERP2077		Na+/H+ antiporter, putative	2077	1.4	**	$U^{II,III,IV}$
SERP2110		hypothetical protein	2110-2109	2.0	***	U^{III}
SERP2126	*feoB*	ferrous iron transport protein B	2127-2125	1.8	**	U II,III
SERP2144	*pyrD*	dihydroorotate dehydrogenase	2144	1.3	**	$U^{III,V}$
SERP2201		sodium:solute symporter family protein	2201	1.7	***	U II,III
SERP2280		SecY/Sec61-alpha family protein	2281-2273	1.4	***	U^{III}
SERP2328		anion transporter family protein	2328	1.5	**	U II
SERP2340		drug resistance transporter, EmrB/QacA family	2340	1.7	***	$U^{III,IV}$
SERP2381		NADH:flavin oxidoreductase/fumarate reductase, flavoprotein subunit, putat	2382-2380	1.5	**	U^{III}
SERP2428	*arsA*	arsenical pump-driving ATPase	2427-2428	1.4	***	U II
SERP2438		cation-transporting ATPase, E1-E2 family	2438	1.5	**	$U^{II,III,V}$
SERP2447		lipoprotein, putative	2447	1.3	**	U^{III}
SERP2491		hypothetical protein	2491	1.3	***	U^{III}
SERP2513		hypothetical protein	2514-2513	1.2	**	U^{III}

The most prominent group of genes in these upregulated clusters were the sodium/proton antiporters. Initial sequencing of the genome reported eight predicted sodium ion/proton exchangers (Gill et al., 2005). Genes on every Na^+/H^+ antiporter operon identified were significantly upregulated as three or more genes on two multisubunit Na^+/H^+ operons, five single-gene operons for Na^+/H^+ antiporters, and one gene coding for a sodium transporter family protein. These systems extrude Na^+ while H^+ enters the cell and are critical in efflux of toxic cations under high salinity and in the maintenance of cytoplasmic cell homeostasis under alkaline conditions (Hiramatsu et al., 1998; Swartz et al., 2005). These results clearly indicate ELF-MF effects on ion transport.

Upregulation of Genes Related
to Transposase Activity in
Response to K^+-tuned ELF-MF (h'=1.8)

While the previous discussed groups of genes have function related to transport systems, the highest enrichment score was for Upregulated Cluster I with 31 genes listed Table 4.6. Genes in this cluster were identified by GOTERM_MF_FAT: "DNA binding" and GOTERM_BP_FAT: "DNA metabolic pathway". Six genes were identified as transcriptional regulators in addition to three response regulators previously identified as components of TCSs. Twelve genes were annotated with GOTERM_BP_FAT: "transposase activity" and related transposase terms. ISSep1-like transposases were particularly predominating.

Table 4.6 Upregulation of transposition genes and related transposase activity identified in Upregulated Cluster I (U^{I}). Three genes listed in two-component systems and one gene listed in ABC transporters were also identified in this cluster and are listed in Tables 4.3 and 4.4. FDR corrections are for a 5% FDR (****), 10% FDR (***), 15% FDR (**), and 20% FDR (*). Clusters are identified for upregulated (U) and downregulated (D) gene clusters with superscript corresponding to individual clusters. Significant genes on the same operon as a clustered gene are also listed.

Upregulated Genes: Cluster I

Locus	Name	Gene Description	Predicted SERP Operon	Fold Change	% FDR	Cluster
SERP0107		transcriptional regulatory protein GltC, putative	0107	1.4	***	U^{I}
SERP0157		transcriptional regulator, GntR family	0157	1.9	***	U^{I}
SERP0160		ISSep1-like transposase	0160	1.4	***	U^{I}
SERP0243		hypothetical protein	0243-0242	1.7	***	U^{I}
SERP0260		ISSep1-like transposase	0260	1.4	***	U^{I}
SERP0349		deoxyribodipyrimidine photolyase, putative	0349	1.7	***	U^{I}
SERP0380		ISSep1-like transposase	0380	1.4	**	U^{I}
SERP0544		ISSep1-like transposase	0544	1.4	**	U^{I}
SERP0558		ISSep1-like transposase	0558	1.4	**	U^{I}
SERP0565		ISSep1-like transposase	0565	1.4	**	U^{I}
SERP0577		ISSep1-like transposase	0577	1.5	***	U^{I}
SERP0697		ISSep1-like transposase	0697	1.3	**	U^{I}
SERP0935		ImpB/MucB/SamB family protein	0935	1.3	**	U^{I}
SERP0991		ISSep1-like transposase	0991	1.4	**	U^{I}
SERP1146	*prmA*	ribosomal protein L11 methyltransferase	1152-1144	-1.6	***	
SERP1147	*dnaJ*	dnaJ protein	1152-1144	1.3	**	U^{I}
SERP1173		transposase, IS200 family	1173	1.3	**	U^{I}
SERP1333		hypothetical protein	1333-1334	2.0	***	U^{I}
SERP1730		ISSep1-like transposase	1730	1.4	***	U^{I}
SERP1846		transcriptional regulator, MarR family	1846-1847	1.8	***	U^{I}
SERP1911		ISSep1-like transposase	1911	1.4	***	U^{I}
SERP1931		DNA-3-methyladenine glycosylase	1931	1.3	***	U^{I}
SERP1972		transcriptional regulator, AraC family	1972-1973	1.4	***	U^{I}
SERP2061		transcriptional regulator, MerR family	2061	1.3	**	U^{I}
SERP2157		transcriptional regulator, LysR family	2157	1.3	**	U^{I}
SERP2429	*arsR-2*	arsenical resistance operon repressor	2429-2431	1.3	**	U^{I}
SERP2498		cassette chromosome recombinase A	2498-2499	1.6	**	U^{I}
SERP2499		cassette chromosome recombinase B	2498-2499	1.9	***	U^{I}

.

Upregulation of Amino Acid Biosynthesis
in Response to K^{+}-tuned ELF-MF (h'=1.8).

The cluster with the lowest enrichment score for upregulated genes, Cluster V, had 33 genes listed in Table 4.7.

Table 4.7 Genes identified in Upregulated Cluster V, amino acid biosynthesis-related activity. FDR corrections are for a 5% FDR (****), 10% FDR (***), 15% FDR (**), and 20% FDR (*). Clusters are identified for upregulated (U) and downregulated (D) gene clusters with superscript corresponding to individual clusters. Significant genes on the same operon as a clustered gene are also listed.

Up-regulated Genes: Cluster 5

Locus	Name	Gene Description	Predicted SERP Operon	Fold Change	% FDR	Cluster
SERP0033		cyclase, putative	0037-0033	1.5	***	
SERP0034	*metE*	5-methyltetrahydropteroyltriglutamate-- homocysteine methyltransferase	0037-0033	1.6	***	U^V
SERP0035		bifunctional homocysteine S-methyltransferase/5,10-methylenetetrahydrofolate reductase protein	0037-0033	2.0	***	
SERP0036		trans-sulfuration enzyme family protein	0037-0033	2.4	***	
SERP0037		trans-sulfuration enzyme family protein	0037-0033	1.6	*	
SERP0298		teichoic acid biosynthesis protein B, putative	0298-0300	1.2	**	U^V
SERP0372		6-pyruvoyl tetrahydrobiopterin synthase, putative	0373-0371	1.4	**	U^V
SERP0373		exsB protein	0373-0371	1.7	**	U^V
SERP0653	*purQ*	phosphoribosylformylglycinamidine synthase I	0649-0659	1.3	**	U^V
SERP0659	*purD*	phosphoribosylamine--glycine ligase	0649-0659	1.5	***	U^V
SERP0769	*carB*	carbamoyl-phosphate synthase large subunit	0764-0771	1.2	*	
SERP0770	*pyrF*	orotidine 5'-phosphate decarboxylase	0764-0771	1.5	**	U^V
SERP0936	*tyrA*	prephenate dehydrogenase	0936	1.5	**	U^V
SERP0964	*asd*	aspartate-semialdehyde dehydrogenase	0963-0970	1.6	***	U^V
SERP0966	*dapB*	dihydrodipicolinate reductase	0963-0970	1.3	*	
SERP0969		alanine racemase family protein	0963-0970	1.2	*	
SERP0970	*lysA*	diaminopimelate decarboxylase	0963-0970	-1.2	*	
SERP1089	*argD*	acetylornithine aminotransferase	1092-1089	1.4	***	U^V
SERP1159		iojap-related protein	1166-1158	-1.2	*	
SERP1162		hypothetical protein	1166-1158	-1.3	**	
SERP1163	*aroE*	shikimate 5-dehydrogenase	1166-1158	1.6	***	U^V
SERP1451		nitric-oxide synthase, oxygenase subunit	1451-1452	1.2	*	
SERP1452	*pheA*	prephenate dehydratase	1451-1452	1.4	**	U^V
SERP1665	*ilvD*	dihydroxy-acid dehydratase	1665-1667	1.4	**	U^V
SERP1667		acetolactate synthase, small subunit, truncation	1665-1667	1.6	*	
SERP1851	*mobA*	molybdopterin-guanine dinucleotide biosynthesis protein A	1855-1850	1.6	**	U^V
SERP1854	*mobB*	molybdopterin-guanine dinucleotide biosynthesis protein B	1855-1850	1.8	**	U^V
SERP1855		molybdopterin biosynthesis MoeA protein, putative	1855-1850	1.4	*	
SERP1937	*fni-2*	isopentenyl pyrophosphate isomerase	1938-1937	1.3	**	U^V
SERP1992	*nirR*	transcriptional regulator NirR	1993-1992	1.5	***	U^V
SERP2041		glutamate synthase-related protein	2041	1.3	***	U^V
SERP2188		precorrin-2 dehydrogenase	2191-2185	1.8	**	U^V
SERP2190	*cysI*	sulfite reductase (NADPH) hemoprotein beta-component	2191-2185	1.6	**	U^V
SERP2253		hypothetical protein	2253	1.4	**	U^V
SERP2300	*hisIE*	phosphoribosyl-AMP pyrophosphatase/phosphoribosyl-ATP cyclohydrolase	2307-2300	1.3	*	
SERP2302	*hisA*	phosphoribosylformimino-5-aminoimidazole carboxamide ribotide isomerase	2307-2300	1.7	***	U^V
SERP2303	*hisH*	amidotransferase HisH	2307-2300	3.1	***	U^V
SERP2304	*hisB*	imidazoleglycerol-phosphate dehydratase	2307-2300	1.8	***	U^V
SERP2307		hypothetical protein	2307-2300	1.7	*	
SERP2382		ApbE family protein	2382-2380	1.3	**	U^V
SERP2396	*bioD*	dethiobiotin synthase	2396-2393	2.9	***	U^V
SERP2536	*purA*	adenylosuccinate synthetase	2536	1.4	**	U^V

Thirty-two of these genes were identified by GOTERM_BP_FAT: "nitrogen compound biosynthetic process" with additional annotations linked to amino-acid biosynthetic processes. Three of the genes in this cluster were part of five upregulated genes of an 8-gene predicted operon involved in histidine biosynthesis including *hisH*, the gene with the third highest fold-change (FC=3.1) of all genes at the 15%FDR

Downregulation of Cell Division, Translation, Glycerolphospholipid Metabolism, and Cell Wall Biosynthesis in Response to K^+-tuned ELF-MF (h'=1.8)

The gene clusters identified for the downregulated genes fell into smaller but more distinct groups with less annotation overlap in comparison to the upregulated clusters (Figure 4.5). Genes identified in downregulated clusters are reported in Table 4.8. Further discussion follows.

The cluster with the highest enrichment score were the 13 genes of Downregulated Cluster I all of which were identified by SP_PIR_KEYWORD: "cell division" within which four had additional annotations for septation or barrier septum formation. *ftsL* and *ftsZ* were identified in this cluster in addition to two unclustered gene on the same operon. Disruption of FtsZ, involved in septum formation during cell division, has been studied as a target for therapeutics to combat staphylococci (Rai et al., 2008; Stokes et al., 2013). In *E. coli*, *ftsZ* is required for localization of GroEL at the site of septum formation during cell division (Ogino et al., 2004). Interestingly, GroEL is one of the heat shock proteins along with DnaJ/K previously reported to be produced in response to ELF-MF in *E. coli* (Chow and Tung, 2000a, b; Del Re et al., 2006; Del Re et al., 2009). The gene *groEL* was also identified as a significantly changing gene in this

study but in Downregulated Cluster IV, along with *dnaK*. These changes in gene expression would indicate an opposing effect to the previous studies measuring protein production from these genes. The gene *dnaJ* was also significant but was upregulated.

The largest cluster of downregulated genes were 26 genes in Cluster II. Genes in this cluster were identified by annotations for GOTERM_BP_FAT: "translation", GOTERM_MF_FAT: "structural molecule activity, SP_PIR_KEYWORD: "rna-binding", and GOTERM_CC_FAT: "intracellular non-membrane-bounded organelles". Another cluster of genes related to translation were identified in Cluster IV. Eight of the 10 genes of Cluster IV fell under the SP_PIR_KEYWORD: "isomerase" with the remainder identified with the GOTERM_BP_FAT: "protein folding". The only major operons identified in this cluster coded for ribosomal proteins.

The 7 genes of Downregulated Cluster III were identified by the KEGG_PATHWAY: "Glycerophospholipid metabolism" and annotations for GOTERM_BP_FAT: "glycerol metabolic process", "alditol metabolic process", and "polyol metabolic process". Both genes of the *glpKD* operon were significantly downregulated although with small FCs.

The final cluster identified were thirteen genes identified in Downregulated Cluster V. Genes of this cluster were identified by a number of annotations although all could be identified as GOTERM_BP_FAT: "polysaccharide metabolic process" and "regulation of cell shape". Other annotations related to cell wall macromolecule metabolic process, cell wall biogenesis, and cell wall organization. Again few full operons were identified although over half of the genes in this cluster had $|FC|>1.5$.

Table 4.8 Downregulated genes identified in DAVID clusters for biofilms grown in the higher potassium tuned magnetic field (h'=1.8). FDR corrections are for a 5% FDR (****), 10% FDR (***), 15% FDR (**), and 20% FDR (*). Genes cluster are identified for downregulated (D) gene clusters with superscript corresponding to individual clusters. Genes on the same operon as clustered genes are also listed.

Downregulated Genes: Cluster I

Locus	Name	Gene Description	Predicted SERP Operon	Fold Change	% FDR	Cluster
SERP0150		cell division protein FtsH, putative	0150	-1.1	***	D^{I}
SERP0703		cell division protein, FtsW/RodA/SpoVE family	0703	-1.6	***	D^{I}
SERP0743	*mraZ*	hypothetical protein	0743-0751	-1.8	**	
SERP0745	*ftsL*	cell division protein FtsL	0743-0751	-2.0	***	D^{I}
SERP0750	*ftsA*	cell division protein FtsA	0743-0751	-1.2	*	
SERP0751	*ftsZ*	cell division protein FtsZ	0743-0751	-1.4	**	D^{I}
SERP0754	*ylmF*	ylmF protein	0752-0755	-1.2	**	D^{I}
SERP0756	*ylmH*	ylmH protein	0756-0757	-1.4	***	
SERP0757		cell-division initiation protein, putative	0756-0757	-1.4	***	D^{I}
SERP1016		hypothetical protein	1018-1016	-1.7	**	$D^{I,V}$
SERP1057	*scpB*	segregation and condensation protein B	1058-1054	-1.2	**	D^{I}
SERP1237		GTP-binding protein	1237	-1.5	***	D^{I}
SERP1239	*tig*	trigger factor	1239	-1.4	***	$D^{I,IV}$
SERP1281		septation ring formation regulator EzrA	1281	-1.9	***	$D^{I,II}$
SERP1689	*murF*	UDP-N-acetylmuramoyl-tripeptide--D-alanyl-D- alanine ligase	1690-1689	-1.3	**	$D^{I,V}$
SERP1731	*murAB*	UDP-N-acetylglucosamine 1-carboxyvinyltransferase	1731	-1.2	**	$D^{I,V}$

Downregulated Genes: Cluster II

SERP0044	*rpsF*	ribosomal protein S6	0044-0046	-1.5	***	D^{II}
SERP0139	*rplY*	ribosomal protein L25	0139-0146	-1.9	***	D^{II}
SERP0144		S4 domain protein	0139-0146	-1.4	**	
SERP0156	*lysS*	lysyl-tRNA synthetase	0156	-1.4	***	D^{II}
SERP0187	*rpsG*	30S ribosomal protein S7	0185-0189	-1.2	**	D^{II}
SERP0450		exoribonuclease, VacB/RNase II family	0449-0451	1.3	*	
SERP0451	*smpB*	SsrA-binding protein	0449-0451	-1.3	***	D^{II}
SERP0526		HesB domain protein	0526	-1.3	**	D^{II}
SERP0609	*prfC*	peptide chain release factor 3	0607-0609	-1.4	***	D^{II}
SERP0676		metallo-beta-lactamase family protein	0677-0676	-1.3	***	D^{II}
SERP0677		hypothetical protein	0677-0676	-1.8	**	
SERP0678	*def*	peptide deformylase	0678	-1.8	***	D^{II}
SERP0805	*rimM*	16S rRNA processing protein RimM	0804-0807	-1.6	**	D^{II}
SERP0806	*trmD*	tRNA (guanine-N1)-methyltransferase	0804-0807	-1.2	**	
SERP0824	*tsf*	elongation factor Ts	0823-0826	-1.3	***	D^{II}
SERP0832		hypothetical protein	0832-0836	-1.3	*	
SERP0833		transcription elongation factor NusA	0832-0836	-1.1	**	
SERP0834		hypothetical protein	0832-0836	-2.1	***	
SERP0835		30S ribosomal protein L7Ae, putative	0832-0836	-1.2	***	D^{II}
SERP0842		metallo-beta-lactamase family protein	0842	-1.4	***	D^{II}
SERP0853		HD/HDIG/KH domain protein	0853	-1.2	**	D^{II}
SERP1023		DNA replication protein DnaD, putative	1029-1021	1.4	*	
SERP1024	*asnS*	asparaginyl-tRNA synthetase	1029-1021	-1.1	***	D^{II}
SERP1028		glycosyl transferase, group 1 family protein	1029-1021	-1.4	**	
SERP1029		hypothetical protein	1029-1021	-1.5	***	
SERP1044		ribosomal protein S1	1044	-1.3	***	D^{II}
SERP1056	*rluB*	pseudouridine synthase RluB	1058-1054	-1.2	**	$D^{II,IV}$
SERP1093	*efp*	elongation factor P	1094-1093	-1.4	**	D^{II}
SERP1210		hypothetical protein	1211-1202	-1.6	***	
SERP1211	*rplU*	ribosomal protein L21	1211-1202	-1.5	***	D^{II}
SERP1244	*infC*	translation initiation factor IF-3	1244-1242	-1.4	**	D^{II}

Downregulated Genes: Cluster II (continued)

Locus	Name	Gene Description	Predicted SERP Operon	Fold Change	% FDR	Cluster
SERP1311		hypothetical protein	1313-1311	-2.4	**	
SERP1312		pseudouridine synthase, family 1	1313-1311	-1.3	**	$D^{II,IV}$
SERP1804	*rplQ*	ribosomal protein L17	1809-1804	-1.3	***	D^{II}
SERP1805	*rpoA*	DNA-directed RNA polymerase alpha subunit	1809-1804	-1.1	**	
SERP1806	*rpsK*	30S ribosomal protein S11	1809-1804	1.1	**	
SERP1808	*rpmJ*	ribosomal protein L36	1809-1804	-2.8	**	D^{II}
SERP1821	*rplN*	ribosomal protein L14	1832-1810	1.2	**	
SERP1822	*rpsQ*	30S ribosomal protein S17	1832-1810	-1.6	**	D^{II}
SERP1825	*rpsC*	30S ribosomal protein S3	1832-1810	1.1	*	
SERP1828	*rplB*	50S ribosomal protein L2	1832-1810	1.1	*	
SERP1830	*rplD*	50S ribosomal protein L4	1832-1810	1.1	*	
SERP1831	*rplC*	ribosomal protein L3	1832-1810	1.2	**	
SERP2538	*rplI*	ribosomal protein L9	2540-2538	-1.3	***	D^{II}
SERP2539		DHH family protein	2540-2538	1.2	**	

Downregulated Genes: Cluster III

Locus	Name	Gene Description	Predicted SERP Operon	Fold Change	% FDR	Cluster
SERP0300	*tagD*	glycerol-3-phosphate cytidylyltransferase	0298-0300	-1.8	***	$D^{III,V}$
SERP0710		glycerophosphoryl diester phosphodiesterase, putative	0710	-1.1	***	D^{III}
SERP0791		hypothetical protein	0791-0792	-1.2	*	
SERP0792		DAK2 domain protein	0791-0792	-1.2	***	D^{III}
SERP0867	*glpK*	glycerol kinase	0867-0868	-1.3	***	D^{III}
SERP0868	*glpD*	aerobic glycerol-3-phosphate dehydrogenase	0867-0868	-1.2	**	D^{III}
SERP1585	*aacA*	6'-aminoglycoside N-acetyltransferase/2''-aminoglycoside phosphotransferase	1586-1585	-1.7	**	D^{III}
SERP2523		glycerophosphoryl diester phosphodiesterase UgpQ, putative	2523-2522	-1.5	***	D^{III}

Downregulated Genes: Cluster IV

Locus	Name	Gene Description	Predicted SERP Operon	Fold Change	% FDR	Cluster
SERP0540		peptidyl-prolyl cis-trans isomerase, cyclophilin-type	0540	-1.8	**	D^{IV}
SERP1146	*prmA*	ribosomal protein L11 methyltransferase	1152-1144	-1.6	***	
SERP1147	*dnaJ*	dnaJ protein	1152-1144	1.3	**	U^{I}
SERP1148	*dnaK*	dnaK protein	1152-1144	-1.2	***	D^{IV}
SERP1231	*hemL-1*	glutamate-1-semialdehyde aminotransferase	1236-1231	-1.2	**	D^{IV}
SERP1236	*hemA*	glutamyl-tRNA reductase	1236-1231	-1.3	***	
SERP1376		protein export protein PrsA, putative	1376	-1.3	**	D^{IV}
SERP1389		hypothetical protein	1390-1388	-1.9	*	
SERP1390		glucosamine-6-phosphate isomerase family protein	1390-1388	-1.6	***	D^{IV}
SERP1484	*groEL*	chaperonin, 60 kDa	1485-1484	-1.3	**	D^{IV}
SERP1485	*groES*	chaperonin, 10 kDa	1485-1484	1.2	**	
SERP1762	*glmM*	phosphoglucosamine mutase	1764-1762	-1.2	**	D^{IV}
SERP1763		hypothetical protein	1764-1762	-1.3	***	

Downregulated Genes: Cluster V

Locus	Name	Gene Description	Predicted SERP Operon	Fold Change	% FDR	Cluster
SERP0520	*dltC*	D-alanine--poly(phosphoribitol) ligase subunit 2	0517-0521	-1.6	***	D^{V}
SERP0521	*dltD*	dltD protein	0517-0521	-1.2	*	
SERP0827	*uppS*	undecaprenyl diphosphate synthase	0827-0828	-1.8	***	D^{V}
SERP0947	*femB*	femB protein	0945-0947	-1.4	***	D^{V}
SERP1019	*recU*	hypothetical protein	1019-1020	-1.3	*	
SERP1020	*pbp2*	penicillin-binding protein 2	1019-1020	-1.3	***	D^{V}
SERP1212		rod shape-determining protein MreD, putative	1213-1212	-1.4	*	
SERP1213	*mreC*	rod shape-determining protein MreC	1213-1212	-1.3	**	D^{V}
SERP1330		N-acetylmuramoyl-L-alanine amidase, family 4	1330	-1.6	***	D^{V}
SERP1412		transglycosylase domain protein	1412	-2.6	***	D^{V}
SERP1891		N-acetylmuramoyl-L-alanine amidase, family 4	1892-1891	-1.1	***	D^{V}
SERP1960	*tagF*	teichoic acid biosynthesis protein F	1960	-1.7	***	D^{V}

Discussion

In this study we sought to explore the use of ELF magnetic fields (ELF-MF) to target bacteria in biofilms. ELF-MFs are currently used in clinical practice for bone healing, supporting the potential use of these fields *in vivo* as a noninvasive treatment strategy. As an exploratory study, we used global gene expression with microarrays to detect potential changes in biological processes. Here we have demonstrated that: 1) Growth of *S. epidermidis* biofilms in an ELF-MF did not affect viable cell counts (Figure 4.4) or growth but did have biological effects on the biofilm as indicated by differential gene expression (Table 4.2); 2) The number of differentially expressed genes were significantly different (p-value$\leq$0.05) between two frequencies on the same order of magnitude with the same static and time-varying magnetic field components (Table 4.2). While a range of frequencies were not tested, the frequency fitting an ion resonance frequency for a calcium ion had almost no effect on differential gene expression while fields fitting an ion resonance frequency for the potassium ion showed larger changes in gene expression. 3) The number of differentially expressed genes increased when the time-varying component of the magnetic field was increased while the static component of the magnetic field and the frequency remained the same (Table 4.2). Peak biological responses at a h'=1.8 were predicted by theory and evidence in eukaryotes (Binhi, 2000); 4) In response to growth in an ELF-MF (K^+ tuning, h'=1.8), *S. epidermidis* biofilms upregulate genes of two-component signal transduction systems (Table 4.3), ABC transporters (Table 4.4), ion transport systems, particularly all of the Na^+/H^+ antiporters (Table 4.5), transposition activity (Table 4.6), and amino acid biosynthesis (Table 4.7).

6) In response to growth in an ELF-MF (K^+ tuning, h'=1.8), *S. epidermidis* biofilms downregulate genes related to cell division, translation and protein folding, glycerophospholipid metabolism, and biogenesis of cell wall components (Table 4.8).

One of the interests of this study was to investigate ion resonance frequencies as a possible targeted approach to ELF-MF application. However, behind this application was the fundamental question of whether a weak ELF-MF would have any effect on biofilm as the magnitudes of fields and frequencies were similar to ELF-MFs in the modern environment. Previous work on planktonic *E. coli* has focused on mutagenic properties of 50Hz (Chow and Tung, 2000a, b; Del Re et al., 2006; Del Re et al., 2009; Li and Chow, 2001) or 60Hz (Cairo et al., 1998) ELF magnetic fields reporting increased production of sigma factors, DnaK/J and GroEL but at time-varying field magnitudes of 0.4-1.2mT (4,000-12,000 mG), 4-20 times the magnitude used in the current study. In this study, *dnaK* and *groEL* were downregulated while *dnaJ* was upregulated. In a study using anomalous viscosity as a measure of DNA relaxation, Belyaev reported frequencies of 7-11Hz with a 430 mG static and 210 mG time-varying component to have a non-toxic but growth stimulatory effect on *E. coli* cultures and, based on peak measurements during frequency scans, may present some evidence for frequency-specific magnetic field tunings (Belyaev, 2011). The only full transcriptome study of *E. coli* found no changes in gene expression in response to 8 min, 1.5 hr, and 18 hr exposures to a 50 Hz, 1mT B_{AC} (10,000 mG) sinusoidal, intermittent sinusoidal, and pulsed ELF-MF (Huwiler et al., 2012). For the work presented here, magnetic field tunings parameters were selected based on ion resonance frequencies for the calcium or potassium ion, both ions of

biological importance. Availability of these ions in the medium were abundant for potassium as potassium phosphate but calcium was only present in trace amounts. This could explain differences in tuning responses and would be a topic of further study. In that medium, 10 genes were perturbed at the Ca^{2+} tuning ($p \leq 0.05$), only one of which had a $FC \geq 1.5$. None of these results were significant after corrections for multiple comparisons and it was concluded that the calcium field had no effect in this system. In contrast, both potassium tunings at $h'=0.7$ and 1.8 found significant changes of 174 and 725 perturbed genes ($p \leq 0.05$), respectively. Although the results of the lower magnitude potassium tuning did not hold up to multiple comparisons testing, these results do indicate some significance of the 23.5 Hz frequency, which correlates to an ion resonance frequency for K^+ in a 600 mG B_o. Together, these results demonstrate biological effects of ELF-MF on *S. epidermidis* biofilms that were specifically observed at a K^+ ion resonance frequency. Further inference into whether these effects could only be observed at this frequency with a different static magnetic field, or different frequencies with the same static magnetic field would require further study, possibly using one of the responses reported here.

Given the responses reported here, what can be said about ELF-MF effects on growing biofilms? While exact mechanisms or effects would be very difficult to pull from the large list of changing genes, insight can be gained from stimuli known to modify genes. Two-component systems (TCSs) are signal transduction systems that are a primary mode bacteria use to sense and respond to changes in their surrounding environments (Capra and Laub, 2012) through use of a sensor protein and a response

regulator that may regulate one or multiple systems. These highly responsive TCSs can thus be used as indicators of the changing environment sensed by the biofilm. Of the 15 reported *S. epidermidis* systems (Gill et al., 2005), 6 TCS sensor histidine kinases, 5 response regulators, and 1 gene with TCS component sensor activity exhibited significant changes in response to the ELF-MF (K^+, h'=1.8) and could be used to infer effects on biofilm.

As the MF frequency corresponding to the K^+ ion resonance frequency had biological effects, it is hypothesized that potassium-related systems might be perturbed. One of the first TCS investigated was the potassium uptake system. The *kdpD/kdeP* TCS regulates *kdpABC* coding for a high affinity K^+ transporter KdpATPase. Biofilms grow in the 23.5Hz, 1,080 mG ELF-MF had upregulated expression of *kdpD* and *kdpABC*. In addition, the single gene operon between the *kdpABC* and *kdpD/kdeP* operons coding for a hypothetical protein (SERP2488) was significantly upregulated with a FC=2.3 (significant at the 10%FDR). In *E. coli*, the KdpD/KdpE TCS responds to intracellular potassium limitation or high osmolarity by activating the *kdpFABC* operon coding for a K^+ uptake system (Heermann and Jung, 2010). In *S. aureus* NCTC8325, *kdpDE* has also been reported to be upregulated in response to potassium limitation but was identified to regulate virulence factors and, in contrast to *E. coli*, negatively regulate *kdpFABC* as knockouts of *kdpE* or *kdpDE* had greater levels of *kdpA* transcripts. In the same study, knocking out *kdpDE* or *kdpFABC* had no significant change in growth curves compared to the wildtype over a range of potassium concentrations, nor was a significant change in

internal K^+ concentrations found between the *kdpFABC* mutant and wildtype strains. The study concluded that KdpFABC is not a major K^+ transporter in *S. aureus* NCTC8325 (Xue et al., 2011). In *S. epidermidis*, these two operons differ (Table 4.9). Interestingly, the homology between components of the *S. aureus* NCTC8325 and *S. epidermidis RP62A* systems was only 52-67% for each component *kdpABC*, *kdpD* and *kdpE* (NCTC8325)/*kdeP* (RP62A). No homology was found for the hypothetical protein of the *kdpFABC S. aureus* operon thought to be *kdpF*, nor was there homology in any genome for the hypothetical single gene operon between the *kdpD/kdeP* and *kdpABC* operons in *S. epidermidis*. Further exploration of these systems found that some *S. aureus* strains have two *kdp* systems, one with >98% homology to the *S. aureus* NCTC8325 system and the other with >99% homology to *S. epidermidis* RP62A (Table 4.9). The redundancy of these systems in the same strains with slightly different homology may suggest different functionality between systems within staphylococcal strains. While further knowledge of the *kdp* system of *S. epidermidis* is clearly needed, the upregulation of *kdpD* is an indicator of potassium limitation in all of the organisms discussed, suggesting a similar role in *S. epidermidis*. The upregulation of *kdpABC* and the hypothetical protein operon preceding that operon in response to the magnetic field may indicate an increase in potassium uptake. As the principal cation involved in maintenance of osmotic and pH homeostasis (White, 2007), perturbations of K^+ systems or concentrations might significantly alter cell function.

Table 4.9 Comparison of homology between *kdp* potassium uptake systems in staphylococcal strains. "X" indicates all three genes were homologous with the comparison strains *S. epidermidis* RP62A or *S. aureus* NCTC 8325 at the cutoff.

	Strain had *kdp* system with >98% homology with *kdpd, kdpA, and kdpB in the reference strain*		
	NCBI Strain Designation	*S. epidermidis* RP62A	*S. aureus* NCTC 8325
	Staphylococcus epidermidis RP62A	X	-
	Staphylococcus aureus aureus NCTC 8325	-	X
ONE kdp system found	*Staphylococcus aureus aureus* COL	-	X
	Staphylococcus aureus RF122	-	X
	Staphylococcus aureus subsp. aureus ED98	-	X
	Staphylococcus aureus subsp. aureus str. JKD6008	-	X
	Staphylococcus aureus subsp. aureus str. JKD6009	-	X
	Staphylococcus aureus subsp. aureus str. Newman	-	X
	Staphylococcus aureus subsp. aureus USA300_FPR3757	-	X
	Staphylococcus aureus subsp. aureus USA300_TCH1516	-	X
	Staphylococcus aureus, MRSA476	-	X
	Staphylococcus aureus, MW2	-	X
TWO kdp systems	*Staphylococcus aureus* subsp. aureus JH1	X	X
	Staphylococcus aureus subsp. aureus JH9	X	X
	Staphylococcus aureus subsp. aureus Mu3	X	X
	Staphylococcus aureus, MRSA252	X	X
	Staphylococcus aureus , Mu50	X	X
	Staphylococcus aureus , N315	X	X

Other systems also suggest that the ELF-MF can affect ion distribution across the cell membrane. The *lytSR* TCS, upregulated by the 23.5Hz, 1080 mG ELF-MF, is induced by collapse of the proton motive force in *S. aureus* (Patton et al., 2006). The *lytS* sensing component is a membrane spanning protein which positively regulates the downstream *lrgAB* operon upon sensing a decrease in the electrical gradient, $\Delta\psi$, in *S. aureus*. While decreases activated the system, increase in $\Delta\psi$ or changes in pH did not have an effect (Patton et al., 2006). Less is known about LytSR regulation in *S. epidermidis* but it has also been reported to positively regulate *lrgAB* as well as control

extracellular murein hydrolase activity, membrane transport, and bacterial cell death (Zhu et al., 2010). While both *lytS* and *lytR* were upregulated in response to the ELF-MF, the changes in gene expression for *lrgAB* were not significant. Additionally, we found upregulation of all of the Na^+/H^+ antiporters in response to the ELF-MF. As H^+, K^+, and Na^+ are the main ions in cell wall homeostasis, detection of a decrease in the $\Delta\psi$ component of the proton motive force (PMF) could be in concert with upregulation of a potassium uptake system and the sodium-proton antiporters which bring in protons in exchange for sodium leaving the cell. All genes on an osmoprotectant uptake operon, the proline/glycine betaine ABC transporter, were upregulated as well as several on glycine betaine systems on other operons. These systems are upregulated by halotolerant staphylococcal species in high salinity environments. While all are effective osmoprotectants, proline betaine and glycine betaine are reported as far more effective than L-proline in staphylococcal species including *S. epidermidis* (Amin et al., 1995). Interestingly, uptake of glycine betaine by two uptake systems in *S. aureus* has been demonstrated to be Na^+-dependent with increased uptake with increasing Na^+ concentrations in media (Pourkomailian and Booth, 1992) which could relate to the Na^+/H^+ antiporter upregulation.

While the results suggest ELF-MF changes on membrane transport, damage to the cell wall was not indicated. The *vraSR* TCS system is activated by damage to cell wall peptidoglycan, and is considered a "sentinel" system for cell wall damage activating a rapid cell wall stress response involving over 40 genes in *S. aureus* (Belcheva and Golemi-Kotra, 2008). The sensor protein *vraS* of the *vraSR* TCS and a hypothetical

protein on the same operon were significantly downregulated. Changes on the other genes on the operon, *vraR* (FC= -1.0, p=0.99) and an additional hypothetical protein (FC= -1.2, p=0.12) were not statistically significant. Genes involved with polysaccharide and cell wall biosynthesis were also downregulated in response to the ELF-MF. While the upregulated TCS systems involved in ion transport may indicate changes in membrane associated transport systems and PMF, the downregulation of these TCS genes suggests that those changes are not damaging the cell wall.

Sinusoidal ELF-MF has been reported to both increase (Chow and Tung, 2000b) and decrease (Del Re et al., 2004; Del Re et al., 2003; Giorgi et al., 2011) transposition activity in *E. coli.* In *S. epidermidis* transposase genes and transposition activity were identified as a significantly upregulated cluster of genes (Table 4.6). While transposition activity was used in earlier ELF-MF studies as possible evidence of mutagenesis, transposition activity has also been indicated in *S. aureus* as a means of changing expression of colony morphology, phenotypes, antibiotic susceptibility, hemolytic activity and gene expression (Cui et al., 2012). Alternating insertion and excision of transposition elements IS256 has been reported as a molecular mechanism for mediating phase variation of virulence factor expression in *S. epidermidis* (Ziebuhr et al., 1999) and has been proposed as an indicator of *S. epidermidis* transition from a commensal to pathogenic organisms *in vivo*. In this study, none of the IS256 transposase were affected but nearly all of the unidentified group of *S. epidermidis* insertion sequences (ISSep1-like transposases) were upregulated and warrant further investigation.

In all discussions of bacterial responses to ELF-MF, the differences and contradictions in effects are discussed as being due to different magnetic field parameters. Mutagenic effects such as DNA damage were studied at 50 and 60 Hz with effects typically observed above 0.2 mT although small responses were observed for the few studies at 0.07 and 0.1 mT (Chow and Tung, 2000a; Del Re et al., 2004), just above the geomagnetic field. While Li and Chow report results at 1.2mT, they also report attempts to study exposures below the geomagnetic field (0.01 and 0.03 mT fields) exposures but determined, if present, the responses were below the resolution of the analysis. They suggested that, while closer to what would be experienced in daily life, the fields would not be strong enough to generate oxidant radicals, thought to be the cause of stress responses in *E. coli,* creating weak activity or effects that bacterial could successfully combat with defense mechanisms (Li and Chow, 2001). In contrast, the studies reporting frequency-dependent biological effects were all found at ELF-MF B_{AC} magnitudes around half of the geomagnetic field. It is possible that mutagenic effects may occur above certain ranges of the AC magnetic field component but at lower field intensities, biological effects are more affected by specific frequencies.

Taking these transcriptomic results together, a prediction of overall processes occurring in *S. epidermidis* biofilms in response to an ELF-MF is presented in Figure 4.6. We have inferred possible protein activity for identifiable systems based on gene expression data only and these predictions would need to be tested further.

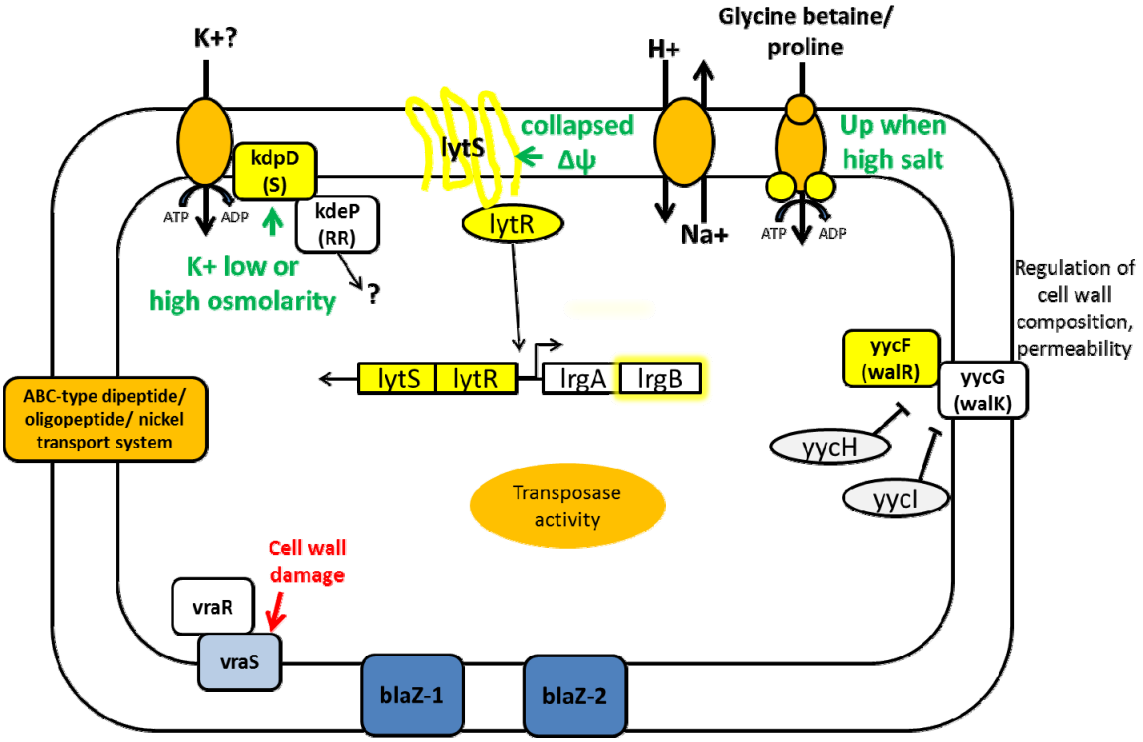

Figure 4.6 Possible cell processes based on transcriptome data for known or predicted bacterial systems. Upregulated genes or proteins are indicated in yellow (1.5≤FC) or orange (2.0≤FC). Downregulated proteins or genes are light blue (-1.5≥FC) or dark blue (-2≥FC). White indicates a |FC|<1.5. Haze indicates a gene upregulated or downregulated as indicated by the colors above but not statistically significant.

In this study we report a change in gene expression in *S. epidermidis* biofilms when grown in an ELF-MF providing evidence that *S. epidermidis* both senses and responds to weak ELF-MFs. The changing systems implicate effects on the cell membrane and processes related to ion flux in and out of the cell that could potentially be exploited to stress or stimulate bacteria in biofilm. No changes in CFU were found and thus these changes do not appear to perturb cell viability, however the downregulation of cell division could indicate changes in cell morphology. The results serve as evidence for ELF-MF effects in biofilm. While the responses were found at the K^+ resonance frequency, the results should only be considered as preliminary support for ion resonance

frequency-related effects in biofilm systems. Study of responses, such as those identified here, across a spectrum of tuning parameters is needed. This work provides directions for future investigations.

CHAPTER 5: CONCLUSIONS

The preceding chapters explored bacterial responses to electric current and magnetic fields as alternative approaches for the treatment of biofilm-related infections. In Chapter 2, the use of low levels of direct electric current (DC) was demonstrated to have killing effects against *S. epidermidis* and *P. aeruginosa* biofilms under varying and physiologically relevant chloride conditions and electrolytic chlorine generation was identified as a primary mechanism of killing. In Chapter 3, a gene level comparison identified similar changes in the global transcriptome profiles with DC and chlorine treatments, providing further evidence for a chlorine generation mechanism during DC exposure, both of which lead to oxidative stress in biofilms. In Chapter 4, global transcriptomics were used to detect evidence of bacterial responses to growth in extremely low-frequency magnetic fields (ELF-MFs) and identify gene level responses specific to particular combinations of frequency and field magnitudes. Here, these chapters are synthesized, electrochemical mechanisms are further explored, and future directions for these two approaches are discussed.

DC Treatment of Biofilms

In Chapters 2 and 3, direct current (DC) treatment of biofilms and the bioelectric effect were investigated using measures of cell viability, solution chemistry, and gene level responses. DC has previously been reported to synergistically enhance antimicrobial efficacy, a phenomenon termed the bioelectric effect (reviewed in Chapters 1 and 2). In the studies presented here, experimental parameters were adjusted to study

DC effects at physiological sodium chloride concentrations more relevant to conditions found *in vivo*. Under these conditions, electrolytic generation of chlorine was identified as a major mode of action by which direct current kills *Staphylococcus epidermidis* and *Pseudomonas aeruginosa* biofilms. This effect was strongest in chloride-containing medium and was greatly reduced or absent in chloride-free medium. Further, no evidence was found for synergistic enhancement of antibiotics effects with DC, identifying DC treatment as an effective means of biofilm treatment independent of other antimicrobials. In Chapter 3, the theory of electrolytic chlorine generation was further tested using full transcriptome analysis of DC and chlorine treated *S. epidermidis* biofilms. Over half of the genes upregulated during DC treatment were also upregulated with chlorine treatment, and conversely just under half of the genes downregulated in response to DC were also downregulated in response to chlorine treatment. Genes and pathways of the DC response agreed well with transcriptome studies of chlorine and hydrogen peroxide treatment of staphylococci in the literature (Chang et al., 2007; Chang et al., 2006; Palazzolo-Ballance et al., 2008), confirming oxidative stress of biofilm due to chlorine and possible other oxidative species in response to DC treatment.

The electrical enhancement of antimicrobials has been an intriguing phenomenon and although this effect was not observed in our study system, many of the initial experimental design parameters were based on studies of the bioelectric effect in the literature. Through the course of this study, experimental parameters were identified that have significant importance in the study of electrolyzed systems. With the potential for many electrochemical reactions, selection of electrode materials and consideration of

electrolytes and media components are important both in *in vitro* assessment of electric current effects as well as for translation to *in vivo* systems. What follows is a discussion of these parameters and the related electrochemistry.

Electrode Material

The electrolytic reactions that occur due to the input of electrical energy are determined by the reduction potential of chemical species present in the system including the electrode material. Reactivity of metal electrodes is of primary concern at the anode, as solid metal electrodes cannot be reduced and oxidization will not occur at the cathode. This property is utilized in industrial applications such as electroplating where electrolysis is used to deposit aqueous metal compounds as a coating on cathodic electrodes. However, reaction and corrosion of non-inert electrodes is typically undesirable and with few exceptions (Secinti et al., 2008) would not be tolerated in potential medical applications of DC.

During preliminary design of the DC setup, Nichrome and stainless steel electrodes were tested in several configurations but were quickly determined to be unsuitable due to extensive corrosion (Sandvik et al., 2013). Corrosion was clearly observable in dilute chloride solutions in as little as 20 minutes of DC application as discoloration and precipitation (Figure A.2) from the anode of stainless steel wire and stainless steel plate electrodes and from both Nichrome electrodes (Figure A.1). Corrosion continued to the extent of covering the coupons within 24 hours (Figure A.1C and D). A very slow switch of polarity (every 30 minutes) did not alleviate corrosion issues (Figure A.2A-E). Alternating polarity every 64 seconds was used in earlier

bioelectric studies (Blenkinsopp et al., 1992b; Blenkinsopp et al., 1991; Costerton et al., 1994; Khoury et al., 1992) presumably to prevent corrosion issues. As both salinity and chlorine are known to corrode stainless steel (Frankel, 1998), these results were not unexpected but the speed and extent of corrosion were surprising. These observations raised questions about the role of electrode corrosion in previous reports of the bioelectric effect, the majority of which used stainless steel electrodes (reviewed in Chapter 1 and 2). While most studies have eliminated chloride effects by omitting this ion, stainless steel corrosion was still reported in chloride-free medium (Blenkinsopp et al., 1991; Khoury et al., 1992) and it is possible that corrosion did occur in other instances but at rates that were not detected. Flow conditions could further obscure detection of corrosion. Recent studies have led to similar speculation concerning the possible contribution of toxic corrosion products in bioelectric studies using stainless steel electrodes. These comments were based on observations of larger killing effects with stainless steel electrodes compared to carbon electrodes within the same system (del Pozo et al., 2009b; Szkotak et al., 2011) and increased gene expression of metal toxicity genes in electrolyzed systems with stainless steel electrodes (Szkotak et al., 2011; Szurmant et al., 2007).

Given these considerations, the work presented in Chapter 2 and 3 used experimental wells with inert, platinum electrodes. No indication of electrode corrosion was observed throughout five years of experimentation. Inert electrodes thus eliminated a potential confounding factor in assessment of predominant electrochemical reactions measured in Chapter 2, as corrosion reactions need not be considered. In Chapter 3, gene responses to DC, electrolysis, and current flow through and around biofilm were

considered without complications of corrosion. In contrast, a transcriptome study of DC effects on *Bacillus subtilis* reported dose-responsive increases in precipitated debris in AFM images along with induction of genes related to metal (zinc, cadmium, and copper) toxicity and nine metal resistance genes using stainless steel electrodes in chloride-containing media, (Szkotak et al., 2011). The decreases in cell viability were reduced when the stainless steel electrodes were replaced with graphite, thus identifying stainless steel corrosion products as an important factor generating biocidal effects with DC (Szkotak et al., 2011).

It is possible that industrial applications could tolerate release of corrosion products from electrodes during DC treatment, assuming corrosion of piping and equipment did not occur. However, release of corrosion products *in vivo* could be detrimental. Corrosion of metal orthopedic implants in living tissue by friction and corrosion reactions, "biocorrosion", has been reported for extracellular metal particles measuring up to 5 mm in diameter resulting in necrotic tissue and foreign body response (Jacobs et al., 1998) and has been implicated in aseptic loosening (Cadosch et al., 2009). The potential to further aggravate infected tissue via electrolytic corrosion products from electrodes or metal components of medical implants with DC should thus raise concern. *In vivo* corrosion of stainless steel electrodes used in DC treatment has already been indicated in a rabbit model as evidenced through discoloration the bone where the wire electrode was wrapped (del Pozo et al., 2009a). Similarly, intentional electrolytic release of titanium clusters into host tissue have been shown to kill bacteria but simultaneously induce substantial host tissue inflammation and damage (Secinti et al., 2008). Electrode

material is thus an important consideration for design of *in vitro* studies to identify mechanisms of the bioelectric effect and avoidance of potential adverse effects *in vivo*. Configurations in which an inert electrode is only used at the anode can eliminate corrosion while still utilizing stainless steel implants as demonstrated *in vivo* by van der Borden et al. (2007) using a stainless steel implant cathode with an inert platinum wire anode on the skin surface.

Electrolyte and Media Composition

The use of DC for biocidal action against bacteria would rarely be employed in highly defined media outside of the laboratory setting. Both in the *in vivo* setting of tissues and in industrial applications, such as waste water treatment, the composition of treated material is likely to contain a mix of organic and inorganic materials including mixed electrolytes. In urine, for instance, sodium, chloride, potassium, and ammonium ions and the organic metabolites urea, creatinine, hippuric acid, and citric acid make up the eight most abundant of 2,651 total metabolites recently identified in the "human urine metabolome" (Bouatra et al., 2013). Such media complexity hinders analysis of simultaneous reactions of medium components in the presence of an electric current. However, insight can be gained first through evaluation of components that could serve as electrolytes.

Chloride. A main difference between the DC work presented here and previous work on the bioelectric effect was inclusion of chloride to more accurately approximate physiological conditions. Chloride serves as a strong electrolyte and simultaneous reactant, carrying current throughout the media while being consumed to release chlorine

gas and generating reactive chlorine species including hypochlorous acid and hypochlorite. Chlorine production was measureable during DC application in chloride-containing media (Figure 2.4). Such chlorine species are known to have strong antimicrobial properties. The positive and negative effects of electrolytic generation of chlorine *in vivo* remains unanswered. One could propose that the natural presence of chloride establishes a mechanism for effective DC therapy that obviates need for an antibiotic. Additionally, these biocidal agents could be generated at the site of a conductive implant potentially delivering highly localized treatment. Sodium hypochlorite as Dakin's Solution has long been used as a topical treatment in wound care (Cornwell et al., 2010) and is the most commonly used endodontic irrigation solution used for debridement of diseased pulp space during root canal treatments, specifically due to its ability to dissolve soft necrotic tissue (Zehnder, 2006). Though complications arising from sodium hypochlorite exposure to tissue outside of the infected zone (discomfort to severe tissue damage) in the oral cavity has made its use somewhat controversial (Chaudhry et al., 2011), it remains a standard in practice owing to its efficacy against recalcitrant chronic wounds (Cornwell et al., 2010). These topical uses illustrate a delicate balance between the utility of sodium hypochlorite for treatment of a diversity of bacterial infections and the potential for damage to the surrounding tissue. Electrolytic generation of hypochlorite for treatment of bacterial/tissue systems could trigger similar adverse consequences but these effects may be reduced by application of lower current levels. The relatively low (100μA), continuous current levels used over 21 days to successfully treat *S. aureus* in an *in vivo* fixator without tissue damage (van der

Borden et al., 2007) support potential for lower rates of chlorine generation with lower current levels.

Electrolytic chlorine generation offers a potent control mechanism against bacteria. Chlorine generation was furthermore identified as the primary mechanism by which DC kills *S. epidermidis* biofilms as the same log reductions (LR) in viable cells were achieved with DC alone or a chlorine dose representative of the chlorine generated for that current level (Figure 2.2). If parallel electrolytic reactions (other than with chloride) were occurring, the contribution to overall killing would be likely negligible but is of interest should chlorine reactions not occur to the degree observed in the treatment wells used in Chapters 2 and 3.

Chloride-free Medium. To identify potential parallel reactions in the standard treatment solution (TSB, 9 g/L NaCl) used in Chapter 2 and 3, electrolyte contribution and reactions of other medium components were first examined. TSB consists of a glucose (dextrose) carbon source, peptone and tryptone as nitrogen sources, NaCl for osmotic balance, and a potassium phosphate buffer. Of these components, sodium chloride and potassium phosphate will both ionize in water and thus should be conductive in solution. The chemical makeup of peptone and tryptone were unknown as undefined protein digests that may retain trace ions and thus conductivity of these solutions was determined experimentally. Preliminary experiments mentioned in Chapter 2 (and documented in APPENDIX A) were performed to investigate the ability of TSB lacking chloride and the individual components of TSB to carry current over a range of voltage levels. Concentrations of individual components were the same as that found in full or

$1/10^{th}$ strength TSB. Solutions of full strength TSB (containing 5g/L NaCl) and 5g/L NaCl carried the same current levels identifying chloride as the electrolyte when present in solution (Figure A.4A). Solutions of NaCl alone also achieved higher current levels at the same voltage than the combined TSB components excluding chloride, consistent with chloride's role as a strong electrolyte (Figures A.4). As independent solutions, potassium phosphate showed current-carrying capacity and to a lesser extent the organic nitrogen sources tryptone and peptone were also capable of supporting current flow albeit at lower levels compared to combined components (Figure A.4). Glucose (dextrose) solutions or NanoPure water should not be conductive if free of trace ions, as was revealed by complete absence of current flow in our solutions. Even though a strong electrolyte such as chloride would predominate in electrolysis reactions, other components may react with the products of electrolysis. The organic components of TSB react with the chlorine product of electrolysis as indicated by the inability to detect measureable free chlorine in TSB solutions when the organics were present (Chapter 2). These reactions could lead to formation of chlorine disinfectant byproducts. Therefore, lack of component involvement in electrolytic processes does not preclude reactivity in the system.

To isolate DC effects unrelated to chlorine generation, the same current levels were applied in chloride-free medium. Despite the electrolyte activity just discussed, TSB lacking chloride did not reach the 2-5mA current level within the 5-12V range of the current controllers used for biofilm experiments (Figure A.4). Thus, the substitute electrolytes sulfate, nitrate, and phosphate were used at equimolar concentrations to generate identical current levels as achieved in chloride-containing solutions (Figure

A.5). These electrolytes were chosen as they were not thought to partake in primary metabolic processes although some decrease in stationary survival was observed, partly due to removal of chloride (Figures A.6 and A.7). Additionally, in contrast to chloride as an electrolyte and reactant, aqueous solutions of sodium sulfate or sodium nitrate would be predicted to serve only as electrolytes, conducting current with the overall reaction resulting in the electrolysis of water. Using these alternate electrolytes would thus remove chlorine generation effects, while pH changes and any effect of current flowing through or around the biofilm would remain. Choice of an equimolar concentration of phosphate as an additional substitute electrolyte also achieved the desired current levels while the increased buffer capacity would diminish pH effects. If water electrolysis was occurring, results in the three substitute electrolytes would be expected to be similar unless phosphate buffering of pH shifts decreased antimicrobial efficacy. Experimentally, the result of DC treatment with the substitute electrolytes nitrate or sulfate resulted in *S. epidermidis* biofilm killing although to a lesser degree than chloride containing medium (Figure 2.5). In contrast, no killing was observed for phosphate substituted medium (Figure 2.5). Several explanations could be considered for killing in sulfate- and nitrate-containing medium.

One explanation for killing in sulfate-substituted media would be formation of electrolytic products specific to a sodium sulfate solution. Neglecting the undefined components in tryptone and peptone, the following reactions could be considered for electrolysis of a TSB solution with 0.154M sodium sulfate substituted for 0.154M sodium chloride accounting for the ions in sodium sulfate, the buffer and the aqueous solvent. At

the cathode, the following reductions could occur where E^o is the standard reduction potential (1M concentration of dissolved species, 1atm, 25°C):

$$K^+(aq) + e^- \rightarrow K(s) \qquad E^o = -2.93 \qquad (5.1)$$

$$Na^+(aq) + e^- \rightarrow Na(s) \qquad E^o = -2.71 \qquad (5.2)$$

$$SO_4^{2-}(aq) + H_2O(l) + 2e^- \rightarrow SO_3^{2-}(aq) + 2OH^-(aq) \qquad E^o = -0.93 \qquad (5.3)$$

$$2H_2O + 2e^- \rightarrow H_2(g) + 2OH^-(aq) \qquad E^o = -0.83 \qquad (5.4)$$

$$2H^+(aq) + 2e^- \rightarrow H_2(g) \qquad E^o = 0.00 \qquad (5.5)$$

Reduction of potassium or sodium will not occur due to the strong negative standard reduction potential. As an anion, sulfate would migrate to the anode and would not be considered as a reactant at the cathode but furthermore would be less favorable to reactions with higher reduction potential. Reduction of the hydrogen ion to hydrogen gas (Equation 5.4) is the most favorable reaction but at neutral pH reaction Equation 5.4 likely predominates. At the anode, the oxidation reactions could result from the following reactions in reverse:

$$O_2(g) + 4H^+(aq) + 4e^- \rightarrow 2H_2O \qquad E^o = +1.23 \qquad (5.6)$$

$$S_2O_8^{2-} + 2e^- \rightarrow 2SO_4^{2-} \qquad E^o = +2.07 \qquad (5.7)$$

The high standard reduction potential of sulfate to peroxydisulfate ($S_2O_8^{2-}$) makes sulfate one of the most difficult anions to oxidize, which is why sulfate is often used as an electrolyte to support electrolysis of water. The lower standard reduction potential (higher oxidation potential) of water oxidation (Equation 5.6) is the favored reaction. Sodium persulfate production can be achieved electrolytically, but in mixtures of nearly saturated sodium sulfate in sulfuric acid (Radimer and McCarthy, 1979) in which the

reactions at cathode and anode are represented by Eq 5.5 and 5.7, respectively. Under neutral conditions, Equation 5.6 would be predicted at the anode and the overall reaction would result in electrolysis of water with formation of oxygen and hydrogen gas with no net effect on sulfate.

$$2H_2O \rightarrow O_2(g) + 2H_2(g) \qquad (5.8)$$

This analysis considers sodium sulfate and the ionic components found in the buffer but cannot account for components in the undefined protein digests found in the media which could contain additional ionic compounds.

A similar analysis of a sodium nitrate solution can be considered. Again, neglecting the undefined components in tryptone and peptone, Equations 5.1-5.2, 5.4-5.6 would still apply. Again, it should be noted that as tryptone and peptone are sources of amino acids and nitrogen in the medium, other species may not be represented in this assessment. During electrolysis, anions are likely oxidized at the anode. For the case of the nitrate anion, an oxidizing agent, nitrogen is at the highest oxidation state and nitrate can only be reduced, eliminating nitrate from reactions at the anode where oxidation of water will again occur (Equation 5.6). Reduction reactions involving nitrate and related species follow:

$$NO_2^-(aq) + H_2O(l) + e^- \rightarrow NO(g) + 2OH^-(aq) \qquad E^o = -0.46\ V \quad (5.8)$$

$$NO_3^-(aq) + 2H^+(aq) + e^- \rightarrow NO_2^-(g) + H_2O(l) \qquad E^o = +0.80V \quad (5.9)$$

$$NO_3^-(aq) + 10H^+(aq) + 8e^- \rightarrow NH_4^+(g) + 3H_2O \qquad E^o = +0.88V \quad (5.10)$$

$$NO_3^-(aq) + 4H^+(aq) + 3e^- \rightarrow NO(g) + 2H_2O \qquad E^o = +0.96V \quad (5.11)$$

$$NO_3^-(aq) + 12H^+(aq) + 10e^- \rightarrow N_2(g) + 6H_2O \qquad E^o = +1.25V \quad (5.12)$$

Considering the above reactions, all reactions for the reduction of nitrate (Equation 5.9-1.12) are favored under acidic conditions. Reduction of nitrite (Equation 5.8) could occur at neutral pH but would first require reduction of nitrate to nitrite or nitrite present in the undefined (tryptone, peptone) portion of the medium. Thus, under neutral pH conditions, such as those under which DC treatment with nitrate electrolyte occurred, water reduction again would be predicted at the cathode and the overall reaction across the treatment well would be electrolysis of water (Equation 5.8). While not predicted at neutral pH, anion reduction of nitrate has been widely studied for nitrate removal from waste streams and can be accomplished electrolytically under alkaline and acidic conditions (da Cunha et al., 2000; Dima et al., 2003). The goal of these applications is to reduce NO_3^- to NH_3 or N_2 gas, however many intermediate nitrogen species including NO_2^-, HNO_2, NO, N_2O, and NH_2OH can form depending on pH, electrode material, the applied potential, and the presence of co-contaminants or supplemental compounds (da Cunha et al., 2000; Dima et al., 2003; Li et al., 1988a; Li et al., 1988b; Peel et al., 2003). On platinum electrodes, measures of nitrate reduction in nitric acid initiates with the formation of NO followed by N_2O (da Cunha et al., 2000), the former of which has antimicrobial properties both in the innate immune system (MacMicking et al., 1997) and in therapeutic applications (Schairer et al., 2012).

pH gradients offer an alternate explanation for DC killing observed in sulfate and nitrate substituted systems. The half reactions for electrolysis of water are:

$$2H_2O \rightarrow O_2(g) + 4H^+(aq) + 4e^- \quad \text{(anode)} \quad (5.13)$$

$$4H_2O + 4e^- \rightarrow 2H_2(g) + 4OH^-(aq) \quad \text{(cathode)} \quad (5.14)$$

While the net change in pH is zero, production of H^+ would result in more acidic condition at the anode versus a higher pH with OH^- production at the cathode. Similar pH gradients were predicted by the half reactions in sodium chloride electrolysis and were measureable as a large pH gradient during current flow (Figure A.3) but no net change in pH over the course of treatment (Figure 2.3). The killing gradients in the chloride systems with increased killing at the cathode compared to coupons towards the center of the well (Figure 2.4) also parallel pH extremes from pH values near 9 at the cathode to near neutral conditions near the center of the well (see Chapter 2 for further discussion of pH effects of electrolyzed chloride solution). In chloride-free medium, a large pH gradient could account for reductions observed in nitrate and sulfate substituted systems but would warrant further investigation. Alkaline treatments with NaOH have been reported to weaken biofilm stability (Simoes et al., 2005). While high pH may impair biofilm structure, high pH with $Ca(OH)_2$ treatment failed to reduce biofilm viability (van der Waal et al., 2011), thus indicating a trend of preferential removal rather than killing of biofilms at high pH, the same trend demonstrated in electrolyzed sodium chloride solutions at high pH (Sun et al., 2012). The strongest support for a pH mechanism of DC in nitrate- and sulfate-substituted systems is lack of biofilm reduction with DC in the phosphate-substituted medium (Figure 2.5). Increasing the phosphate concentration allowed for current flow in the medium while additionally increasing the buffering capacity. Within the buffering capacity of the solution, pH changes would not be observed. Thus, if a pH mechanism of DC efficacy is supported, killing would not be predicted in the buffered system.

Future Direct Current Work

Assessment of Tissue Damage Associated with DC. Based on the *in vitro* findings, we have reason to predict that chlorine would be generated if DC was used *in vivo* based on chloride presence in the body. The most fundamental question yet to answer is what effects does DC have on host tissue? Based on well-designed animal studies utilizing an inert anode, DC can be effective with little tissue damage (van der Borden et al., 2007) but an in-depth study of histology and other factors is needed. It is possible that simultaneous treatment could be addressed *in vitro* using a co-culture method in which tissue and biofilm are grown together such as the biofilm/human kerotinocytes scratch model described by Kirker et al. (2009). Using the system, human keratinocytes, cells of the epidermis, are grown in the bottom of a plate under a bacterial biofilm separated by a 0.2 μm porous membrane (Kirker et al., 2009). Modifications of this method and appropriate cell lines would need to be assessed. However, to fully assess tissue damage, *in vivo* experiments would likely be necessary.

Current Flow in an Internal Joint and Measures of Zone of Efficacy. The practical application of current to an artificial joint through skin, muscle, and bone is a further consideration. To be used for orthopedic implants, electrode attachment would need to protrude through the skin. While insertion of electrodes was originally thought to be a strong deterrent to implementation, patients suffering from infected orthopedics implants are often facing a second surgery to remove and replace the device or cannot go through the surgery because of multiple co-morbidities. In such cases, a DC therapy may outweigh the risk of potential tissue damage. Chlorine is highly reactive and may react

so readily with organics immediately adjacent to the electrode as to limit its diffusion radius. An assessment of current flow should include measures of diffusion zones of biocide and biocide reaction products in a tissue system.

Repeat of Previous Bioelectric Experiments with Inert Electrodes. One phenomenon we have not addressed is the bioelectric effect, as no synergistic enhancement of antibiotics with DC was observed in *S. epidermidis* with ciprofloxacin or *P. aeuruginosa* with tobramycin (Chapter 2). The results of studies reporting synergistic enhancement of antibiotics (reviewed in Chapters 1 and 2) are intriguing however questions arise concerning possible contribution of toxic corrosion products from stainless steel electrodes in those studies. The cleanest means of resolving this issue would be to repeat one or several of the bioelectric effect experiments as reported, simply replacing the electrodes with inert electrodes such as platinum. This would be an interesting assessment of DC synergy with antibiotics which could potentially then be expanded to chloride-containing medium.

ELF-MF Treatment of Biofilms

In Chapter 4, global transcriptomics were used to determine if *S. epidermidis* biofilms respond to growth in an extremely low-frequency magnetic field (ELF-MF). Unlike the DC work discussed above, there is no basis for anticipating electrolytic reactions in a magnetic field. Furthermore, ELF-MFs will penetrate tissues without electrodes or direct contact with the body and could be administered noninvasively. The frequency of the ELF-MF were selected based on ion resonance frequencies for calcium

and potassium, ions of biological importance, and static components of the ELF-MF were on the magnitude of the geomagnetic field. Microarray analysis identified differential gene expression for biofilm grown in ELF-MFs at the potassium ion resonance frequency but minimal to no effect at the calcium frequency. Further, an enhanced response was observed at the same potassium resonance frequency with an increase of the magnitude of the time-varying component of the MF (which also increases *h'*, the ratio of time-varying to static MF components). To our knowledge, this is the first transcriptome study of ELF-MFs effects in biofilm, and the first study to identify conditions under which differential gene expression occurs in bacteria in response to ELF-MFs (no changes in gene expression were found in a recent transcriptome study of *E. coli* exposed to a 50Hz, 1mT ELF-MF (Huwiler et al., 2012)).

ELF-MF Field Parameters.

In eukaryotic systems, ELF-MF elicit a variety of biological responses specific to ion resonance frequencies (reviewed in Chapter 1, summarized in Table 1.1, (Liboff, 2005)). These effective frequencies are identified by a peak in the biological response during scans across a range of frequencies. Evidence also exists for ion resonance frequencies in bacteria, identifying peak DNA relaxation and DNA-protein associations at resonance frequencies in *E. coli* (Belyaev and Alipov, 2001). The biological responses to ELF-MFs studied in bacteria primarily relate to potential mutagenic effects (reviewed in Chapter 4). We chose to use ELF-MF at ion resonance frequencies to determine if ion resonance frequencies could also be effective in *S. epidermidis* biofilms. As the effects of those ion resonance frequencies were unknown, microarray technology allowed for

simultaneous examination of every gene in the organism at the transcriptional level. If no differentially expressed genes were detected, it is likely bacteria were not sensing and responding to the magnetic fields.

MF tuning parameters were calculated for fundamental resonance frequencies (Equations 1.16 or 1.17 for n=1) for two biologically relevant ions, Ca^{2+} and K^{+}. Three parameters described the magnetic field for each setting: the static component of the magnetic field (B_o), set for these experiments to the geomagnetic field, the time-varying component of the magnetic field (B_{AC}), and the frequency of the time-varying component (f). The ion resonance frequency is only a function of B_o and the charge to mass ratio for the ion and is independent of B_{AC}. Full transcriptome profiles were compared for colony biofilms grown for 24 hours in three time-varying magnetic field tunings compared to control biofilms in the same chamber experiencing the static magnetic field only (Table 4.1). All of the MF tunings had the same B_o (600 mG). Two of the MF tunings had the same B_{AC} (400 mG) and only differed in f set to the Ca^{2+} resonance frequency (45.9 Hz) or the K^{+} resonance frequency (23.5 Hz) corresponding to a B_o=600mG. The third tuning had the same frequency at the K^{+} tuning (23.5Hz) but the magnitude of the time-varying component of the MF was increased to 1,080 mG. Variation of B_{AC} was based on theoretical and experimental evidence for maximum biological response to MFs tuned to ion resonance frequencies at a ratio of $h'=B_{AC}/B_o$ around 1.8 compared to greatly decreased responses at the ratio used for the previous tunings, h'=0.7 (Binhi, 2000).

The number of differentially expressed genes for the three tunings suggest responses may depend on both frequency and the ratio of the time-varying and static MF

components (Table 4.2). For the two fields that differed only in frequencies, minimal response was identified for the 45.9 Hz field tuned to the Ca^{2+} resonance frequency (4 upregulated and 6 downregulated genes of 2,536 total genes with p-values≤0.05, any FC) whereas a moderate response was observed in response to growth in the 23.5 Hz field tuned to the K^+ resonance frequency (77 upregulated and 102 downregulated genes with p-values≤0.05, any FC), suggesting a frequency-dependent MF effect. When the B_{AC} of the 23.5 Hz K^+ field was increased from 40 μT (400 mG) to 108 μT (1,080 mG), corresponding to an increase from h'=0.7 to 1.8, a larger effect was observed (339 upregulated and 386 downregulated genes with p-values≤0.05, any FC) demonstrating a clear effect of the time-varying amplitude and/or h' on the number of genes changing in response to the MF. The only other transcriptome study of bacterial MF effects did not target ion resonance frequencies, using a powerline freauency of 50 Hz with a B_{AC} of 1 mT (10,000 mG), and did not identify any significant changes in gene expression for p-values≤0.01, any |FC|≥2 (Huwiler et al., 2012). These same cutoffs applied to the three tunings in Chapter 4 indicate 0, 3, and 34 genes differentially expressed genes for the lower Ca^{2+} tuning, the lower K^+ tuning, and the higher K^+ tuning, respectively.

The larger response observed for the K^+ tuning with B_{AC} of 1,080 mG was further analyzed (Chapter 4). Of particular interest were potential links to ion transport (similar to eukaryotic responses) and mutagenic and/or stimulatory effects (seen in bacteria). Annotations and gene clustering identified significant changes in gene expression in response to the ELF-MF with upregulation of genes coding for two-component signal transduction systems (TCS) and membrane transport systems including the bacterial

kdpATPase high affinity K^+ uptake system, 8 operons for Na^+/H^+ antiporters, the *lytSR* TCS responsive to drops in membrane potential, several operons coding for osmoprotectant systems, and a large group of ABC transporters (summarized in Figure 4.6). Together, this evidence supports an ELF-MF response affecting membrane systems and ion transport as has been seen in a wide range of eukaryotic systems (see Chapter 1, Magnetic Fields) and may support MF effects specific to ion resonance tunings. Additionally, upregulation of genes with transposase and DNA binding activity was observed in *S. epidermidis* grown in the MF while cell division and cell wall biosynthesis were downregulated. Genes of these groups may parallel changes in the rate of transfer of transposable genetic elements, the extent of DNA damage and coiling, and the bacterial heat shock response in *E. coli* that have been reported widely in response to MF at power-line frequencies of 50 and 60 Hz (See Chapter 4, Introduction). Those studies were not designed for tuning to resonance frequencies and while it is possible the powerline frequencies hit a resonance frequency for a certain ion (depending on B_o), it is likely that this represents a separate bacterial stress response to MFs, a stress response that was also seen in the differentially expressed genes reported Chapter 4.

The transcriptome approach uniquely offers a global profile of all genes and systems sensing and responding to growth in the MF and indication of the strongest responses therein. As a means of maximizing potential responses, frequencies were selected based on the ion resonance frequency theory (Equation 1.16), however, due to limitations of microarray experiments, only three experimental conditions were selected. While the advantage of microarray was a wide breadth of responses, there are not

sufficient measurements across a range of MF parameters to draw conclusions on a mechanism or theory, only to support it. Interestingly, the set of significant genes associated with ion homeostasis, membrane transport, and signal transduction systems are consistent with a number of studies, regardless of mechanism. If we were to assume the ICR theory (Liboff, 2005), we would predict that an ELF-MF at the K^+ ion resonance frequency would modify K^+ transport through protein channels. As a primary ion responsible for bacterial cell wall homeostasis, the effect could modify signal transduction and a number of membrane transport responses as the cell compensates for the modified flux of ions. Indeed, results indicate upregulation of genes coding for the *kdpATPase* potassium uptake system as well as *kdpD*, the sensor of the TCS that responds to intercellular K^+ limitation and osmotic stress. Intriguingly, similar responses would be predicted by the mechanism of charge transfer proposed by Blank and Goodman in which ELF-MF modify transport through the Na^+/K^+-ATPase in eukaryotic cells via modification of charge distribution in the protein channel (Blank and Goodman, 2008). The theory surrounding eukaryotic responses proposed by Blank and Goodman also predicts enhanced activity of the Na^+/K^+-ATPase that in turn modifies a cascade of signal transduction systems (Blank and Goodman, 2008; Blank and Goodman, 2009) supporting significant genes of two-component signal transduction systems seen in *S. epidermidis* biofilm (Table 4.3). In this sense we are comparing a prokaryotic system to a eukaryotic system yet they serve similar functions in cells, maintaining homeostasis. As an exploratory experiment this work has opened a number of possible research directions.

Future ELF-MF Work.

Evaluation of Frequency Dependence. While the microarray approach allowed for study of the full transcriptome, it was limiting in the ability to perform studies over a range of field tuning parameters. The benefit of the approach was identification of a variety of responses for design of assays for follow-up screenings. The ICR and ion paramagnetic resonance theories were motivated by observations of peak biological responses when measured across a range of frequencies, originally reported as "frequency windows" in chick embryos (Delgado et al., 1982) and observed in many systems including for Ca^{2+} and K^{+} resonance frequencies in *E. coli* (Belyaev and Alipov, 2001). The data show that, at the same field magnitudes, the K^{+} frequency (23.5 Hz) had a greater response than the higher Ca^{2+} frequency (45.9 Hz) both in the number of changing genes and the magnitude of those changes. However, with only two settings, both frequencies may represent local maxima on a frequency scan or may not represent maxima at all, existing only as points on a linear distribution, independent of a resonance frequency. Identification of peaks in biological responses across frequency (or lack of) may provide evidence for the mechanism(s) of action. Furthermore, larger biological responses may be found by scanning frequency.

Evaluation of B_{AC} or h' Dependence. Similar to the question of frequency-dependent responses is the effect of B_{AC} and/or the ratio of the static and time-varying field components, $h'=B_{AC}/B_o$, across a range of MF tunings. Binhi proposed a theoretical model that predicted a nonlinear function to describe the probability of dissociation of ion-protein complexes across a range of h' (2000). He compared this model for fixed

ion-protein complexes with six previous studies at cyclotron resonance frequencies by normalizing "magnetobiological responses" and overlaying plots for h'=0.1-12, demonstrating significant correlation with peak responses around h'=1.8 (see Figure 1, (Binhi, 2000). The increase in the number of differentially expressed genes observed in our study for K^+ tunings at h'=1.8 compared to h'=0.7 correspond to Binhi's prediction. Using a biological response, such as one identified in the microarray data, assessment across a range of field magnitudes should consider the possibility of a linear or non-linear response to B_{AC} incorporating consideration of h' as a possible parameter to predict peak biological responses.

Evaluation of Transposase Activity. Finally, the highest upregulated cluster of genes was related to transposition activity including a number of transposases of unknown function. Transposition activity was also found to be responsive to ELF-MF in *E. coli* studies and was primarily used as a measure of mutagenesis (Chow and Tung, 2000b; Del Re et al., 2004; Del Re et al., 2003; Giorgi et al., 2011). Increased genetic mobility induced by MF may prove to be a damaging effect on bacteria but could also enhance adaptation to MF exposure. Contradictory responses reported in the *E. coli* literature of MF-induced transposition (Chow and Tung, 2000b), DNA degradation (Li and Chow, 2001), as well as DNA repair (Chow and Tung, 2000a) justify further exploration into the role of transposition and DNA damage and repair in ELF-MF effects in bacterial biofilms.

Perspectives on Electromagnetic Treatment Strategies for Biofilm

The work presented in this dissertation has explored bacterial responses to electromagnetic exposure as potential treatments for biofilm infections, particularly in the context of device-related infections. Biofilms establish on implanted devices *in vivo* and for many reasons, including impeded antimicrobial penetration into the biofilm, decreased bacterial metabolism, and antibiotic resistance, are extremely difficult to treat causing recalcitrant and recurrent infections. Electromagnetic therapies were explored for potential use in conjunction with or in place of traditional antibiotic therapies. While both direct electric current (DC) and extremely low-frequency magnetic fields (ELF-MF) are electromagnetic treatments, the strategies are distinct.

DC exposure has a biocidal effect on biofilm. At physiological chloride concentration, DC kills *S. epidermidis* and *P. aeruginosa* biofilms primarily via electrochemical generation of chlorine compounds (hypochlorous acid and hypochlorite) (Sandvik et al., 2013). These are potent disinfectants known to eradicate bacteria naturally in the innate immune system (Foote et al., 1983; King et al., 1997; Sam and Lu, 2009). Chlorine disinfectants also eradicate bacteria in applied treatments in topical treatments including wound care (Cornwell et al., 2010) and oral surgery (Zehnder, 2006), and in the broad historical use of chorine as a household and industrial disinfectant. Additionally, DC can generate other chemical changes such as pH gradients (Figure A.3) and microarray data indicate potential H_2O_2 responses consistent with an oxidative stress response (Chapter 3). If stainless steel or other non-inert electrodes are used, these biocidal effects may be due to release of metal corrosion products from the

electrodes (Szkotak et al., 2011). DC effects are thus very system-specific and require assessment of all potential reactive species. For DC therapy *in vivo*, electrode connection would be required. For an indwelling orthopedic device, this would require penetration through the skin, potentially using components of the implant as an electrode. The generated electrolytic products originate at these electrodes at the interface of the implant, biofilm, and surrounding tissues. As the reaction of chlorine, an oxidizing agent, with organic material is non-specific (Chapman, 2003), generated chlorine species would consequently react with both biofilm and host tissue. pH changes on or in the immediate vicinity of the electrode may additionally modify biofilm attachment to implants. While possible tissue damage with DC needs to be assessed, a balance of low current levels and minimal tissue damage may be achieved, rendering DC as a viable treatment particularly when co-morbidities preclude surgical intervention to remove infected implants.

In contrast, ELF-MF exposure does not require direct contact and thus offers a potential noninvasive therapy. ELF-MF will penetrate tissues and biofilm matrix unimpeded and thus ELF-MF therapy is independent of the physical properties of the biofilm that may hinder other antimicrobial treatments. The ELF-MFs used in Chapter 4 did not have biocidal effects, however they modified the expression of ion transport systems suggesting potentially perturbed cell homeostasis. The effect ELF-MF-modified ion transport may have on the proton motive force (PMF) could be of interest whether the PMF was dissipated or increased. Many bacterial drug efflux pumps require energy generated from the PMF (Paulsen et al., 1996). The mode of action of certain drugs such as bacteriocins depends on dissipation of the PMF by formation of nonspecific, cation-

specific, or anion-specific pores in Gram-positive organisms, including staphylococcal species (Hechard and Sahl, 2002). The bacteriostatic agent chlorpromazine inhibits potassium efflux in *S. aureus* (Kristiansen et al., 1982). Related mechanisms of action of phenothiazines and thioxanthenes reduce the PMF of *S. aureus* (Kaatz et al., 2003) and PMF-targeted therapies are now emerging as a target particularly in the context of drug resistant organisms including staphylococci (Farha et al., 2013). Identifying optimal ELF-MF that deplete PMF may be a mechanism of inhibiting bacteria. Alternatively, drugs such as aminoglycosides require PMF for uptake (Taber et al., 1987). A potential mechanism by which bacterial persisters tolerate antibiotics is depletion of the PMF and several studies have used carbon sources to measurably increase the PMF in persister cells rendering cells sensitive to aminoglycosides (Allison et al., 2011; Barraud et al., 2013). Due to the high frequency of persister cells in biofilm, a noninvasive means of increasing the PMF via ELF-MF in conjunction with aminoglycosides may serve to target biofilm persisters or stimulate slow-growing bacteria in biofilms without the complications of carbon delivery *in vivo*.

In-vitro DC and ELF-MF effects on bacterial biofilms have been identified in the studies reported here. In the case of DC, future directions should include assessment of current flow and tissue damage in complex tissue systems. The ELF-MF work is the first to identify ELF-MF changes in gene expression in bacteria opening a number of directions for future investigation. *In-vitro* work is required to validate the responses and to assess whether these ELF-MF responses could be manipulated to develop treatment therapies. Within this assessment, investigations of optimal ELF-MF tuning parameters

should be further investigated to determine if responses are frequency or field magnitude-dependent. Specificity to tuning parameters could provide a means of targeted therapy.

REFERENCES CITED

Alipov, Y. D., and I. Y. Belyaev, 1996, Difference in frequency spectrum of extremely-low-frequency effects on the genome conformational state of AB1157 and EMG2 *E. coli* cells: Bioelectromagnetics, v. 17, p. 384-387.

Alipov, Y. D., I. Y. Belyaev, and O. A. Aizenberg, 1994, Systematic reaction of *Escherichia coli* cells to weak electromagnetic fields of extremely low frequency: Bioelectrochemistry and Bioenergetics, v. 34, p. 5-12.

Allison, K. R., M. P. Brynildsen, and J. J. Collins, 2011, Metabolite-enabled eradication of bacterial persisters by aminoglycosides: Nature, v. 473, p. 216-20.

Amin, U. S., T. D. Lash, and B. J. Wilkinson, 1995, Proline betaine is a highly effective osmoprotectant for *Staphylococcus aureus*: Archives of Microbiology, v. 163, p. 138-142.

Anderl, J. N., M. J. Franklin, and P. S. Stewart, 2000, Role of antibiotic penetration limitation in *Klebsiella pneumoniae* biofilm resistance to ampicillin and ciprofloxacin: Antimicrobial Agents and Chemotherapy, v. 44, p. 1818-1824.

ASTM E2562 - 07, 2007, Standard Test Method for Quantification of *Pseudomonas aeruginosa* Biofilm Grown with High Shear and Continuous Flow using CDC Biofilm Reactor, West Conshohocken, PA, American Society for Testing and Materials International. DOI: 10.1520/E2562-07. www.astm.org.

Barranco, S. D., J. A. Spadaro, T. J. Berger, and R. O. Becker, 1974, *In-vitro* effect of weak direct current on *Staphylococcus aureus*: Clinical Orthopaedics and Related Research, p. 250-255.

Barraud, N., A. Buson, W. Jarolimek, and S. Rice, 2013, Mannitol Enhances Antibiotic Sensitivity of Persister Bacteria in *Pseudomonas aeruginosa* Biofilms, PLOS ONE, p. e84220.

Bawin, S. M., and W. R. Adey, 1976, Sensitivity of calcium binding in cerebral tissue to weak environmental electric fields oscillating at low-frequency: Proceedings of the National Academy of Sciences of the United States of America, v. 73, p. 1999-2003.

Becker, R. O., and J. A. Spadaro, 1978, Treatment of Orthopedic Infections with Electrically Generated Silver Ions - Preliminary Report: Journal of Bone and Joint Surgery-American Volume, v. 60, p. 871-881.

Belcheva, A., and D. Golemi-Kotra, 2008, A close-up view of the VraSR two-component system - A mediator of *Staphylococcus aureus* response to cell wall damage: Journal of Biological Chemistry, v. 283, p. 12354-12364.

Belyaev, I., 2011, Toxicity and SOS-response to ELF magnetic fields and nalidixic acid in *E. coli* cells: Mutation Research-Genetic Toxicology and Environmental Mutagenesis, v. 722, p. 56-61.

Belyaev, I. Y., and E. D. Alipov, 2001, Frequency-dependent effects of ELF magnetic field on chromatin conformation in *Escherichia coli* cells and human lymphocytes: Biochimica Et Biophysica Acta-General Subjects, v. 1526, p. 269-276.

Belyaev, I. Y., Y. D. Alipov, and A. Y. Matronchik, 1998, Cell density dependent response of *E. coli* cells to weak ELF magnetic fields: Bioelectromagnetics, v. 19, p. 300-309.

Belyaev, I. Y., Y. D. Alipov, A. Y. Matronchik, and S. P. Radko, 1995, Cooperativity in *Escherichia coli* cell response to resonance effect of weak extremely low frequency electromagnetic field: Bioelectrochemistry and Bioenergetics, v. 37, p. 85-90.

Benjamini, Y., and Y. Hochberg, 1995, Controlling the false discovery rate - A practical and powerful approach to multiple testing: Journal of the Royal Statistical Society Series B-Methodological, v. 57, p. 289-300.

Berger, T. J., J. A. Spadaro, R. Bierman, S. E. Chapin, and R. O. Becker, 1976a, Antifungal properties of electrically generated metallic-ions: Antimicrobial Agents and Chemotherapy, v. 10, p. 856-860.

Berger, T. J., J. A. Spadaro, S. E. Chapin, and R. O. Becker, 1976b, Electrically generated silver ions - quantitative effect on bacterial and mammalian cells: Antimicrobial Agents and Chemotherapy, v. 9, p. 357-358.

Binhi, V. N., 2000, Amplitude and frequency dissociation spectra of ion-protein complexes rotating in magnetic fields: Bioelectromagnetics, v. 21.

Binhi, V. N., Y. D. Alipov, and I. Y. Belyaev, 2001, Effect of static magnetic field on *E. coli* cells and individual rotations of ion-protein complexes: Bioelectromagnetics, v. 22, p. 79-86.

Blackman, C. F., S. G. Benane, D. E. House, and W. T. Joines, 1985, Effects of ELF (1-20 Hz) and modulated (50Hz) RF Fields on the efflux of calcium ions from brain tissue *in-vitro*: Bioelectromagnetics, v. 6, p. 1-11.

Blackman, C. F., S. G. Benane, L. S. Kinney, W. T. Joines, and D. E. House, 1982, Effects of ELF fields on calcium ion efflux from brain tissue *in-vitro*: Radiation Research, v. 92, p. 510-520.

Blanchard, J. P., and C. F. Blackman, 1994, Clarification and application of an ion parametric resonance model for magnetic field interactions with biological systems: Bioelectromagnetics, v. 15, p. 217-238.

Blank, M., 1992, Na,K-ATPase function in alternating electric fields: FASEB J, v. 6, p. 2434-8.

Blank, M., 1995, Electric and magnetic field signal transduction in the membrane Na^+/K^+-adenosinetriphosphatase: Electromagnetic Fields: Biological Interactions and Mechanisms, v. 250, p. 339-348.

Blank, M., 2005, Do electromagnetic fields interact with electrons in the Na,K-ATPase?: Bioelectromagnetics, v. 26, p. 677-83.

Blank, M., 2008, Protein and DNA reactions stimulated by electromagnetic fields: Electromagnetic Biology and Medicine, v. 27, p. 3-23.

Blank, M., and R. Goodman, 1997, Do electromagnetic fields interact directly with DNA?: Bioelectromagnetics, v. 18, p. 111-5.

Blank, M., and R. Goodman, 2002, Low-frequency electromagnetic fields evoke the stress response: Mechanism of interaction with DNA and biomedical applications: IEEE Transactions on Plasma Science, v. 30, p. 1497-1500.

Blank, M., and R. Goodman, 2004, Initial interactions in electromagnetic field-induced biosynthesis: Journal of Cellular Physiology, v. 199, p. 359-363.

Blank, M., and R. Goodman, 2008, A mechanism for stimulation of biosynthesis by electromagnetic fields: Charge transfer in DNA and base pair separation: Journal of Cellular Physiology, v. 214, p. 20-26.

Blank, M., and R. Goodman, 2009, Electromagnetic fields stress living cells: Pathophysiology : the official journal of the International Society for Pathophysiology / ISP, v. 16, p. 71-8.

Blank, M., and L. Soo, 1993, The Na,K-ATPase as a model for electromagnetic field effects on cells: Bioelectrochemistry and Bioenergetics, v. 30, p. 85-92.

Blank, M., and L. Soo, 1996a, Enzyme activation level determines electromagnetic (EM) signal transduction in Na,K-ATPase: Biophysical Journal, v. 70, p. SUAM1-SUAM1.

Blank, M., and L. Soo, 1996b, The threshold for Na,K-ATPase stimulation by electromagnetic fields: Bioelectrochemistry and Bioenergetics, v. 40, p. 63-65.

Blank, M., and L. Soo, 1997, Frequency dependence of Na,K-ATPase function in magnetic fields: Bioelectrochemistry and Bioenergetics, v. 42, p. 231-234.

Blank, M., and L. Soo, 2001a, Electromagnetic acceleration of electron transfer reactions: Journal of Cellular Biochemistry, v. 81, p. 278-283.

Blank, M., and L. Soo, 2001b, Optimal frequencies for magnetic acceleration of cytochrome oxidase and Na,K-ATPase reactions: Bioelectrochemistry, v. 53, p. 171-174.

Blank, M., L. Soo, and V. Papstein, 1995, Effects of low-frequency magnetic fields on Na,K-ATPase activity: Bioelectrochemistry and Bioenergetics, v. 38, p. 267-273.

Blenkinsopp, S., A. Khoury, and J. Costerton, 1992a, Electrical enhancement of biocide efficacy against *Pseudomonas aeruginosa* biofilms.: Applied and Environmental Microbiology, v. 58, p. 3770-3.

Blenkinsopp, S. A., C. P. Anderson, B. D. Ellis, K. Lam, J. W. Costerton, and A. E. Khoury, 1992b, Electrical enhancement of bacterial biocides against sessile populations: Abstracts of the General Meeting of the American Society for Microbiology, v. 92, p. 379-379.

Blenkinsopp, S. A., A. E. Khoury, and W. J. Costerton, 1991, Electrical Enhancement of Biocide Effectiveness against Bacterial Biofilms: 4th International IGT Symposium on Gas, Oil, and Environmental Biotechnology.

Borriello, G., E. Werner, F. Roe, A. M. Kim, G. D. Ehrlich, and P. S. Stewart, 2004, Oxygen limitation contributes to antibiotic tolerance of *Pseudomonas aeruginosa* in biofilms: Antimicrobial Agents and Chemotherapy, v. 48, p. 2659-2664.

Bouatra, S., F. Aziat, R. Mandal, A. C. Guo, M. R. Wilson, C. Knox, T. C. Bjorndahl, R. Krishnamurthy, F. Saleem, P. Liu, Z. T. Dame, J. Poelzer, J. Huynh, F. S. Yallou, N. Psychogios, E. Dong, R. Bogumil, C. Roehring, and D. S. Wishart, 2013, The Human Urine Metabolome: Plos One, v. 8.

Brezonik, P. L., 1994, Chemical kinetics and process dynamics in aquatic systems: Boca Raton, Lewis, 754 p. p.

Buckingham-Meyer, K., D. Goeres, and M. Hamilton, 2007, Comparative evaluation of biofilm disinfectant efficacy tests.: Journal of Microbiological Methods, v. 70, p. 236-44.

Cadosch, D., E. Chan, O. P. Gautschi, and L. Filgueira, 2009, Metal is not inert: Role of metal ions released by biocorrosion in aseptic loosening-Current concepts: Journal of Biomedical Materials Research Part A, v. 91A, p. 1252-1262.

Cairo, P., B. Greenebaum, and E. Goodman, 1998, Magnetic field exposure enhances mRNA expression of sigma(32) in *E. coli*: Journal of Cellular Biochemistry, v. 68, p. 1-7.

Capra, E. J., and M. T. Laub, 2012, Evolution of Two-Component Signal Transduction Systems, in S. Gottesman, C. S. Harwood, and O. Schneewind, eds., Annual Review of Microbiology, Vol 66: Annual Review of Microbiology, v. 66: Palo Alto, Annual Reviews, p. 325-347.

Chang, M. W., F. Toghrol, and W. E. Bentley, 2007, Toxicogenomic response to chlorination includes induction of major virulence genes in *Staphylococcus aureus*: Environmental Science & Technology, v. 41, p. 7570-7575.

Chang, R., 1987, Chemistry: New York, Random House, xxiv, 1046, A47 p. p.

Chang, W., D. A. Small, F. Toghrol, and W. E. Bentley, 2006, Global transcriptome analysis of *Staphylococcus aureus* response to hydrogen peroxide: Journal of Bacteriology, v. 188, p. 1648-1659.

Chapman, A. L. P., M. B. Hampton, R. Senthilmohan, C. C. Winterbourn, and A. J. Kettle, 2002, Chlorination of bacterial and neutrophil proteins during phagocytosis and killing of *Staphylococcus aureus*: Journal of Biological Chemistry, v. 277, p. 9757-9762.

Chapman, J. S., 2003, Biocide resistance mechanisms: International Biodeterioration & Biodegradation, v. 51.

Chaudhry, H., T. M. Wildan, S. Popat, R. Anand, and D. Dhariwal, 2011, Before you reach for the bleach: British Dental Journal, v. 210, p. 157-160.

Chow, K. C., and W. L. Tung, 2000a, Magnetic field exposure enhances DNA repair through the induction of DnaK/J synthesis: Febs Letters, v. 478.

Chow, K. C., and W. L. Tung, 2000b, Magnetic field exposure stimulates transposition through the induction of DnaK/J synthesis: Biochemical and Biophysical Research Communications, v. 270.

Cooksey, B., and K. E. Cooksey, 1980, Calcium is necessary for motility in the diatom *Amphora coffeaeformis*: Plant Physiology, v. 65, p. 129-131.

Cornwell, P., M. Arnold-Long, S. B. Barss, and M. F. Varnado, 2010, The Use of Dakin's Solution in Chronic Wounds A Clinical Perspective Case Series: Journal of Wound Ostomy and Continence Nursing, v. 37, p. 94-104.

Costerton, J. W., B. Ellis, K. Lam, F. Johnson, and A. E. Khoury, 1994, Mechanism of electrical enhancement of efficacy of antibiotics in killing biofilm bacteria: Antimicrobial Agents and Chemotherapy, v. 38, p. 2803-2809.

Cui, L. Z., H. M. Neoh, A. Iwamoto, and K. Hiramatsu, 2012, Coordinated phenotype switching with large-scale chromosome flip-flop inversion observed in bacteria: Proceedings of the National Academy of Sciences of the United States of America, v. 109, p. E1647-E1656.

da Cunha, M., J. P. I. De Souza, and F. C. Nart, 2000, Reaction pathways for reduction of nitrate ions on platinum, rhodium, and platinum-rhodium alloy electrodes: Langmuir, v. 16, p. 771-777.

Dalman, M. R., A. Deeter, G. Nimishakavi, and Z.-H. Duan, 2012, Fold change and p-value cutoffs significantly alter microarray interpretations: BMC Bioinformatics, v. 13.

Darouiche, R., 2004, Treatment of infections associated with surgical implants.: New England Journal of Medicine, v. 350, p. 1422-9.

Davies, D. G., M. R. Parsek, J. P. Pearson, B. H. Iglewski, J. W. Costerton, and E. P. Greenberg, 1998, The involvement of cell-to-cell signals in the development of a bacterial biofilm: Science, v. 280, p. 295-298.

Davis, C. P., D. Arnett, and M. M. Warren, 1982, Iontophoretic killing of *Escherichia coli* in static fluid and in a model catheter system: Journal of Clinical Microbiology, v. 15, p. 891-894.

Davis, C. P., M. E. Shirtliff, N. M. Trieff, S. L. Hoskins, and M. M. Warren, 1994, Quantification, qualification, and microbial killing efficiencies of antimicrobial chlorine-based substances produced by iontophoresis: Antimicrobial Agents and Chemotherapy, v. 38, p. 2768-2774.

Davis, C. P., N. Wagel, M. D. Anderson, and M. M. Warren, 1993, Iontophoresis and chloride-containing compounds - Parameters required for killing: Journal of Urology, v. 150, p. 1172-1175.

Davis, C. P., N. Wagle, M. D. Anderson, and M. M. Warren, 1991, Bacterial and fungal killing by iontophoresis with long-lived electrodes: Antimicrobial Agents and Chemotherapy, v. 35, p. 2131-2134.

Davis, C. P., N. Wagle, M. D. Anderson, and M. M. Warren, 1992, Iontophoresis generates an antimicrobial effect that remains after iontophoresis ceases: Antimicrobial Agents and Chemotherapy, v. 36, p. 2552-2555.

Davis, C. P., S. Weinberg, M. D. Anderson, G. M. Rao, and M. M. Warren, 1989, Effects of microamperage, medium, and bacterial concentration on iontophoretic killing of bacteria in fluid: Antimicrobial Agents and Chemotherapy, v. 33, p. 442-447.

Davison, W. M., B. Pitts, and P. S. Stewart, 2010, Spatial and temporal patterns of biocide action against *Staphylococcus epidermidis* biofilms: Antimicrobial Agents and Chemotherapy, v. 54, p. 2920-2927.

DeBeer, D., R. Srinivasan, and P. S. Stewart, 1994a, Direct measurement of chlorine penetration into biofilms during disinfection: Applied and Environmental Microbiology, v. 60, p. 4339-4344.

DeBeer, D., P. Stoodley, F. Roe, and Z. Lewandowski, 1994b, Effects of bilfilm structures on oxygen distribution and mass-transport: Biotechnology and Bioengineering, v. 43, p. 1131-1138.

Deibert, M. C., B. R. McLeod, S. Smith, and A. Liboff, 1989, Cyclotron-resonance stimulation of bone healing in rabbits with fibular osteotomies: Clinical Research, v. 37, p. A223-A223.

Deibert, M. C., B. R. McLeod, S. D. Smith, and A. R. Liboff, 1994, Ion resonance electromagnetic field stimulation of fracture healing in rabbits with a fibular ostectomy: Journal of Orthopaedic Research, v. 12, p. 878-885.

del Pozo, J. L., M. S. Rouse, G. Euba, C.-I. Kang, J. N. Mandrekar, J. M. Steckelberg, and R. Patel, 2009a, The electricidal effect is active in an experimental model of *Staphylococcus epidermidis* chronic foreign body osteomyelitis: Antimicrobial Agents and Chemotherapy, v. 53.

del Pozo, J. L., M. S. Rouse, J. N. Mandrekar, M. F. Sampedro, J. M. Steckelberg, and R. Patel, 2009b, Effect of electrical current on the activities of antimicrobial agents against *Pseudomonas aeruginosa*, *Staphylococcus aureus*, and *Staphylococcus epidermidis* biofilms: Antimicrobial Agents and Chemotherapy, v. 53, p. 35-40.

del Pozo, J. L., M. S. Rouse, J. N. Mandrekar, J. M. Steckelberg, and R. Patel, 2009c, The electricidal effect: reduction of *Staphylococcus* and *Pseudomonas* biofilms by prolonged exposure to low-intensity electrical current: Antimicrobial Agents and Chemotherapy, v. 53, p. 41-45.

Del Re, B., F. Bersani, C. Agostini, P. Mesirca, and G. Giorgi, 2004, Various effects on transposition activity and survival of *Escherichia coli* cells due to different ELF-MF signals: Radiation and Environmental Biophysics, v. 43.

Del Re, B., F. Bersani, P. Mesirca, and G. Giorgi, 2006, Synthesis of DnaK and GroEL in *Escherichia coli* cells exposed to different magnetic field signals: Bioelectrochemistry, v. 69, p. 99-103.

Del Re, B., F. Garoia, P. Mesirca, C. Agostini, F. Bersani, and G. Giorgi, 2003, Extremely low frequency magnetic fields affect transposition activity in *Escherichia coli*: Radiation and Environmental Biophysics, v. 42.

Del Re, B., P. Marcantonio, F. Bersani, and G. Giorgi, 2009, Extremely low frequency magnetic field exposure affects DnaK and GroEL expression in *E. coli* cells with impaired heat shock response: General Physiology and Biophysics, v. 28.

Delgado, J. M. R., J. Leal, J. L. Monteagudo, and M. G. Gracia, 1982, Embryological changes inducced by weak, extremely low-frequency electromagnetic fields: Journal of Anatomy, v. 134, p. 533-551.

Dima, G. E., A. C. A. de Vooys, and M. T. M. Koper, 2003, Electrocatalytic reduction of nitrate at low concentration on coinage and transition-metal electrodes in acid solutions: Journal of Electroanalytical Chemistry, v. 554, p. 15-23.

Dubrac, S., and T. Msadek, 2008, Tearing down the wall: Peptidoglycan metabolism and the WalK/WalR (YycG/YycF) essential two-component system: Bacterial Signal Transduction: Networks and Drug Targets, v. 631, p. 214-228.

Ehrlich, G. D., F. Z. Hu, Q. Lin, J. W. Costerton, and J. C. Post, 2004, Intelligent implants to battle biofilms: ASM News, v. 70, p. 127-133.

Farha, M. A., C. P. Verschoor, D. Bowdish, and E. D. Brown, 2013, Collapsing the Proton Motive Force to Identify Synergistic Combinations against *Staphylococcus aureus*: Chemistry & Biology, v. 20, p. 1168-1178.

Flemming, H.-C., and J. Wingender, 2010, The biofilm matrix: Nature Reviews Microbiology, v. 8, p. 623-633.

Fojt, L., L. Strasak, V. Vetterl, and J. Smarda, 2004, Comparison of the low-frequency magnetic field effects on bacteria *Escherichia coli*, *Leclercia adecarboxylata* and *Staphylococcus aureus*: Bioelectrochemistry, v. 63, p. 337-341.

Foote, C. S., T. E. Goyne, and R. I. Lehrer, 1983, Assessment of chlorination by human neutrophils: Nature, v. 301, p. 715-716.

Frankel, G. S., 1998, Pitting corrosion of metals - A review of the critical factors: Journal of the Electrochemical Society, v. 145, p. 2186-2198.

Gill, S. R., D. E. Fouts, G. L. Archer, E. F. Mongodin, R. T. DeBoy, J. Ravel, I. T. Paulsen, J. F. Kolonay, L. Brinkac, M. Beanan, R. J. Dodson, S. C. Daugherty, R. Madupu, S. V. Angiuoli, A. S. Durkin, D. H. Haft, J. Vamathevan, H. Khouri, T. Utterback, C. Lee, G. Dimitrov, L. X. Jiang, H. Y. Qin, J. Weidman, K. Tran, K. Kang, I. R. Hance, K. E. Nelson, and C. M. Fraser, 2005, Insights on evolution of virulence and resistance from the complete genome analysis of an early

methicillin-resistant *Staphylococcus aureus* strain and a biofilm-producing methicillin-resistant *Staphylococcus epidermidis* strain: Journal of Bacteriology, v. 187.

Giorgi, G., P. Marcantonio, F. Bersani, E. Gavoci, and B. Del Re, 2011, Effect of extremely low-frequency magnetic field exposure on DNA transposition in relation to frequency, wave shape and exposure time: International Journal of Radiation Biology, v. 87.

Hechard, Y., and H. G. Sahl, 2002, Mode of action of modified and unmodified bacteriocins from Gram-positive bacteria: Biochimie, v. 84, p. 545-557.

Heermann, R., and K. Jung, 2010, The complexity of the 'simple' two-component system KdpD/KdpE in *Escherichia coli*: FEMS Microbiology Letters, v. 304, p. 97-106.

Herigstad, B., M. Hamilton, and J. Heersink, 2001, How to optimize the drop plate method for enumerating bacteria: Journal of Microbiological Methods, v. 44, p. 121-129.

Hiramatsu, T., K. Kodama, T. Kuroda, T. Mizushima, and T. Tsuchiya, 1998, A putative multisubunit Na^+/H^+ antiporter from *Staphylococcus aureus*: Journal of Bacteriology, v. 180, p. 6642-6648.

Hong, S. H., J. Jeong, S. Shim, H. Kang, S. Kwon, K. H. Ahn, and J. Yoon, 2008, Effect of electric currents on bacterial detachment and inactivation: Biotechnology and Bioengineering, v. 100, p. 379-386.

Horsburgh, M. J., M. O. Clements, H. Crossley, E. Ingham, and S. J. Foster, 2001a, PerR controls oxidative stress resistance and iron storage proteins and is required for virulence in *Staphylococcus aureus*: Infection and Immunity, v. 69, p. 3744-3754.

Horsburgh, M. J., E. Ingham, and S. J. Foster, 2001b, In *Staphylococcus aureus*, Fur is an interactive regulator with PerR, contributes to virulence, and is necessary for oxidative stress resistance through positive regulation of catalase and iron homeostasis: Journal of Bacteriology, v. 183, p. 468-475.

Huang, D. W., B. T. Sherman, and R. A. Lempicki, 2009a, Bioinformatics enrichment tools: paths toward the comprehensive functional analysis of large gene lists: Nucleic Acids Research, v. 37.

Huang, D. W., B. T. Sherman, and R. A. Lempicki, 2009b, Systematic and integrative analysis of large gene lists using DAVID bioinformatics resources: Nature Protocols, v. 4.

Huwiler, S. G., C. Beyer, J. Froehlich, H. Hennecke, T. Egli, D. Schuermann, H. Rehrauer, and H.-M. Fischer, 2012, Genome-wide transcription analysis of

Escherichia coli in response to extremely low-frequency magnetic fields: Bioelectromagnetics, v. 33, p. 488-496.

Inhan-Garip, A., B. Aksu, Z. Akan, D. Akakin, A. N. Ozaydin, and T. San, 2011, Effect of extremely low frequency electromagnetic fields on growth rate and morphology of bacteria: International Journal of Radiation Biology, v. 87, p. 1155-1161.

Irizarry, R. A., B. Hobbs, F. Collin, Y. D. Beazer-Barclay, K. J. Antonellis, U. Scherf, and T. P. Speed, 2003, Exploration, normalization, and summaries of high density oligonucleotide array probe level data: Biostatistics, v. 4, p. 249-264.

Jacobs, J. J., J. L. Gilbert, and R. M. Urban, 1998, Corrosion of metal orthopaedic implants: Journal of Bone and Joint Surgery-American Volume, v. 80A, p. 268-282.

Jass, J., J. W. Costerton, and H. M. Lappin-Scott, 1995, The effect of electrical currents and tobramycin on *Pseudomonas aeruginosa* biofilms: Journal of Industrial Microbiology, v. 15, p. 234-242.

Jass, J., and H. M. Lappin-Scott, 1996, The efficacy of antibiotics enhanced by electrical currents against *Pseudomonas aeruginosa* biofilms: Journal of Antimicrobial Chemotherapy, v. 38, p. 987-1000.

Jensen, L. J., M. Kuhn, M. Stark, S. Chaffron, C. Creevey, J. Muller, T. Doerks, P. Julien, A. Roth, M. Simonovic, P. Bork, and C. von Mering, 2009, STRING 8-a global view on proteins and their functional interactions in 630 organisms: Nucleic Acids Research, v. 37, p. D412-D416.

Kaatz, G. W., V. V. Moudgal, S. M. Seo, and J. E. Kristiansen, 2003, Phenothiazines and thioxanthenes inhibit multidrug efflux pump activity in *Staphylococcus aureus*: Antimicrobial Agents and Chemotherapy, v. 47, p. 719-726.

Khoury, A. E., K. Lam, B. Ellis, and J. W. Costerton, 1992, Prevention and control of bacterial infections associated with medical devices: ASAIO journal (American Society for Artificial Internal Organs : 1992), v. 38.

King, C. C., M. M. Jefferson, and E. L. Thomas, 1997, Secretion and inactivation of myeloperoxidase by isolated neutrophils: Journal of Leukocyte Biology, v. 61.

Kirker, K. R., P. R. Secor, G. A. James, P. Fleckman, J. E. Olerud, and P. S. Stewart, 2009, Loss of viability and induction of apoptosis in human keratinocytes exposed to *Staphylococcus aureus* biofilms in vitro: Wound Repair and Regeneration, v. 17, p. 690-699.

Kristiansen, J. E. H., I. Mortensen, and B. Nissen, 1982, Membrane stabilizers inhibit potassium efflux from *Staphylococcus aureus* strain No U2275: Biochimica Et Biophysica Acta, v. 685, p. 379-382.

Kuhl, M., L. F. Rickelt, and R. Thar, 2007, Combined imaging of bacteria and oxygen in biofilms: Applied and Environmental Microbiology, v. 73, p. 6289-6295.

König, D., J. Schierholz, U. Münnich, and J. Rütt, 2001, Treatment of staphylococcal implant infection with rifampicin-ciprofloxacin in stable implants.: Arch Orthop Trauma Surgery, v. 121, p. 297-9.

Lang, S., M. A. Livesley, P. A. Lambert, W. A. Littler, and T. S. J. Elliott, 2000, Identification of a novel antigen from *Staphylococcus epidermidis*: Fems Immunology and Medical Microbiology, v. 29, p. 213-220.

Lednev, V. V., 1991, Possible mechanism for the influence of weak magnetic fields on biological systems: Bioelectromagnetics, v. 12, p. 71-75.

Lenz, A. P., K. S. Williamson, B. Pitts, P. S. Stewart, and M. J. Franklin, 2008, Localized gene expression in *Pseudomonas aeruginosa* Biofilms: Applied and Environmental Microbiology, v. 74, p. 4463-4471.

Levinger, O., T. Bikels-Goshen, E. Landau, M. Fichman, and R. Shapira, 2012, Epigallocatechin Gallate Induces Upregulation of the Two-Component VraSR System by Evoking a Cell Wall Stress Response in *Staphylococcus aureus*: Applied and Environmental Microbiology, v. 78, p. 7954-7959.

Lewis, K., 2012, Persister cells: molecular mechanisms related to antibiotic tolerance: Handbook of experimental pharmacology, p. 121-33.

Li, H. L., J. Q. Chambers, and D. T. Hobbs, 1988a, Electroreduction of nitrate ions in concentrated sodium hydroxide solutions at lead, zinc, nickel and phthalocyanine-modified electrodes: Journal of Applied Electrochemistry, v. 18, p. 454-458.

Li, H. L., D. H. Robertson, J. Q. Chambers, and D. T. Hobbs, 1988b, Electrochemical reduction of nitrate and nitrite in concentrated sodium hydroxide at platinum and nickel electrodes: Journal of the Electrochemical Society, v. 135, p. 1154-1158.

Li, S. H., and K. C. Chow, 2001, Magnetic field exposure induces DNA degradation: Biochemical and Biophysical Research Communications, v. 280.

Li, X. Y., H. F. Diao, F. X. J. Fan, J. D. Gu, F. Ding, and A. S. F. Tong, 2004, Electrochemical wastewater disinfection: Identification of its principal germicidal actions: Journal of Environmental Engineering-Asce, v. 130, p. 1217-1221.

Liboff, A. R., 1985, Geomagnetic Cyclotron Resonance in Living Cells: Journal of Biological Physics, v. 13, p. 99-102.

Liboff, A. R., 2005, The Charge-to-Mass ICR Signature in Weak ELF Bioelectromagnetic Effects, *in* J. C. Lin, and SpringerLink (Online service), eds., Advances in electromagnetic fields in living systems. Volume 4, v. 4: New York, NY, Springer, p. 189-218.

Liu, W. K., M. R. W. Brown, and T. S. J. Elliott, 1997, Mechanisms of the bactericidal activity of low amperage electric current (DC): Journal of Antimicrobial Chemotherapy, v. 39, p. 687-695.

Maalej, S., I. Dammak, and S. Dukan, 2006, The impairment of superoxide dismutase coordinates the derepression of the PerR regulon in the response of *Staphylococcus aureus* to HOCl stress: Microbiology-Sgm, v. 152, p. 855-861.

MacMicking, J., Q. W. Xie, and C. Nathan, 1997, Nitric oxide and macrophage function: Annual Review of Immunology, v. 15, p. 323-350.

Madkan, A., M. Blank, E. Elson, K.-C. Chou, M. S. Geddis, and R. Goodman, 2009, Steps to the clinic with ELF EMF: Natural Science, v. 1, p. 157-165.

Martin, P. K., T. Li, D. X. Sun, D. P. Biek, and M. B. Schmid, 1999, Role in cell permeability of an essential two-component system in *Staphylococcus aureus*: Journal of Bacteriology, v. 181, p. 3666-3673.

McLeod, B. R., S. Fortun, J. W. Costerton, and P. S. Stewart, 1999, Enhanced bacterial biofilm control using electromagnetic fields in combination with antibiotics: Biofilms, v. 310, p. 656-670.

McLeod, B. R., and E. L. Sandvik, 2010, A biofilm growth protocol and the design of a magnetic field exposure setup to be used in the study of magnetic fields as a means of controlling bacterial biofilms: Bioelectromagnetics, v. 31, p. 56-63.

McLeod, B. R., S. D. Smith, K. E. Cooksey, and A. R. Liboff, 1987a, Ion cyclotron resonance frequencies enhance Ca^{++}-dependent motility in diatoms: Journal of Bioelectricity, v. 6, p. 1-12.

McLeod, B. R., S. D. Smith, and A. R. Liboff, 1987b, Calcium and Potassium Cyclotron Resonance Curves and Harmonics in Diatoms (*Amphora coffeaeformis*): Journal of Bioelectricity, v. 6, p. 153-168.

Montanaro, L., P. Speziale, D. Campoccia, S. Ravaioli, I. Cangini, G. Pietrocola, S. Giannini, and C. R. Arciola, 2011, Scenery of *Staphylococcus* implant infections in orthopedics: Future Microbiology, v. 6, p. 1329-1349.

Nelson, N., 1994, Energizing porters by proton motive force: Journal of Experimental Biology, v. 196, p. 7-13.

Ogino, H., M. Wachi, A. Ishii, N. Iwai, T. Nishida, S. Yamada, K. Nagai, and M. Sugai, 2004, FtsZ-dependent localization of GroEL protein at possible division sites: Genes to Cells, v. 9, p. 765-771.

Oubekka, S. D., R. Briandet, M. P. Fontaine-Aupart, and K. Steenkeste, 2012, Correlative Time-Resolved Fluorescence Microscopy To Assess Antibiotic Diffusion-Reaction in Biofilms: Antimicrobial Agents and Chemotherapy, v. 56, p. 3349-3358.

Palazzolo-Ballance, A. M., M. L. Reniere, K. R. Braughton, D. E. Sturdevant, M. Otto, B. N. Kreiswirth, E. P. Skaar, and F. R. Deleo, 2008, Neutrophil microbicides induce a pathogen survival response in community-associated methicillin-resistant *Staphylococcus aureus*: Journal of Immunology, v. 180, p. 500-509.

Pareilleux, A., and N. Sicard, 1970, Lethal Effects of Electric Current on *Escherichia coli*: Applied Microbiology, v. 19, p. 421-424.

Patton, T. G., S. J. Yang, and K. W. Bayles, 2006, The role of proton motive force in expression of the *Staphylococcus aureus cid* and *lrg* operons: Molecular Microbiology, v. 59, p. 1395-1404.

Paulsen, I. T., M. H. Brown, and R. A. Skurray, 1996, Proton-dependent multidrug efflux systems: Microbiological Reviews, v. 60, p. 575-&.

Pavoni, G., M. Giannella, M. Falcone, L. Scorzolini, M. Liberatore, B. Carlesimo, P. Serra, and M. Venditti, 2004, Conservative medical therapy of prosthetic joint infections: retrospective analysis of an 8-year experience.: Clinical Microbiology and Infection, v. 10, p. 831-7.

Peel, J. W., K. J. Reddy, B. P. Sullivan, and J. M. Bowen, 2003, Electrocatalytic reduction of nitrate in water: Water Research, v. 37, p. 2512-2519.

Peschel, A., M. Otto, R. W. Jack, H. Kalbacher, G. Jung, and F. Gotz, 1999, Inactivation of the dlt operon in *Staphylococcus aureus* confers sensitivity to defensins, protegrins, and other antimicrobial peptides: Journal of Biological Chemistry, v. 274, p. 8405-8410.

Peterson, J. D., L. A. Umayam, T. Dickinson, E. K. Hickey, and O. White, 2001, The Comprehensive Microbial Resource: Nucleic Acids Research, v. 29, p. 123-125.

Pinheiro, J., D. Bates, S. DebRoy, D. Sarkar, and The R Development Core Team, 2011, nlme: Linear and Nonlinear Mixed Effects Models. R package version 3.1-98.

Poortinga, A. T., R. Bos, and H. J. Busscher, 2001a, Lack of effect of an externally applied electric field on bacterial adhesion to glass: Colloids and Surfaces B-Biointerfaces, v. 20, p. 189-194.

Poortinga, A. T., J. Smit, H. C. van der Mei, and H. J. Busscher, 2001b, Electric field induced desorption of bacteria from a conditioning film covered substratum: Biotechnology and Bioengineering, v. 76, p. 395-399.

Pourkomailian, B., and I. R. Booth, 1992, Glycine betaine transport by *Staphylococcus aureus* - Evidence for 2 transport systems and for their possible roles in osmoregulation: Journal of General Microbiology, v. 138, p. 2515-2518.

Proctor, A. R., and W. E. Kloos, 1973, Tryptophan biosynthetic enzymes of *Staphylococcus aureus*: Journal of Bacteriology, v. 114, p. 169-177.

Qin, Z. Q., Y. Z. Ou, L. A. Yang, Y. L. Zhu, T. Tolker-Nielsen, S. Molin, and D. Qu, 2007, Role of autolysin-mediated DNA release in biofilm formation of *Staphylococcus epidermidis*: Microbiology-Sgm, v. 153, p. 2083-2092.

R Development Core Team, 2010, R: A language and environment for statistical computing, Vienna, Austria, R Foundation for Statistical Computing. ISBN 3-900051-07-0, URL http://www.R-project.org/.

Rabinovitch, C., and P. S. Stewart, 2006, Removal and inactivation of *Staphylococcus epidermidis* biofilms by electrolysis: Applied and Environmental Microbiology, v. 72, p. 6364-6366.

Radimer, K., and M. McCarthy, 1979, Electrolytic production of sodium persulfate, *in* U. S. Patent, ed., United States.

Rai, D., J. K. Singh, N. Roy, and D. Panda, 2008, Curcumin inhibits FtsZ assembly: an attractive mechanism for its antibacterial activity: Biochemical Journal, v. 410, p. 147-155.

Rani, S. A., B. Pitts, H. Beyenal, R. A. Veluchamy, Z. Lewandowski, W. M. Davison, K. Buckingham-Meyer, and P. S. Stewart, 2007, Spatial patterns of DNA replication, protein synthesis, and oxygen concentration within bacterial biofilms reveal diverse physiological states: Journal of Bacteriology, v. 189, p. 4223-4233.

Regling, G., 2001, Magnetic fields and connective tissue regulation: Electro- and Magnetobiology, v. 20, p. 255-258.

Saginur, R., M. Stdenis, W. Ferris, S. Aaron, F. Chan, C. Lee, and K. Ramotar, 2006, Multiple combination bactericidal testing of staphylococcal biofilms from implant-associated infections.: Antimicrobial Agents and Chemotherapy, v. 50, p. 55-61.

Sam, C. H., and H. K. Lu, 2009, The role of hypochlorous acid as one of the reactive oxygen species in periodontal disease: Journal of Dental Sciences, v. 4, p. 45-54.

Sandvik, E. L., B. R. McLeod, A. E. Parker, and P. S. Stewart, 2013, Direct electric current treatment under physiologic saline conditions kills *Staphylococcus epidermidis* biofilms via electrolytic generation of hypochlorous acid: PLOS ONE, v. 8.

Schairer, D. O., J. S. Chouake, J. D. Nosanchuk, and A. J. Friedman, 2012, The potential of nitric oxide releasing therapies as antimicrobial agents: Virulence, v. 3, p. 271-279.

Secinti, K. D., M. Ayten, G. Kahilogullari, G. Kaygusuz, H. C. Ugur, and A. Attar, 2008, Antibacterial effects of electrically activated vertebral implants: Journal of Clinical Neuroscience, v. 15, p. 434-439.

Shirtliff, M., A. Bargmeyer, and A. Camper, 2005, Assessment of the ability of the bioelectric effect to eliminate mixed-species biofilms.: Applied and Environmental Microbiology, v. 71, p. 6379-82.

Simoes, M., M. O. Pereira, and M. J. Vieira, 2005, Effect of mechanical stress on biofilms challenged by different chemicals: Water Research, v. 39, p. 5142-5152.

Singh, R., P. Ray, A. Das, and M. Sharma, 2010, Penetration of antibiotics through *Staphylococcus aureus* and *Staphylococcus epidermidis* biofilms: Journal of Antimicrobial Chemotherapy, v. 65, p. 1955-1958.

Smith, S. D., B. R. McLeod, and A. R. Liboff, 1991, Effects of Resonant Magnetic Fields on Chick Femoral Development *in-vitro*: Journal of Bioelectricity, v. 10, p. 81-99.

Smith, S. D., B. R. McLeod, and A. R. Liboff, 1995, Testing the ion cyclotron resonance theory of electromagnetic field interaction with odd and even harmonic tuning for cations: Bioelectrochemistry and Bioenergetics, v. 38, p. 161-167.

Smith, S. D., B. R. McLeod, A. R. Liboff, and K. Cooksey, 1987, Calcium Cyclotron Resonance and Diatom Mobility: Bioelectromagnetics, v. 8, p. 215-227.

Stewart, P. S., W. Wattanakaroon, L. Goodrum, S. M. Fortun, and B. R. McLeod, 1999, Electrolytic generation of oxygen partially explains electrical enhancement of tobramycin efficacy against *Pseudomonas aeruginosa* biofilm: Antimicrobial Agents and Chemotherapy, v. 43, p. 292-296.

Stokes, N. R., N. Baker, J. M. Bennett, J. Berry, I. Collins, L. G. Czaplewski, A. Logan, R. Macdonald, L. MacLeod, H. Peasley, J. P. Mitchell, N. Nayal, A. Yadav, A. Srivastava, and D. J. Haydon, 2013, An Improved Small-Molecule Inhibitor of

FtsZ with Superior In Vitro Potency, Drug-Like Properties, and In Vivo Efficacy: Antimicrobial Agents and Chemotherapy, v. 57, p. 317-325.

Stoodley, P., D. DeBeer, and H. M. Lappin-Scott, 1997, Influence of electric fields and pH on biofilm structure as related to the bioelectric effect: Antimicrobial Agents and Chemotherapy, v. 41, p. 1876-1879.

Sun, J.-L., S.-K. Zhang, J.-Y. Chen, and B.-Z. Han, 2012, Efficacy of acidic and basic electrolyzed water in eradicating *Staphylococcus aureus* biofilm: Canadian Journal of Microbiology, v. 58, p. 448-454.

Swartz, T. H., S. Ikewada, O. Ishikawa, M. Ito, and T. A. Krulwich, 2005, The Mrp system: a giant among monovalent cation/proton antiporters?: Extremophiles, v. 9, p. 345-354.

Szkotak, R., T. H. R. Niepa, N. Jawrani, J. L. Gilbert, M. B. Jones, and D. Ren, 2011, Differential Gene Expression to Investigate the Effects of Low-level Electrochemical Currents on *Bacillus subtilis*: AMB Express, v. 1, p. 39.

Szurmant, H., M. A. Mohan, P. M. Imus, and J. A. Hoch, 2007, YycH and YycI interact to regulate the essential YycFG two-component system in *Bacillus subtilis*: Journal of Bacteriology, v. 189, p. 3280-3289.

Taber, H. W., J. P. Mueller, P. F. Miller, and A. S. Arrow, 1987, Bacterial uptake of aminoglycoside antibiotics: Microbiological Reviews, v. 51.

Ueda, S., and Y. Kuwabara, 2007, Susceptibility of biofilm *Escherichia coli*, *Salmonella enteritidis* and *Staphylococcus aureus* to detergents and sanitizers: Biocontrol Science, v. 12, p. 149-153.

van der Borden, A. J., P. G. M. Maathuis, E. Engels, G. Rakhorst, H. C. van der Mei, H. J. Busscher, and P. K. Sharma, 2007, Prevention of pin tract infection in external stainless steel fixator frames using electric current in a goat model: Biomaterials, v. 28, p. 2122-2126.

van der Borden, A. J., H. C. van der Mei, and H. Busscher, 2005, Electric block current induced detachment from surgical stainless steel and decreased viability of *Staphylococcus epidermidis*: Biomaterials, v. 26, p. 6731-6735.

van der Borden, A. J., H. C. van der Mei, and H. J. Busscher, 2004a, Electric-current-induced detachment of *Staphylococcus epidermidis* strains from surgical stainless steel: Journal of Biomedical Materials Research Part B-Applied Biomaterials, v. 68B, p. 160-164.

van der Borden, A. J., H. van der Werf, H. C. van der Mei, and H. J. Busscher, 2004b, Electric current-induced detachment of *Staphylococcus epidermidis* biofilms from

surgical stainless steel: Applied and Environmental Microbiology, v. 70, p. 6871-6874.

van der Waal, S. V., L. W. M. van der Sluis, A. R. Ozok, R. A. M. Exterkate, J. van Marle, P. R. Wesselink, and J. J. de Soet, 2011, The effects of hyperosmosis or high pH on a dual-species biofilm of *Enterococcus faecalis* and *Pseudomonas aeruginosa*: an in-vitro study: International Endodontic Journal, v. 44, p. 1110-1117.

Venkitanarayanan, K. S., G. O. Ezeike, Y. C. Hung, and M. P. Doyle, 1999, Efficacy of electrolyzed oxidizing water for inactivating *Escherichia coli* O157 : H7, *Salmonella enteritidis*, and *Listeria monocytogenes*: Applied and Environmental Microbiology, v. 65.

Vergidis, P., and R. Patel, 2012, Novel Approaches to the Diagnosis, Prevention, and Treatment of Medical Device-Associated Infections: Infectious Disease Clinics of North America, v. 26, p. 173-+.

Verschaeve, L., R. Anthonissen, M. Grudniewska, J. Wudarski, L. Gevaert, and A. Maes, 2011, Genotoxicity Investigation of ELF-Magnetic Fields in *Salmonella typhimurium* With the Sensitive SOS-Based VITOTOX Test: Bioelectromagnetics, v. 32, p. 580-584.

von Eiff, C., G. Peters, and C. Heilmann, 2002, Pathogenesis of infections due to coagulase-negative staphylococci: Lancet Infectious Diseases, v. 2.

Wattanakaroon, W., and P. S. Stewart, 2000, Electrical enhancement of *Streptococcus gordonii* biofilm killing by gentamicin: Archives of Oral Biology, v. 45, p. 167-171.

Weidenmaier, C., A. Peschel, V. A. J. Kempf, N. Lucindo, M. R. Yeaman, and A. S. Bayer, 2005, DltABCD- and MprF-mediated cell envelope modifications of *Staphylococcus aureus* confer resistance to platelet microbicidal proteins and contribute to virulence in a rabbit endocarditis model: Infection and Immunity, v. 73, p. 8033-8038.

Wellman, N., S. Fortun, and B. McLeod, 1996, Bacterial biofilms and the bioelectric effect: Antimicrob Agents and Chemotherapy, v. 40, p. 2012-4.

White, D., 2007, The physiology and biochemistry of prokaryotes: New York, Oxford University Press, xix, 628 p. p.

Winterbourn, C. C., 2002, Biological reactivity and biomarkers of the neutrophil oxidant, hypochlorous acid: Toxicology, v. 181, p. 223-227.

Xue, T., Y. B. You, D. Hong, H. P. Sun, and B. L. Sun, 2011, The *Staphylococcus aureus* KdpDE Two-Component System Couples Extracellular K^+ Sensing and Agr Signaling to Infection Programming: Infection and Immunity, v. 79, p. 2154-2167.

Xulu, B. A., and M. T. Ashby, 2010, Small Molecular, Macromolecular, and Cellular Chloramines React with Thiocyanate To Give the Human Defense Factor Hypothiocyanite: Biochemistry, v. 49, p. 2068-2074.

Yang, L., K. B. Barken, M. E. Skindersoe, A. B. Christensen, M. Givskov, and T. Tolker-Nielsen, 2007, Effects of iron on DNA release and biofilm development by *Pseudomonas aeruginosa*: Microbiology-Sgm, v. 153, p. 1318-1328.

Zehnder, M., 2006, Root canal irrigants: Journal of Endodontics, v. 32, p. 389-398.

Zheng, Z. L., and P. S. Stewart, 2002, Penetration of rifampin through *Staphylococcus epidermidis* biofilms: Antimicrobial Agents and Chemotherapy, v. 46, p. 900-903.

Zhu, T., Q. Lou, Y. Wu, J. Hu, F. Yu, and D. Qu, 2010, Impact of the *Staphylococcus epidermidis* LytSR two-component regulatory system on murein hydrolase activity, pyruvate utilization and global transcriptional profile: Bmc Microbiology, v. 10.

Ziebuhr, W., V. Krimmer, S. Rachid, I. Lossner, F. Gotz, and J. Hacker, 1999, A novel mechanism of phase variation of virulence in *Staphylococcus epidermidis*: evidence for control of the polysaccharide intercellular adhesin synthesis by alternating insertion and excision of the insertion sequence element IS256: Molecular Microbiology, v. 32.

Zimmerli, W., A. Widmer, M. Blatter, R. Frei, and P. Ochsner, 1998, Role of rifampin for treatment of orthopedic implant-related staphylococcal infections: a randomized controlled trial. Foreign-Body Infection (FBI) Study Group.: JAMA, v. 279, p. 1537-41.

APPENDICES

APPENDIX A

PRELIMINARY AND SUPPLEMENTAL DATA FOR CHAPTER 2

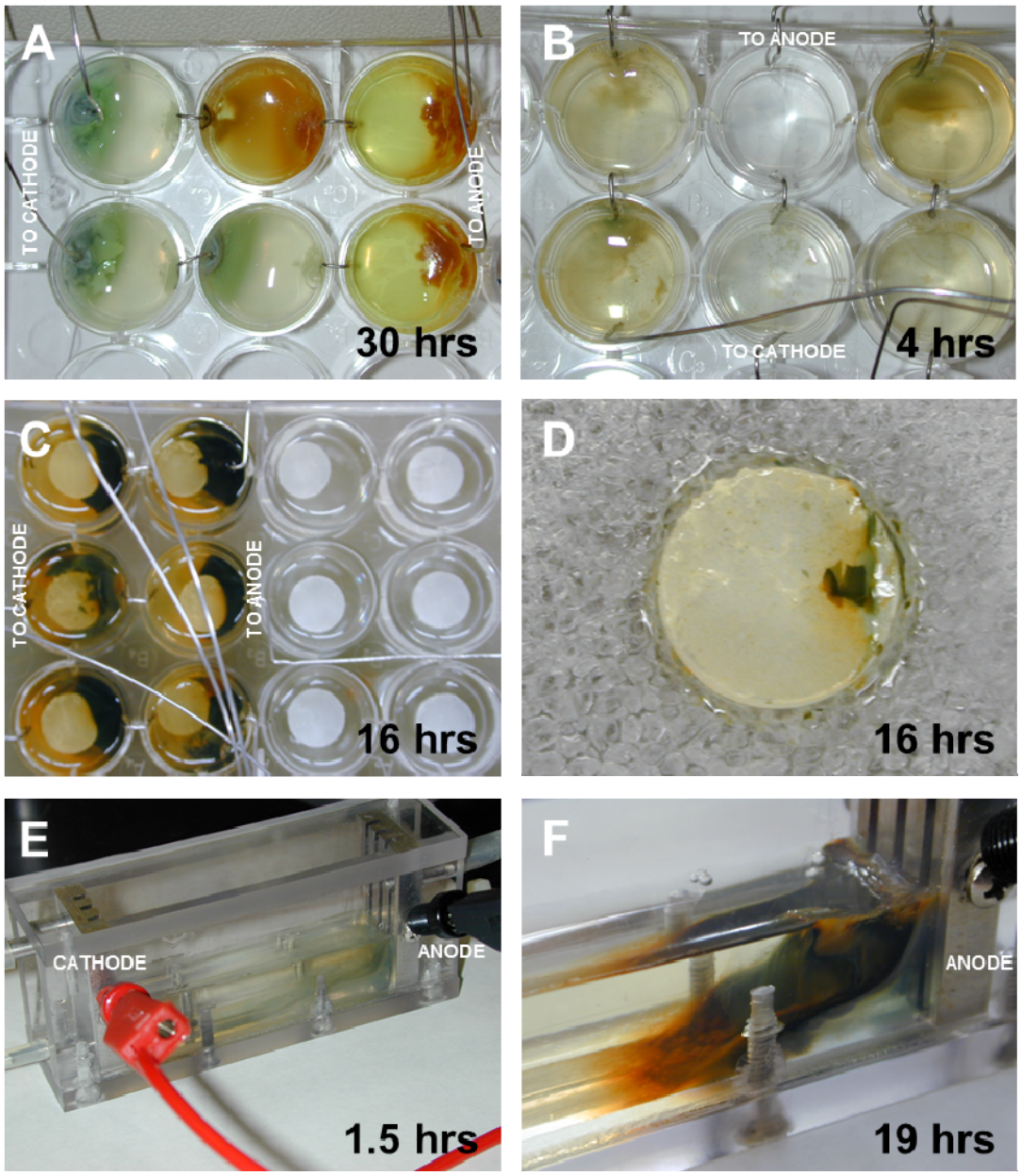

Figure A.1 Electrode corrosion in 1/10th strength TSB (0.5 g/L total NaCl). Electrode material and current settings were as follows: (A) 20 mil nichrome electrodes, 0.5 mA split to two parallel circuits of three wells in series, (B) 30 mil 316 stainless steel electrodes, 0.75 mA split to three parallel circuits each with two wells in series, (C) 20 mil 316 stainless steel electrodes, 0.25 mA through 3 independent circuits each with two wells containing biofilm coupons in series (left) and untreated control coupons (right). (D) Close up of *S. epidermidis* biofilm from well in (C). Precipitation formed with 2 mA DC with stainless steel plate electrodes at (E) 1.5 hrs and (F) 19 hrs.

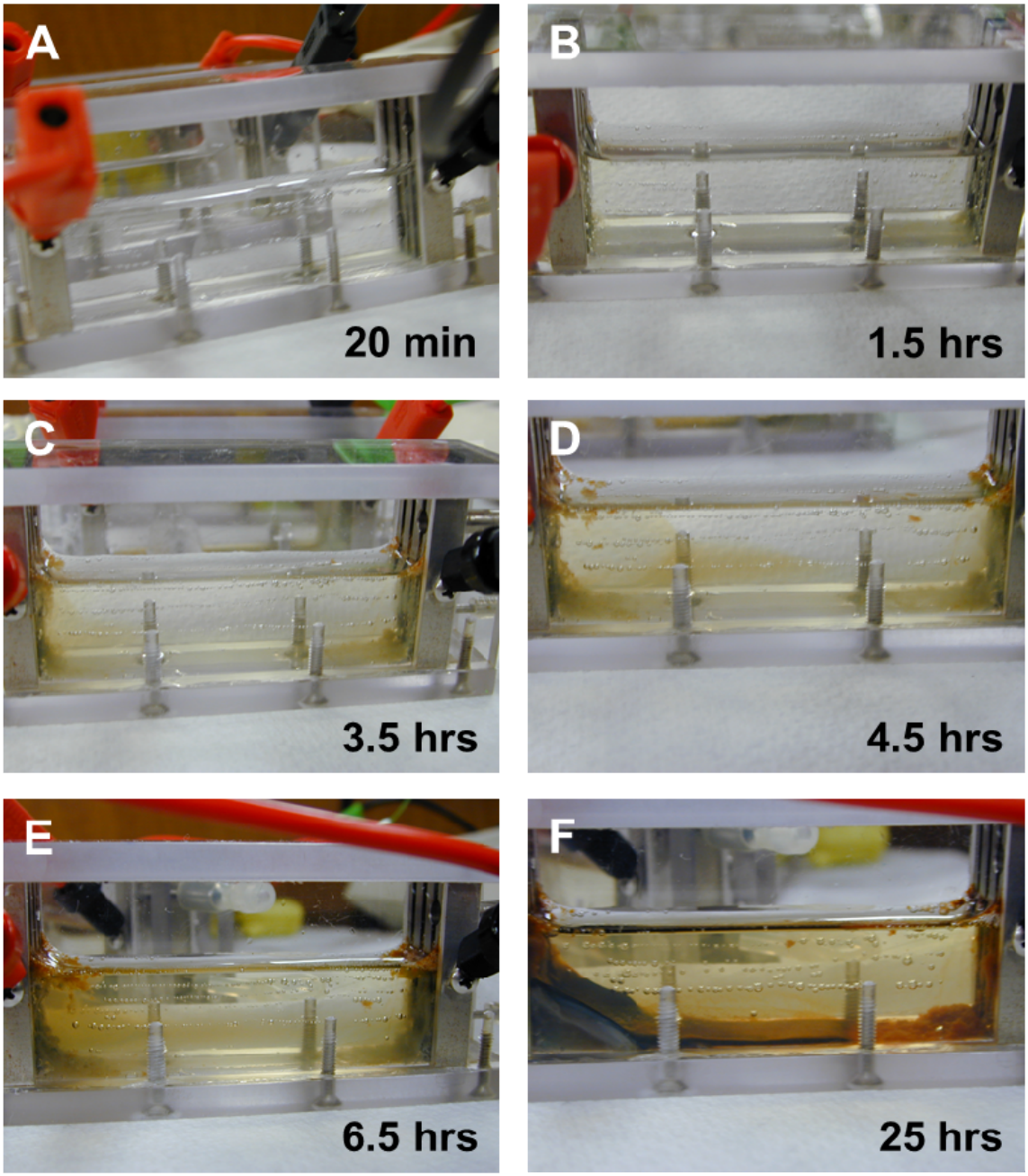

Figure A.2 Time course of stainless steel plate electrode corrosion from 1 mA of DC, alternating the electrode polarity every 30 minutes. After the initial 6.5 hours (A-E), the current was continued without alternating the polarity and observed at 25 hours (F). Wells contained 20 mL of 1/10th strength TSB (0.5 g/L total NaCl).

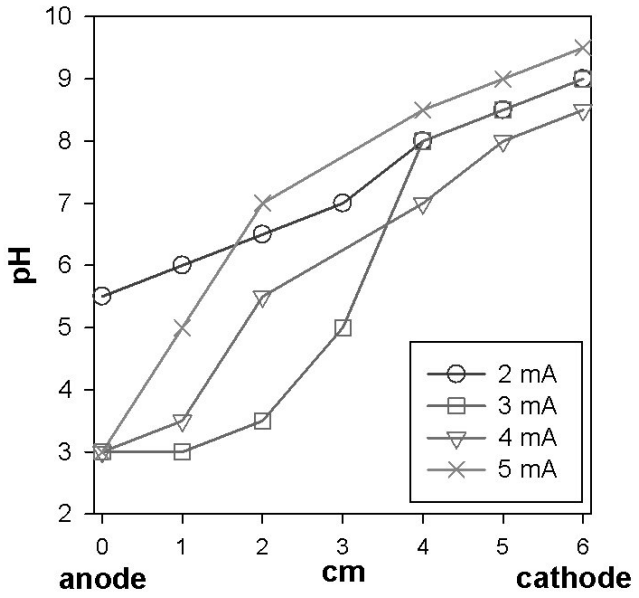

Figure A.3 pH gradient across treatment well with DC running. DC was applied to 20 mL of $1/10^{th}$ TSB (9 g/L NaCl) for 5 minutes. ph strips were inserted at 1cm distances in a styrofoam lid and dipped simultaneously into treatment well for measurement.

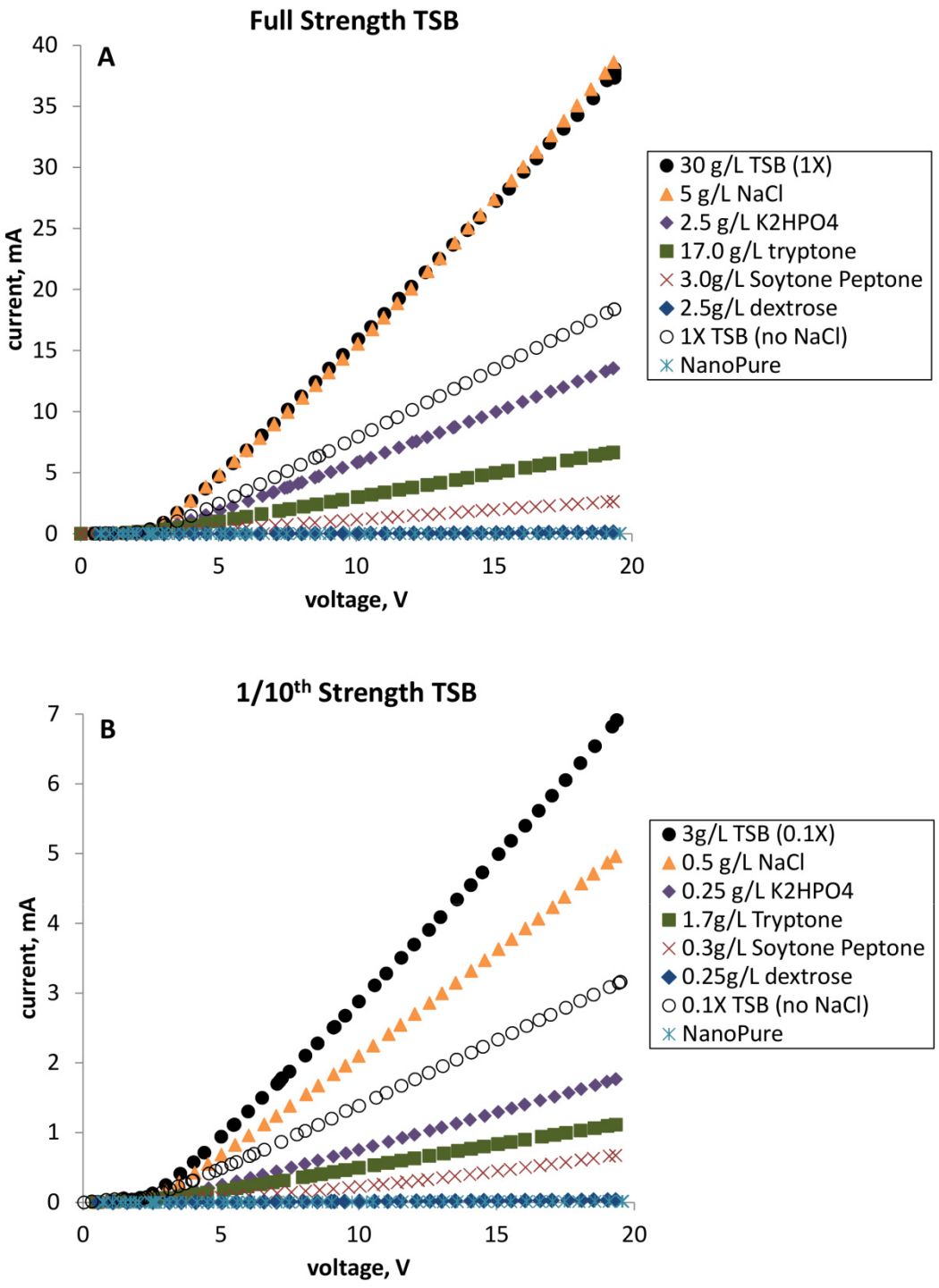

Figure A.4 Current vs. voltage measurements of TSB components. Current was applied from an adjustable voltage DC generator and current was increased ~0.5 V/reading (3 or 5 second interval readings). Treatment wells (described in Chapter 2) contained 20 mL of solution as indicated at concentrations of (A) full strength TSB or (B) 1/10th strength TSB.

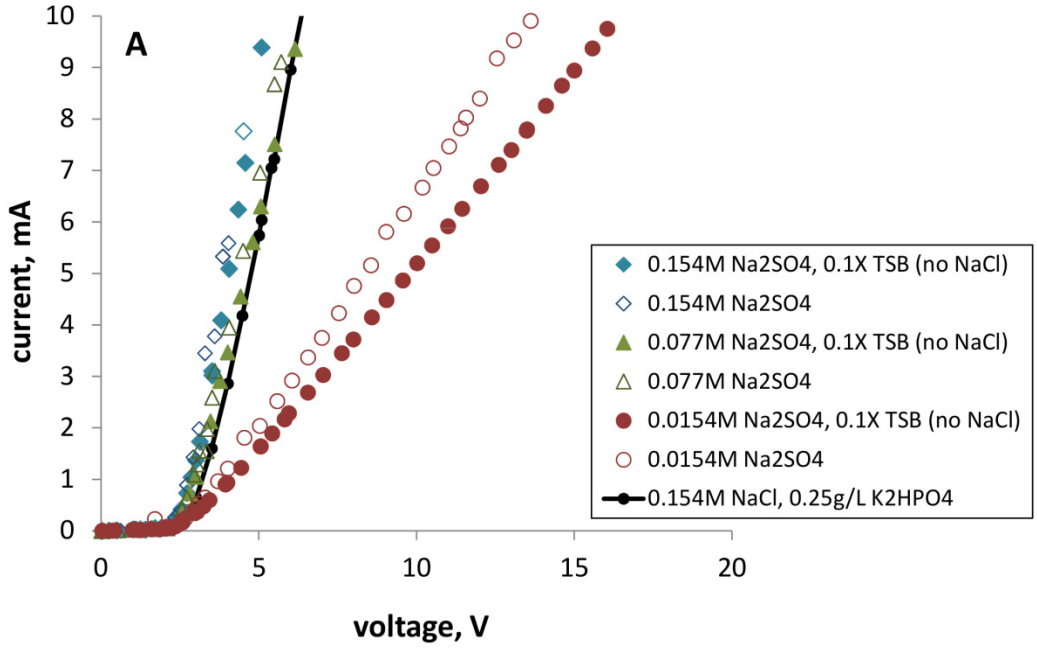
A
current, mA
voltage, V
0.154M Na2SO4, 0.1X TSB (no NaCl)
0.154M Na2SO4
0.077M Na2SO4, 0.1X TSB (no NaCl)
0.077M Na2SO4
0.0154M Na2SO4, 0.1X TSB (no NaCl)
0.0154M Na2SO4
0.154M NaCl, 0.25g/L K2HPO4

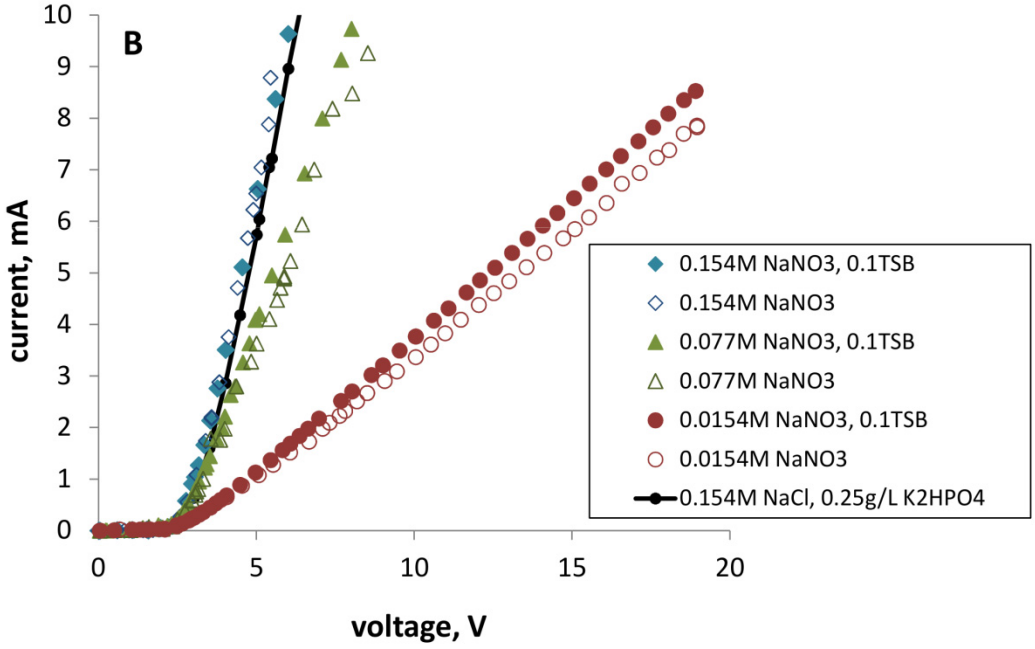
B
current, mA
voltage, V
0.154M NaNO3, 0.1TSB
0.154M NaNO3
0.077M NaNO3, 0.1TSB
0.077M NaNO3
0.0154M NaNO3, 0.1TSB
0.0154M NaNO3
0.154M NaCl, 0.25g/L K2HPO4

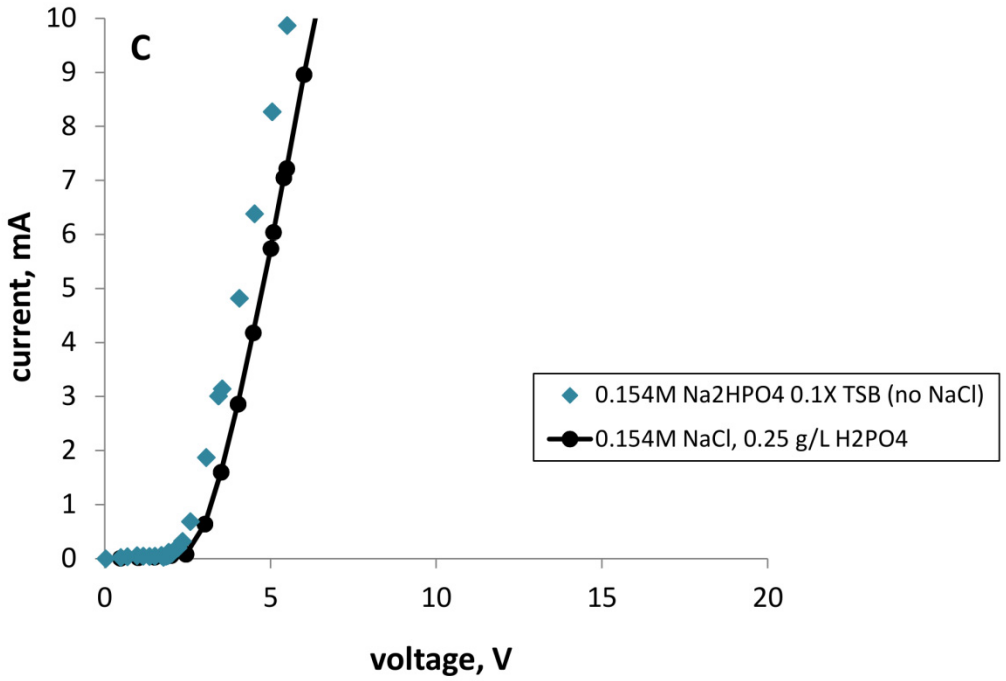

Figure A.5 Current vs. voltage measurements across solutions containing TSB components with alternate electrolytes as (A) sulfate, (B) nitrate or (C) phosphate. Current was applied from an adjustable voltage DC generator and current was increased ~0.5 V/reading (3 or 5 second interval readings). Treatment wells (Chapter 2) contained 20 mL of solution as indicated.

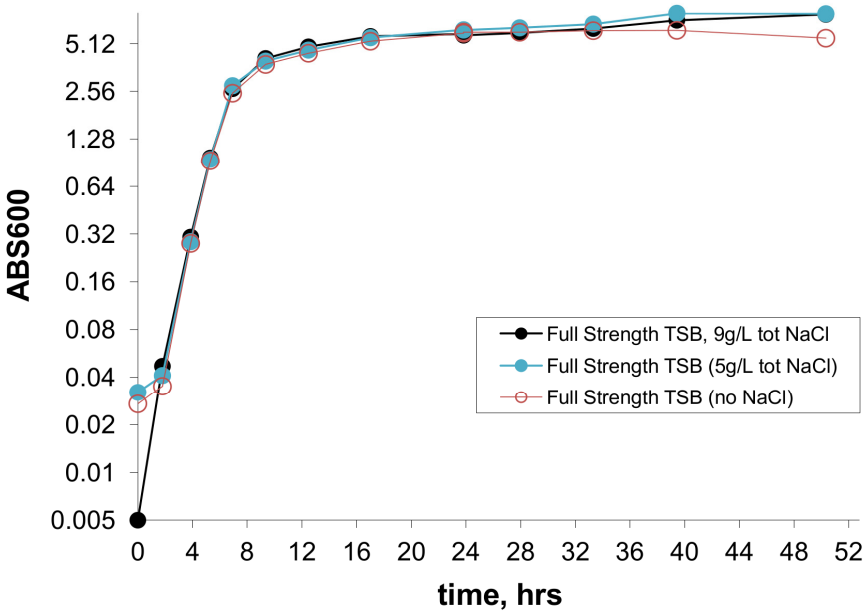

Figure A.6 Growth of *S. epidermidis* ATCC#35984 with varying concentrations of NaCl from 9 g/L (0.154 M) to no NaCl. Flasks were inoculated with 100 µL of an overnight culture grown in TSB (no NaCl) from frozen stock grown in a 37°C environmental shaker.

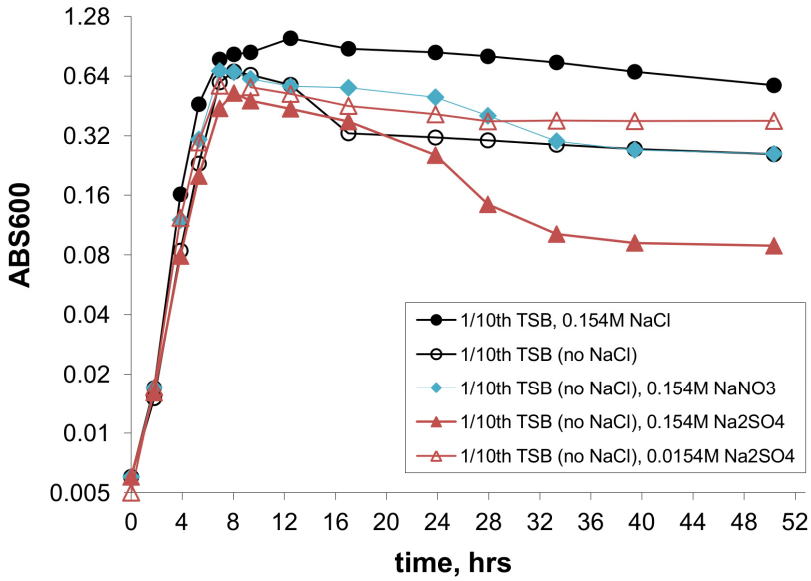

Figure A.7 Growth of *S. epidermidis* ATCC#35984 with substitute electrolytes at equimolar concentrations to 9 g/L NaCl. Flasks were inoculated with 100µL of an overnight culture grown in TSB (no NaCl) from frozen stock grown in a 37°C environmental shaker.

APPENDIX B

SUPPLEMENTAL DATA FOR DC AND CHLORINE MICROARRAYS

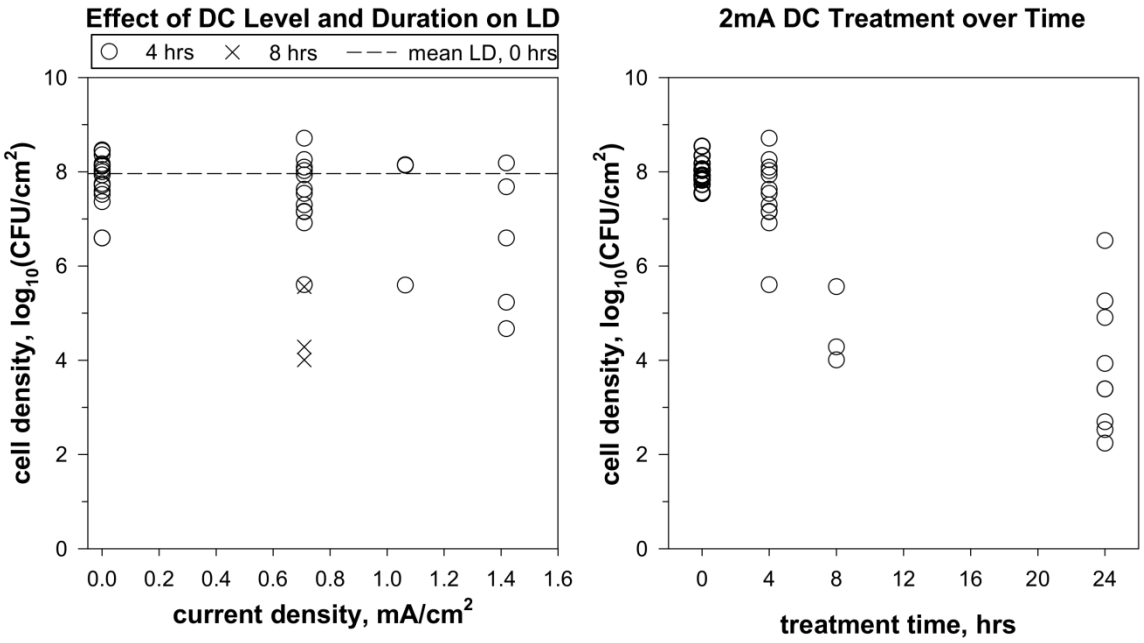

Figure B.1 Preliminary experiments decreasing DC level and duration for DC gene expression experiments. Current was applied to *S. epidermidis* biofilms in 20 mL of a 3 g/L TSB solution with 9 g/L total NaCl.

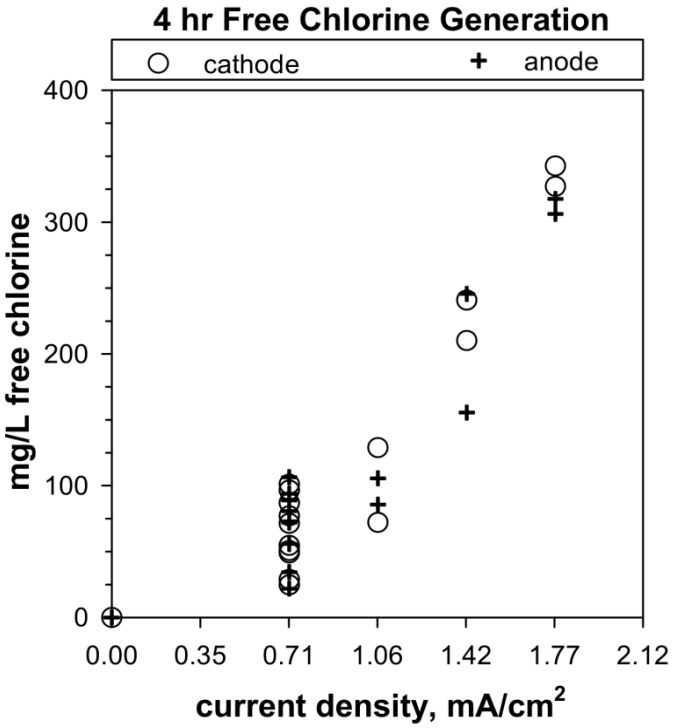

Figure B.2 Free chlorine generated over 4 hrs of direct current exposure. Free chlorine was measured simultaneously at each electrode immediately after the current was turned off. The solution contained 9 g/L NaCl and 0.25 g/L K_2HPO_4, equivalent to the treatment solution used in DC biofilm experiments with organic sources of chlorine demand removed.

Table B.1 DAVID Cluster output (with enrichment score ≥1) for gene lists from biofilm in response to DC treatment. Columns indicate the number of genes in the input list with the annotation (count , Ct.), the percentage of genes in the input list with the annotation (%), the number of genes in the input list with an annotation in the annotation category (list total, List Tot.), the number of all genes on the array that have the specific annotation (population total, Pop Hits), and the number of genes within the background (all genes on the array) with an annotation in the annotation category (population total, Pop Tot.). The p-values are EASE scores, a modified fisher's exact p-value used by the DAVID database (p-val). The fold-enrichment (FE) and false-discovery rate (FDR) calculated within the DAVID database are also indicated.

Annotation DC Up Cluster 1 **Enrichment Score: 1.93**

Category	Term	Ct.	%	p-val	List Tot.	Pop Hits	Pop Tot.	FE	FDR
GOTERM_BP_FAT	GO:0006412~translation	14	13.6	0.001	66	94	1152	2.6	1.8
SP_PIR_KEYWORDS	rRNA-binding	7	6.8	0.002	103	33	2508	5.2	1.9
SP_PIR_KEYWORDS	ribonucleoprotein	8	7.8	0.005	103	54	2508	3.6	5.7
SP_PIR_KEYWORDS	ribosomal protein	8	7.8	0.007	103	56	2508	3.5	6.9
GOTERM_MF_FAT	GO:0019843~rRNA binding	7	6.8	0.008	71	33	1265	3.8	9.1
KEGG_PATHWAY	sep03010:Ribosome	8	7.8	0.010	39	49	735	3.1	9.0
GOTERM_CC_FAT	GO:0043232~intracellular non-membrane-bounded organelle	9	8.7	0.010	20	68	383	2.5	6.9
GOTERM_CC_FAT	GO:0043228~non-membrane-bounded organelle	9	8.7	0.010	20	68	383	2.5	6.9
GOTERM_CC_FAT	GO:0005840~ribosome	8	7.8	0.013	20	57	383	2.7	9.4
GOTERM_CC_FAT	GO:0030529~ribonucleoprotein complex	8	7.8	0.015	20	58	383	2.6	10.3
KEGG_PATHWAY	ser03010:Ribosome	8	7.8	0.016	39	54	735	2.8	14.9
GOTERM_MF_FAT	GO:0003735~structural constituent of ribosome	8	7.8	0.026	71	54	1265	2.6	27.2
SP_PIR_KEYWORDS	rna-binding	7	6.8	0.026	103	57	2508	3.0	24.7
GOTERM_MF_FAT	GO:0005198~structural molecule activity	8	7.8	0.028	71	55	1265	2.6	29.4
GOTERM_CC_FAT	GO:0033279~ribosomal subunit	4	3.9	0.032	20	15	383	5.1	21.5
GOTERM_MF_FAT	GO:0003723~RNA binding	9	8.7	0.086	71	84	1265	1.9	66.5

Annotation DC Up Cluster 2 **Enrichment Score: 1.67**

Category	Term	Ct.	%	p-val	List Tot.	Pop Hits	Pop Tot.	FE	FDR
SP_PIR_KEYWORDS	glycolysis	5	4.9	0.004	103	17	2508	7.2	4.3
GOTERM_BP_FAT	GO:0006007~glucose catabolic process	6	5.8	0.005	66	21	1152	5.0	6.0
GOTERM_BP_FAT	GO:0019320~hexose catabolic process	6	5.8	0.005	66	21	1152	5.0	6.0

GOTERM_BP_FAT	GO:0006006~glucose metabolic process	7	6.8	0.005	66	30	1152	4.1	6.3
GOTERM_BP_FAT	GO:0019318~hexose metabolic process	7	6.8	0.006	66	31	1152	3.9	7.4
GOTERM_BP_FAT	GO:0046365~monosaccharide catabolic process	6	5.8	0.009	66	24	1152	4.4	10.7
GOTERM_BP_FAT	GO:0046164~alcohol catabolic process	6	5.8	0.013	66	26	1152	4.0	14.8
GOTERM_BP_FAT	GO:0006096~glycolysis	5	4.9	0.019	66	19	1152	4.6	21.1
GOTERM_BP_FAT	GO:0044275~cellular carbohydrate catabolic process	6	5.8	0.027	66	31	1152	3.4	28.4
GOTERM_BP_FAT	GO:0005996~monosaccharide metabolic process	7	6.8	0.030	66	43	1152	2.8	31.5
KEGG_PATHWAY	ser00030:Pentose phosphate pathway	4	3.9	0.052	39	17	735	4.4	40.8
KEGG_PATHWAY	ser00010:Glycolysis / Gluconeogenesis	6	5.8	0.054	39	41	735	2.8	41.5
GOTERM_BP_FAT	GO:0016052~carbohydrate catabolic process	6	5.8	0.064	66	39	1152	2.7	55.8
SP_PIR_KEYWORDS	Isomerase	4	3.9	0.232	103	41	2508	2.4	93.9
GOTERM_BP_FAT	GO:0006091~generation of precursor metabolites and energy	5	4.9	0.350	66	53	1152	1.6	99.5

Annotation DC Up Cluster 3 **Enrichment Score: 1.04**

Category	Term	Ct.	%	p-val	List Tot.	Pop Hits	Pop Tot.	FE	FDR
INTERPRO	IPR013027:FAD-dependent pyridine nucleotide-disulphide oxidoreductase	5	4.9	0.008	92	18	1937	5.8	10.3
INTERPRO	IPR000103:Pyridine nucleotide-disulphide oxidoreductase, class-II	3	2.9	0.020	92	5	1937	12.6	22.8
INTERPRO	IPR001327:Pyridine nucleotide-disulphide oxidoreductase, NAD-binding region	4	3.9	0.025	92	14	1937	6.0	27.9
GOTERM_MF_FAT	GO:0050662~coenzyme binding	9	8.7	0.046	71	74	1265	2.2	43.9
SP_PIR_KEYWORDS	nadp	4	3.9	0.094	103	27	2508	3.6	65.1
SP_PIR_KEYWORDS	Redox-active center	3	2.9	0.095	103	13	2508	5.6	65.6
SP_PIR_KEYWORDS	oxidoreductase	10	9.7	0.105	103	138	2508	1.8	69.2
GOTERM_MF_FAT	GO:0050660~FAD binding	4	3.9	0.118	71	22	1265	3.2	78.2
SP_PIR_KEYWORDS	FAD	3	2.9	0.209	103	21	2508	3.5	91.8
GOTERM_MF_FAT	GO:0048037~cofactor binding	9	8.7	0.242	71	108	1265	1.5	96.5
GOTERM_MF_FAT	GO:0009055~electron carrier activity	4	3.9	0.290	71	34	1265	2.1	98.4

SP_PIR_KEYWORDS	Flavoprotein	3	2.9	0.301	103	27	2508	2.7	97.8
GOTERM_BP_FAT	GO:0055114~oxidation reduction	11	10.7	0.358	66	153	1152	1.3	99.6

Annotation DC Down Cluster 1 **Enrichment Score: 1.03**

Category	Term	Ct.	%	p-val	List Tot.	Pop Hits	Pop Tot.	FE	FDR
INTERPRO	IPR004107:Integrase, N-terminal SAM-like, phage	3	3.2	0.025	72	7	1937	11.5	25.8
SP_PIR_KEYWORDS	dna integration	3	3.2	0.025	93	7	2508	11.6	22.0
INTERPRO	IPR013762:Integrase-like, catalytic core, phage	3	3.2	0.069	72	12	1937	6.7	57.4
INTERPRO	IPR002104:Integrase, catalytic core, phage	3	3.2	0.069	72	12	1937	6.7	57.4
GOTERM_BP_FAT	GO:0015074~DNA integration	3	3.2	0.122	40	18	1152	4.8	78.6
GOTERM_BP_FAT	GO:0006259~DNA metabolic process	8	8.5	0.149	40	132	1152	1.7	85.4
SP_PIR_KEYWORDS	dna recombination	3	3.2	0.152	93	19	2508	4.3	80.4
GOTERM_BP_FAT	GO:0032196~transposition	3	3.2	0.232	40	27	1152	3.2	95.6
GOTERM_BP_FAT	GO:0006310~DNA recombination	4	4.3	0.303	40	57	1152	2.0	98.6

Table B.2 Differentially expressed genes in response to a 70 ppm dose of free chlorine over 4 hrs. All genes were significant with a p-value≤0.05 with fold change (FC) with respect to parallel no treatment controls.

Locus	Gene Name	Gene Description	Predicted Operon	DC FC	Chlor FC
SEA0002		truncated IS431mec-like transposase			2.5
SEA0003	*blaZ-2*	beta-lactamase	0003		1.8
SEA0005	*blaI-2*	penicillinase repressor			2.1
SEA0006		site-specific recombinase, resolvase family	0006	-1.3	-1.5
SEA0009		transcriptional regulator, putative	0009	1.4	1.5
SEA0010	*aphA*	aminoglycoside 3'-phosphotransferase			-1.1
SEA0019		hypothetical protein			1.8
SEA0024		sulfate permease family protein			1.6
SEA0026		hypothetical protein	0026		-1.6
SEA0027		mobilization protein			2.3
SEA0028		hypothetical protein	0029-0028		2.8
SEA0031		hypothetical protein			2.0
SERP0002	*rnpA*	ribonuclease P			-1.4
SERP0003	*trmE*	tRNA modification GTPase			2.2
SERP0004	*gidA*	glucose-inhibited division protein A			2.3
SERP0005	*gidB*	glucose-inhibited division protein B			2.2
SERP0006		chromosome partioning protein, ParB family			1.5
SERP0007		hypothetical protein			1.8
SERP0009		hypothetical protein			-1.6
SERP0013		hypothetical protein			-2.4
SERP0019		hypothetical protein	0021-0019		2.0
SERP0028		hypothetical protein	0029-0028	-2.2	-2.2
SERP0029		transcriptional regulator, Cro/CI family	0029-0028	-1.6	-1.7
SERP0031		hypothetical protein	0031		1.3
SERP0035		bifunctional homocysteine S-methyltransferase/5,10-methylenetetrahydrofolate reductase protein	0037-0033		2.1
SERP0036		trans-sulfuration enzyme family protein	0037-0033		2.1
SERP0037		trans-sulfuration enzyme family protein	0037-0033		1.8
SERP0040		hypothetical protein			-1.6
SERP0042		hypothetical protein	0043-0042		-1.4
SERP0043		lysozyme domain protein	0043-0042		1.3
SERP0046	*rpsR*	ribosomal protein S18	0044-0046		-3.0
SERP0057		hypothetical protein			-1.9
SERP0059	*ahpF*	alkyl hydroperoxide reductase, F subunit	0060-0059	1.3	1.5
SERP0060	*ahpC*	alkyl hydroperoxide reductase, C subunit	0060-0059		1.3

Table B.2 (continued)

Locus	Gene Name	Gene Description	Predicted Operon	DC FC	Chlor FC
SERP0063		sodium:dicarboxylate symporter family protein			2.2
SERP0064		hypothetical protein	0066-0064	-1.4	-3.6
SERP0066		hypothetical protein	0066-0064		-1.3
SERP0067	*xpt*	xanthine phosphoribosyltransferase			-1.5
SERP0068	*pbuX*	xanthine permease			-1.3
SERP0069	*guaB*	inosine-5'-monophosphate dehydrogenase			-1.5
SERP0071		hypothetical protein			-2.2
SERP0073		hypothetical protein			-2.4
SERP0074		hypothetical protein			-2.3
SERP0075		hypothetical protein			-1.9
SERP0080		cobalamin synthesis protein, putative			1.5
SERP0086		hypothetical protein			3.3
SERP0087		hypothetical protein			-1.8
SERP0088		hypothetical protein			-1.5
SERP0093		hypothetical protein			-3.1
SERP0094		cysteine synthase/cystathionine beta-synthase family protein			2.7
SERP0095		trans-sulfuration enzyme family protein			2.3
SERP0096		hypothetical protein	0096-0099	1.3	2.0
SERP0097		ABC transporter, ATP-binding protein	0096-0099		2.1
SERP0098		ABC transporter, permease protein	0096-0099		1.7
SERP0100		LysM domain protein			-1.7
SERP0102		hypothetical protein			-2.2
SERP0104		hypothetical protein			2.3
SERP0109	*gltD*	glutamate synthase, small subunit			1.5
SERP0117		hypothetical protein			2.5
SERP0121		hypothetical protein			-2.0
SERP0122		DNA polymerase III, delta prime subunit, putative	0122-0127		-1.7
SERP0123		hypothetical protein	0122-0127		-1.3
SERP0127		methyltransferase, tetrapyrrole family	0122-0127	-1.3	-1.3
SERP0130		primase-related protein			-1.6
SERP0133	*ispE*	4-diphosphocytidyl-2-C-methyl-D-erythritol kinase			-1.5
SERP0134	*purR*	purine operon repressor			-1.3
SERP0146		hypothetical protein	0139-0146		-2.0
SERP0151	*hslO*	chaperonin, 33 kDa			3.4
SERP0152	*cysK*	cysteine synthase			1.6

Table B.2 (continued)

Locus	Gene Name	Gene Description	Predicted Operon	DC FC	Chlor FC
SERP0159		hypothetical protein	0158-0159	1.5	-1.7
SERP0161	*nupC*	nucleoside permease NupC			-1.4
SERP0162	*ctsR*	transcriptional regulator CtsR			2.3
SERP0163		UvrB/UvrC domain protein			2.3
SERP0164		putative ATP:guanido phosphotransferase			2.2
SERP0165	*clpC*	ATP-dependent Clp protease, ATP-binding subunit ClpC			1.9
SERP0166	*radA*	DNA repair protein RadA			1.6
SERP0169	*cysE*	serine acetyltransferase			2.6
SERP0170	*cysS*	cysteinyl-tRNA synthetase			2.3
SERP0171		hypothetical protein			1.5
SERP0172		RNA methyltransferase, TrmH family, group 3			1.7
SERP0173		hypothetical protein			3.1
SERP0174		RNA polymerase sigma factor sigW, putative			2.1
SERP0176	*secE*	preprotein translocase, SecE subunit			1.4
SERP0177	*nusG*	transcription termination/antitermination factor NusG			1.6
SERP0180	*rplJ*	ribosomal protein L10	0178-0182		-1.4
SERP0181	*rplL*	50S ribosomal protein L7/L12	0178-0182		-2.2
SERP0183	*rpoB*	DNA-directed RNA polymerase beta subunit	0183-0184	1.2	1.3
SERP0184	*rpoC*	DNA-directed RNA polymerase beta' subunit	0183-0184		1.2
SERP0191		acetyltransferase, GNAT family			1.4
SERP0195	*ilvE*	branched-chain amino acid aminotransferase			-1.7
SERP0199		hydrolase, haloacid dehalogenase-like family			1.9
SERP0201		3-ketoacyl-(acyl-carrier-protein) reductase			1.6
SERP0203		deoxynucleoside kinase family protein	0203-0202		-1.6
SERP0205		hydrolase, haloacid dehalogenase-like family	0205-0206	1.3	1.8
SERP0207		sdrG protein			2.0
SERP0209	*arsC-1*	arsenate reductase	0211-0209	-1.3	1.5
SERP0210		arsenical pump membrane protein	0211-0209		1.4
SERP0211	*arsR-1*	arsenical resistance operon repressor	0211-0209		2.5
SERP0212		hypothetical protein			2.3
SERP0213		hypothetical protein	0214-0213		3.2
SERP0214		hypothetical protein	0214-0213	1.4	3.1
SERP0215	*nagB*	glucosamine-6-phosphate isomerase	0215-0222		2.2
SERP0217		SIS domain protein	0215-0222		-1.3
SERP0218		hydrolase, haloacid dehalogenase-like family	0215-0222		-2.0
SERP0221		hypothetical protein	0215-0222		-1.3
SERP0222		hypothetical protein	0215-0222		-1.9

Table B.2 (continued)

Locus	Gene Name	Gene Description	Predicted Operon	DC FC	Chlor FC
SERP0231		hypothetical protein			1.6
SERP0232		amino acid permease family protein			1.6
SERP0236	*pta*	phosphate acetyltransferase	0236-0237		-1.3
SERP0237		lipoate-protein ligase A family protein	0236-0237	-1.2	-1.2
SERP0242		pyridine nucleotide-disulfide oxidoreductase family protein	0243-0242	1.9	6.9
SERP0243		hypothetical protein	0243-0242	2.2	10.1
SERP0248		hypothetical protein			1.8
SERP0251		HD domain protein			1.3
SERP0254		AIR carboxylase, putative	0056-0053		1.5
SERP0255		hypothetical protein	0056-0053	-1.4	-1.4
SERP0263		endonuclease III, putative			1.4
SERP0271		hypothetical protein			-1.8
SERP0272		hypothetical protein			-1.9
SERP0273		hydrolase, alpha/beta hydrolase fold family			4.1
SERP0276		hypothetical protein			2.2
SERP0277		hypothetical protein			2.0
SERP0281		Na+/H+ antiporter, MnhA component, putative	0281-0287		2.7
SERP0282		Na+/H+ antiporter, MnhB component, putative	0281-0287		2.1
SERP0283		Na+/H+ antiporter, MnhC component, putative	0281-0287		1.8
SERP0284		Na+/H+ antiporter, MnhD component, putative	0281-0287		1.9
SERP0285		Na+/H+ antiporter, MnhE component, putative	0281-0287		5.2
SERP0286		Na+/H+ antiporter, MnhF component, putative	0281-0287		1.8
SERP0287		Na+/H+ antiporter, MnhG component, putative	0281-0287		1.7
SERP0289		Na+/H+ antiporter, putative	0289		2.1
SERP0293	*sirR*	iron-dependent repressor	0293		-2.0
SERP0294		hypothetical protein			-1.5
SERP0302		hypothetical protein			1.9
SERP0303	*abcA*	ABC transporter, ATP-binding/permease protein			-1.4
SERP0304		nucleoside permease NupC, putative			-1.5
SERP0305		hypothetical protein			-1.3
SERP0310		acetyltransferase, GNAT family			-1.9
SERP0311		hypothetical protein	0311-0315		-1.5

Table B.2 (continued)

Locus	Gene Name	Gene Description	Predicted Operon	DC FC	Chlor FC
SERP0312		DNA-binding response regulator	0311-0315		-3.0
SERP0313		sensor histidine kinase	0311-0315		-1.5
SERP0314		ABC transporter, ATP-binding protein	0311-0315		-1.7
SERP0315		ABC transporter, permease protein	0311-0315		-1.6
SERP0316		hypothetical protein			-3.4
SERP0317		phosphate transporter family protein			-2.9
SERP0332		lipoprotein, putative			-1.6
SERP0333		hypothetical protein			-2.0
SERP0334		acetyltransferase, GNAT family			1.6
SERP0336		hypothetical protein			1.6
SERP0338		hypothetical protein			1.3
SERP0340		ABC transporter, ATP-binding protein, MsbA family	0340-0341		4.8
SERP0341		ABC transporter, ATP-binding protein, MsbA family	0340-0341	1.4	4.4
SERP0342	*norR*	transcriptional regulator, MarR family			-2.5
SERP0350		hypothetical protein			1.8
SERP0351		hypothetical protein			1.6
SERP0352		hypothetical protein			1.4
SERP0353	*norA*	quinolone resistance protein NorA	0353	1.4	2.4
SERP0355		ebsC protein, putative			-1.7
SERP0357		transcriptional regulator, DeoR family			1.9
SERP0358	*fruK*	1-phosphofructokinase			1.8
SERP0359	*fruA*	PTS system, fructose-specific IIABC components			2.0
SERP0360	*nagA*	N-acetylglucosamine-6-phosphate deacetylase			2.3
SERP0369		IS1272-like transposase, degenerate			4.0
SERP0370		hypothetical protein			-1.6
SERP0385		ABC transporter, ATP-binding protein			1.6
SERP0386		ABC transporter, permease protein			2.0
SERP0388		hypothetical protein			-1.6
SERP0389		alcohol dehydrogenase, iron-containing			-1.2
SERP0394		hypothetical protein			-1.9
SERP0398	*nrdF-1*	ribonucleotide-diphosphate reductase beta subunit			-1.7
SERP0408		hypothetical protein			-1.9
SERP0414		glycosyl transferase, group 4 family protein			-1.5
SERP0415		hypothetical protein			-1.3
SERP0416		DegV family protein			-2.1
SERP0420	*secA*	translocase			1.4

Table B.2 (continued)

Locus	Gene Name	Gene Description	Predicted Operon	DC FC	Chlor FC
SERP0421	*prfB*	peptide chain release factor 2			1.4
SERP0422		LysM domain protein			1.7
SERP0423		HD domain protein, putative			-1.4
SERP0425		hypothetical protein			2.1
SERP0426	*uvrB*	excinuclease ABC subunit B	0426-0427		2.2
SERP0427	*uvrA*	excinuclease ABC, A subunit	0426-0427		2.0
SERP0429	*lgt*	prolipoprotein diacylglyceryl transferase	0428-0432		1.2
SERP0431	*yvcD*	yvcD protein	0428-0432		2.2
SERP0432	*trxB*	thioredoxin-disulfide reductase	0428-0432	1.4	3.2
SERP0433		hypothetical protein			1.6
SERP0434		hypothetical protein			1.6
SERP0435		hypothetical protein			1.6
SERP0439		hypothetical protein			-2.4
SERP0447		hypothetical protein			-2.7
SERP0449	*est*	carboxylesterase	0449-0451		1.5
SERP0452		hypothetical protein			1.8
SERP0455		lipoprotein, putative			-1.5
SERP0457		hypothetical protein			-1.8
SERP0459		hypothetical protein			3.3
SERP0462		hypothetical protein			-2.5
SERP0464		hypothetical protein			2.4
SERP0466		cold shock protein, CSD family			-3.6
SERP0472		hypothetical protein			-2.3
SERP0478		IS1272-like transposase, degenerate			1.8
SERP0483		thioredoxin, putative	0483	1.9	2.2
SERP0484		hypothetical protein	0484-0485		-1.5
SERP0487		Toprim domain protein			-1.7
SERP0491		ABC transporter, substrate-binding protein	0489-0491		-2.0
SERP0492		hypothetical protein			1.4
SERP0496	*sufC*	FeS assembly ATPase SufC	0496-0499	1.3	1.8
SERP0497	*sufD*	FeS assembly protein SufD	0496-0499		2.7
SERP0498	*sufS*	cysteine desulfurase SufS	0496-0499		2.2
SERP0499		NifU domain protein	0496-0499	1.2	2.0
SERP0500	*sufB*	FeS assembly protein SufB			2.0
SERP0503		hypothetical protein			-4.6
SERP0505		hypothetical protein			-1.7
SERP0510		5'-nucleotidase family protein	0508-0510		2.0
SERP0523		hypothetical protein			-1.5
SERP0524		NADH dehydrogenase, putative	0524	-1.5	-1.7
SERP0526		HesB domain protein	0526		1.7
SERP0528		cytosol aminopeptidase			2.1

Table B.2 (continued)

Locus	Gene Name	Gene Description	Predicted Operon	DC FC	Chlor FC
SERP0531		hypothetical protein			1.5
SERP0539	*kapB*	kinase-associated protein B	0539		-1.9
SERP0541		general stress protein 13			-5.1
SERP0542		NADH-dependent flavin oxidoreductase, Oye family	0542	1.7	2.7
SERP0549	*argG*	argininosuccinate synthase			1.6
SERP0551		hypothetical protein			-1.5
SERP0552	*spsA*	signal peptidase IA, inactive			-1.4
SERP0553	*spsB*	signal peptidase IB			-1.9
SERP0556		fumarylacetoacetate hydrolase family protein			1.2
SERP0559		IS1272-like transposase, degenerate			4.2
SERP0560		coenzyme A disulfide reductase			2.5
SERP0561		hydrolase, haloacid dehalogenase-like family			2.1
SERP0563		hypothetical protein			-1.3
SERP0564	*clpB*	ATP-dependent Clp protease, ATP-binding subunit ClpB			1.6
SERP0566		hypothetical protein			-3.4
SERP0567	*fabH*	3-oxoacyl-(acyl carrier protein) synthase	0567-0568	1.7	2.7
SERP0568	*fabF*	3-oxoacyl-(acyl-carrier-protein) synthase II	0567-0568	1.4	1.6
SERP0570	*oppB*	oligopeptide ABC transporter, permease protein	0570-0574		1.4
SERP0575	*trpS*	tryptophanyl-tRNA synthetase			-1.5
SERP0576		transcriptional regulator Spx			-1.8
SERP0578		adaptor protein			1.8
SERP0579		competence protein, putative			4.0
SERP0580	*pepF*	oligoendopeptidase F			1.7
SERP0582		protozoan/cyanobacterial globin family protein	0583-0581		1.6
SERP0583		hypothetical protein	0583-0581	1.6	1.5
SERP0584		hypothetical protein			1.5
SERP0593		transposase, putative, truncation			1.8
SERP0595		daunorubicin resistance protein DrrC, putative			2.1
SERP0596		hypothetical protein			1.8
SERP0600		transposase, IS200 family, truncation			1.6
SERP0603		hypothetical protein			-1.3
SERP0604		hypothetical protein			-3.2
SERP0605		hypothetical protein			1.5
SERP0606	*ypfP*	ypfP protein			1.5

Table B.2 (continued)

Locus	Gene Name	Gene Description	Predicted Operon	DC FC	Chlor FC
SERP0607	*murE*	UDP-N-acetylmuramoylalanyl-D-glutamate--2, 6-diaminopimelate ligase	0607-0609		-1.5
SERP0611		serine protease, putative			-1.5
SERP0616		lipoate-protein ligase A family protein	0616	1.6	2.5
SERP0617		hypothetical protein			-2.9
SERP0628		hypothetical protein			1.7
SERP0629		isochorismate synthase family protein			1.6
SERP0630	*menD*	2-succinyl-6-hydroxy-2, 4-cyclohexadiene-1-carboxylic acid synthase/2-oxoglutarate decarboxylase			1.5
SERP0634		hypothetical protein	0634-0633	1.2	1.4
SERP0635		transcriptional regulator, MarR family			-1.7
SERP0637		acetyltransferase, GNAT family			2.1
SERP0639		hypothetical protein			-3.0
SERP0640		transcriptional regulator, putative			-1.8
SERP0646	*qoxB*	quinol oxidase, subunit II			-1.2
SERP0647		chitinase-related protein			-1.7
SERP0648	*folD*	methylenetetrahydrofolate dehydrogenase/methenyltetrahydrofolate cyclohydrolase			-1.8
SERP0666		hypothetical protein			-2.2
SERP0668		hypothetical protein			1.8
SERP0669	*ptsH*	phosphocarrier protein HPr			-1.4
SERP0672	*cydA*	cytochrome d ubiquinol oxidase, subunit I	0672-0674		4.5
SERP0673	*cydB*	cytochrome d ubiquinol oxidase, subunit II	0672-0674		4.9
SERP0674		potassium uptake protein TrkA	0672-0674		1.9
SERP0680	*pdhA*	pyruvate dehydrogenase complex E1 component, alpha subunit	0680-0683		-1.2
SERP0681	*pdhB*	pyruvate dehydrogenase complex E1 component, beta subunit	0680-0683		-1.2
SERP0685		transcriptional regulator, Cro/CI family			1.8
SERP0686	*potA*	spermidine/putrescine ABC transporter, ATP-binding protein			1.7
SERP0691		hypothetical protein			-1.9
SERP0695		hypothetical protein			-1.6
SERP0702		hypothetical protein			-2.2
SERP0703		cell division protein, FtsW/RodA/SpoVE family	0703		-1.6
SERP0704	*pyc*	pyruvate carboxylase			-1.3
SERP0705	*ctaA*	cytochrome oxidase assembly protein	0705		-2.5
SERP0706	*ctaB*	protoheme IX farnesyltransferase	0706-0707		-1.5

Table B.2 (continued)

Locus	Gene Name	Gene Description	Predicted Operon	DC FC	Chlor FC
SERP0708		hypothetical protein			1.5
SERP0711		hypothetical protein			2.4
SERP0714		hypothetical protein			1.3
SERP0720		RNA methyltransferase, TrmH family			-1.9
SERP0723	*rnhC*	ribonuclease HIII			-2.0
SERP0724		hypothetical protein			-3.8
SERP0725		bacteriocin production protein, putative			-2.0
SERP0727		recombination and DNA strand exchange inhibitor protein			1.5
SERP0729	*uvrC*	excinuclease ABC subunit C	0729	1.4	3.0
SERP0732		succinate dehydrogenase			-1.3
SERP0736		phenol soluble modulin beta 1			-3.7
SERP0737		phenol soluble modulin beta 1			-1.7
SERP0742		hypothetical protein			1.4
SERP0745	*ftsL*	cell division protein FtsL	0743-0751		-2.1
SERP0747	*mraY*	phospho-N-acetylmuramoyl-pentapeptide-transferase	0743-0751		-1.4
SERP0756	*ylmH*	ylmH protein	0756-0757		1.5
SERP0760		glyoxalase family protein			1.4
SERP0761		LysM domain protein			1.6
SERP0764	*pyrR*	pyrimidine regulatory protein PyrR	0764-0771		-3.5
SERP0767	*pyrC*	dihydroorotase	0764-0771		1.4
SERP0768	*carA*	carbamoyl-phosphate synthase small subunit	0764-0771		1.3
SERP0773		hypothetical protein			-1.4
SERP0774		hypothetical protein			-1.5
SERP0775	*fbe*	fibronectin/fibrinogen binding protein	0775	1.2	2.0
SERP0777	*rpoZ*	DNA-directed RNA polymerase, omega subunit			-3.4
SERP0781	*def-2*	polypeptide deformylase	0781-0786	1.2	1.6
SERP0786		serine/threonine protein kinase, putative	0781-0786		-1.5
SERP0787		hypothetical protein	0787-0789	-1.1	-1.3
SERP0788	*rpe*	ribulose-phosphate 3-epimerase	0787-0789		-1.3
SERP0794		transcriptional regulator of fatty acid biosynthesis	0794-0803		1.5
SERP0796	*fabD*	malonyl CoA-acyl carrier protein transacylase	0794-0803	1.4	1.4
SERP0797	*fabG*	3-oxoacyl-(acyl-carrier-protein) reductase	0794-0803		1.2
SERP0798	*acpP*	acyl carrier protein	0794-0803		-2.3
SERP0811		GTP-binding protein, putative			-1.4
SERP0816	*topA*	DNA topoisomerase I			1.4
SERP0817		glucose-inhibited division protein A			1.5
SERP0818	*xerC*	tyrosine recombinase XerC			1.7

Table B.2 (continued)

Locus	Gene Name	Gene Description	Predicted Operon	DC FC	Chlor FC
SERP0819	*hslV*	ATP-dependent protease peptidase subunit			1.9
SERP0822		hypothetical protein			2.2
SERP0828	*cdsA*	phosphatidate cytidylyltransferase	0827-0828		-1.5
SERP0829		membrane-associated zinc metalloprotease, putative			1.6
SERP0830	*proS*	prolyl-tRNA synthetase			1.6
SERP0831		DNA polymerase III, alpha subunit, Gram-positive type			1.5
SERP0832		hypothetical protein	0832-0836		-1.5
SERP0839	*ribF*	riboflavin biosynthesis protein RibF	0837-0841	1.2	1.8
SERP0842		metallo-beta-lactamase family protein	0842		-1.4
SERP0850	*pgsA*	CDP-diacylglycerol--glycerol-3-phosphate 3-phosphatidyltransferase			-1.9
SERP0853		HD/HDIG/KH domain protein	0853		-1.2
SERP0854		hypothetical protein			-3.3
SERP0860	*miaB*	tRNA-i(6)A37 modification enzyme MiaB			1.3
SERP0861		hypothetical protein			-1.5
SERP0869		hydrolase, alpha/beta hydrolase fold family			1.7
SERP0870	*miaA*	tRNA delta(2)-isopentenylpyrophosphate transferase			1.6
SERP0871		host factor-I protein, putative			-1.9
SERP0872	*gpxA-1*	glutathione peroxidase			1.4
SERP0873		GTP-binding protein, putative	0873-0874	1.3	2.7
SERP0874		hypothetical protein	0873-0874		2.1
SERP0883		hypothetical protein			1.6
SERP0885	*cls-1*	cardiolipin synthetase			-1.4
SERP0886		ABC transporter, ATP-binding protein	0886-0889		-1.4
SERP0887		ABC transporter, permease protein	0886-0889		-1.7
SERP0888		sensor histidine kinase, putative	0886-0889	-1.3	-1.9
SERP0889		DNA-binding response regulator, LuxR family	0886-0889		-1.7
SERP0891		thermonuclease precursor family protein			-1.7
SERP0893		hypothetical protein			-2.4
SERP0894		hypothetical protein	0894	-1.2	-1.5
SERP0895		hypothetical protein			-2.4
SERP0896		aspartate kinase			1.6
SERP0901		hypothetical protein			-2.2
SERP0903	*katA*	catalase			1.2
SERP0905	*rpsN-1*	30S ribosomal protein S14			3.0
SERP0908		hypothetical protein			2.6
SERP0910		hypothetical protein			-1.6
SERP0911		hypothetical protein			3.0

Table B.2 (continued)

Locus	Gene Name	Gene Description	Predicted Operon	DC FC	Chlor FC
SERP0912	*tkt*	transketolase	0912	1.2	1.3
SERP0914		hypothetical protein			-2.3
SERP0918	*sbcC*	exonuclease SbcC			-1.6
SERP0919	*mscL*	large conductance mechanosensitive channel protein			-1.6
SERP0920		choline/carnitine/betaine transporter	0920	1.2	-1.4
SERP0924		hypothetical protein			-1.9
SERP0927		amino acid carrier protein	0927	1.2	1.6
SERP0929		hypothetical protein			-1.7
SERP0931	*msrA-1*	methionine sulfoxide reductase A			-2.0
SERP0932		transcriptional regulator, putative			-1.9
SERP0939	*trpD*	anthranilate phosphoribosyltransferase	0937-0943		1.6
SERP0940	*trpC*	indole-3-glycerol phosphate synthase	0937-0943	-1.2	1.5
SERP0941	*trpF*	N-(5'phosphoribosyl)-anthranilate isomerase	0937-0943		1.6
SERP0942	*trpB*	tryptophan synthase subunit beta	0937-0943		1.8
SERP0948		hydrolase-related protein			-1.4
SERP0950		peptide ABC transporter, ATP-binding protein, putative	0953-0950		-1.6
SERP0954		hypothetical protein	0954		-2.6
SERP0955		oligoendopeptidase F, putative	0955	1.3	1.6
SERP0961		hypothetical protein	0961		-2.6
SERP0962		ABC transporter, ATP-binding protein	0962		-1.8
SERP0965	*dapA*	dihydrodipicolinate synthase	0963-0970		2.0
SERP0966	*dapB*	dihydrodipicolinate reductase	0963-0970		2.1
SERP0967	*dapD*	2,3,4,5-tetrahydropyridine-2,6-dicarboxylate N-succinyltransferase	0963-0970		2.2
SERP0968		amidohydrolase family protein	0963-0970		2.6
SERP0969		alanine racemase family protein	0963-0970		1.9
SERP0981		hypothetical protein			-1.4
SERP0982		hypothetical protein			-1.5
SERP0983		hypothetical protein			-2.2
SERP0984		ABC transporter, ATP-binding protein			-2.7
SERP0987		hypothetical protein			1.9
SERP0988	*arlS*	sensor histidine kinase ArlS	0989-0988		-1.4
SERP0992		PAP2 family protein			-1.5
SERP0995		hypothetical protein			1.5
SERP0998		PTS system, IIA component	1000-1997		2.0
SERP0999	*msrB*	methionine sulfoxide reductase B	1000-1997		2.6
SERP1000	*msrA-2*	methionine sulfoxide reductase A	1000-1997	1.2	1.6
SERP1003	*thyA-1*	thymidylate synthase			-1.3
SERP1005		ABC transporter, permease protein			1.6

Table B.2 (continued)

Locus	Gene Name	Gene Description	Predicted Operon	DC FC	Chlor FC
SERP1006		hypothetical protein			1.8
SERP1008		hypothetical protein			1.8
SERP1010		cell wall enzyme EbsB, putative			-1.6
SERP1012		5'-3' exonuclease, putative			1.2
SERP1018		hypothetical protein	1018-1016		-1.6
SERP1020	*pbp2*	penicillin-binding protein 2	1019-1020	1.2	-1.2
SERP1022	*nth*	endonuclease III	1029-1021		1.4
SERP1028		glycosyl transferase, group 1 family protein	1029-1021		1.9
SERP1029		hypothetical protein	1029-1021		1.5
SERP1031		hypothetical protein			1.4
SERP1034	*aroA*	3-phosphoshikimate 1-carboxyvinyltransferase			1.3
SERP1035	*aroB*	3-dehydroquinate synthase			1.5
SERP1037		nucleoside diphosphate kinase			-5.0
SERP1039		ubiquinone/menaquinone biosynthesis methyltransferase			1.3
SERP1046	*ansA*	L-asparaginase			1.6
SERP1047		pyridine nucleotide-disulfide oxidoreductase family protein	1047	1.5	1.5
SERP1050		hypothetical protein			-1.4
SERP1052		hypothetical protein	1052	2.1	1.8
SERP1053		hypothetical protein	1053	1.7	1.6
SERP1055	*srrA*	DNA-binding response regulator SrrA	1058-1054		-1.5
SERP1056	*rluB*	pseudouridine synthase RluB	1058-1054		-1.7
SERP1057	*scpB*	segregation and condensation protein B	1058-1054		-1.9
SERP1059		hypothetical protein			1.3
SERP1060	*xerD*	tyrosine recombinase XerD	1062-1060		1.3
SERP1061		transcriptional regulator, Fur family	1062-1060	1.3	1.8
SERP1063		oxidoreductase, aldo/keto reductase family	1063		1.9
SERP1064		oxidoreductase, short-chain dehydrogenase/reductase family	1064		1.6
SERP1065	*proC*	pyrroline-5-carboxylate reductase	1065		-1.5
SERP1066		AtsA/ElaC family protein	1066	-1.3	-2.3
SERP1070	*malA*	alpha-glucosidase	1072-1070		1.3
SERP1071	*gnd*	6-phosphogluconate dehydrogenase	1072-1070	1.1	1.1
SERP1072		peptidase T-like protein	1072-1070		2.8
SERP1075		hypothetical protein	1074-1075		-1.7
SERP1078		2-oxoisovalerate dehydrogenase, E1 component, alpha subunit	1079-1076		1.6
SERP1082	*ispA*	geranyltranstransferase	1088-1082		1.5
SERP1084	*xseA*	exodeoxyribonuclease VII, large subunit	1088-1082		1.7

Table B.2 (continued)

Locus	Gene Name	Gene Description	Predicted Operon	DC FC	Chlor FC
SERP1085	*nusB*	transcription antitermination protein NusB	1088-1082	1.2	1.7
SERP1086		hypothetical protein	1088-1082		-1.2
SERP1087	*accC*	acetyl-CoA carboxylase	1088-1082		-1.6
SERP1090	*argB*	acetylglutamate kinase	1092-1089		1.5
SERP1091	*argJ*	bifunctional ornithine acetyltransferase/N-acetylglutamate synthase protein	1092-1089		1.9
SERP1095		lipoprotein, putative			-2.2
SERP1096		hypothetical protein			-1.6
SERP1097		lipoate-protein ligase A family protein			-2.0
SERP1105		hypothetical protein			1.5
SERP1121		ABC transporter, permease protein			2.0
SERP1122		ABC transporter, ATP-binding protein			2.1
SERP1126		hypothetical protein			1.3
SERP1129		hypothetical protein			-1.6
SERP1130		CBS domain protein			-1.7
SERP1139		hypothetical protein			-1.8
SERP1141		hypothetical protein			-1.6
SERP1144		hypothetical protein	1152-1144		1.2
SERP1146	*prmA*	ribosomal protein L11 methyltransferase	1152-1144		1.4
SERP1147	*dnaJ*	dnaJ protein	1152-1144		1.7
SERP1148	*dnaK*	dnaK protein	1152-1144		1.4
SERP1149	*grpE*	heat shock protein GrpE	1152-1144		2.4
SERP1154		hypothetical protein			-1.6
SERP1162		hypothetical protein	1166-1158		-1.3
SERP1165		hydrolase, HAD-superfamily, subfamily IIIA	1166-1158		-1.6
SERP1166	*mtn*	5'-methylthioadenosine/S-adenosylhomocysteine nucleosidase	1166-1158		-2.3
SERP1173		transposase, IS200 family	1173		1.8
SERP1177		peptidase, U32 family			1.6
SERP1182	*alaS*	alanyl-tRNA synthetase			1.5
SERP1183		helicase, putative, RecD/TraA family			1.4
SERP1187		bacterial luciferase family protein	1187	1.7	2.6
SERP1193	*hisS*	histidyl-tRNA synthetase			-1.4
SERP1195	*dtd*	D-tyrosyl-tRNA deacylase			-1.2
SERP1198	*apt*	adenine phosphoribosyltransferase	1199-1198		-1.6
SERP1201		protein-export membrane protein SecDF			-1.5
SERP1202	*yajC*	preprotein translocase, YajC subunit	1211-1202		-2.3
SERP1207		hypothetical protein	1211-1202	1.3	1.5
SERP1213	*mreC*	rod shape-determining protein MreC	1213-1212		-1.8
SERP1215		hypothetical protein			-2.2
SERP1218		Tn554, hypothetical protein			1.4

Table B.2 (continued)

Locus	Gene Name	Gene Description	Predicted Operon	DC FC	Chlor FC
SERP1222	*tnpC-1*	Tn554, transposase C			-1.6
SERP1223	*tnpB-1*	Tn554, transposase B	1226-1223		1.5
SERP1230		hypothetical protein			2.2
SERP1231	*hemL-1*	glutamate-1-semialdehyde aminotransferase	1236-1231		1.3
SERP1232	*hemB*	delta-aminolevulinic acid dehydratase	1236-1231		1.4
SERP1233	*hemD*	uroporphyrinogen-III synthase	1236-1231		1.7
SERP1238	*clpX*	ATP-dependent protease ATP-binding subunit			-1.2
SERP1240		hypothetical protein			-2.3
SERP1241		MutT/nudix family protein			-2.0
SERP1242	*rplT*	50S ribosomal protein L20	1244-1242		-2.2
SERP1246	*thrS*	threonyl-tRNA synthetase			-1.6
SERP1247	*dnaI*	primosomal protein DnaI			1.5
SERP1255	*phoR*	sensory box histidine kinase PhoR	1256-1255		-2.4
SERP1256	*phoP*	alkaline phosphatase synthesis transcriptional regulatory protein PhoP	1256-1255		-2.3
SERP1260		amino acid permease family protein			-1.3
SERP1264	*accD*	acetyl-CoA carboxylase beta subunit			1.4
SERP1266	*dnaE*	DNA polymerase III, alpha subunit			-1.2
SERP1267		DHH family protein			-1.5
SERP1269		universal stress protein family	1269	-1.2	-2.5
SERP1272	*ald*	alanine dehydrogenase			-1.8
SERP1276		hypothetical protein			1.5
SERP1277		thiol peroxidase, putative			1.6
SERP1280		aminotransferase, class V	1280-1278		1.4
SERP1281		septation ring formation regulator EzrA	1281		-2.4
SERP1282		GAF domain protein			1.6
SERP1286		OsmC/Ohr family protein			1.6
SERP1287		aminotransferase, class V			1.6
SERP1289		hydrolase, haloacid dehalogenase-like family			-1.5
SERP1290		PTS system, IIBC components			-1.8
SERP1291		1-acyl-sn-glycerol-3-phosphate acyltransferase, putative			-3.4
SERP1292		serine protease HtrA, putative			1.9
SERP1295	*fhs*	formate--tetrahydrofolate ligase	1295	1.8	1.8
SERP1297		3-deoxy-7-phosphoheptulonate synthase			-2.1
SERP1298		hypothetical protein			1.4
SERP1300	*murC*	UDP-N-acetylmuramate--L-alanine ligase	1305-1300		2.2
SERP1301		FtsK/SpoIIIE family protein	1305-1300	1.3	1.7
SERP1302		hypothetical protein	1305-1300		1.5
SERP1303		hypothetical protein	1305-1300	1.4	1.2

Table B.2 (continued)

Locus	Gene Name	Gene Description	Predicted Operon	DC FC	Chlor FC
SERP1304		thioredoxin, putative	1305-1300		1.7
SERP1307	*trmB*	tRNA (guanine-N(7)-)-methyltransferase			-2.6
SERP1309	*dat*	D-alanine aminotransferase			1.4
SERP1310		dipeptidase family protein			1.7
SERP1312		pseudouridine synthase, family 1	1313-1311		-1.3
SERP1314		hypothetical protein			2.2
SERP1315		hypothetical protein	1315	1.3	1.7
SERP1320		hypothetical protein			1.8
SERP1322	*rot*	repressor of toxins			-3.3
SERP1323		lysophospholipase, putative			-2.5
SERP1324	*putA*	proline dehydrogenase			-2.6
SERP1326	*ribBA*	3,4-dihydroxy-2-butanone-4-phosphate synthase/GTP cyclohydrolase II	1328-1325		2.3
SERP1327	*ribE*	riboflavin synthase subunit alpha	1328-1325	1.7	2.6
SERP1328	*ribD*	riboflavin biosynthesis protein RibD	1328-1325	1.6	2.1
SERP1338		CrcB family protein	1337-1339	1.4	1.6
SERP1341		Tn554, hypothetical protein			1.4
SERP1345	*tnpC-2*	Tn554, transposase C	1345	-1.2	-1.6
SERP1346	*tnpB-2*	Tn554, transposase B	1347-1346		1.5
SERP1348		ISSep1-like transposase			1.5
SERP1351		hypothetical protein			-2.3
SERP1357		O-succinylbenzoic acid synthetase, putative			2.1
SERP1358	*menE*	O-succinylbenzoic acid--CoA ligase			1.9
SERP1366	*hemG*	protoporphyrinogen oxidase			1.8
SERP1367	*hemH*	ferrochelatase			1.4
SERP1368	*hemE*	uroporphyrinogen decarboxylase			1.7
SERP1370		cadmium resistance family protein			-1.5
SERP1375		hypothetical protein	1375	1.2	-1.5
SERP1376		protein export protein PrsA, putative	1376		-2.8
SERP1378	*cbf1*	cmp-binding-factor 1			-2.0
SERP1379		hypothetical protein			-1.9
SERP1380		DNA repair exonuclease family protein			-1.9
SERP1382		hypothetical protein			-1.6
SERP1383		transcriptional regulator, Cro/CI family			-1.7
SERP1386		ribosomal large subunit pseudouridine synthase, RluD subfamily			-2.4
SERP1388		hypothetical protein	1390-1388		1.3
SERP1394		amino acid ABC transporter, ATP-binding protein, putative	1395-1394		-1.3
SERP1397	*sspA*	glutamyl endopeptidase precursor SspA			-7.2
SERP1398		transcriptional regulator, Fur family			-1.9

Table B.2 (continued)

Locus	Gene Name	Gene Description	Predicted Operon	DC FC	Chlor FC
SERP1402		hypothetical protein			-2.4
SERP1403		ABC transporter, permease/ATP-binding protein			2.8
SERP1404		hypothetical protein			2.1
SERP1405		hypothetical protein			-2.1
SERP1406	*mutY*	A/G-specific adenine glycosylase			1.9
SERP1408		hypothetical protein			-2.2
SERP1409		ABC transporter, ATP-binding protein			-1.6
SERP1412		transglycosylase domain protein	1412		-2.0
SERP1415		Radical SAM superfamily domain protein			-1.3
SERP1420		hypothetical protein			-2.3
SERP1422	*vraR*	DNA-binding response regulator VraR	1425-1422		-1.9
SERP1426	*map*	methionine aminopeptidase			-1.3
SERP1427		hypothetical protein			-2.1
SERP1428		immunodominant antigen B, putative			-2.7
SERP1433	*dinP*	DNA-damage-inducible protein P			2.3
SERP1434		hypothetical protein			-1.4
SERP1437	*gatB*	aspartyl/glutamyl-tRNA amidotransferase subunit B	1439-1437	1.3	1.3
SERP1442	*ligA*	DNA ligase, NAD-dependent			1.3
SERP1445		hypothetical protein			-2.7
SERP1446	*purB*	adenylosuccinate lyase			-2.0
SERP1448		hypothetical protein			2.0
SERP1450		nicotinate phosphoribosyltransferase			1.3
SERP1455	*ppaC*	putative manganese-dependent inorganic pyrophosphatase			-1.6
SERP1457		hypothetical protein			1.7
SERP1458		hypothetical protein			1.8
SERP1463		hypothetical protein			-2.1
SERP1466		Tn554-related, transposase A			-2.6
SERP1469		hypothetical protein			-1.4
SERP1472		hypothetical protein			-1.3
SERP1474		hypothetical protein	1478-1474		-1.5
SERP1477		ABC transporter, ATP-binding protein	1478-1474		-1.6
SERP1479		hypothetical protein			-1.4
SERP1481		hypothetical protein			-1.7
SERP1482		cell wall surface anchor family protein			1.5
SERP1483		cell wall surface anchor family protein			1.6
SERP1484	*groEL*	chaperonin, 60 kDa	1485-1484		1.8
SERP1485	*groES*	chaperonin, 10 kDa	1485-1484		1.3
SERP1486		abortive infection family protein			-1.5

Table B.2 (continued)

Locus	Gene Name	Gene Description	Predicted Operon	DC FC	Chlor FC
SERP1487	*sdrH*	sdrH protein			1.7
SERP1488		hydrolase, carbon-nitrogen family			-1.4
SERP1490	*agrB*	accessory gene regulator protein B	1490-1493		-1.3
SERP1492	*agrC*	accessory gene regulator protein C	1490-1493		-3.0
SERP1493	*agrA*	accessory gene regulator protein A	1490-1493		-2.6
SERP1494		fructokinase, putative	1495-1494	-1.4	-1.4
SERP1497	*scrR*	sucrose operon repressor	1498-1496	-1.5	-1.5
SERP1498		ammonium transporter family protein	1498-1496		1.5
SERP1503		hypothetical protein	1506-1503		1.4
SERP1507		hypothetical protein			-1.5
SERP1508		thioredoxin, putative	1508	-1.4	-1.3
SERP1512		HNH endonuclease family protein	1512	-1.4	1.5
SERP1527		hypothetical protein			1.5
SERP1534		DNA ligase, ATP-dependent			-2.2
SERP1535		hypothetical protein			-1.7
SERP1536		hypothetical protein			-1.2
SERP1540		hypothetical protein			-2.7
SERP1541		hypothetical protein			-1.7
SERP1545		hypothetical protein			1.7
SERP1555		serine/threonine protein phosphatase, putative	1556-1552		1.7
SERP1556		hypothetical protein	1556-1552		1.6
SERP1557		hypothetical protein			1.4
SERP1565		hypothetical protein			1.4
SERP1571		hypothetical protein			1.6
SERP1572		hypothetical protein			1.6
SERP1576		hypothetical protein			1.2
SERP1583		IS431mec-like transposase			2.8
SERP1586		acetyltransferase, GNAT family	1586-1585		1.5
SERP1588		IS431mec-like transposase			2.0
SERP1589		hypothetical protein			-1.3
SERP1590		single-stranded-DNA-specific exonuclease RecJ, putative	1592-1590	-1.4	-1.4
SERP1591		hypothetical protein	1592-1590		-1.5
SERP1593		hypothetical protein	1593	-1.3	-2.0
SERP1594		hypothetical protein	1595-1594		-1.7
SERP1595		hypothetical protein	1595-1594	-1.4	-2.1
SERP1596		hypothetical protein	1596	-1.6	-2.1
SERP1599		hypothetical protein			-2.3
SERP1600		hypothetical protein			-2.3
SERP1603		hypothetical protein			-2.0

Table B.2 (continued)

Locus	Gene Name	Gene Description	Predicted Operon	DC FC	Chlor FC
SERP1604		hypothetical protein			-2.1
SERP1605		hypothetical protein			-1.9
SERP1606		hypothetical protein			-3.1
SERP1607		hypothetical protein			-1.7
SERP1608		hypothetical protein	1608	-1.6	-1.9
SERP1614		hypothetical protein	1614	-2.1	-2.1
SERP1621		DNA-binding protein HU, putative	1621	-1.7	-2.4
SERP1622		hypothetical protein			-2.4
SERP1625		prophage, terminase, ATPase subunit, putative			-1.9
SERP1626		hypothetical protein			-2.2
SERP1627		hypothetical protein			-1.7
SERP1628		hypothetical protein			-2.9
SERP1629		hypothetical protein			-2.1
SERP1630		hypothetical protein			-2.3
SERP1631		hypothetical protein			-2.2
SERP1633		hypothetical protein			-1.8
SERP1635		hypothetical protein			-1.6
SERP1636		hypothetical protein			-2.7
SERP1640		M23/M37 peptidase domain protein			-1.5
SERP1642		hypothetical protein	1641-1643		-1.5
SERP1644		hypothetical protein			-1.7
SERP1645		hypothetical protein			-1.7
SERP1646		hypothetical protein			-1.8
SERP1647		hypothetical protein			-1.4
SERP1648	*xhlB*	prophage, holin, SPP1 family			-1.7
SERP1650		prophage, amidase, putative			-1.5
SERP1652		hypothetical protein			-1.5
SERP1653		hypothetical protein			-1.3
SERP1656		hypothetical protein			-1.2
SERP1658		ABC transporter, ATP-binding protein			1.2
SERP1659		hypothetical protein			2.0
SERP1660		MutS family protein			-1.7
SERP1665	*ilvD*	dihydroxy-acid dehydratase	1665-1667		1.6
SERP1671	*leuC*	isopropylmalate isomerase large subunit	1668-1673		1.7
SERP1672	*leuD*	3-isopropylmalate dehydratase, small subunit	1668-1673		1.7
SERP1673	*ilvA*	threonine dehydratase	1668-1673		1.4
SERP1677	*rpoF*	sigma factor B	1680-1677	-1.3	-1.5
SERP1678	*rsbW*	serine-protein kinase RsbW	1680-1677	-1.3	1.3
SERP1680	*rsbU*	sigma factor B regulator protein	1680-1677	-1.3	-1.7

Table B.2 (continued)

Locus	Gene Name	Gene Description	Predicted Operon	DC FC	Chlor FC
SERP1682		hypothetical protein			-2.1
SERP1685		hypothetical protein			-1.5
SERP1686		hypothetical protein			-1.3
SERP1687		hypothetical protein			-1.7
SERP1691		cell division protein, FtsW/RodA/SpoVE family			-1.6
SERP1693		hypothetical protein			-2.2
SERP1694		hypothetical protein			-2.4
SERP1696		HD domain protein			-1.3
SERP1699	*thiM*	hydroxyethylthiazole kinase			1.6
SERP1700	*thiD-2*	phosphomethylpyrimidine kinase			2.0
SERP1701		transcriptional regulator, TenA family			2.3
SERP1702	*sceD*	sceD protein			2.4
SERP1704	*ywpF*	ywpF protein			-1.3
SERP1706	*murAA*	UDP-N-acetylglucosamine 1-carboxyvinyltransferase	1707-1705		1.6
SERP1707		hypothetical protein	1707-1705	1.6	1.7
SERP1709	*atpD*	ATP synthase subunit B	1715-1708		-1.3
SERP1711	*atpA*	ATP synthase subunit A	1715-1708		-1.2
SERP1713	*atpF*	ATP synthase F0, B subunit	1715-1708		-1.3
SERP1714	*atpE*	ATP synthase subunit C	1715-1708		-1.3
SERP1715	*atpB*	ATP synthase subunit A	1715-1708		-1.4
SERP1717		UDP-N-acetylglucosamine 2-epimerase			-1.2
SERP1725	*prfA*	peptide chain release factor 1			-1.2
SERP1729		aldehyde dehydrogenase			1.9
SERP1731	*murAB*	UDP-N-acetylglucosamine 1-carboxyvinyltransferase	1731		-1.2
SERP1734	*pyrG*	CTP synthetase			-1.5
SERP1737		hypothetical protein			-2.5
SERP1739		hypothetical protein			1.8
SERP1740		amidohydrolase family protein			1.9
SERP1744	*pdp*	pyrimidine-nucleoside phosphorylase			1.4
SERP1745	*deoC*	deoxyribose-phosphate aldolase			1.6
SERP1749		hypothetical protein			-3.1
SERP1750		hypothetical protein			-1.7
SERP1752	*manA-1*	mannose-6-phosphate isomerase, class I			-2.2
SERP1753		hypothetical protein			2.7
SERP1755	*czrA*	transcriptional regulator CzrA			-1.9
SERP1756		cation efflux family protein			-2.1
SERP1764		hypothetical protein	1764-1762		-1.7
SERP1765		ATP-binding protein, Mrp/Nbp35 family	1766-1765	1.8	2.5

Table B.2 (continued)

Locus	Gene Name	Gene Description	Predicted Operon	DC FC	Chlor FC
SERP1771		hypothetical protein			-1.9
SERP1774		hypothetical protein			-1.3
SERP1778		hypothetical protein			2.1
SERP1779		hypothetical protein			1.9
SERP1780		transporter, putative			1.9
SERP1781		hypothetical protein			1.3
SERP1783		hypothetical protein			4.5
SERP1785		alcohol dehydrogenase, zinc-containing			1.5
SERP1786		alcohol dehydrogenase, zinc-containing			1.6
SERP1790	*lacE*	PTS system, lactose-specific IIBC components	1795-1789		1.2
SERP1791	*lacF*	PTS system, lactose-specific IIA component	1795-1789		1.3
SERP1792	*lacD*	tagatose 1,6-diphosphate aldolase	1795-1789	-1.2	1.2
SERP1793	*lacC*	tagatose-6-phosphate kinase	1795-1789		1.2
SERP1796	*lacR*	lactose phosphotransferase system repressor			-1.6
SERP1797		transcriptional regulator, Sir2 family			-2.7
SERP1799	*rplM*	50S ribosomal protein L13			-1.3
SERP1821	*rplN*	ribosomal protein L14	1832-1810		-1.4
SERP1838		sugar transporter, putative			1.5
SERP1841		hypothetical protein			-1.8
SERP1842		hypothetical protein			-1.9
SERP1843		AcrB/AcrD/AcrF family protein			1.4
SERP1845		hypothetical protein			1.3
SERP1846		transcriptional regulator, MarR family	1846-1847		1.9
SERP1861	*modA*	molybdenum ABC transporter, molybdenum-binding protein ModA			-1.6
SERP1865		inosine-uridine preferring nucleoside hydrolase family protein			1.4
SERP1866		acyl-CoA dehydrogenase-related protein			1.7
SERP1867		hypothetical protein			1.3
SERP1874	*ureG*	urease accessory protein UreG			-1.2
SERP1876	*sarR*	Staphylococcal accessory regulator R	1876		-2.8
SERP1880		secretory antigen precursor SsaA	1880	2.1	2.2
SERP1883		hypothetical protein			-2.3
SERP1887	*sugE-2*	sugE protein	1886-1888		1.6
SERP1888		glycerate dehydrogenase	1886-1888		1.9
SERP1892		hypothetical protein	1892-1891		-1.3
SERP1893		transcriptional regulator, putative			-1.9
SERP1904		hypothetical protein			-1.9
SERP1908		hypothetical protein			-2.3

Table B.2 (continued)

Locus	Gene Name	Gene Description	Predicted Operon	DC FC	Chlor FC
SERP1910		phosphosugar-binding transcriptional regulator			-2.2
SERP1914		Na+/H+ antiporter, putative	1914		1.5
SERP1916		hypothetical protein			1.9
SERP1917		oxidoreductase, short chain dehydrogenase/reductase family			2.1
SERP1918		amidohydrolase family protein			2.8
SERP1919	*hutG*	formiminoglutamase			1.6
SERP1920		abortive infection family protein			-2.6
SERP1922		hypothetical protein			-2.9
SERP1924	*rpiA*	ribose 5-phosphate isomerase			-1.7
SERP1925		hypothetical protein			-1.9
SERP1926	*galM*	aldose 1-epimerase			-1.4
SERP1928		hypothetical protein			-1.4
SERP1929		hypothetical protein			1.8
SERP1938	*corA*	magnesium and cobalt transport protein CorA	1938-1937		-1.6
SERP1940		hypothetical protein			-1.4
SERP1942		hypothetical protein			-1.6
SERP1945		drug transporter, putative	1945-1944	-1.3	-2.0
SERP1947	*tcaB*	tcaB protein	1048-1947		-1.3
SERP1948	*tcaA*	tcaA protein	1048-1947	-1.3	-1.7
SERP1949	*tcaR*	transcriptional regulator TcaR			-2.7
SERP1953		DNA-binding response regulator	1953-1954	1.3	2.2
SERP1954		sensor histidine kinase	1953-1954		1.5
SERP1956		glycosyl transferase, group 1 family protein			1.6
SERP1957		L-lactate permease			-1.3
SERP1959		lipoprotein, putative			-1.8
SERP1964		hypothetical protein			-2.3
SERP1968		PTS system, sucrose-specific IIBC components			-1.3
SERP1977		hypothetical protein			-1.9
SERP1980		nitrite extrusion protein	1980		-1.8
SERP1991		hypothetical protein			2.9
SERP1994		ABC transporter, substrate-binding protein	1994		-1.2
SERP1996		acetyltransferase, GNAT family			1.6
SERP1997		formate/nitrite transporter family protein			-1.9
SERP1998		hypothetical protein			-1.3
SERP1999		glutaredoxin, putative	2000-1999	-1.4	-2.5
SERP2000		lipoprotein, putative	2000-1999		-2.1
SERP2001	*fmhA*	fmhA protein			-1.8

Table B.2 (continued)

Locus	Gene Name	Gene Description	Predicted Operon	DC FC	Chlor FC
SERP2003		amino acid ABC transporter, ATP-binding protein	2005-2003		2.8
SERP2004		amino acid ABC transporter, permease protein	2005-2003		2.1
SERP2005		amino acid ABC transporter, amino acid-binding protein	2005-2003		1.6
SERP2007	*gpm*	phosphoglycerate mutase			-1.8
SERP2009		hypothetical protein			-1.7
SERP2010		hypothetical protein			-1.9
SERP2013		hypothetical protein			-1.4
SERP2015		hypothetical protein			1.6
SERP2016		hypothetical protein	2016	1.2	1.8
SERP2019		fmtA-like protein			1.6
SERP2022		2-dehydropantoate 2-reductase			1.2
SERP2025	*lytR*	response regulator LytR	2024-2027		-1.3
SERP2029		amino acid ABC transporter, amino acid-binding protein	2031-2028		1.2
SERP2031		amino acid ABC transporter, ATP-binding protein	2031-2028	-1.2	1.3
SERP2032		sorbitol dehydrogenase, putative			-1.2
SERP2033		hypothetical protein			1.4
SERP2035		carboxylesterase family protein			1.5
SERP2036		major facilitator superfamily protein			1.6
SERP2043		peptidase, M42 family			2.2
SERP2044		hypothetical protein			2.5
SERP2045		short chain dehydrogenase			1.9
SERP2048		acetylornithine deacetylase			1.4
SERP2049		oxidoreductase, short-chain dehydrogenase/reductase family			1.5
SERP2050		hypothetical protein			2.4
SERP2052		helicase, putative			-1.3
SERP2053		MutT/nudix family protein			-1.4
SERP2054		glycosyl transferase, group 1 family protein			-1.6
SERP2056	*galU*	UTP-glucose-1-phosphate uridylyltransferase			-1.2
SERP2069		major facilitator superfamily protein			-1.7
SERP2070		thiamine-phosphate pyrophosphorylase, putative			2.0
SERP2071		glycine oxidase, putative			2.1
SERP2073		thiazole synthase			1.8
SERP2074		HesA/MoeB/ThiF family protein			1.7
SERP2076		fructose-1,6-bisphosphatase, putative			1.6

Table B.2 (continued)

Locus	Gene Name	Gene Description	Predicted Operon	DC FC	Chlor FC
SERP2077		Na+/H+ antiporter, putative	2077		1.9
SERP2079		hypothetical protein			1.7
SERP2083		glyoxalase family protein			3.6
SERP2084	*aldA-2*	aldehyde dehydrogenase	2085-2084	1.3	2.2
SERP2085		hypothetical protein	2085-2084		4.9
SERP2086	*frp*	NAD(P)H-flavin oxidoreductase			1.8
SERP2087		2-hydroxyacid dehydrogenase			1.8
SERP2089	*srtA*	sortase			-1.7
SERP2091		hypothetical protein			1.3
SERP2092		IS1272-like transposase, degenerate			1.6
SERP2101		ribose transport protein	2102-2100		-1.4
SERP2102		hypothetical protein	2102-2100		-1.5
SERP2103	*dep*	gamma-glutamyltranspeptidase			1.6
SERP2106	*capC*	capC protein			1.4
SERP2109		esterase, putative	2110-2109	1.4	1.7
SERP2110		hypothetical protein	2110-2109		1.6
SERP2113		abortive infection family protein			-1.3
SERP2114		PTS system, IIABC components			-1.4
SERP2118		transcriptional regulator, LysR family	2118	-1.4	-1.6
SERP2129		oxidoreductase, short-chain dehydrogenase/reductase family			1.6
SERP2131		cation-transporting ATPase, E1-E2 family			1.6
SERP2135		hypothetical protein			1.5
SERP2136		secretory antigen precursor SsaA	2136	2.2	2.3
SERP2138		immunodominant antigen A, putative			-1.6
SERP2139		hypothetical protein			2.3
SERP2140		hypothetical protein			-1.4
SERP2142		amino acid permease family protein	2142	-1.5	-1.4
SERP2144	*pyrD*	dihydroorotate dehydrogenase	2144		-1.6
SERP2145		hypothetical protein			-1.9
SERP2151	*panC*	pantoate--beta-alanine ligase			1.5
SERP2152	*panB*	3-methyl-2-oxobutanoate hydroxymethyltransferase			1.8
SERP2155	*budB*	alpha-acetolactate synthase			1.2
SERP2156	*ldh*	L-lactate dehydrogenase			1.3
SERP2159		4-aminobutyrate aminotransferase			1.5
SERP2160		hypothetical protein			1.3
SERP2161		lipoprotein, putative	2161	-1.5	-1.8
SERP2167		lipoprotein, putative			-2.6
SERP2168	*mqo-2*	malate:quinone oxidoreductase			-1.6
SERP2170	*ppdK*	pyruvate phosphate dikinase			1.9

Table B.2 (continued)

Locus	Gene Name	Gene Description	Predicted Operon	DC FC	Chlor FC
SERP2172		acetyl-CoA synthetase, putative			1.7
SERP2173		hypothetical protein			1.8
SERP2174		hypothetical protein			1.6
SERP2180		anaerobic C4-dicarboxylate transporter			-1.2
SERP2182	*nrdG*	anaerobic ribonucleoside-triphosphate reductase activating protein	2183-2182	1.0	-1.2
SERP2183	*nrdD*	anaerobic ribonucleoside triphosphate reductase	2183-2182		-1.2
SERP2184		hypothetical protein	2184	-2.0	-2.7
SERP2185	*cysC*	adenylylsulfate kinase	2191-2185		1.7
SERP2186	*sat*	sulfate adenylyltransferase	2191-2185		1.7
SERP2187		hypothetical protein	2191-2185		2.3
SERP2188		precorrin-2 dehydrogenase	2191-2185		1.6
SERP2190	*cysI*	sulfite reductase (NADPH) hemoprotein beta-component	2191-2185		1.9
SERP2191	*cysJ*	sulfite reductase (NADPH) flavoprotein alpha-component	2191-2185		1.9
SERP2192	*cysH*	phosophoadenylyl-sulfate reductase			3.6
SERP2193		hypothetical protein			20.9
SERP2194	*gpxA-2*	glutathione peroxidase	2196-2194		4.4
SERP2195		alpha keto acid dehydrogenase complex, E3 component, lipoamide dehydrogenase, putative	2196-2194		1.8
SERP2196		transcriptional regulator, MarR family	2196-2194	1.5	9.6
SERP2199		hypothetical protein	2199	1.3	2.0
SERP2200		hypothetical protein			2.0
SERP2202		hypothetical protein			-2.2
SERP2206		DNA-binding response regulator	2207-2203	-1.5	-1.8
SERP2207		hypothetical protein	2207-2203		-2.4
SERP2209		hypothetical protein			2.0
SERP2212		hypothetical protein			2.0
SERP2213		hypothetical protein			1.2
SERP2221		cadmium resistance family protein			-2.6
SERP2222	*cadC*	transcriptional regulator CadC			-2.4
SERP2225		transcriptional regulator, ArsR family			-1.3
SERP2226		hypothetical protein			1.5
SERP2227		hypothetical protein			2.2
SERP2228		hypothetical protein			1.5
SERP2230		hypothetical protein			2.0
SERP2232		major facilitator superfamily protein			1.7
SERP2233		transcriptional regulator, LysR family			-1.5

Table B.2 (continued)

Locus	Gene Name	Gene Description	Predicted Operon	DC FC	Chlor FC
SERP2235		hypothetical protein			-3.1
SERP2240		transposase, IS200 family			1.6
SERP2241		transcriptional regulator, putative			-1.6
SERP2243		hypothetical protein			5.1
SERP2244		capA-related protein	2244	-1.6	-2.7
SERP2246		transcriptional regulator, Crp/Fnr family			-4.0
SERP2247	*arcD*	arginine/ornithine antiporter			-1.8
SERP2248		hypothetical protein			-3.9
SERP2249	*arcB-1*	ornithine carbamoyltransferase			-1.5
SERP2250	*arcA*	arginine deiminase			-1.4
SERP2251		transcriptional regulator, ArgR family			-2.8
SERP2253		hypothetical protein	2253		1.6
SERP2254		hypothetical protein			-2.7
SERP2255		hypothetical protein	2255-2256	-1.5	-1.5
SERP2256		hypothetical protein	2255-2256		-1.3
SERP2265		organic hydroperoxide resistance protein, putative	2265	1.6	3.2
SERP2266		hypothetical protein			3.0
SERP2267		hypothetical protein			-2.5
SERP2272		methionine sulfoxide reductase A			1.4
SERP2274		hypothetical protein	2281-2273		1.7
SERP2275		glycosyl transferase, group 1 family protein	2281-2273		1.9
SERP2276		translocase	2281-2273		1.9
SERP2278		hypothetical protein	2281-2273		2.4
SERP2279		hypothetical protein	2281-2273		2.5
SERP2280		SecY/Sec61-alpha family protein	2281-2273		2.3
SERP2281		serine threonine rich antigen	2281-2273		1.8
SERP2282		hypothetical protein			-1.4
SERP2286		phosphonate ABC transporter, phosphonate-binding protein	2286-2283		-2.1
SERP2287		hypothetical protein	2287		1.7
SERP2292	*icaR*	intercellular adhesion regulator	2292		-1.8
SERP2299		N-acetyltransferase family protein			1.7
SERP2300	*hisIE*	phosphoribosyl-AMP pyrophosphatase/phosphoribosyl-ATP cyclohydrolase	2307-2300		1.5
SERP2301	*hisF*	imidazoleglycerol phosphate synthase, cyclase subunit	2307-2300		1.7
SERP2302	*hisA*	phosphoribosylformimino-5-aminoimidazole carboxamide ribotide isomerase	2307-2300		1.7
SERP2304	*hisB*	imidazoleglycerol-phosphate dehydratase	2307-2300		1.6

Table B.2 (continued)

Locus	Gene Name	Gene Description	Predicted Operon	DC FC	Chlor FC
SERP2305	*hisD*	histidinol dehydrogenase	2307-2300		2.0
SERP2306	*hisG*	ATP phosphoribosyltransferase	2307-2300		1.8
SERP2307		hypothetical protein	2307-2300		1.8
SERP2309		transcriptional regulator, AsnC family			-2.6
SERP2313		hypothetical protein			1.1
SERP2315	*drp35*	drp35 protein			1.5
SERP2317	*pcp*	pyrrolidone-carboxylate peptidase			1.3
SERP2319		hypothetical protein			-1.6
SERP2323		IS1272-like transposase, degenerate			1.9
SERP2329		hypothetical protein			2.4
SERP2330		thiamine biosynthesis protein, putative			2.2
SERP2332		hypothetical protein			2.1
SERP2333		hypothetical protein			2.1
SERP2334		major facilitator superfamily protein			-1.7
SERP2336		lipase, putative			1.8
SERP2342		drug transporter, putative			1.5
SERP2347	*bioB*	biotin synthase			2.0
SERP2350		hypothetical protein			-1.6
SERP2351	*arcB-2*	ornithine carbamoyltransferase	2351-2352	-1.1	-1.6
SERP2352	*arcC*	carbamate kinase	2351-2352		-1.3
SERP2355		amino acid ABC transporter, permease protein	2358-2354		1.9
SERP2357		amino acid ABC transporter, permease protein	2358-2354		1.8
SERP2358		amino acid ABC transporter, ATP-binding protein	2358-2354		1.6
SERP2359		hypothetical protein			2.0
SERP2360		3-hydroxyacyl-CoA dehydrogenase family protein			2.2
SERP2361		hypothetical protein			2.8
SERP2362		transcriptional regulator, TetR family			2.1
SERP2367		transporter, putative	2375-2367		1.5
SERP2368		peptide ABC transporter, ATP-binding protein	2375-2367		1.4
SERP2369		peptide ABC transporter, ATP-binding protein	2375-2367		1.6
SERP2370		peptide ABC transporter, permease protein	2375-2367		1.7
SERP2372		peptide ABC transporter, peptide-binding protein	2375-2367		1.7
SERP2373		hypothetical protein	2375-2367		2.2
SERP2374		hypothetical protein	2375-2367		1.7

Table B.2 (continued)

Locus	Gene Name	Gene Description	Predicted Operon	DC FC	Chlor FC
SERP2375		diaminopimelate epimerase family protein	2375-2367		1.6
SERP2382		ApbE family protein	2382-2380		-1.7
SERP2384		hypothetical protein	2384-2386		2.4
SERP2385		hypothetical protein	2384-2386	-1.5	1.8
SERP2386		cobalamin synthesis protein, putative	2384-2386		2.2
SERP2392	*bhp*	cell wall associated biofilm protein			1.7
SERP2394		aminotransferase, class II	2396-2393		1.4
SERP2395	*bioA*	adenosylmethionine--8-amino-7-oxononanoate aminotransferase	2396-2393		1.9
SERP2396	*bioD*	dethiobiotin synthase	2396-2393		2.0
SERP2402		hypothetical protein			4.4
SERP2405		sensor histidine kinase	2404-2406		1.6
SERP2406		DNA-binding response regulator, AraC family	2404-2406		1.8
SERP2411		oxidoreductase, short chain dehydrogenase/reductase family			-1.9
SERP2414		lipoprotein, putative			-2.5
SERP2420		hypothetical protein			1.5
SERP2423		lipoprotein, putative			1.9
SERP2424		hypothetical protein			7.0
SERP2425		hypothetical protein			10.0
SERP2426		transcriptional regulator, ArsR family			8.6
SERP2427	*arsD*	arsenical resistance operon trans-acting repressor	2427-2428	1.8	3.7
SERP2428	*arsA*	arsenical pump-driving ATPase	2427-2428		3.4
SERP2429	*arsR-2*	arsenical resistance operon repressor	2429-2431		2.2
SERP2430	*arsB*	arsenical pump membrane protein	2429-2431	1.3	3.2
SERP2431	*arsC-2*	arsenate reductase	2429-2431		1.7
SERP2432		hypothetical protein			2.5
SERP2433		hypothetical protein			1.7
SERP2434		rhodanese-like domain protein			2.7
SERP2435		metallo-beta-lactamase family protein			3.1
SERP2436		hypothetical protein			2.2
SERP2439		hypothetical protein			-2.3
SERP2441		transporter, putative			-1.7
SERP2442		hypothetical protein			1.4
SERP2445		lipoprotein, putative			-1.5
SERP2453		lipoprotein, putative			-1.4
SERP2454		hypothetical protein	2454	-1.5	-2.5
SERP2455		hypothetical protein	2463-2455		-2.7
SERP2456		hypothetical protein	2463-2455	-1.5	-2.6
SERP2457		CRISPR-associated protein, TM1807 family	2463-2455		-1.9

Table B.2 (continued)

Locus	Gene Name	Gene Description	Predicted Operon	DC FC	Chlor FC
SERP2458		CRISPR-associated protein, TM1808 family	2463-2455		-1.8
SERP2459		CRISPR-associated protein, TM1792 family	2463-2455		-2.6
SERP2461		CRISPR-associated protein, TM1811 family	2463-2455		-1.9
SERP2462		CRISPR-associated protein Cas2	2463-2455		-2.9
SERP2463	*cas1*	CRISPR-associated protein Cas1	2463-2455		-3.1
SERP2464		hypothetical protein			-1.4
SERP2467		hypothetical protein			1.8
SERP2470		spermidine N1-acetyltransferase, putative			-3.3
SERP2471		type I restriction-modification system, S subunit, EcoA family	2474-2471		-1.7
SERP2472	*hsdM*	type I restriction-modification system, M subunit	2474-2471	-1.8	-2.0
SERP2473		hypothetical protein	2474-2471		-1.3
SERP2474	*hsdR*	type I restriction-modification system, R subunit	2474-2471		-1.5
SERP2475		hypothetical protein			-1.7
SERP2481		hypothetical protein			-1.4
SERP2485	*kdpC*	K+-transporting ATPase, C subunit	2485-2487	-1.7	-2.7
SERP2494		hypothetical protein			-2.0
SERP2496		hypothetical protein			1.6
SERP2497		hypothetical protein			2.3
SERP2498		cassette chromosome recombinase A	2498-2499		1.9
SERP2499		cassette chromosome recombinase B	2498-2499		1.8
SERP2500		hypothetical protein			1.8
SERP2501		hypothetical protein	2501-2505		1.7
SERP2502		hypothetical protein	2501-2505		1.6
SERP2503		hypothetical protein	2501-2505		1.7
SERP2504		hypothetical protein	2501-2505		1.8
SERP2507	*tnpB-3*	transposase B	2506-2507		1.6
SERP2508	*tnpC-3*	transposase C			-1.6
SERP2512		hypothetical protein			1.5
SERP2513		hypothetical protein	2514-2513		2.5
SERP2514		hypothetical protein	2514-2513		2.5
SERP2515		rhodanese-like domain protein			2.2
SERP2520	*mecR1*	methicillin-resistance regulatory protein MecR1			-2.0
SERP2521	*mecA*	penicillin-binding protein 2'			-1.5
SERP2522		MaoC domain protein	2523-2522		-1.4
SERP2528		hypothetical protein			-2.5
SERP2529		hypothetical protein			-2.0
SERP2530	*yycJ*	metallo-beta-lactamase family protein YycJ	2530		1.4

Table B.2 (continued)

Locus	Gene Name	Gene Description	Predicted Operon	DC FC	Chlor FC
SERP2534	*yycF*	DNA-binding response regulator YycF	2534-2531		-1.8
SERP2536	*purA*	adenylosuccinate synthetase	2536		1.5
SERP2537	*dnaB*	replicative DNA helicase			1.7
SERP2541		homoserine O-acetyltransferase, putative			1.9
SERP2543		azlC protein, putative	2543-2542		1.5
SERP2544	*hlb*	beta-hemolysin			1.5
SERP2545	*serS*	seryl-tRNA synthetase			-2.3
SERP2546		hypothetical protein			-5.7
SERP2549	*gyrB*	DNA gyrase, B subunit	2551-2548		-1.2
SERP2553	*dnaA*	chromosomal replication initiation protein			-1.6

APPENDIX C

A BIOFILM GROWTH PROTOCOL AND THE DESIGN OF A MAGNETIC FIELD EXPOSURE SETUP TO BE USED IN THE STUDY OF MAGNETIC FIELDS AS A MEANS OF CONTROLLING BACTERIAL BIOFILMS

A BIOFILM GROWTH PROTOCOL AND THE DESIGN OF A MAGNETIC FIELD EXPOSURE SETUP TO BE USED IN THE STUDY OF MAGNETIC FIELDS AS A MEANS OF CONTROLLING BACTERIAL BIOFILMS

Contribution of Authors and Co-Authors

Manuscript(s) in Appendix C

Author: Bruce R. McLeod

Contributions: Designed, built, and tested electrical parameters for exposure system. Wrote manuscript.

Co-Author: Elizabeth L. Sandvik

Contributions: Assisted with design of microbial and aseptic aspects of the exposure system and testing. Contributed sections to the manuscript.

Manuscript Information Page

Bruce R. McLeod and Elizabeth L. Sandvik
Bioelectromagnetics
Status of Manuscript:
____ Prepared for submission to a peer-reviewed journal
____ Officially submitted to a peer-review journal
____ Accepted by a peer-reviewed journal
_X_ Published in a peer-reviewed journal

John Wiley & Sons, Inc.
Submitted September 22, 2008
Published online July 23, 2009
Issue 31: 56-63

Abstract

The use of prosthetic implants is increasing both in the United States and around the world and there is a concomitant rise in cases of biofilm based, persistent infections that are quite serious and virtually impervious to antibiotic treatment. The development of alternate therapies that do not involve the long term use of high levels of antibiotics or surgical intervention is needed. Based on the success of using electric or magnetic fields to alter certain physiological processes, it is hypothesized that relatively low level magnetic fields in conjunction with the appropriate antibiotic may be able to help control and eventually clear the bacterial biofilms on a prosthetic. In order to test this hypothesis, it is necessary to first develop a means of growing laboratory grade biofilms on specific materials in a way that is repeatable between experiments and that can be reproduced by other laboratories. Secondly, a means of applying controlled magnetic fields to the surfaces supporting the biofilms at a defined temperature must be developed. This paper addresses both of these points.

Keywords: *Staphylococcus epidermidis*, prosthetic implants, orthopedic device associated infections, EMF, solenoid

Introduction

Bacterial biofilm growth on a prosthetic implant can be the primary cause of persistent infections resulting in serious medical problems [Darouiche, 2004; Konig, et al., 2001; Pavoni, et al., 2004; Saginur, et al., 2006]. Bacterial biofilms have a well-known ability to be nearly impervious to antibiotic treatment with resistance to antibiotics at 1,000 to as high as 5,000 times the concentration effective on the same species in a planktonic (free-floating) culture [Costerton and Stewart, 2000, del Pozo, et al, 2008]. Extensive antimicrobial therapy with multiple antibiotics has been used as a treatment for implant associated infections [Konig, et al., 2001; Pavoni, et al., 2004; Zimmerli, et al., 1998] but if this course of action fails, it is probable that the removal and replacement of the device in a one or two stage surgical process in addition to another extensive course of antibiotics will be necessary [Pavoni, et al., 2004]. An effective treatment method that improves antibiotic treatment and does not include surgery is clearly needed.

One alternate approach to traditional antimicrobial treatment is the use of electric or magnetic fields alone or in conjunction with an appropriate antibiotic to enhance the efficacy of the antibiotic against the biofilm. A 1992 study first showed that the action of several specific biocides against *Pseudomonas aeruginosa* biofilms could be significantly enhanced with the application of low levels of direct current (DC) whereas the biocide or current alone had little to no effect [Blenkinsopp, et al., 1992]. A number of similar papers have since appeared [del Pozo, et al., 2008; Ehrlich, et al., 2005; Shirtliff, et al., 2005; Caubet, et al., 2004; O'Gara, et al., 2001; Stewart, et al., 1999; Masterson, et al., 1997; Wellman, et al., 1996] indicating the effectiveness of this direct current approach.

While this approach may show promise in clinical treatment, it requires the placement of two electrodes in contact with the patient.

A recent paper in Antimicrobial Agents & Chemotherapy suggests AC electric fields alone can inhibit the growth of planktonic bacteria [Giladi, et al., 2008]. Time varying (AC) and non-time varying (DC) electric and magnetic fields have been investigated for quite some time with respect to their use in medicine and biology (for instance, see the papers from the First World Congress for Electricity and Magnetism in Biology and Medicine, Orlando, Florida, 1992, Martin Blank, editor) and their clinical use in aiding bone repair is well established (Aaron, et al. 2004; Pilla, 2006). There are, however, very few reports of using AC or combined AC and DC magnetic fields in conjunction with antibiotics to explore the possibility of controlling a bacterial biofilm. A potential advantage of using AC magnetic fields rather than direct current to achieve the control is that no direct contact to the patient is required making this method entirely noninvasive.

In order to explore this approach, a growth protocol for biofilms is needed that allows the biofilms to be grown in a controlled, repeatable manner on specific surfaces and then exposed to well characterized and defined magnetic fields. Additionally, the entire process must take place at a set temperature. This paper first details an approach for growing *Staphylococcus epidermidis* biofilms on selected materials and then a magnetic field exposure system design is described that allows for up to seven variations of biofilm experimental conditions (e.g., antibiotic level, antibiotic type, trace minerals,

nutrients, type of material, specific biofilm) to be studied during a single experiment done in a uniform magnetic field at a selected temperature.

Biofilm Growth and Quantification

The first challenge in biofilm research is to develop a protocol that results in a routinely repeatable biofilm on a desired material. An example of such research would be growing *Staphylococcus epidermidis* or *Staphylococcus aureus* biofilms on materials normally used in prosthetic knees (such as ASTM-75 metal or Ultra High Molecular Weight Polyethylene (UHMWPE)). The requirement for repeatability must hold between experiments as well as between separate laboratories. The Center for Biofilm Engineering (CBE) at Montana State University has developed a number of growth methods, protocols, and reactors. It should be noted that reactor choice is critical since the growth protocol can affect observed antimicrobial response even when the same microorganism is used. A recent study investigating fluid dynamics as a critical control parameter looked at two different bacterial species grown in five different growth systems used to study biofilms and the response to three different antimicrobials. Even though treatments were applied in exactly the same way, the log reduction for the same antimicrobial at the same concentration was significantly different between the different growth systems [Buckingham-Meyer, et al, 2007].

The CDC Biofilm Reactor is a continuous flow system with biofilms grown under high shear (shown in Figure 1a). Figure 1b shows the CDC Reactor in use in a typical growth setup. The CDC Reactor is an excellent choice for growing biofilms because of its versatility (it can be used for many different organisms grown on different types of

material) and because it can be used to produce biofilms on up to 24 sampling surfaces during a single growth procedure. An example growth protocol for *Staphylococcus epidermidis* ATCC #35984 using this reactor follows which has yielded biofilms with repeatable cell densities (+/- 0.25 $\log_{10}$CFU/cm^2) both within and between experiments.

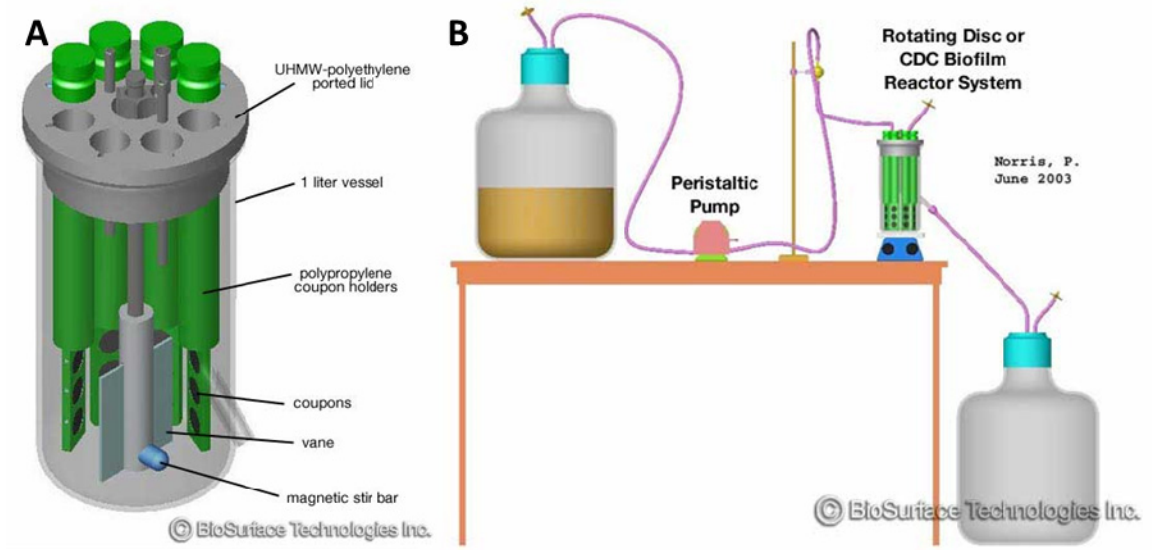

Figure C.1 (A) The CDC reactor. Biofilms are grown on 12.7 mm diameter disks, or coupons, suspended in the bulk fluid by 8 polypropylene coupon holders with the possibility of 24 repeat coupons from each growth protocol. The coupons can be made from a variety of materials as desired. Biofilm growth can be controlled with specific changes in the growth medium, temperature, the flow rate, the rotation speed of the baffled stir bar and other growth conditions. The CDC reactor is available from BioSurfaces Technologies Corp., Bozeman, Montana. (B) A biofilm growth setup using the CDC reactor is shown. A typical experiment would start with inoculation of the sterile reactor containing a nutrient solution and a period of batch operation with the effluent port clamped. Following the batch phase, the effluent port would be unclamped and a flow of a sterile fresh nutrient solution from the carboy seen on the left would start for a phase of continuous flow operation. A glass flow break in the feed line before the reactor prevents backcontamination of the feed carboy and maintains the influent sterility. A detailed species-specific growth protocol is described in the text.

While this protocol can be used as a basic guide, some modifications may be needed if a different strain or species of microorganism is to be studied. Additionally, a biofilm sampling process is described. This section was included to indicate how one might evaluate the effect on the biofilm after a magnetic field experiment but it should be noted that several other sampling processes might work equally well. Both the growth and sampling protocols parallel the methods of ASTM Method E 2562–07 for *Pseudomonas aeruginosa* biofilms grown with high shear and continuous flow using the CDC Biofilm Reactor [ASTM International, 2007].

Biofilm Growth Protocol. *Staphylococcus epidermidis* ATCC#35984 biofilms were to be grown on polycarbonate coupons (12.7 mm diameter, surface area 126.7 mm^2) in the CDC Biofilm Reactor. The sterilized reactor containing 450 mL of full strength tryptic soy broth (TSB, Fischer Scientific #DF0370075) with the effluent tube clamped was inoculated from a frozen stock of *S. epidermidis*. The reactor was placed in a 37˚C incubator and operated in batch with stirring at 125 rpm for 24 hours. After 24 hours, a continuous flow of sterile $1/10^{th}$ strength tryptic soy broth (TSB) was started with a reactor residence time of 30 minutes. Continuous flow ran for 16 hours at the end of which biofilm coated coupons were ready for use in experimental protocols. It should be noted that the two faces of the coupon (facing inward towards the baffled stir bar versus outwards towards the glass) experience different amounts of shear stress which is a critical control in biofilm growth. The inward facing side of the coupon was always of interest for these experiments.

Biofilm Sampling Protocol. Growth control coupons sampled at the end of the growth protocol were aseptically removed from the rod, gently dipped in 10 mL of sterile dilution water (42.2 mg KH2PO4/L, 406.5 mg/L MgCl2·6H2O/L in reagent-grade water) to remove planktonic cells, and placed on a sterile Plexiglas board for sampling with the inward facing side up. The top of the coupon was scraped for 30 seconds with a sterile wooden stick held perpendicular to the surface and then rinsed by swirling in 9 mL of dilution water. This process was repeated such that the coupon was scraped three times. After scraping, the coupon was held over the dilution tube and the scraped surface was rinsed with 1 mL of dilution water to remove any remaining biofilm resulting in a final volume of 10 mL in the dilution tube. The sample was homogenized at 10,000 rpm for one minute to disaggregate biofilm clumps, serially diluted, and drop plated on tryptic soy agar (Fischer Scientific #DF0369078). After overnight incubation at 37˚C, the colony forming units (CFU) on the plates were counted and a biofilm density (mean colony forming units per cm^2) for each coupon was calculated using the surface area of the coupon. Using the above protocol a mean cell density for 13 separate experiments was 8.37 +/- 0.25 log CFU/cm^2. Coupons (in place in the rods) to be used in experimental protocols would be dipped to remove planktonic cells upon removal from the CDC Reactor just prior to transfer to the exposure setup. Following exposure, coupons would be removed from the rods and scraped as described above.

The Magnetic Field Exposure Setup

Design requirements for the magnetic field exposure setup included being able to achieve a constant elevated temperature (above room temperature), to develop and

maintain a controlled, uniform magnetic field, and to have multiple experimental conditions tested simultaneously along with a control. Inside a typical laboratory incubator, the AC magnetic fields due to motors and heaters switching on and off render it virtually useless for controlled magnetic field experiments. Therefore, a totally non-magnetic enclosure for the exposure setup was designed in which the temperature could be set and maintained. Since a uniform applied magnetic field was needed throughout a large volume, either a solenoid or a pair of Helmholtz coils had to be designed to apply the magnetic fields. A solenoid was selected since it could be designed to accommodate multiple laboratory scale biofilms and conditions during initial experimentation as well as being able to accommodate a full scale prosthetic knee joint in future work. Finally, a treatment unit was designed that would allow the magnetic field exposure of biofilms while the biofilms were immersed in support medium. The top unit described below was designed to be used in conjunction with the CDC Biofilm Reactor such that biofilms would first be grown in the CDC Reactor and then aseptically moved to the individual compartments of the top unit during exposure.

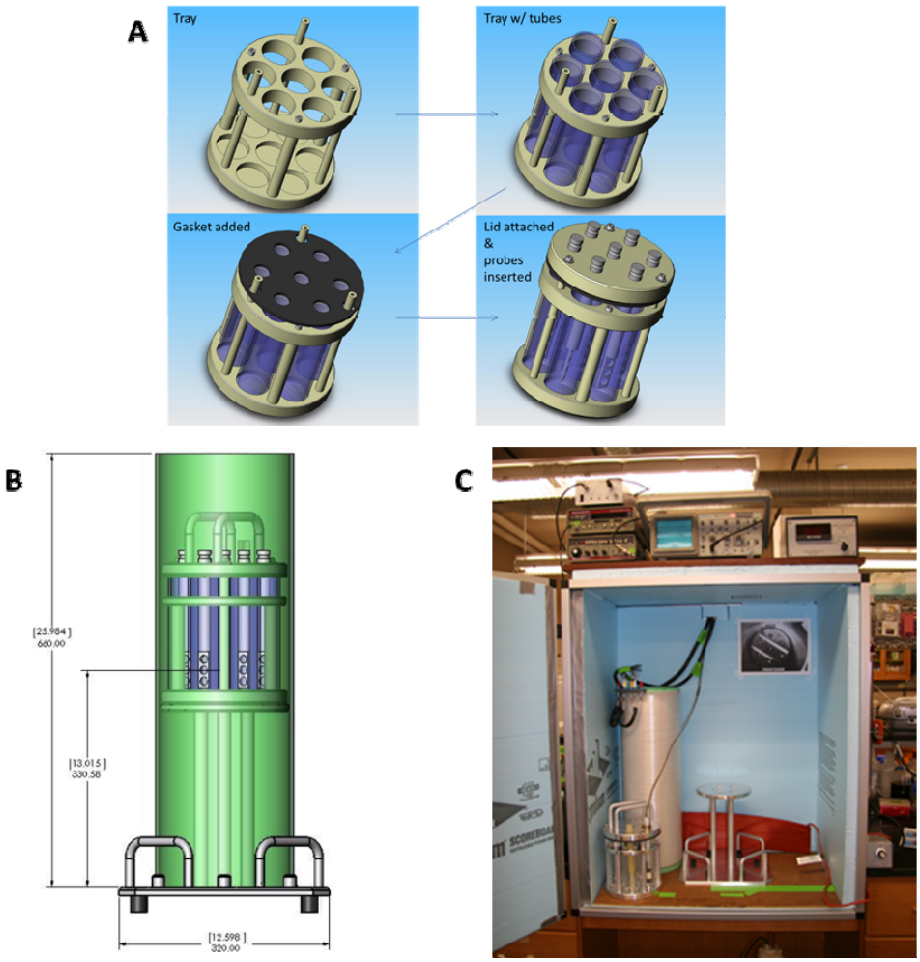

Figure C.2 The magnetic field exposure setup to be used during treatment. (A) Four views of the top unit showing the tray, the tray with the seven glass tubes inserted, the rubber gasket in place and the assembled top unit including the lid with seven CDC polypropylene coupon holders projecting through the lid and into the glass tubes. (B) A view of the top unit sitting on the pedestal inside of the solenoid coil form and the coordinate system. The handles used to lift the top unit in and out of the solenoid are shown in place on the top unit and coupons upon which the biofilms are grown are shown near the center of the solenoid coil form in place in the top unit. (C) The non-magnetic bench top environmental chamber is seen with the door open to show the exposure setup top unit, the pedestal, the solenoid and the heating pad. All electrical connections pass through the small port at the top, center of the chamber. The magnetometer probe is shown in place in the top unit on the r = 60 mm ring of coupon holders but it can be placed in any one of the seven positions. The N4L Model LPA01 power amplifier, the Circuitmate UC 10 Universal Frequency Counter, the Circuitmate FG2 Function Generator (AC/DC power supply), the Tektronix 2201 Digital Storage Oscilloscope, and the Schoenstedt Instrument Company Model 2220-S5 magnetometer are shown (top to bottom, left to right) in place on top of the chamber.

Non-magnetic Environmental Box: An economical, easy to build non-magnetic environmental box is shown in Figure 2c. The frame of the box is made from 25.4 mm square "snap together" aluminum tubes (manufactured by 80/20 Inc, Columbia City, IN) with the top, sides, bottom and door made with 50.8 mm thick, closed cell Styrofoam insulation. The dimensions of the environmental box were chosen to fit a typical chemistry laboratory bench top and to accommodate the solenoid, top unit, pedestal and base plate (see Figure 2a and Figure 2b) in addition to control biofilms not exposed to the magnetic field. A small heating pad (seen at the back of the chamber and behind the solenoid in Figure 2c) is used to hold the temperature in the chamber at 37˚C +/- 1˚. The 60 Hz magnetic field generated by the heating pad was measured using a Schonstedt Instrument Company DM 2220-S5 digital magnetometer and a Tektronix 2201 oscilloscope and established as being less than 6 milligauss peak to peak at the level of the biofilm coated coupons.

Solenoid: The design parameters for the solenoid included making the length at least three times the radius (to achieve a uniform magnetic field volume inside the solenoid), having an inside diameter large enough to allow the placement of a full size prosthetic knee inside the coil, and having a coil form that was something "off the shelf". In order to minimize skin effect in the coil wires if frequencies above several hundred Hz were to be used, the wire chosen for the solenoid coils was Litzendraht (Litz) wire from New England Wire (Type 2, # 12, 5x5x42/42). The Litz wire is manufactured using number 42 AWG insulated wire with five bundles of five wires each (all bundles are individually twisted) with 42 of these bundles twisted to form the final 1,050 strand wire

(with an outside diameter, including insulation, of 3 mm). The coil form needed to have a wall thickness sufficient to allow the machining of spiral grooves to properly space three separate, non-overlapping coils of 47 turns wrapped on the form. The use of three windings was incorporated in the design of the solenoid in order to have flexibility in setting up the magnetic field and in the choice of the drive current in the coils. For instance, one coil can be used to add to or zero out the geomagnetic field, all three coils can be used in series to achieve a higher magnetic field at a given drive current, or one coil can be used to apply an AC field and two coils can be used to apply a DC field. Standard 203.2 mm (eight inch ID) PVC drain pipe with a wall thickness of approximately 9.5 mm was selected for the form as it is readily available and is easy to machine. The 660 mm long solenoid coil form with the exposure setup inside is shown in Figure 2b and can be seen in Figure 2c with the coil wires in place and connected to the terminal strip bonded to the top of the coil form.

Top Unit: During treatment, the biofilms-coated coupons are aseptically transferred from the CDC biofilm reactor via the holders to the individual glass cylinders of the top unit for treatment (Figure 2a). The top unit is then placed in the solenoid, sitting on the pedestal as seen in Figure 2b. Six of the coupon holders are arranged on ring ($r = 60$ mm, $\varphi = n*60^{\circ}$; where $n = 0 \ldots 5$) with one holder centered along the z axis (the coordinate system is shown in Figure 2b). Each coupon holder holds three coupons and is contained in an individual glass cylinder (see Figure 2a), 181 mm in height with an outer diameter of 50.8 mm (Technical Glass Products, Inc., part number RPMUSB50-3.5-7.125), which allows samples to be exposed in triplicate to each solution during a

magnetic field exposure. The r = 60 mm radius was selected for the ring of coupon holders since this is approximately the radius needed to achieve the closest packing of the six glass cylinders and to have them within the uniform magnetic field volume of the solenoid. A casing for the Schonstedt magnetometer probe was designed to be the same length and diameter as one of the coupon holders so the casing and probe could be inserted in place of a coupon holder and magnetic field data obtained at each position. The rubber gasket seen in Figure 2a on the underside of the top plate prevents any cross contamination between the glass treatment cylinders during the experiment and the entire top unit can be autoclaved. It should be noted that the coupon holders shown will allow the magnetic field to be applied parallel to the surface containing the biofilm. A second set of coupon holders are planned that rotate the surface of the coupons by 90o making the biofilm surface perpendicular to the magnetic field (i.e., the z axis).

The pedestal and base plate were designed to support the top unit and vertically locate the center coupon of the three biofilm coupons in the z = 0 plane of the solenoid. The height of the environmental box was chosen to allow the top unit to be moved into and out of the solenoid when preparing an experimental exposure.

Measurements

Figure 3 illustrates the measured and calculated magnetic fields, both inside and outside the solenoid. The calculated values for the magnetic field along the z axis were done using the Biot-Savart law [Hayt, 1989] and for the magnetic fields off the z axis, special expressions for the radial and z components of the magnetic field were used [Stratton, 1941].

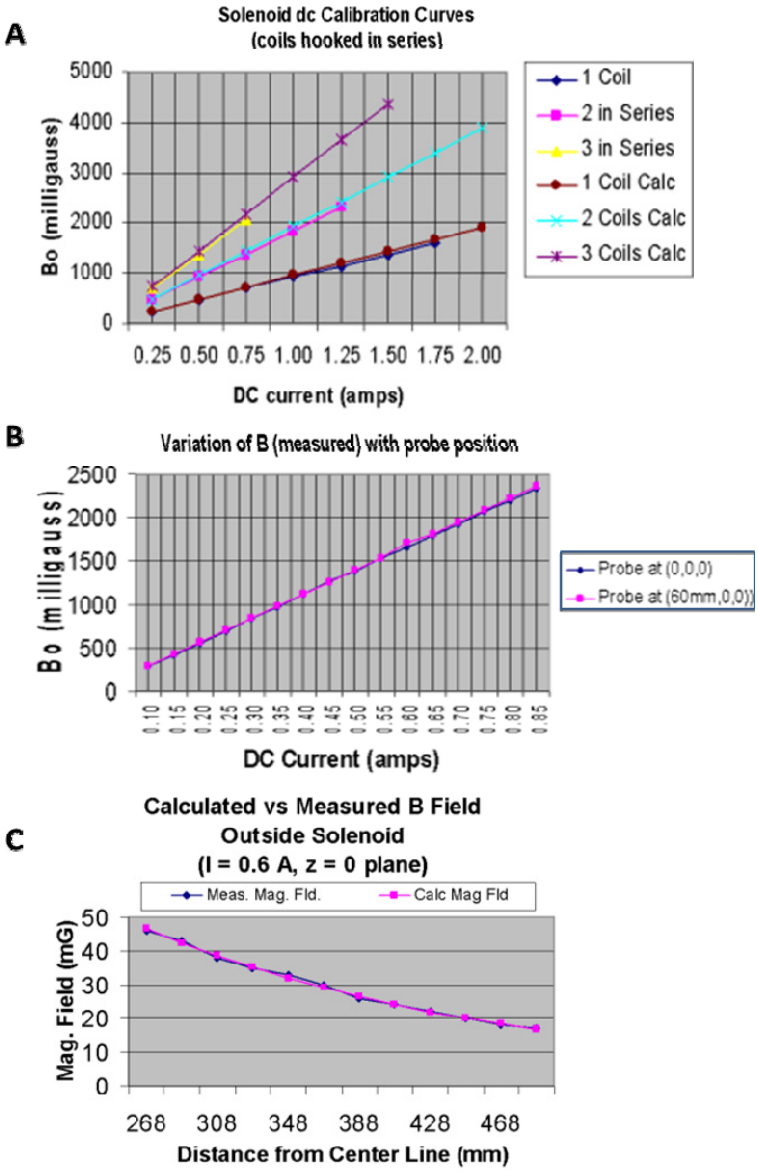

Figure C.3 Chart (A) shows both calculated and measured values at (0,0,0) for a single coil, two coils in series (fields adding) and three coils in series (fields adding) versus the DC drive current. All magnetic field measurements were done with a single Schonstedt Instrument DM 2220-S5 digital magnetometer. Chart (B) shows the measured magnetic fields versus DC current with three coils in series at the origin (0,0,0) and at one of the positions on the outer ring (60 mm,0,0). Differences are negligible out to at least 60% of the radius of the solenoid. Chart (C) compares calculated and measured values for the magnetic field outside the solenoid and in the z = 0 plane for (r) between 268 mm (closest to the solenoid) and 488 mm (near the right side wall of the environmental chamber) again using a 0.6 amp DC drive current.

The data outside the solenoid were developed in order to ascertain how non-exposed control biofilms could be positioned in the environmental box in order to receive a minimum amount of the magnetic field generated by the solenoid. Comparing data at a DC drive current of 0.6 amp, the magnetic field inside the solenoid is around 1700 mG at (0,0,0) while outside the coil at (468 mm,0,0) the field is approximately 17 mG. The scale (radius values) in Figure 3c resulted from the method used to measure the magnetic field outside the solenoid. The pedestal and top unit were used outside of the solenoid to position the magnetometer probe in the same vertical plane as the internal probe placement (z = 0 plane) to measure the decrease of the external magnetic field generated by the solenoid with distance from the solenoid. Due to the width of the base of the pedestal, the closest position of the probe to the solenoid was 268 mm and each data point (starting from 268 mm) is, thereafter, a change in the r value of 20 mm.One of the design goals for the solenoid was to be able to apply both low level and high level AC magnetic fields from frequencies below 100 Hz to frequencies as high as 1 kHz. As noted above, the wire selected for the solenoid was type 2 Litz wire which has an operating frequency range up to 350 kHz and a current capacity of about 5 amps. Laboratory measurements with the three coils in series show an AC magnetic field (sine wave) of 3.2 gauss (peak to peak) can be achieved with a frequency of 100 Hz and 0.46 gauss (peak to peak) can be achieved at 1kHz. These data were obtained using a Circuitmate FG2 function generator in series with a N4L model LPA01 laboratory power amplifier to drive the coils.

The data in Figure 3 show that the magnetic fields inside the solenoid at (0,0,0) are in close agreement with the fields at (60 mm,0,0) as expected (see Fig. 3b) and the field is essentially constant across this radius. Measurements and calculations (not shown) also indicate the magnetic field variation along the z (vertical) axis of the solenoid was less than 1% over the dimension of the biofilm coupons and less than 5% for z = +/- 150 mm. Therefore, the constant, cylindrical magnetic field volume is at least 60 mm in radius with a height of at least z = +/- 150 mm.

Conclusions

This paper was focused on two points. First, a well characterized, repeatable and "exportable" method of growing bacterial biofilms on material surfaces is extremely important when doing any biofilm work. Biofilms can be grown on various surfaces by a number of means but growing "laboratory grade" biofilms can prove to be a challenge. The growth protocol described was optimized for *Staphylococcus epidermidis* ATCC#35984 grown in the CDC Reactor and the resulting biofilms show a high level of repeatability. Secondly, an exposure setup was described that was designed to study how magnetic fields might be used alone or in conjunction with antibiotics to control bacterial biofilms on materials typically found in prosthetic implants. Since bacterial biofilm experiments often require a controlled and elevated temperature (in this case body temperature) and since laboratory incubators incorporate so many uncontrollable magnetic fields, one design of a non-magnetic environmental chamber is described. The exposure setup presented was specifically designed to be compatible with the CDC Biofilm Reactor and to allow the testing of up to seven different solutions with varying

levels of antibiotics, nutrient content, trace metals, etc in each experimental run. This system will aid in the study of magnetic fields applied to biofilms which are found on orthopedic implants. The system is capable of applying magnetic fields, both DC and AC fields (up to about 1 kHz), from tens to several thousand milligauss. Additionally, the system can be modified for different bacterial species and as the coupons in the CDC reactor can be made of a variety of materials, the system is sufficiently flexible to allow it to be useful for the study of other applications.

Acknowledgements

The artwork and manufacturing design drawings for the solenoid and experimental exposure setup were done by Mr. Joe Eldring, Manager, Technical Services, Montana State University College of Engineering.

References (Bioelectromagnetics Article)

Aaron R, Ciombor D, Simon B. 2004. Treatment of nonunions with electric and electromagnetic fields. Clin Orthop Relat Res(419):21-9.

ASTM Standard E 5895-07. "Quantification of + Biofilm Grown with High Shear and Continuous Flow using CDC Biofilm Reactor." ASTM International. West Conshohocken, PA. 2007. DOI: 10.1520/E2562-07. www.astm.org.

Blank M. 1993. Electricity and magnetism in biology and medicine : review and research papers presented at the First World Congress for Electricity and Magnetism in Biology and Medicine, Orlando, Florida, 1992. San Francisco, CA, USA: San Francisco Press. xv, 936 p. p.

Blenkinsopp S, Khoury A, Costerton J. 1992. Electrical enhancement of biocide efficacy against *Pseudomonas aeruginosa* biofilms. Appl Environ Microbiol 58(11):3770-3.

Buckingham-Meyer K, Goeres D, Hamilton M. 2007. Comparative evaluation of biofilm disinfectant efficacy tests. J Microbiol Methods 70(2):236-44.

Caubet R, Pedarros-Caubet F, Chu M, Freye E, de Belém Rodrigues M, Moreau J, Ellison W. 2004. A radio frequency electric current enhances antibiotic efficacy against bacterial biofilms. Antimicrob Agents Chemother 48(12):4662-4.

Costerton JW, Stewart PS. "Biofilms and Device-Related Infections" in: Nataro JP, Blaser MJ, Cunningham-Rundles S. 2000. *Persistent bacterial infections*. Washington, DC: ASM Press. xv, 453 pp 423-439.

Darouiche R. 2004. Treatment of infections associated with surgical implants. N Engl J Med 350(14):1422-9.

del Pozo J, Rouse M, Patel R. 2008. Bioelectric effect and bacterial biofilms. A systematic review. Int J Artif Organs 31(9):786-95.

Ehrlich G, Stoodley P, Kathju S, Zhao Y, McLeod B, Balaban N, Hu F, Sotereanos N, Costerton J, Stewart P and others. 2005. Engineering approaches for the detection and control of orthopaedic biofilm infections. Clin Orthop Relat Res(437):59-66.

Giladi M, Porat Y, Blatt A, Wasserman Y, Kirson E, Dekel E, Palti Y. 2008. Microbial growth inhibition by alternating electric fields. Antimicrob Agents Chemother 52(10):3517-22.

Goeres D, Loetterle L, Hamilton M, Murga R, Kirby D, Donlan R. 2005. Statistical

assessment of a laboratory method for growing biofilms. Microbiology 151(Pt 3):757-62.

Hayt WH. 1989. *Engineering electromagnetics*. New York: McGraw-Hill. xiii, 472 p. p.

König D, Schierholz J, Münnich U, Rütt J. 2001. Treatment of staphylococcal implant infection with rifampicin-ciprofloxacin in stable implants. Arch Orthop Trauma Surg 121(5):297-9.

Masterson E, Masri B, Duncan C. 1998. Treatment of infection at the site of total hip replacement. Instr Course Lect 47:297-306.

O'Gara J, Humphreys H. 2001. *Staphylococcus epidermidis* biofilms: importance and implications. J Med Microbiol 50(7):582-7.

Pavoni G, Giannella M, Falcone M, Scorzolini L, Liberatore M, Carlesimo B, Serra P, Venditti M. 2004. Conservative medical therapy of prosthetic joint infections: retrospective analysis of an 8-year experience. Clin Microbiol Infect 10(9):831-7.

Pilla L, Valenti R, Marrari A, Patuzzo R, Santinami M, Parmiani G, Rivoltini L. 2006. Vaccination: role in metastatic melanoma. Expert Rev Anticancer Ther 6(8):1305-18.

Saginur R, Stdenis M, Ferris W, Aaron S, Chan F, Lee C, Ramotar K. 2006. Multiple combination bactericidal testing of staphylococcal biofilms from implant-associated infections. Antimicrob Agents Chemother 50(1):55-61.

Shirtliff M, Bargmeyer A, Camper A. 2005. Assessment of the ability of the bioelectric effect to eliminate mixed-species biofilms. Appl Environ Microbiol 71(10):6379-82.

Stewart P, Wattanakaroon W, Goodrum L, Fortun S, McLeod B. 1999. Electrolytic generation of oxygen partially explains electrical enhancement of tobramycin efficacy against *Pseudomonas aeruginosa* biofilm. Antimicrob Agents Chemother 43(2):292-6.

Stratton JA. 1941. *Electromagnetic theory*. New York, London,: McGraw-Hill book company, inc. xv, 615 p. p.

Wellman N, Fortun S, McLeod B. 1996. Bacterial biofilms and the bioelectric effect. Antimicrob Agents Chemother 40(9):2012-4.

Zimmerli W, Widmer A, Blatter M, Frei R, Ochsner P. 1998. Role of rifampin for treatment of orthopedic implant-related staphylococcal infections: a randomized controlled trial. Foreign-Body Infection (FBI) Study Group. JAMA 279(19):1537-41.

APPENDIX D

SUPPLEMENTAL DATA FOR BIOFILM MICROARRAY EXPERIMENTS IN RESPONSE TO ELF-MF

Table D.1 DAVID Cluster output (enrichment score ≥1) for FDR≤15% gene lists for *S. epidermidis* biofilm grown in a K+ tuned field (*h'*=1.8). Columns indicate the number of genes in the input list with the annotation (count , Ct.), the percentage of genes in the input list with the annotation (%), the number of genes in the input list with an annotation in the annotation category (list total, List Tot), the number of all genes on the array that have the specific annotation (population total, Pop Hits), and the number of genes within the background (all genes on the array) with an annotation in the annotation category (population total, Pop Tot.). The p-values are EASE scores, a modified fisher's exact p-value used by the DAVID database (p-val). The fold-enrichment (FE) and false-discovery rate (FDR) calculated within the DAVID database are also indicated.

Annotation Up Cluster 1 **Enrichment Score: 3.20**

Category	Term	Ct.	%	p-val	List Tot.	Pop Hits	Pop Tot.	FE	FDR
INTERPRO	IPR003346:Transposase, IS116/IS110/IS902	11	4.0	0.000	232	25	3694	7.0	0.0
GOTERM_MF_FAT	GO:0004803~transposase activity	12	4.4	0.000	138	41	2340	5.0	0.0
GOTERM_BP_FAT	GO:0006313~transposition, DNA-mediated	12	4.4	0.000	124	45	2117	4.6	0.0
GOTERM_BP_FAT	GO:0032196~transposition	12	4.4	0.000	124	51	2117	4.0	0.1
GOTERM_BP_FAT	GO:0006310~DNA recombination	14	5.1	0.013	124	114	2117	2.1	16.3
GOTERM_BP_FAT	GO:0006259~DNA metabolic process	19	6.9	0.238	124	259	2117	1.3	97.6
GOTERM_MF_FAT	GO:0003677~DNA binding	29	10.5	0.270	138	425	2340	1.2	98.4

Annotation Up Cluster 2 **Enrichment Score: 2.04**

Category	Term	Ct.	%	p-val	List Tot.	Pop Hits	Pop Tot.	FE	FDR
GOTERM_BP_FAT	GO:0006811~ion transport	21	7.6	0.000	124	155	2117	2.3	0.6
SP_PIR_KEYWORDS	ion transport	11	4.0	0.002	275	62	4790	3.1	2.7
GOTERM_BP_FAT	GO:0006812~cation transport	16	5.8	0.003	124	118	2117	2.3	3.6
GOTERM_BP_FAT	GO:0030001~metal ion transport	12	4.4	0.005	124	78	2117	2.6	6.0
GOTERM_MF_FAT	GO:0015662~ATPase activity, coupled to transmembrane movement of ions, phosphorylative mechanism	5	1.8	0.005	138	13	2340	6.5	6.7
GOTERM_BP_FAT	GO:0015672~monovalent inorganic cation transport	9	3.3	0.017	124	58	2117	2.6	21.0
GOTERM_MF_FAT	GO:0042625~ATPase activity, coupled to transmembrane movement of ions	6	2.2	0.021	138	28	2340	3.6	24.3

GOTERM_MF_FAT	GO:0022890~inorganic cation transmembrane transporter activity	9	3.3	0.033	138	65	2340	2.3	35.9
GOTERM_MF_FAT	GO:0015077~monovalent inorganic cation transmembrane transporter activity	6	2.2	0.062	138	37	2340	2.7	56.4
GOTERM_BP_FAT	GO:0006814~sodium ion transport	5	1.8	0.084	124	29	2117	2.9	69.9

Annotation Up Cluster 3 **Enrichment Score: 1.77**

Category	Term	Ct.	%	p-val	List Tot.	Pop Hits	Pop Tot.	FE	FDR
SP_PIR_KEYWORDS	transport	27	9.8	0.001	275	233	4790	2.0	0.8
SP_PIR_KEYWORDS	ion transport	11	4.0	0.002	275	62	4790	3.1	2.7
SP_PIR_KEYWORDS	transmembrane	33	12.0	0.006	275	356	4790	1.6	6.7
SP_PIR_KEYWORDS	cell membrane	30	10.9	0.022	275	346	4790	1.5	22.5
SP_PIR_KEYWORDS	membrane	31	11.3	0.030	275	369	4790	1.5	29.2
GOTERM_CC_FAT	GO:0016021~integral to membrane	41	14.9	0.030	55	436	710	1.2	22.6
GOTERM_CC_FAT	GO:0031224~intrinsic to membrane	42	15.3	0.042	55	457	710	1.2	30.0
UP_SEQ_FEATURE	transmembrane region	14	5.1	0.070	62	183	1314	1.6	59.0
GOTERM_CC_FAT	GO:0005886~plasma membrane	30	10.9	0.208	55	337	710	1.1	85.5

Annotation Up Cluster 4 **Enrichment Score: 1.42**

Category	Term	Ct.	%	p-val	List Tot.	Pop Hits	Pop Tot.	FE	FDR
GOTERM_MF_FAT	GO:0015297~antiporter activity	10	3.6	0.003	138	54	2340	3.1	4.4
GOTERM_MF_FAT	GO:0015298~solute:cation antiporter activity	5	1.8	0.086	138	29	2340	2.9	69.0
GOTERM_MF_FAT	GO:0015299~solute:hydrogen antiporter activity	5	1.8	0.086	138	29	2340	2.9	69.0
GOTERM_MF_FAT	GO:0015300~solute:solute antiporter activity	5	1.8	0.086	138	29	2340	2.9	69.0

Annotation Up Cluster 5 **Enrichment Score: 1.08**

Category	Term	Ct.	%	p-val	List Tot.	Pop Hits	Pop Tot.	FE	FDR
GOTERM_BP_FAT	GO:0044271~nitrogen compound biosynthetic process	32	11.6	0.004	124	336	2117	1.6	5.3
GOTERM_BP_FAT	GO:0008652~cellular amino acid biosynthetic process	14	5.1	0.094	124	151	2117	1.6	74.2
GOTERM_BP_FAT	GO:0009309~amine biosynthetic process	14	5.1	0.110	124	155	2117	1.5	79.8

GOTERM_BP_FAT	GO:0046394~carboxylic acid biosynthetic process	15	5.5	0.196	124	188	2117	1.4	95.1
SP_PIR_KEYWORDS	amino-acid biosynthesis	9	3.3	0.204	275	99	4790	1.6	92.4
GOTERM_BP_FAT	GO:0016053~organic acid biosynthetic process	16	5.8	0.215	124	207	2117	1.3	96.4

Annotation Down Cluster 1 **Enrichment Score: 2.05**

Category	Term	Ct.	%	p-val	List Tot.	Pop Hits	Pop Tot.	FE	FDR
SP_PIR_KEYWORDS	cell division	13	4.0	0.000	326	53	4790	3.6	0.2
GOTERM_BP_FAT	GO:0051301~cell division	12	3.7	0.001	155	53	2117	3.1	1.5
SP_PIR_KEYWORDS	cell cycle	10	3.1	0.003	326	46	4790	3.2	3.7
GOTERM_BP_FAT	GO:0007049~cell cycle	11	3.4	0.005	155	55	2117	2.7	7.0
SP_PIR_KEYWORDS	septation	4	1.2	0.053	326	13	4790	4.5	47.5
GOTERM_BP_FAT	GO:0032506~cytokinetic process	4	1.2	0.063	155	13	2117	4.2	59.3
GOTERM_BP_FAT	GO:0000910~cytokinesis	4	1.2	0.063	155	13	2117	4.2	59.3
GOTERM_BP_FAT	GO:0000917~barrier septum formation	4	1.2	0.063	155	13	2117	4.2	59.3

Annotation Down Cluster 2 **Enrichment Score: 1.67**

Category	Term	Ct.	%	p-val	List Tot.	Pop Hits	Pop Tot.	FE	FDR
GOTERM_CC_FAT	GO:0005840~ribosome	11	3.4	0.003	43	65	710	2.8	2.4
GOTERM_CC_FAT	GO:0030529~ribonucleoprotein complex	11	3.4	0.004	43	67	710	2.7	3.1
SP_PIR_KEYWORDS	rna-binding	13	4.0	0.004	326	75	4790	2.5	4.8
GOTERM_BP_FAT	GO:0006412~translation	17	5.2	0.006	155	113	2117	2.1	8.4
GOTERM_CC_FAT	GO:0043232~intracellular non-membrane-bounded organelle	12	3.7	0.009	43	88	710	2.3	7.7
GOTERM_CC_FAT	GO:0043228~non-membrane-bounded organelle	12	3.7	0.009	43	88	710	2.3	7.7
KEGG_PATHWAY	ser03010:Ribosome	9	2.8	0.019	86	54	1318	2.6	18.8
SP_PIR_KEYWORDS	ribosomal protein	10	3.1	0.027	326	64	4790	2.3	27.9
GOTERM_MF_FAT	GO:0005198~structural molecule activity	10	3.1	0.030	171	61	2340	2.2	32.9
SP_PIR_KEYWORDS	ribonucleoprotein	9	2.8	0.040	326	58	4790	2.3	38.4
GOTERM_MF_FAT	GO:0003735~structural constituent of ribosome	9	2.8	0.060	171	59	2340	2.1	56.2
SP_PIR_KEYWORDS	rrna-binding	6	1.8	0.093	326	36	4790	2.4	68.4
GOTERM_MF_FAT	GO:0019843~rRNA binding	6	1.8	0.116	171	36	2340	2.3	80.5
KEGG_PATHWAY	sep03010:Ribosome	6	1.8	0.489	86	71	1318	1.3	99.9

Annotation Down Cluster 3 **Enrichment Score: 1.41**

Category	Term	Ct.	%	p-val	List Tot.	Pop Hits	Pop Tot.	FE	FDR
KEGG_PATHWAY	ser00564:Glycerophospholipid metabolism	5	1.5	0.007	86	13	1318	5.9	7.6
GOTERM_BP_FAT	GO:0006071~glycerol metabolic process	5	1.5	0.061	155	21	2117	3.3	58.1
GOTERM_BP_FAT	GO:0019400~alditol metabolic process	5	1.5	0.061	155	21	2117	3.3	58.1
GOTERM_BP_FAT	GO:0019751~polyol metabolic process	5	1.5	0.081	155	23	2117	3.0	68.7

Annotation Down Cluster 4 **Enrichment Score: 1.25**

Category	Term	Ct.	%	p-val	List Tot.	Pop Hits	Pop Tot.	FE	FDR
GOTERM_BP_FAT	GO:0006457~protein folding	5	1.5	0.030	155	17	2117	4.0	34.7
SP_PIR_KEYWORDS	Rotamase	3	0.9	0.040	326	5	4790	8.8	38.2
GOTERM_MF_FAT	GO:0016859~cis-trans isomerase activity	3	0.9	0.045	171	5	2340	8.2	46.0
GOTERM_MF_FAT	GO:0003755~peptidyl-prolyl cis-trans isomerase activity	3	0.9	0.045	171	5	2340	8.2	46.0
SP_PIR_KEYWORDS	Isomerase	8	2.5	0.234	326	74	4790	1.6	95.7

Annotation Down Cluster 5 **Enrichment Score: 1.17**

Category	Term	Ct.	%	p-val	List Tot.	Pop Hits	Pop Tot.	FE	FDR
GOTERM_BP_FAT	GO:0008360~regulation of cell shape	9	2.8	0.012	155	44	2117	2.8	15.6
GOTERM_BP_FAT	GO:0022604~regulation of cell morphogenesis	9	2.8	0.012	155	44	2117	2.8	15.6
SP_PIR_KEYWORDS	cell shape	8	2.5	0.017	326	40	4790	2.9	17.8
GOTERM_BP_FAT	GO:0010382~cellular cell wall macromolecule metabolic process	10	3.1	0.027	155	60	2117	2.3	31.3
KEGG_PATHWAY	ser00550:Peptidoglycan biosynthesis	5	1.5	0.030	86	19	1318	4.0	27.4
GOTERM_BP_FAT	GO:0044038~cell wall macromolecule biosynthetic process	9	2.8	0.046	155	56	2117	2.2	48.2
GOTERM_BP_FAT	GO:0070589~cellular component macromolecule biosynthetic process	9	2.8	0.046	155	56	2117	2.2	48.2
GOTERM_BP_FAT	GO:0044036~cell wall macromolecule metabolic process	10	3.1	0.063	155	70	2117	2.0	59.6
GOTERM_BP_FAT	GO:0000270~peptidoglycan metabolic process	8	2.5	0.079	155	52	2117	2.1	67.9

GOTERM_BP_FAT	GO:0006022~aminoglycan metabolic process	8	2.5	0.079	155	52	2117	2.1	67.9
GOTERM_BP_FAT	GO:0030203~glycosaminoglycan metabolic process	8	2.5	0.079	155	52	2117	2.1	67.9
GOTERM_BP_FAT	GO:0005976~polysaccharide metabolic process	11	3.4	0.080	155	84	2117	1.8	68.2
SP_PIR_KEYWORDS	cell wall biogenesis/degradation	7	2.1	0.081	326	45	4790	2.3	63.1
SP_PIR_KEYWORDS	peptidoglycan synthesis	6	1.8	0.085	326	35	4790	2.5	64.8
GOTERM_BP_FAT	GO:0042546~cell wall biogenesis	9	2.8	0.102	155	66	2117	1.9	77.4
GOTERM_BP_FAT	GO:0009273~peptidoglycan-based cell wall biogenesis	9	2.8	0.102	155	66	2117	1.9	77.4
GOTERM_BP_FAT	GO:0000271~polysaccharide biosynthetic process	9	2.8	0.124	155	69	2117	1.8	83.9
GOTERM_BP_FAT	GO:0006023~aminoglycan biosynthetic process	6	1.8	0.127	155	37	2117	2.2	84.6
GOTERM_BP_FAT	GO:0006024~glycosaminoglycan biosynthetic process	6	1.8	0.127	155	37	2117	2.2	84.6
GOTERM_BP_FAT	GO:0009252~peptidoglycan biosynthetic process	6	1.8	0.127	155	37	2117	2.2	84.6
GOTERM_BP_FAT	GO:0007047~cell wall organization	7	2.1	0.141	155	49	2117	2.0	87.8
GOTERM_BP_FAT	GO:0045229~external encapsulating structure organization	7	2.1	0.184	155	53	2117	1.8	94.0
GOTERM_BP_FAT	GO:0016051~carbohydrate biosynthetic process	9	2.8	0.285	155	86	2117	1.4	99.0

Annotation Preturbed Cluster 1 **Enrichment Score: 1.40**

Category	Term	Ct.	%	p-val	List Tot.	Pop Hits	Pop Tot.	FE	FDR
GOTERM_BP_FAT	GO:0006457~protein folding	8	1.3	0.004	279	17	2117	3.6	5.3
SP_PIR_KEYWORDS	Chaperone	8	1.3	0.030	601	25	4790	2.6	30.7
GOTERM_MF_FAT	GO:0051082~unfolded protein binding	4	0.7	0.053	309	7	2340	4.3	53.4
SP_PIR_KEYWORDS	stress response	4	0.7	0.432	601	19	4790	1.7	99.9

Annotation Preturbed Cluster 2 **Enrichment Score: 1.34**

Category	Term	Ct.	%	p-val	List Tot.	Pop Hits	Pop Tot.	FE	FDR
INTERPRO	IPR003346:Transposase, IS116/IS110/IS902	11	1.8	0.001	509	25	3694	3.2	1.6
GOTERM_MF_FAT	GO:0004803~transposase activity	12	2.0	0.014	309	41	2340	2.2	17.9
GOTERM_BP_FAT	GO:0006313~transposition, DNA-mediated	12	2.0	0.027	279	45	2117	2.0	32.7
GOTERM_BP_FAT	GO:0032196~transposition	12	2.0	0.062	279	51	2117	1.8	60.4

GOTERM_BP_FAT	GO:0006310~DNA recombination	17	2.8	0.428	279	114	2117	1.1	100.0
GOTERM_BP_FAT	GO:0006259~DNA metabolic process	28	4.7	0.933	279	259	2117	0.8	100.0

Annotation Preturbed Cluster 3 **Enrichment Score: 1.28**

Category	Term	Ct.	%	p-val	List Tot.	Pop Hits	Pop Tot.	FE	FDR
GOTERM_BP_FAT	GO:0006457~protein folding	8	1.3	0.004	279	17	2117	3.6	5.3
SP_PIR_KEYWORDS	Rotamase	3	0.5	0.121	601	5	4790	4.8	79.2
GOTERM_MF_FAT	GO:0016859~cis-trans isomerase activity	3	0.5	0.132	309	5	2340	4.5	86.4
GOTERM_MF_FAT	GO:0003755~peptidyl-prolyl cis-trans isomerase activity	3	0.5	0.132	309	5	2340	4.5	86.4

Annotation Preturbed Cluster 4 **Enrichment Score: 1.22**

Category	Term	Ct.	%	p-val	List Tot.	Pop Hits	Pop Tot.	FE	FDR
SP_PIR_KEYWORDS	rna-binding	18	3.0	0.010	601	75	4790	1.9	11.3
GOTERM_MF_FAT	GO:0003723~RNA binding	26	4.3	0.016	309	124	2340	1.6	20.7
SP_PIR_KEYWORDS	rrna-binding	10	1.7	0.030	601	36	4790	2.2	30.7
KEGG_PATHWAY	ser03010:Ribosome	13	2.2	0.034	169	54	1318	1.9	31.9
GOTERM_MF_FAT	GO:0019843~rRNA binding	10	1.7	0.039	309	36	2340	2.1	42.8
GOTERM_CC_FAT	GO:0005840~ribosome	15	2.5	0.045	98	65	710	1.7	34.8
GOTERM_MF_FAT	GO:0005198~structural molecule activity	14	2.3	0.050	309	61	2340	1.7	51.1
SP_PIR_KEYWORDS	ribosomal protein	14	2.3	0.051	601	64	4790	1.7	47.0
SP_PIR_KEYWORDS	ribonucleoprotein	13	2.2	0.052	601	58	4790	1.8	48.1
GOTERM_CC_FAT	GO:0030529~ribonucleoprotein complex	15	2.5	0.057	98	67	710	1.6	41.9
GOTERM_MF_FAT	GO:0003735~structural constituent of ribosome	13	2.2	0.078	309	59	2340	1.7	68.2
GOTERM_BP_FAT	GO:0006412~translation	21	3.5	0.094	279	113	2117	1.4	76.2
GOTERM_CC_FAT	GO:0043232~intracellular non-membrane-bounded organelle	16	2.7	0.203	98	88	710	1.3	87.6
GOTERM_CC_FAT	GO:0043228~non-membrane-bounded organelle	16	2.7	0.203	98	88	710	1.3	87.6
KEGG_PATHWAY	sep03010:Ribosome	9	1.5	0.705	169	71	1318	1.0	100.0

Table D.2 Differentially expressed genes of *S. epidermidis* biofilm grown in a K^+ tuned ELF-MF (*h'*=1.8) not listed in Chapter 4. FDR corrections are for a 5% FDR (****), 10% FDR (***), 15% FDR (**), and 20% FDR (*).

Table D.2 (continued)

Locus	Gene Name	Gene Description	FC	% FDR
SEA0001		replication-associated protein	-1.7	**
SEA0008		IS431mec-like transposase	-1.3	*
SEA0009		transcriptional regulator, putative	-1.8	***
SEA0013		hypothetical protein	-2.8	*
SEA0024		sulfate permease family protein	1.5	*
SEA0026		hypothetical protein	1.5	*
SEA0029		rlx protein, putative	1.6	***
SEA0030		mobilization protein	1.7	***
SEA0033	*repA*	replication-associated protein RepA	1.6	*
SERP0003	*trmE*	tRNA modification GTPase	-1.2	*
SERP0008		hypothetical protein	-2.6	*
SERP0018		lipase, putative	1.4	*
SERP0022		hypothetical protein	-1.4	***
SERP0023		hypothetical protein	1.6	**
SERP0026		sdrF protein, truncation	1.6	*
SERP0028		hypothetical protein	1.3	*
SERP0029		transcriptional regulator, Cro/CI family	-1.5	*
SERP0042		hypothetical protein	2.0	***
SERP0049		hypothetical protein	-2.0	**
SERP0054		hypothetical protein	1.3	*
SERP0078	*pfoR*	perfringolysin O regulator protein	1.5	**
SERP0079		hypothetical protein	-2.5	**
SERP0080		cobalamin synthesis protein, putative	1.6	**
SERP0087		hypothetical protein	-2.1	**
SERP0091		hypothetical protein	-1.6	***
SERP0093		hypothetical protein	-1.6	***
SERP0094		cysteine synthase/cystathionine beta-synthase family protein	2.1	*
SERP0101		glycosyl transferase, group 1 family protein	1.2	*
SERP0103		MutT/nudix family protein	-1.5	***
SERP0105		hypothetical protein	1.2	*
SERP0106		hypothetical protein	1.2	**
SERP0115		hypothetical protein	-1.3	**
SERP0120	*tmk*	thymidylate kinase	1.8	*
SERP0121		hypothetical protein	-1.2	*
SERP0122		DNA polymerase III, delta prime subunit, putative	-1.5	***
SERP0123		hypothetical protein	-1.5	***
SERP0127		methyltransferase, tetrapyrrole family	1.5	***
SERP0129		deoxyribonuclease, TatD family	-1.4	***

Table D.2 (continued)

Locus	Gene Name	Gene Description	FC	% FDR
SERP0132		hypothetical protein	-1.6	***
SERP0133	*ispE*	4-diphosphocytidyl-2-C-methyl-D-erythritol kinase	1.3	***
SERP0134	*purR*	purine operon repressor	-1.2	*
SERP0149	*hpt*	hypoxanthine phosphoribosyltransferase	-1.3	*
SERP0152	*cysK*	cysteine synthase	-1.2	**
SERP0154	*folB*	dihydroneopterin aldolase	1.4	*
SERP0159		hypothetical protein	-1.4	*
SERP0165	*clpC*	ATP-dependent Clp protease, ATP-binding subunit ClpC	-1.2	*
SERP0169	*cysE*	serine acetyltransferase	1.3	*
SERP0173		hypothetical protein	-1.3	*
SERP0174		RNA polymerase sigma factor sigW, putative	-1.3	*
SERP0177	*nusG*	transcription termination/antitermination factor NusG	-1.1	**
SERP0179	*rplA*	50S ribosomal protein L1	-1.7	*
SERP0200		hypothetical protein	1.2	***
SERP0202		deoxynucleoside kinase family protein	-1.3	***
SERP0204		cytidine/deoxycytidylate deaminase family protein	1.3	**
SERP0206		azoreductase	-1.4	***
SERP0208		glycosyl transferase, group 1 family protein	1.5	*
SERP0210		arsenical pump membrane protein	1.4	*
SERP0213		hypothetical protein	1.8	***
SERP0214		hypothetical protein	1.2	**
SERP0227		penicillin V acylase, putative	1.4	***
SERP0228	*ung*	uracil-DNA glycosylase	1.4	*
SERP0229		hypothetical protein	1.6	*
SERP0233		hypothetical protein	1.5	**
SERP0234		hypothetical protein	1.5	**
SERP0235		hypothetical protein	-1.7	***
SERP0236	*pta*	phosphate acetyltransferase	-1.1	*
SERP0237		lipoate-protein ligase A family protein	1.2	***
SERP0239	*mvaD*	mevalonate diphosphate decarboxylase	1.2	*
SERP0241		hypothetical protein	1.3	*
SERP0247		transcriptional regulator, putative	-1.2	*
SERP0249		IS431mec-like transposase	-1.4	*
SERP0252		hypothetical protein	-1.5	***
SERP0253		hypothetical protein	1.4	**
SERP0270		hypothetical protein	-1.9	*
SERP0274	*sarA*	Staphylococcal accessory regulator A	-1.6	**
SERP0275		hypothetical protein	2.0	***
SERP0276		hypothetical protein	1.4	*
SERP0293	*sirR*	iron-dependent repressor	-1.5	***
SERP0316		hypothetical protein	-1.2	**

Table D.2 (continued)

Locus	Gene Name	Gene Description	FC	% FDR
SERP0322		hypothetical protein	-1.1	*
SERP0323		hypothetical protein	-1.5	**
SERP0325		flavohemoprotein, putative	1.2	*
SERP0327		hypothetical protein	-1.4	*
SERP0328		transcriptional regulator, LysR family	1.3	*
SERP0329		sugar efflux transporter, putative	1.3	*
SERP0331		hypothetical protein	1.7	**
SERP0334		acetyltransferase, GNAT family	-1.6	**
SERP0342	*norR*	transcriptional regulator, MarR family	-1.3	***
SERP0343		hypothetical protein	-2.4	**
SERP0360	*nagA*	N-acetylglucosamine-6-phosphate deacetylase	1.5	***
SERP0361		CBS domain protein	-1.6	***
SERP0368		hypothetical protein	2.2	
SERP0370		hypothetical protein	1.7	
SERP0374	*pabA*	para-aminobenzoate synthase, glutamine amidotransferase, component II	1.8	***
SERP0379		sulfatase family protein	-1.4	
SERP0393		hypothetical protein	-3.2	
SERP0395		hypothetical protein	1.5	
SERP0396	*nrdI-1*	hypothetical protein	-1.2	**
SERP0406		hypothetical protein	1.2	*
SERP0407		lipoprotein, putative	-2.2	***
SERP0409		glycerate kinase family protein	-1.5	***
SERP0412		hypothetical protein	1.4	*
SERP0414		glycosyl transferase, group 4 family protein	1.4	*
SERP0419		ribosomal subunit interface protein	-1.7	**
SERP0422		LysM domain protein	1.3	**
SERP0423		HD domain protein, putative	-1.2	*
SERP0424		hypothetical protein	-2.0	***
SERP0437		hypothetical protein	-1.9	***
SERP0438		hypothetical protein	-1.3	**
SERP0439		hypothetical protein	-1.4	**
SERP0440		hypothetical protein	2.1	***
SERP0446	*eno*	enolase	-1.1	*
SERP0448	*secG*	protein-export membrane protein	-1.7	**
SERP0455		lipoprotein, putative	1.3	*
SERP0457		hypothetical protein	-2.0	**
SERP0459		hypothetical protein	1.5	**
SERP0462		hypothetical protein	-2.5	**
SERP0463		hypothetical protein	1.7	**
SERP0466		cold shock protein, CSD family	-2.5	**

Table D.2 (continued)

Locus	Gene Name	Gene Description	FC	% FDR
SERP0470		flagellar hook-length control protein-related protein	-2.5	***
SERP0472		hypothetical protein	-1.4	*
SERP0476		phosphoglycerate mutase family protein	-1.5	***
SERP0477		acetyltransferase, GNAT family	-2.6	**
SERP0482		nitroreductase family protein	-1.2	*
SERP0483		thioredoxin, putative	-1.4	*
SERP0484		hypothetical protein	-1.4	***
SERP0485	*gcvH*	glycine cleavage system protein H	-1.8	***
SERP0486		hypothetical protein	-1.8	**
SERP0487		Toprim domain protein	-1.4	**
SERP0488		thioredoxin, putative	-1.9	*
SERP0494		hypothetical protein	-3.1	**
SERP0497	*sufD*	FeS assembly protein SufD	1.4	*
SERP0498	*sufS*	cysteine desulfurase SufS	1.3	**
SERP0501		hypothetical protein	1.5	*
SERP0507		CBS domain protein	-1.3	*
SERP0512		hypothetical protein	-1.9	***
SERP0514		hypothetical protein	-1.4	*
SERP0527		NADH dehydrogenase, putative	-1.1	*
SERP0531		hypothetical protein	1.5	*
SERP0542		NADH-dependent flavin oxidoreductase, Oye family	-1.2	*
SERP0552	*spsA*	signal peptidase IA, inactive	-1.7	**
SERP0556		fumarylacetoacetate hydrolase family protein	-1.2	**
SERP0557		hypothetical protein	-1.6	*
SERP0560		coenzyme A disulfide reductase	1.3	*
SERP0562		hypothetical protein	-1.8	**
SERP0569		hypothetical protein	1.5	**
SERP0578		adaptor protein	-1.5	*
SERP0580	*pepF*	oligoendopeptidase F	-1.3	**
SERP0581		hypothetical protein	1.2	*
SERP0582		protozoan/cyanobacterial globin family protein	1.3	*
SERP0583		hypothetical protein	-1.4	*
SERP0585		hypothetical protein	-2.5	***
SERP0586	*relA-1*	GTP pyrophosphokinase	-1.2	*
SERP0602		hypothetical protein	1.5	**
SERP0604		hypothetical protein	1.1	*
SERP0606	*ypfP*	ypfP protein	-1.3	**
SERP0614		abortive infection family protein	-1.6	**
SERP0615		hypothetical protein	-2.0	**
SERP0623		hypothetical protein	1.2	**
SERP0624		hypothetical protein	2.1	**

Table D.2 (continued)

Locus	Gene Name	Gene Description	FC	% FDR
SERP0626		acetyltransferase, GNAT family	-1.7	***
SERP0631		hydrolase, alpha/beta hydrolase fold family	1.6	***
SERP0633		aminotransferase, class I	1.3	**
SERP0638		IS1272-like transposase, degenerate	1.8	***
SERP0641		fmt protein	-2.1	***
SERP0644	*qoxC*	quinol oxidase, subunit III	-1.7	***
SERP0648	*folD*	methylenetetrahydrofolate dehydrogenase/methenyltetrahydrofolate cyclohydrolase	-1.5	***
SERP0649	*purE*	phosphoribosylaminoimidazole carboxylase, catalytic subunit	1.6	*
SERP0651	*purC*	phosphoribosylaminoimidazole-succinocarboxamidesynthase	-1.3	**
SERP0663		67 kDa Myosin-crossreactive antigen	-1.1	***
SERP0665		hypothetical protein	-2.7	*
SERP0666		hypothetical protein	-1.2	**
SERP0667		hypothetical protein	-1.2	**
SERP0668		hypothetical protein	-1.4	***
SERP0670	*ptsI*	phosphoenolpyruvate-protein phosphotransferase	-1.4	**
SERP0672	*cydA*	cytochrome d ubiquinol oxidase, subunit I	1.6	*
SERP0673	*cydB*	cytochrome d ubiquinol oxidase, subunit II	1.6	***
SERP0674		potassium uptake protein TrkA	-1.2	**
SERP0691		hypothetical protein	-1.7	*
SERP0693		hypothetical protein	-1.8	***
SERP0694		inositol monophosphatase family protein	-1.4	***
SERP0700		hypothetical protein	-1.4	**
SERP0701		hypothetical protein	-1.9	***
SERP0708		hypothetical protein	-1.4	***
SERP0713		hypothetical protein	1.3	**
SERP0717		hypothetical protein	1.4	**
SERP0719		cell wall surface anchor family protein	1.4	****
SERP0721	*pheS*	phenylalanyl-tRNA synthetase, alpha subunit	1.4	*
SERP0722	*pheT*	phenylalanyl-tRNA synthetase, beta subunit	1.3	*
SERP0728	*trxA*	thioredoxin	-1.5	***
SERP0731		succinate dehydrogenase	-1.1	*
SERP0732		succinate dehydrogenase	-1.2	*
SERP0733	*murI*	glutamate racemase	1.4	**
SERP0735		phosphoesterase, putative	-1.3	***
SERP0738		phenol soluble modulin beta 1	-1.4	*
SERP0739		phenol soluble modulin beta 1	-1.7	*
SERP0740		hydrolase, haloacid dehalogenase-like family	-1.2	*
SERP0760		glyoxalase family protein	1.5	**
SERP0761		LysM domain protein	1.9	***
SERP0773		hypothetical protein	-1.6	**

Table D.2 (continued)

Locus	Gene Name	Gene Description	FC	% FDR
SERP0776	*gmk*	guanylate kinase	-1.5	***
SERP0778	*coaBC*	phosphopantothenoylcysteine decarboxylase/phosphopantothenate--cysteine ligase	1.2	**
SERP0779	*priA*	primosomal protein N'	1.3	*
SERP0787		hypothetical protein	-1.3	***
SERP0789		hypothetical protein	-1.2	**
SERP0797	*fabG*	3-oxoacyl-(acyl-carrier-protein) reductase	-1.3	**
SERP0799	*rnc*	ribonuclease III	1.6	***
SERP0802		hypothetical protein	-2.6	**
SERP0813	*sucC*	succinyl-CoA synthetase subunit beta	-1.3	**
SERP0820	*hslU*	ATP-dependent protease ATP-binding subunit	-1.2	**
SERP0821	*codY*	transcriptional repressor CodY	1.1	*
SERP0822		hypothetical protein	-1.8	**
SERP0841	*pnp*	polyribonucleotide nucleotidyltransferase	-1.1	*
SERP0848		ACT domain protein	-1.3	***
SERP0849		transcriptional regulator, Cro/CI family	-1.6	***
SERP0852	*recA*	recombinase A	-1.2	**
SERP0859		hypothetical protein	-2.0	**
SERP0860	*miaB*	tRNA-i(6)A37 modification enzyme MiaB	-1.4	***
SERP0861		hypothetical protein	-1.5	**
SERP0870	*miaA*	tRNA delta(2)-isopentenylpyrophosphate transferase	-1.6	**
SERP0884		hypothetical protein	-1.6	***
SERP0894		hypothetical protein	1.8	*
SERP0900		hydrolase, haloacid dehalogenase-like family	-1.4	*
SERP0906	*guaC*	guanosine 5'-monophosphate oxidoreductase	-1.5	**
SERP0909	*lexA*	LexA repressor	-1.4	*
SERP0912	*tkt*	transketolase	-1.2	**
SERP0914		hypothetical protein	-1.8	***
SERP0916		hypothetical protein	-1.6	**
SERP0917	*sbcD*	exonuclease SbcD	-1.4	**
SERP0922		thioesterase family protein	-1.6	**
SERP0924		hypothetical protein	-1.8	***
SERP0925	*parE*	DNA topoisomerase IV subunit B	1.2	*
SERP0928		transcriptional antiterminator LicT, putative	-1.4	**
SERP0934	*dmpI*	4-oxalocrotonate tautomerase	-1.5	*
SERP0948		hydrolase-related protein	1.5	*
SERP0955		oligoendopeptidase F, putative	1.3	*
SERP0977	*brnQ-1*	branched-chain amino acid transport system II carrier protein	1.3	*
SERP0979		CbbQ/NirQ/NorQ/GpvN family protein	1.5	**
SERP0992		PAP2 family protein	1.3	*
SERP0997		hypothetical protein	1.4	*

Table D.2 (continued)

Locus	Gene Name	Gene Description	FC	% FDR
SERP0999	*msrB*	methionine sulfoxide reductase B	-1.3	*
SERP1000	*msrA-2*	methionine sulfoxide reductase A	-1.3	***
SERP1001		DegV family protein	1.4	**
SERP1008		hypothetical protein	-1.4	***
SERP1014		hypothetical protein	-1.4	*
SERP1030		hypothetical protein	-1.2	**
SERP1033		hypothetical protein	-1.5	***
SERP1036	*aroC*	chorismate synthase	1.3	*
SERP1038		polyprenyl synthetase	1.2	*
SERP1043		GTP-binding protein EngA	-1.1	*
SERP1063		oxidoreductase, aldo/keto reductase family	-1.2	*
SERP1064		oxidoreductase, short-chain dehydrogenase/reductase family	1.6	***
SERP1065	*proC*	pyrroline-5-carboxylate reductase	-1.4	**
SERP1070	*malA*	alpha-glucosidase	-1.2	**
SERP1071	*gnd*	6-phosphogluconate dehydrogenase	-1.1	**
SERP1072		peptidase T-like protein	1.2	*
SERP1074		hypothetical protein	-1.3	***
SERP1080	*recN*	DNA repair protein RecN	-1.3	*
SERP1081	*argR*	arginine repressor	-1.5	**
SERP1082	*ispA*	geranyltranstransferase	-1.5	***
SERP1084	*xseA*	exodeoxyribonuclease VII, large subunit	1.2	*
SERP1085	*nusB*	transcription antitermination protein NusB	-1.3	**
SERP1086		hypothetical protein	-1.2	*
SERP1088	*accB*	acetyl-CoA carboxylase, biotin carboxyl carrier protein	-1.5	***
SERP1096		hypothetical protein	-1.8	***
SERP1098		rhodanese-like domain protein	-1.8	**
SERP1101		glycine dehydrogenase subunit 1	1.3	***
SERP1104		hypothetical protein	-1.6	*
SERP1107	*comGC*	comG operon protein 3	1.4	*
SERP1108		comG operon protein 2, putative	1.3	***
SERP1111		hypothetical protein	-2.1	**
SERP1112	*glk*	glucokinase	1.2	*
SERP1115		5-formyltetrahydrofolate cyclo-ligase family protein	-1.3	**
SERP1124		ATP-dependent RNA helicase, DEAD/DEAH box family	1.4	*
SERP1131		hypothetical protein	-2.8	***
SERP1132	*glyS*	glycyl-tRNA synthetase	-1.2	*
SERP1133		DNA repair protein RecO family	1.5	*
SERP1137		hypothetical protein	-1.2	*
SERP1139		hypothetical protein	-1.7	*
SERP1140		hypothetical protein	-1.1	*
SERP1143	*rpsU*	ribosomal protein S21	-2.9	*

Table D.2 (continued)

Locus	Gene Name	Gene Description	FC	% FDR
SERP1156		comE operon protein 2	-1.5	**
SERP1169		acetyl-CoA carboxylase, biotin carboxylase, putative	-1.2	*
SERP1172		hypothetical protein	1.5	**
SERP1174	*greA*	transcription elongation factor GreA	-1.2	**
SERP1175	*udk*	uridine kinase	-1.2	**
SERP1179		hypothetical protein	-1.9	***
SERP1180		hypothetical protein	-1.2	*
SERP1181		hypothetical protein	-1.7	*
SERP1184		TPR domain protein	-1.3	***
SERP1189		Rrf2 family protein	-2.0	***
SERP1190		ATPase, AAA family	-1.2	*
SERP1193	*hisS*	histidyl-tRNA synthetase	1.6	*
SERP1195	*dtd*	D-tyrosyl-tRNA deacylase	-1.3	***
SERP1202	*yajC*	preprotein translocase, YajC subunit	-1.8	*
SERP1215		hypothetical protein	-2.1	***
SERP1220	*ermA-1*	Tn554, rRNA adenine N-6-methyltransferase	-1.4	*
SERP1225		truncated DNA repair protein RadC	1.9	*
SERP1226		type III leader peptidase family protein	1.9	**
SERP1228	*valS*	valyl-tRNA synthetase	1.2	*
SERP1250	*gapA-2*	glyceraldehyde 3-phosphate dehydrogenase	-1.4	*
SERP1253	*fpg*	formamidopyrimidine-DNA glycosylase	-1.2	**
SERP1254	*polA*	DNA polymerase I	-1.3	***
SERP1257	*icd*	isocitrate dehydrogenase	-1.2	**
SERP1264	*accD*	acetyl-CoA carboxylase beta subunit	-1.3	***
SERP1272	*ald*	alanine dehydrogenase	-1.3	**
SERP1277		thiol peroxidase, putative	-1.6	**
SERP1285		glycerophosphoryl diester phosphodiesterase, putative	-1.3	*
SERP1286		OsmC/Ohr family protein	1.5	***
SERP1287		aminotransferase, class V	1.5	**
SERP1288	*serA*	D-3-phosphoglycerate dehydrogenase	1.4	*
SERP1291		1-acyl-sn-glycerol-3-phosphate acyltransferase, putative	1.4	*
SERP1296	*ccpA*	catabolite control protein A	-1.4	***
SERP1299		hypothetical protein	-2.0	**
SERP1306		hypothetical protein	-1.7	*
SERP1308		hypothetical protein	-1.3	***
SERP1319		drug transporter, putative	1.6	*
SERP1322	*rot*	repressor of toxins	-1.6	**
SERP1323		lysophospholipase, putative	-1.5	**
SERP1324	*putA*	proline dehydrogenase	-1.6	***
SERP1331		hypothetical protein	-2.3	*
SERP1336	*tal*	transaldolase	-1.2	***

Table D.2 (continued)

Locus	Gene Name	Gene Description	FC	% FDR
SERP1337		hypothetical protein	-1.6	*
SERP1338		CrcB family protein	-2.1	**
SERP1340		ISSep1-like transposase	1.4	***
SERP1341		Tn554, hypothetical protein	-1.2	**
SERP1343	*ermA-2*	Tn554, rRNA adenine N-6-methyltransferase	-1.5	*
SERP1344	*spc-2*	Tn554, streptomycin 3''-adenylyltransferase	-1.5	**
SERP1356		hypothetical protein	1.4	**
SERP1357		O-succinylbenzoic acid synthetase, putative	1.4	***
SERP1358	*menE*	O-succinylbenzoic acid--CoA ligase	1.4	***
SERP1361		hypothetical protein	1.4	*
SERP1362		hypothetical protein	1.3	*
SERP1365		hypothetical protein	-1.3	**
SERP1373		HIT family protein	-1.8	**
SERP1374		hypothetical protein	-1.9	**
SERP1378	*cbf1*	cmp-binding-factor 1	-1.4	***
SERP1379		hypothetical protein	-1.4	*
SERP1381		hypothetical protein	-2.7	*
SERP1398		transcriptional regulator, Fur family	-1.3	*
SERP1399		D-isomer specific 2-hydroxyacid dehydrogenase family protein	-1.2	***
SERP1410		hypothetical protein	-1.6	***
SERP1413		ThiJ/PfpI family protein	-1.6	**
SERP1414		hypothetical protein	-1.5	**
SERP1416		cytosolic long-chain acyl-CoA thioester hydrolase family protein	1.2	*
SERP1417		aminopeptidase family protein	1.9	**
SERP1419		phosphotyrosine protein phosphatase	-1.3	*
SERP1427		hypothetical protein	1.6	*
SERP1428		immunodominant antigen B, putative	-1.4	**
SERP1429		cobyric acid synthase, putative	-1.5	****
SERP1431		ferritin family protein	-1.5	***
SERP1436		hypothetical protein	-1.1	*
SERP1444		PcrB-like protein	-1.5	***
SERP1448		hypothetical protein	-1.5	***
SERP1457		hypothetical protein	-1.3	**
SERP1459	*blaI-1*	penicillinase repressor	-1.4	*
SERP1464		Tn554-related, transposase C	-2.1	**
SERP1465		Tn554-related, transposase B	1.6	*
SERP1470		hypothetical protein	-1.5	*
SERP1471		hypothetical protein	-1.7	***
SERP1474		hypothetical protein	1.6	***
SERP1480		hypothetical protein	1.7	***

Table D.2 (continued)

Locus	Gene Name	Gene Description	FC	% FDR
SERP1496		hypothetical protein	-1.4	*
SERP1498		ammonium transporter family protein	1.2	*
SERP1499		hypothetical protein	1.3	*
SERP1514		hypothetical protein	2.1	**
SERP1515	*nrdI-2*	nrdI protein	1.9	*
SERP1536		hypothetical protein	1.7	*
SERP1541		hypothetical protein	1.9	***
SERP1543		hypothetical protein	-2.0	*
SERP1546		hypothetical protein	1.9	*
SERP1549		death-on-curing family protein	-2.0	*
SERP1551		hypothetical protein	-2.6	**
SERP1552		hypothetical protein	2.8	**
SERP1556		hypothetical protein	2.7	***
SERP1561		hypothetical protein	3.8	*
SERP1569		hypothetical protein	2.5	**
SERP1573		hypothetical protein	1.8	**
SERP1576		hypothetical protein	1.7	*
SERP1610		hypothetical protein	2.1	***
SERP1614		hypothetical protein	1.8	*
SERP1628		hypothetical protein	1.7	**
SERP1643		hypothetical protein	2.1	*
SERP1663		hypothetical protein	-1.1	**
SERP1664		hypothetical protein	-1.2	***
SERP1670	*leuB*	3-isopropylmalate dehydrogenase	1.9	*
SERP1673	*ilvA*	threonine dehydratase	1.4	*
SERP1685		hypothetical protein	1.9	**
SERP1687		hypothetical protein	-1.9	**
SERP1691		cell division protein, FtsW/RodA/SpoVE family	-1.2	*
SERP1693		hypothetical protein	-2.8	***
SERP1697		hypothetical protein	-1.8	*
SERP1698	*thiE*	thiamine-phosphate pyrophosphorylase	-1.5	*
SERP1701		transcriptional regulator, TenA family	1.6	*
SERP1704	*ywpF*	ywpF protein	1.3	*
SERP1719	*glyA*	serine hydroxymethyltransferase	-1.2	**
SERP1722		Sua5/YciO/YrdC/YwlC family protein	1.5	*
SERP1724		modification methylase, HemK family	-1.3	**
SERP1728	*rho*	transcription termination factor Rho	1.2	*
SERP1735	*rpoE*	DNA-directed RNA polymerase, delta subunit	-1.9	***
SERP1736		acetyltransferase, GNAT family	-1.4	**
SERP1742		hypothetical protein	-1.4	*
SERP1744	*pdp*	pyrimidine-nucleoside phosphorylase	-1.1	*

Table D.2 (continued)

Locus	Gene Name	Gene Description	FC	% FDR
SERP1745	*deoC*	deoxyribose-phosphate aldolase	-1.3	*
SERP1748		Dps family protein	-1.4	*
SERP1749		hypothetical protein	1.4	**
SERP1750		hypothetical protein	-1.3	***
SERP1751		hypothetical protein	-1.6	***
SERP1754		hypothetical protein	-1.8	**
SERP1757		hypothetical protein	-1.6	***
SERP1758		lytic regulatory protein, putative	-1.4	**
SERP1760	*glmS*	D-fructose-6-phosphate amidotransferase	-1.1	*
SERP1770		UTP-glucose-1-phosphate uridylyltransferase family protein	-1.8	***
SERP1772		hypothetical protein	-1.5	**
SERP1773		hypothetical protein	-2.6	***
SERP1782		alkaline shock protein 23	-1.5	*
SERP1788		hypothetical protein	1.7	***
SERP1790	*lacE*	PTS system, lactose-specific IIBC components	1.3	*
SERP1793	*lacC*	tagatose-6-phosphate kinase	1.3	*
SERP1797		transcriptional regulator, Sir2 family	1.4	*
SERP1818	*rpsN-2*	ribosomal protein S14	1.3	**
SERP1838		sugar transporter, putative	-1.2	***
SERP1840		hypothetical protein	-1.3	***
SERP1845		hypothetical protein	1.4	***
SERP1864		BioY family protein	1.3	*
SERP1868		transporter, putative	1.6	*
SERP1872	*ureE*	urease accessory protein UreE	1.5	**
SERP1876	*sarR*	Staphylococcal accessory regulator R	-1.8	**
SERP1877		hypothetical protein	-1.1	*
SERP1882		NAD/NADP octopine/nopaline dehydrogenase family protein	1.4	**
SERP1893		transcriptional regulator, putative	-1.4	*
SERP1901		phosphosugar-binding transcriptional regulator, RpiR family	1.2	*
SERP1904		hypothetical protein	-1.3	***
SERP1905		hypothetical protein	-1.9	***
SERP1913		hypothetical protein	-2.2	**
SERP1915		hypothetical protein	2.0	***
SERP1917		oxidoreductase, short chain dehydrogenase/reductase family	1.5	**
SERP1934		transcriptional regulator, PadR family	1.7	***
SERP1941		esterase, putative	-1.2	**
SERP1945		drug transporter, putative	1.9	***
SERP1948	*tcaA*	tcaA protein	-1.2	*
SERP1950		hypothetical protein	1.4	**
SERP1962		alcohol dehydrogenase, zinc-containing	-1.3	**
SERP1963		acetyltransferase, GNAT family	-1.3	***

Table D.2 (continued)

Locus	Gene Name	Gene Description	FC	% FDR
SERP1968		PTS system, sucrose-specific IIBC components	1.2	*
SERP1974		hypothetical protein	-2.1	**
SERP1979	*sarZ*	transcriptional regulator, MarR family	-2.5	***
SERP1989	*nirD*	nitrite reductase [NAD(P)H], small subunit	-2.2	**
SERP1995		IS1272-like transposase, degenerate	2.0	*
SERP1997		formate/nitrite transporter family protein	-1.3	**
SERP1999		glutaredoxin, putative	-1.4	**
SERP2000		lipoprotein, putative	-1.9	**
SERP2002		IS1272-like transposase, degenerate	1.9	**
SERP2008		cation efflux family protein	-1.4	**
SERP2010		hypothetical protein	-1.4	**
SERP2013		hypothetical protein	-1.4	**
SERP2018		hypothetical protein	1.7	***
SERP2036		major facilitator superfamily protein	1.2	**
SERP2037		hypothetical protein	1.7	***
SERP2039		conserved domain protein, truncation	1.6	***
SERP2042		lipoprotein, putative	-2.4	**
SERP2043		peptidase, M42 family	1.3	**
SERP2046		exopolyphosphatase	1.5	***
SERP2047	*ppk*	polyphosphate kinase	1.2	**
SERP2056	*galU*	UTP-glucose-1-phosphate uridylyltransferase	-1.4	***
SERP2057	*gntP*	gluconate transporter, permease protein	1.3	**
SERP2058	*gntK*	gluconokinase	1.3	**
SERP2063		esterase, putative	-1.6	***
SERP2064		PAP2 family protein	1.5	**
SERP2066		hypothetical protein	-1.9	**
SERP2067		hypothetical protein	1.6	***
SERP2068		hypothetical protein	-1.7	**
SERP2069		major facilitator superfamily protein	-1.1	**
SERP2072	*thiS*	thiamine biosynthesis protein ThiS	1.9	*
SERP2076		fructose-1,6-bisphosphatase, putative	1.4	*
SERP2078		hypothetical protein	2.0	***
SERP2081		adhesion lipoprotein, putative	1.4	*
SERP2083		glyoxalase family protein	1.6	***
SERP2087		2-hydroxyacid dehydrogenase	1.9	***
SERP2097		hypothetical protein	2.5	*
SERP2105	*capA*	capA protein	1.9	***
SERP2113		abortive infection family protein	-1.3	**
SERP2119		hypothetical protein	-1.4	*
SERP2121		hydroxymethylglutaryl-CoA reductase, degradative	-1.2	***
SERP2127		FeoA family protein	-1.4	**

Table D.2 (continued)

Locus	Gene Name	Gene Description	FC	% FDR
SERP2128		delta-1-pyrroline-5-carboxylate dehydrogenase, putative	-1.1	*
SERP2133		2-hydroxyacid dehydrogenase	1.8	***
SERP2145		hypothetical protein	-1.4	*
SERP2150	*panD*	aspartate 1-decarboxylase precursor	-1.8	***
SERP2166	*fdaB*	fructose-bisphosphate aldolase	-1.4	**
SERP2173		hypothetical protein	-1.3	*
SERP2175		amidohydrolase family protein	1.4	***
SERP2179	*0*	choline/carnitine/betaine transporter	1.5	*
SERP2186	*sat*	sulfate adenylyltransferase	1.9	**
SERP2187		hypothetical protein	1.7	*
SERP2198		hypothetical protein	1.6	*
SERP2200		hypothetical protein	1.5	***
SERP2207		hypothetical protein	-2.5	***
SERP2210		glycosyl transferase, group 1 family protein	1.3	*
SERP2211		hypothetical protein	-1.8	*
SERP2212		hypothetical protein	1.4	***
SERP2217				
SERP2218		ADP-ribosylglycohydrolase, putative	1.2	*
SERP2220		universal stress protein family, putative	-2.0	*
SERP2222	*cadC*	transcriptional regulator CadC	-2.5	***
SERP2224		metallothionein 2-related protein	-1.6	**
SERP2227		hypothetical protein	1.3	**
SERP2232		major facilitator superfamily protein	1.9	***
SERP2234		hypothetical protein	-1.2	*
SERP2236		hypothetical protein	1.4	*
SERP2238		hypothetical protein	-2.5	**
SERP2244		capA-related protein	1.4	*
SERP2246		transcriptional regulator, Crp/Fnr family	-1.9	**
SERP2248		hypothetical protein	1.8	***
SERP2256		hypothetical protein	1.9	*
SERP2261	*manA-2*	mannose-6-phosphate isomerase, class I	1.3	*
SERP2264		cell wall surface anchor family protein	1.4	**
SERP2270		major facilitator superfamily protein	1.3	*
SERP2271		hypothetical protein	2.0	**
SERP2287		hypothetical protein	2.0	***
SERP2288		5'-nucleotidase family protein	1.4	***
SERP2289		transporter, putative	1.9	***
SERP2299		N-acetyltransferase family protein	2.0	***
SERP2312	*mqo-3*	malate:quinone oxidoreductase	1.5	***
SERP2314		hypothetical protein	-2.0	**
SERP2317	*pcp*	pyrrolidone-carboxylate peptidase	1.2	*

Table D.2 (continued)

Locus	Gene Name	Gene Description	FC	% FDR
SERP2318		hypothetical protein	1.6	*
SERP2321		immunodominant antigen B, putative	-2.0	***
SERP2324		dihydrolipoamide acetyltransferase	-1.2	*
SERP2331	*rarD*	rarD protein	1.3	*
SERP2332		hypothetical protein	-1.2	*
SERP2333		hypothetical protein	1.2	*
SERP2335		hypothetical protein	1.3	**
SERP2336		lipase, putative	1.6	**
SERP2338		peptide synthetase	1.2	***
SERP2341		hypothetical protein	-1.6	**
SERP2342		drug transporter, putative	1.8	***
SERP2343		hypothetical protein	-1.6	***
SERP2344		DAK2 domain protein	-1.4	*
SERP2359		hypothetical protein	1.9	***
SERP2361		hypothetical protein	1.8	*
SERP2379		oxidoreductase, short-chain dehydrogenase/reductase family	-1.4	*
SERP2384		hypothetical protein	1.6	**
SERP2385		hypothetical protein	2.0	**
SERP2386		cobalamin synthesis protein, putative	3.4	***
SERP2390	*sspB*	cysteine protease precursor SspB	2.4	***
SERP2391	*sspC*	SspC protein	1.5	**
SERP2392	*bhp*	cell wall associated biofilm protein	1.2	*
SERP2410		hypothetical protein	-1.7	**
SERP2411		oxidoreductase, short chain dehydrogenase/reductase family	-1.4	***
SERP2413		hypothetical protein	1.5	**
SERP2420		hypothetical protein	1.3	*
SERP2421		hypothetical protein	-1.5	**
SERP2423		lipoprotein, putative	-1.4	*
SERP2425		hypothetical protein	1.8	***
SERP2435		metallo-beta-lactamase family protein	1.5	***
SERP2437		lipoprotein, putative	-1.8	**
SERP2441		transporter, putative	1.4	*
SERP2454		hypothetical protein	-1.3	**
SERP2455		hypothetical protein	-1.5	**
SERP2456		hypothetical protein	-1.2	*
SERP2457		CRISPR-associated protein, TM1807 family	-1.4	***
SERP2460		CRISPR-associated protein, TM1810 family	-2.2	**
SERP2462		CRISPR-associated protein Cas2	-1.8	***
SERP2463	*cas1*	CRISPR-associated protein Cas1	-1.2	*
SERP2467		hypothetical protein	1.8	*
SERP2468		hypothetical protein	1.7	**

Table D.2 (continued)

Locus	Gene Name	Gene Description	FC	% FDR
SERP2470		spermidine N1-acetyltransferase, putative	-2.1	**
SERP2471		type I restriction-modification system, S subunit, EcoA family	-1.4	*
SERP2472	*hsdM*	type I restriction-modification system, M subunit	1.3	*
SERP2475		hypothetical protein	-1.6	**
SERP2480		hypothetical protein	-1.3	*
SERP2481		hypothetical protein	1.2	**
SERP2483		hypothetical protein	1.4	***
SERP2488		hypothetical protein	2.3	**
SERP2495		hypothetical protein	1.5	*
SERP2496		hypothetical protein	1.8	***
SERP2501		hypothetical protein	2.0	**
SERP2502		hypothetical protein	1.7	*
SERP2504		hypothetical protein	2.2	**
SERP2510	*ermA-3*	rRNA adenine N-6-methyltransferase	-1.4	*
SERP2512		hypothetical protein	-1.2	*
SERP2517	*xylR*	xylose repressor	-1.4	**
SERP2519	*mecI*	methicillin-resistance regulatory protein MecI	-2.1	**
SERP2528		hypothetical protein	-1.6	*
SERP2529		hypothetical protein	1.5	**
SERP2535		hypothetical protein	-2.9	**
SERP2541		homoserine O-acetyltransferase, putative	1.4	***
SERP2542		hypothetical protein	2.9	***
SERP2543		azlC protein, putative	2.0	***
SERP2550	*recF*	recombination protein F	-1.1	*
SERP2551		hypothetical protein	-2.0	**
SERP2552	*dnaN*	DNA polymerase III subunit beta	-1.3	***

APPENDIX E

IN-VITRO TESTING OF STAPHYLOCOCCUS EPIDERMIDIS BIOFILM GROWTH ON SURGICAL MESH AND TREATMENT WITH DIRECT ELECTRIC CURRENT

IN-VITRO TESTING OF STAPHYLOCOCCUS EPIDERMIDIS BIOFILM GROWTH ON SURGICAL MESH AND TREATMENT WITH DIRECT ELECTRIC CURRENT

Motivation

In Chapters 2 and 3, biofilm-coated coupons were treated with direct current (DC) in liquid medium containing chloride. The following experiments investigated biofilm growth and DC treatment on surgical meth in liquid broth and on an agar surface. Surgical mesh was selected based on a subcutaneous animal model in which a small square of surgical mesh inoculated with bacteria is inserted under the skin of an animal with growth occurring in conjunction or prior to testing of treatment agents. One aim of these experiments was to investigate zones of efficacy and degrees of chlorine generation in semisolid medium. The other aim was to gather preliminary data on DC current levels and duration of electric current application (as DC) for the treatment of biofilm on mesh if an animal model were to be used.

Two *in-vitro* growth systems were investigated with biofilms grown on the mesh and treated in nutrient broth or on an agar plate. The assessment of growth and treatment efficacy was based on confocal microscopy and bacterial enumeration by plate counts. The agar, "colony" growth system was thought to be a better representation of the rat model and was used to generate dose-response curves for both current level (0, 2, and 5 mA) and time (2 and 4 hrs). Log reductions following 4 hrs of DC at 5 mA were close to total kill. What follows is a report of the results. Detailed methods can be found at the end of the document.

Results and Discussion

Growth Systems

Staphylococcus epidermidis biofilms were grown on surgical mesh in two growth systems. Platinum electrodes were woven through surgical mesh to provide contact. The broth growth system used a twelve-well plate containing 4 mL/well tryptic soy broth with the mesh suspended in the broth by the electrodes (Figure E.1). The colony mesh system sat flesh with the surface of a tryptic soy agar plate (Figure E.2). For both systems, the mesh was dipped in an overnight culture of *S. epidermidis* RP62A and grown for 24hours at 37˚C.

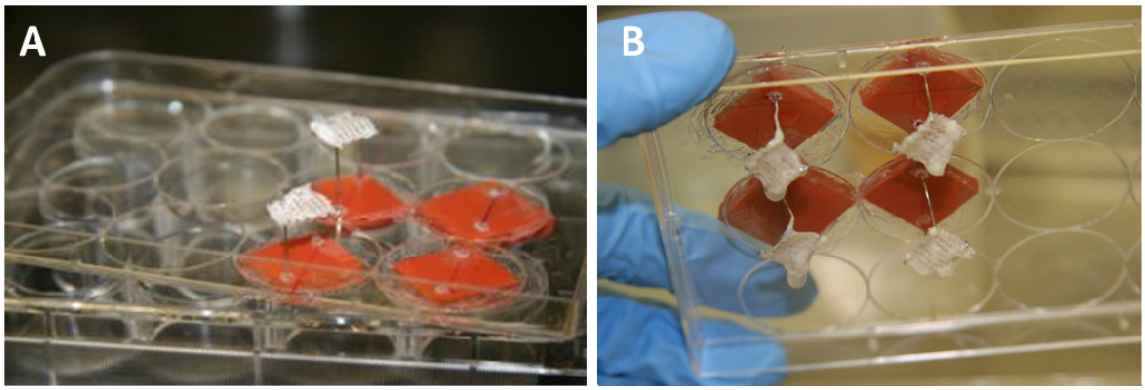

Figure E.1 *S. epidermidis* biofilm grown on surgical mesh in nutrient broth. (A) Electrodes attached to surgical mesh were inserted through the lid of a twelve well plate, held in place by rubber sheeting on the outside lid. Mesh was suspended in broth during growth in a shaker. (B) Broth growth system following 24h growth.

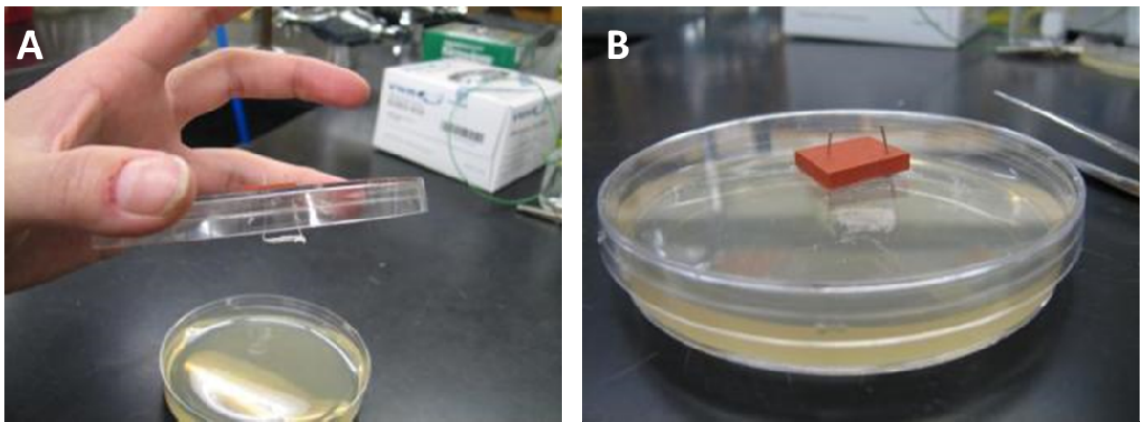

Figure E.2 *S. epidermidis* biofilm grown on surgical mesh on an agar plate. (A) Electrodes were inserted through the lid of a petri plate and held in place by rubber sheeting on the outer lid. (B) Following inoculation, mesh rested flat on the surface of the agar.

Confocal Imaging of Biofilms
Grown and Treated in the Broth System

The broth growth system produced biofilm with large clusters loosely anchored to the mesh as visible by the naked eye (Figure E.1B) and confocal imaging with LIVE/DEAD staining (Figure E.3A,B). After 24 hrs of growth, the biofilms were transferred to fresh medium and treated with DC. After 24 hrs of 4mA of DC, cells and clusters were very difficult to locate and the mesh looked essentially clean (Figure E.3C). When the treatment was decreased to 5mA for 2hr, cells were visible in the treated sample although the density of cells was significantly decreased (Figure E.3D-F). Plate counts for samples treated in parallel indicated cell densities of 10.04 $\log_{10}(CFU/cm^2)$ for a no-current control sample (n=1 sample) and 8.30 $\log_{10}(CFU/cm^2)$ for the 5mA treated sample (n=1 sample) over 2 hours.

An interesting observation was a staining gradient from one electrode to the other across the treated mesh after staining with LIVE/DEAD stain. Confocal images were

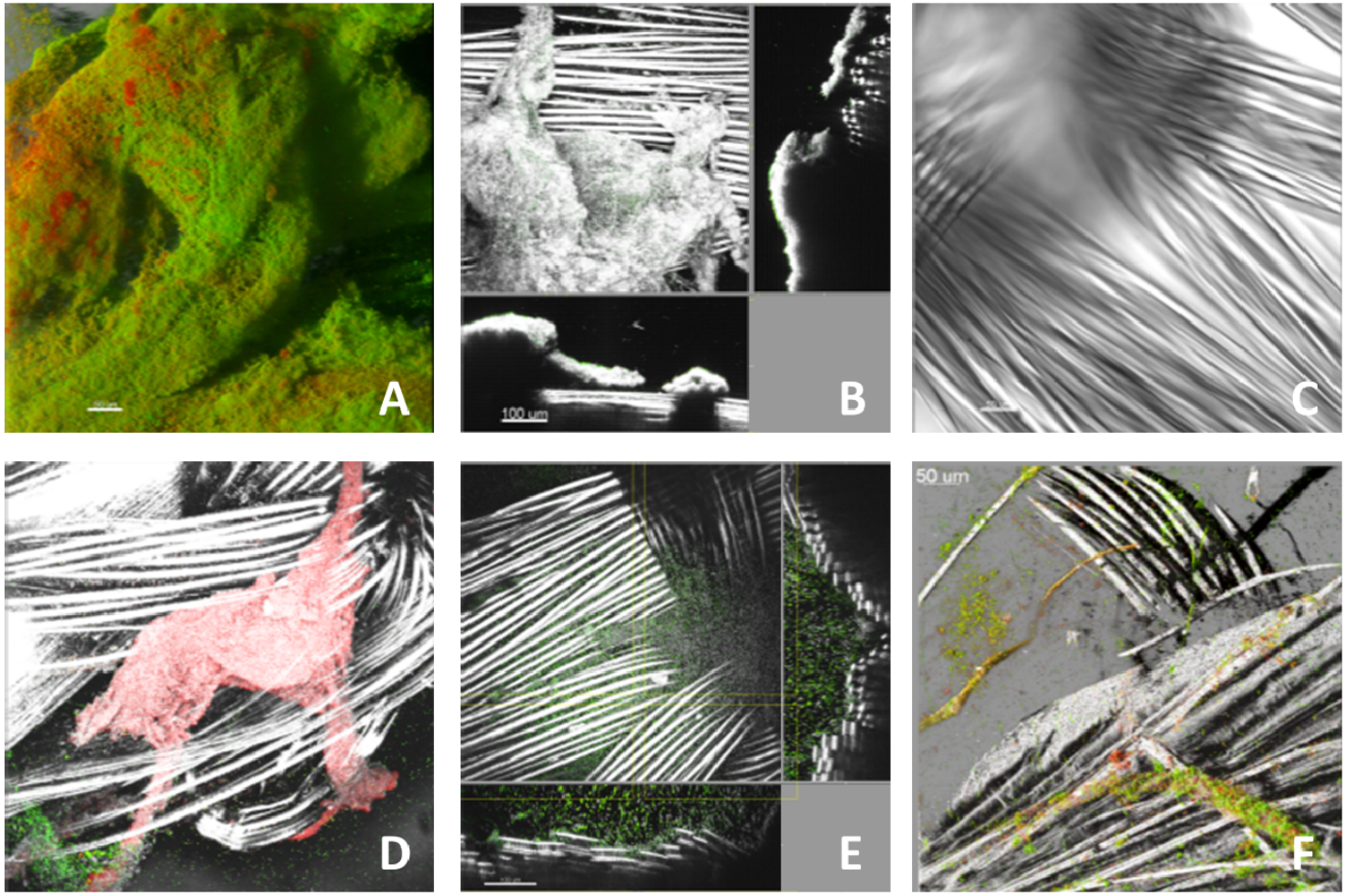

Figure E.3 Confocal images with LIVE/DEAD stained ("live" in green, "dead" in red) of *S. epidermidis* biofilms grown and DC treated in the broth mesh system. (A,B) Biofilms after 24 hours of growth. (C) Essentially clean mesh after 24 hour treatment of biofilm with 4mA DC. Two hour treatments of biofilm with 5mA DC at the (D) anode. (E) middle of the mesh, and (F) cathode.

taken of cells remaining at each electrode and in the middle of the mesh and the stained cells presented differently. More red cells were found at the anode while more green cells were seen at the cathode. The image from the center of the mesh indicates green cells above the mesh surface, however large clusters could not be found and, in the absence of visible matrix, the cells appear planktonic. While it is tempting to interpret this as "live" cells (green) at the anode and "dead" cells (red) at the cathode, the chemical gradients present with DC could significantly affect the staining process. As significant differences in pH and chlorine are both expected and have been observed at the different electrodes (Figure A.3), caution should be taken in direct interpretation of the color in these images. Regardless, it is evident that treatment with current has decreased the amount of biofilm on the mesh.

Confocal Imaging and Kill
Curve for Biofilms Grown and
Treated in the Colony Mesh System

In contrast to the broth system, the colony mesh system produced biofilm coating the strands of the mesh (Figure E.4). The close association allowed for visualization of the mesh location with LIVE/DEAD staining of the cells and did not require imaging with reflected light. The confocal images of samples treated for 2 hours with 5mA of direct current showed a decrease in visible biofilm (B and C). Cells that remained after the two hour treatment appeared to still be adhered to the mesh surface however the biofilm was sparse in comparison to the no-current control.

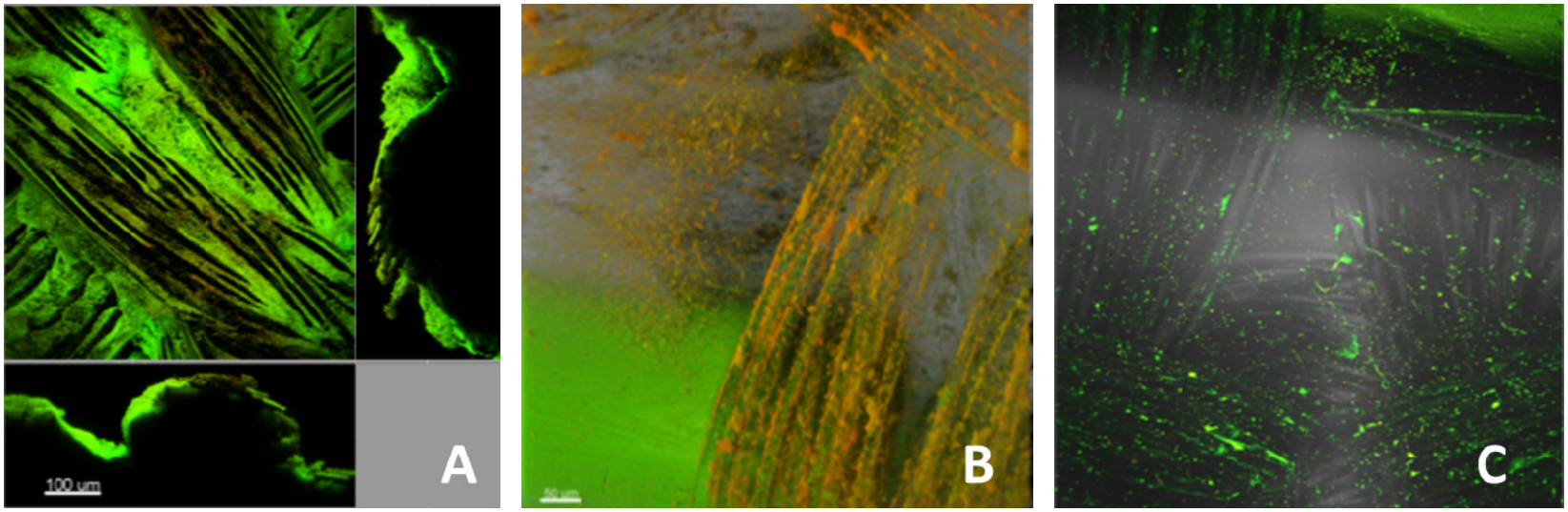

Figure E.4 Confocal images with LIVE/DEAD staining ("live" in green, "dead" in red) of *S. epidermidis* biofilm growtn in the colony mesh growth system. (A) Biofilm after 24 hours of growth. Biofilms following 2 hours of DC at 5mA at the (B) anode and (C)cathode. Electrodes are visible in the treated samples.

A color gradient was again noted across the treated mesh after staining. Staining patterns similar to that seen in the broth system were observed, with more red cells at the anode and green cells at the cathode. Again, the large electrolytic chemical gradients could modify cell staining, caution should be taken to directly interpret these staining patters as either "live" or "dead" however variations are clearly present.

Based on the confocal images, it was thought that the colony mesh biofilm more closely represented the type of biofilm that might be found in the wound bed of the animal model. Kill curves to determine current levels and duration for effective treatment were performed at 2 and 5mA for 2 or 4hrs (Figure E.5). DC treatment was dose-responsive with respect to both current level and treatment duration. Treatment with 2mA of current resulted in 2- to 3-log reductions for 2 and 4hrs of treatment, respectively. Treatment with 5mA of current approaching the detection limit for some samples at 2hrs and were at or below the limit of detection at 4hrs.

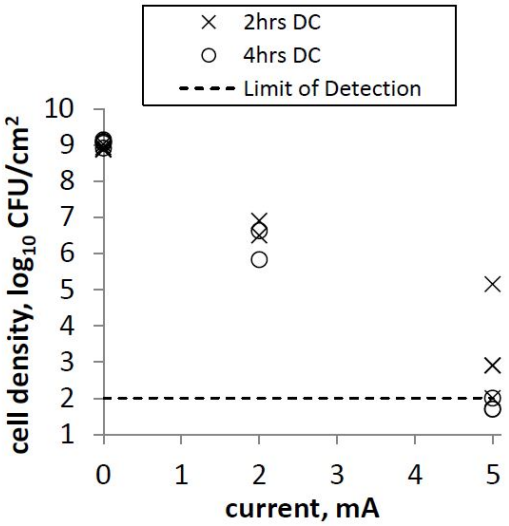

Figure E.5 Log reductions for 24hr *S. epidermidis* biofilms exposed to direct current using the colony mesh system. Data are the result of three experiments (Exp1=0 and 5mA, 4hrs; Exp2=0 and 5mA, 2hrs; Exp3=0 and 2mA, 2 and 4hrs).

For a rough estimate of enhanced killing at one electrode over the other, some mesh samples for the 2mA experiment were cut in half after treatment and plated separately. Between electrodes, differences of only 0.5-1 $\log_{10}$CFU/cm^2 were observed for a given sample with three of the four samples higher at the cathode although results were inconclusive. Overall, treatment with direct current seems to induce killing across the whole mesh sample although local variation between electrodes may exist.

Conclusions

- Growth of *S. epidermidis* biofilm on surgical mesh in a broth system produced a thick biofilm with large clusters loosely tethered to the mesh. Growth on the surgical mesh on an agar surface produced biofilms coating the strands of the mesh and was thought to be a preferred *in-vitro* system to mimic the animal model.
- In both mesh system, electric current at levels of 2-5 mA DC for 2, 4 or 24hrs decreased biofilm density of an established, 24hr old biofilm in all treated samples when examined by confocal microscopy and plate counts.
- In the colony mesh system, dose-responsive killing was observed. The dose-response curve indicates a current level of 5 mA for 2-4 hrs to establish total kill of a 9 $\log_{10}$CFU/cm^2 biofilm on surgical mesh.
- The decreases in biofilm density from direct current were observed across the whole mesh surface and at both electrodes suggesting chemistry in semisolid agar medium similar to that seen in TSB liquid medium (Chapters 2 and 3) in which biofilm were effectively treated when between but not in contact with electrodes.

- Differences in staining across the DC-treated mesh may support pH and chemical gradients, which could lead to killing gradients.
- Finally, for trial animal experiments, a very basic system for adding electrodes to the mesh system by weaving was used that we believe is compatible with the animal model. Once in place, the mesh seems relatively secure on the electrodes while maintaining flexibility of the mesh with two stiff 1cm segments of wire that would lie parallel to the skin. Used as is, the wire would exit the skin in two locations (opposite on the diagonal of the square mesh segment). Electrodes could then be cut down as only a small amount of exposed electrode is needed for connection to the power supply. Future modifications could be made as needed, should animal experiments continue.

Methods

Mesh Preparation and Electrodes

Biofilms were grown on Tyco polypropylene clear (undyed) SURGIPRO Mesh (0.57mm thick, REF SPM-35). The mesh was cut to 1cm square using a flame heated inoculating wire and placed in a sterile petri plate. The hot wire was necessary to prevent fraying when wire was woven through mesh in comparison to cutting. Platinum wire (0.5mm (0.02in) dia, Premion, 99.997% (metal basis), Alfa Aesar 10957) was woven through mesh and bent to a 90 degree angle at 1 cm. Wire at the opposite end of the mesh was bent slightly to prevent mesh from sliding off the wire during growth and treatment.

Broth Mesh Protocol

The electrodes (woven through mesh) were inserted through the lid of the twelve well plate held in place with rubber sheeting adhered with silicone to the outer lid of the plate. The lid was moved to a plate with wells containing 4mL of overnight inoculum (*S. epidermidis* RP62A in tryptic soy broth) and placed on a 37˚C shaker for 30 minutes. The lid was then transferred to a fresh 12-well plate with 4mL of tryptic soy broth in each well and returned to the shaker for 24hrs.

For treatment with electric current, the lid with biofilm was transferred to a new 12-well plate with 4mL per well of a treatment solution ($1/10^{th}$ strength tryptic soy broth with 9 g/L total NaCl). Current was applied in a 37˚C incubator using the system previously described (Sandvik et al., 2013). Control samples remained suspended by the electrodes but electrodes were not connected to the power supply.

Colony Mesh Protocol

The electrodes (woven through mesh) were inserted through the lid of a petri plate (1 sample per plate) and held in place with rubber sheeting adhered with silicone to the outer lid of the plate. Each mesh sample was dipped in an overnight inoculum (*S. epidermidis* RP62A in tryptic soy broth) and placed on a tryptic soy agar plate. The electrodes were adjusted such that the mesh lay flat on the agar surface. Control samples were $1cm^2$ pieces of mesh without electrodes and were dipped and placed on agar. Biofilms were grown upright in a 37˚C incubator for 24hrs.

For treatment with electric current, the lid with mesh was removed, the mesh was dipped in a treatment solution ($1/10^{th}$ strength tryptic soy broth with 9 g/L total NaCl) and

transferred to a fresh agar plate (to maintain moisture and conductivity). Again, electrodes were adjusted such that the mesh lay flat on the agar surface. Control samples were transferred to fresh plates with sterile forceps also dipping in the treatment solution. Current was applied in a 37˚C incubator.

Sampling Protocol for Bacterial Counts

When biofilms were grown on the mesh on an agar plate, the mesh was gently lifted off the agar surface with sterile forceps and placed in a test tube containing 10mL of sterile phosphate buffered saline (PBS, pH 7.2). When the sample was attached via electrodes, the electrodes were gently pulled from the lid of the growth system and the biofilm coated mesh with electrodes was placed in a test tube containing 10mL of PBS. For a rough estimate of a killing gradient across treated samples, some mesh samples were cut in half (by eye) with sterile scissors at the midpoint between electrodes following treatment and processed as separate samples. For disruption, each sample was vortexed for 30 seconds, sonicated in a water bath for 2 minutes, and vortexed again for 30 seconds. Samples were serially diluted and drop plated on tryptic soy agar using the 10 drop method. Colony forming units were counted after overnight incubation at 37˚C.

LIVE/DEAD Staining and Microscopy

For confocal imaging, biofilm samples were stained using Invitrogen's LIVE/DEAD BacLight Bacterial Viability Kit. 3 uL of Components A (SYTO 9 nucleic acid stain) and B (propidium iodide) where added to 0.5 mL of filter sterilized water. The biofilm samples were moved from the treatment system to a sterile petri plate. The stain was gently applied to form a bubble over the mesh and incubated in the dark for 30

minutes. The sample was then gently rinsed with filter sterilized water and transferred to a fresh petri plate. The samples were imaged while submerged in filter-sterilized water. While the green-fluorescent SYTO 9 can penetrate both healthy and compromised cells, the red-fluorescent propidium iodide stain only penetrates cells with damaged membranes. Thus, staining using this technique generates images of "live" (green) cells and "dead" (red) cells although literal interpretation of the viability of the cells is debated. Confocal images of red and green fluorescence were taken simultaneously at a given location on the sample. When needed, an additional stack of images was taken at the same location using reflected light to identify location of the mesh strands.